THE EFFECT OF GRADATION AND FINES CONTENT ON THE UNDRAINED

LOADING RESPONSE OF SAND

by

Ralph H. Kuerbis

B.A.Sc., The University of British Columbia, 1985

A THESIS SUBMITTED IN PARTIAL FULFILLMENT OF

THE REQUIREMENTS FOR THE DEGREE OF

MASTER OF APPLIED SCIENCE

in

THE FACULTY OF GRADUATE STUDIES

Department of Civil Engineering

We accept this thesis as conforming

to the required standard

THE UNIVERSITY OF BRITISH COLUMBIA

June 1989

© Ralph H. Kuerbis

In presenting this thesis in partial fulfilment of the requirements for an advanced degree at the University of British Columbia, I agree that the Library shall make it freely available for reference and study. I further agree that permission for extensive copying of this thesis for scholarly purposes may be granted by the head of my department or by his or her representatives. It is understood that copying or publication of this thesis for financial gain shall not be allowed without my written permission.

Department of ___Civil Engineering___

The University of British Columbia
Vancouver, Canada

Date ___July 5, 1989___

ABSTRACT

A systematic study of the effect of grain size, gradation and silt content on the monotonic and cyclic undrained loading response of sand is presented. The objective of the study is to gain an improved understanding of the behaviour of fluvial and hydraulic fill sands. A slurry method of deposition is developed to prepare homogeneous specimens of well-graded and silty sands, and to simulate hydraulic fill or fluvial deposition processes. Various soil gradations consolidated from loosest state of slurry deposition are shown to have similar triaxial compression loading behaviour, but quite different triaxial extension loading behaviour. Well-graded sands are shown to be generally more resistant to soil liquefaction. Loose silty sands are shown to possess similar cyclic strengths regardless of silt content, even though they have widely different void ratios. The concept of sand skeleton void ratio is introduced in order to explain the observed behaviour of silty sands with varying fines content. The effect of soil sample preparation technique on laboratory test results is discussed. Water pluviated sand is shown to have a characteristic fabric and strength anisotropy. An interpretation of the factors which contribute to sand fabric and strength anisotropy is provided. The practical performance of water pluviated sand is discussed.

TABLE OF CONTENTS

LIST OF FIGURES

LIST OF TABLES

NOTATIONS

CSR	Critical effective stress ratio
Dr	Relative density
Dr_c	Relative density after consolidation
$Dr_{c(skel)}$	Sand skeleton relative density after consolidation
e	Void ratio
e_c	Void ratio after consolidation
$e_{c(skel)}$	Sand skeleton void ratio after consolidation
e_j, Dr_j	Initial density after set-up and consolidation to 20 kPa
N	Number of loading cycles
N_1	Number of loading cycles to initial liquefaction (2.5% strain)
U	Porewater pressure
ΔU	Excess porewater pressure
$\epsilon_a, \epsilon_r, \epsilon_v$	Axial, radial and volumetric strain
ϵ_1, ϵ_3	Strains in maximum and minimum stress directions
ϕ_{ult}	Undrained loading boundary envelope effective friction angle
ϕ_{pt}	Effective friction angle at phase transformation
σ'_a, σ'_r	Axial and radial effective stress
σ'_1, σ'_3	Maximum and minimum effective stress
σ_d	Deviator stress
σ'_c	Effective isotropic consolidation stress
σ'_{3c}	Effective confining stress
m	Membrane penetration factor (see Appendix A)
B	Bulk modulus during consolidation

ACKNOWLEDGEMENTS

CHAPTER 1

INTRODUCTION

The occurrence of sand liquefaction or loss of strength during rapid loading has been the focus of considerable soils engineering research in the past fifty years. Extensive damage due to soil foundation failures during the 1964 earthquakes in Niigata (Japan) and Alaska (U.S.A.) sparked considerable interest in understanding the undrained and dynamic loading behaviour of saturated sand. Much effort has gone into the development of sand liquefaction evaluation techniques, including laboratory testing, in situ testing, and the development of predictive models. The dynamic loading behaviour of sand has been shown to be the critical design factor in many geotechnical projects.

In the past, an understanding of the fundamentals of sand liquefaction behaviour has been derived from laboratory tests and observations. To ensure that fundamental material strength properties determined in the laboratory are applicable to practical field problems, two fundamental questions must be considered: (1) is the soil sample tested in the laboratory representative of the in situ soil being modelled; and (2) does the laboratory testing technique employed simulate the loading conditions that occur in situ. Differences in opinion about soil behaviour and methods of stability evaluation can often be directly attributed to these questions. To address these questions one must be

able to define representative in situ soil and loading conditions. This is a very difficult process, as soil properties are dependent upon many different factors. In addition, the loading conditions on any specific soil element are difficult to quantify because they are controlled to a large extent by the mechanical properties of adjacent soil elements. Material properties may also be changed dramatically by the process of loading.

Most fundamental laboratory studies of sand liquefaction behaviour conducted in the past have been performed using poorly-graded clean sands, to ensure homogeneity and repeatability of soil samples for systematic comparison of results. Many natural sands which are encountered in geotechnical design problems are silty or well-graded. In order to successfully evaluate the liquefaction susceptibility of such in situ sands, it would be useful to identify the effects of silt content and gradation upon the behaviour of laboratory sand samples. This has been identified as a major research objective by the U.S. N.R.C. (1985) report on earthquake engineering.

Some silty and well-graded sands have been tested in the past, but due to the different methods employed in sample preparation and laboratory test evaluation, contradictory conclusions as to the effects of silt content and sand gradation have been reported by various researchers. Samples have generally been prepared in a dry or moist state. Such sample preparation methods do not

simulate the depositional fabric of hydraulic fill or natural fluvial deposits, where sediment settles through water. A majority of loose sandy materials which are prone to liquefaction and of practical concern in geotechnical designs are deposited by natural fluvial deposition or artificial hydraulic fill placement.

Previous laboratory testing programs performed on silty and well-graded sand have also generally concentrated on one particular type of laboratory strength test, such as triaxial compression loading, even though numerous laboratory test results have shown sand strength properties to be highly dependent upon direction and type of loading.

This thesis presents a systematic study of undrained sand response, with the objective of gaining an improved understanding of the behaviour and performance of natural fluvial and hydraulic fill sands. The effects of gradation and fines content on undrained behaviour are investigated. Selective sieving of a tailings sand was employed to obtain uniform and well-graded sands. Silty sands were simulated by adding various percentages of a cohesionless silt to the processed sand. Identical soil mineralogy in various soil gradations is ensured by use of the same parent material.

Fundamental studies of material behaviour require tests on homogeneous specimens. Homogeneity of laboratory test specimens is mandatory in order to determine elemental soil properties. Consequently, a slurry method of deposition was developed that yields homogeneous specimens of well-graded

as well as silty sands. This method of sample preparation simulates well the placement of sand through water in a hydraulic fill or fluvial sand deposit.

The behaviour of each material after consolidation from loosest state of slurry deposition is studied under undrained monotonic loading conditions. Both triaxial extension and compression tests are conducted to explore the effect of loading direction upon material properties. The behaviour of silty sand at various densities is also studied under cyclic loading. Test results are evaluated to determine if there is a systematic variation in sand behaviour with change in gradation and silt content.

CHAPTER 2

THE UNDRAINED BEHAVIOUR OF SAND - BACKGROUND CONCEPTS

Several approaches have been developed for modeling and evaluating soil behaviour under undrained loading conditions, based upon the observed behaviour of various laboratory and field soils. The different approaches to mechanical behaviour modeling can be divided into two groups: 1) limit state models where a soil is deemed either stable when applied shear stress is below shear strength or unstable when shear stress is above shear strength, and 2) strain development models where strains induced within a soil are directly related to stresses applied. Limit state models have been developed specifically for flow slide forms of failure, where soil is observed to flow in a manner similar to that of a viscous fluid. Strain development models have been developed for use in numerical analysis, specifically for denser soils which may not be susceptable to flow failure, but nevertheless may be subject to large undesirable strains under cyclic loading conditions. The applicability of any given soil model or soil evaluation method to a specific stability problem is determined by the soil being modeled, the conditions under which the soil exists in the field, and the mechanism of expected field loading which will be applied to the soil.

2.1 MONOTONIC LOADING BEHAVIOUR

The range of undrained monotonic loading stress-strain response of sand is shown in Figure 2.1. (e.g., Castro, 1969, Castro et. al., 1982, Chern, 1985). Types 1 and 2 are characteristic of contractive response exhibited by loose sand and sand at higher effective confining stress. Type 1 response is generally associated with flow failure. Type 3 is a characteristic dilative response exhibited by dense sand and sand at lower effective confining stresses.

Type 1 and 2 response represent strain softening behaviour. In soils responding in this manner, Type 1 behaviour has been called liquefaction (Castro, 1969). To avoid confusion with other uses of the term "liquefaction" Type 1 resonse will henceforth be called steady-state liquefaction. In Type 1 response, sand ultimately reaches a minimum constant shear strength at which unlimited shear strain may occur at constant shear and effective confining stresses. This shear strength called the steady-state undrained strength is considered to be uniquely related to the void ratio of the sand, and is believed to be independent of factors such as soil structure (which may be affected by the method of sample preparation), or prior strain history (Castro, 1982). Type 2 response has been called limited liquefaction (Castro, 1969). The term "limited" implies that strain hardening follows strain softening after a minimum in undrained strength. This
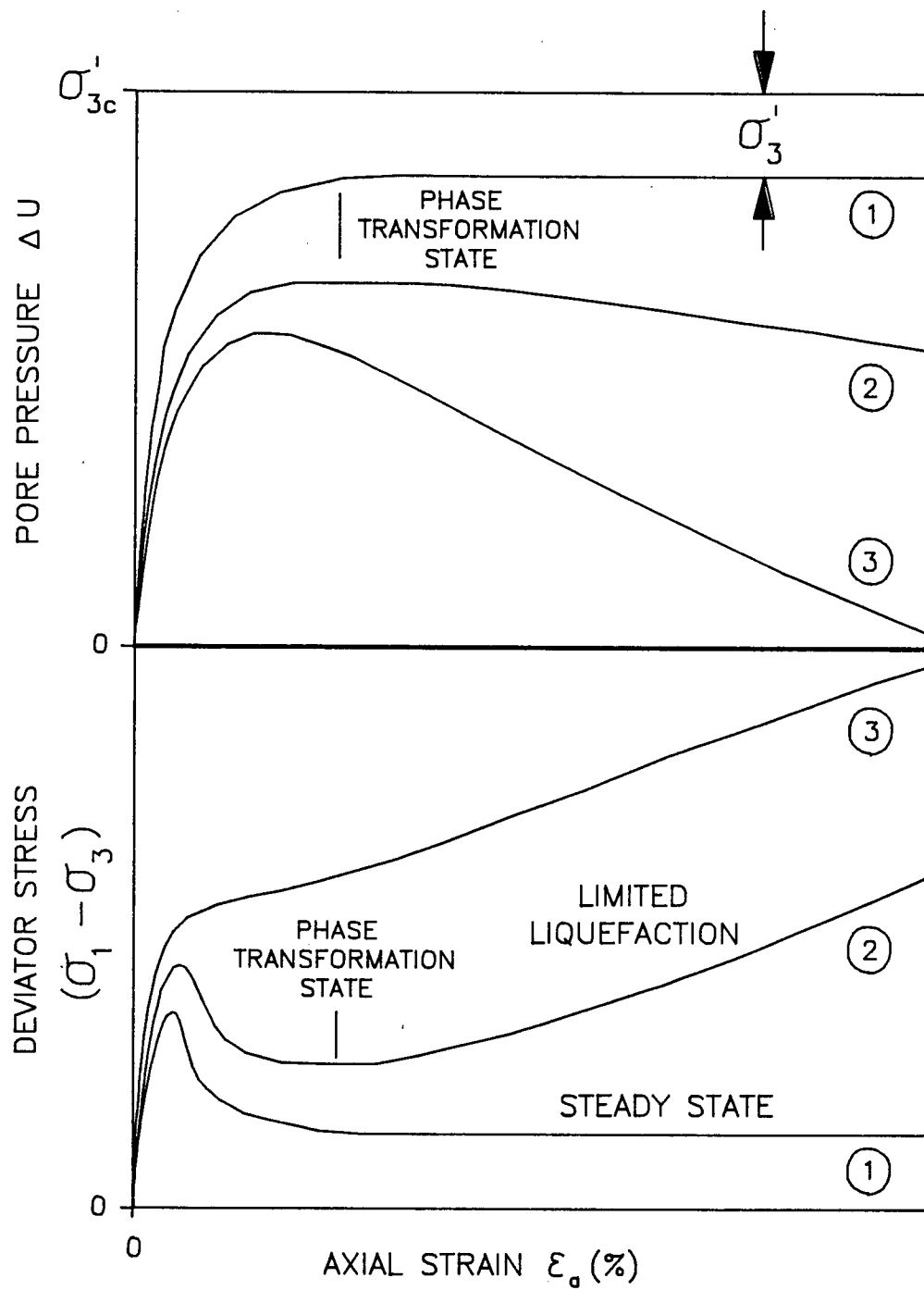
Figure 2.1(a)   Characteristic monotonic undrained loading stress-
            strain response of sandy soils
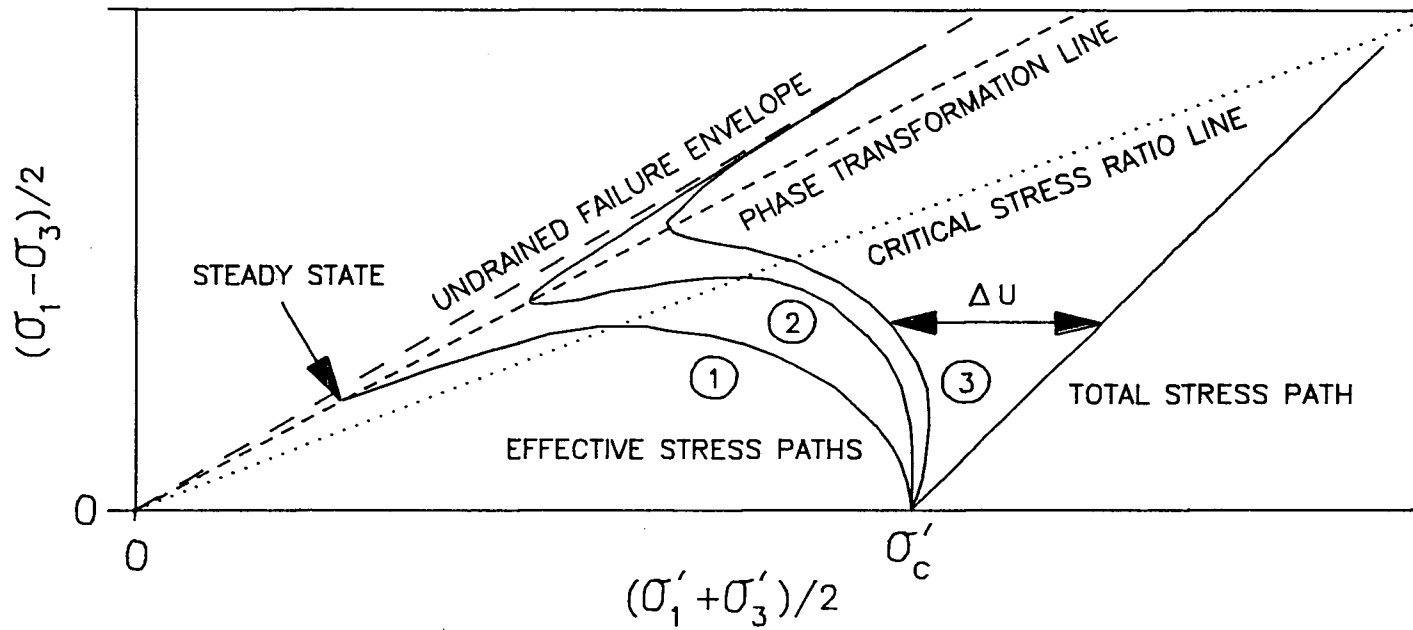
Figure 2.1(b)   Characteristic monotonic undrained loading effective stress
path response of sandy soils   (modified Mohr diagram)

strain hardening that is accompanied by increasing effective confining stress and decreasing pore pressure limits the amount of shear strain possible under constant shear stress.

2.1.1 Critical Stress Ratio Line

Critical stress ratio (CSR) refers to the effective principal stress ratio at which contractive deformation of either steady-state liquefaction or limited liquefaction types is triggered. CSR has been shown to be unique for a given strain softening sand in triaxial compression loading (Vaid and Chern, 1985; Chung, 1985) but dependent upon deposition void ratio in triaxial extension loading (Chung, 1985). Other researchers such as Sladen et. al. (1985) and Castro (1982) however, show test data which implies that CSR varies as a function of confining stress level in triaxial compression loading. These differences may be attributed to their specimen preparation by moist tamping as opposed to pluviation by Vaid and Chern and Chung. Specimen uniformity and fabric is difficult to control by the moist tamping method. Chung (1985) shows that triaxial extension CSR values are considerably lower than compression CSR values.

2.1.2 Phase Transformation State

The point at which the induced pore pressure stops increasing and starts decreasing in responses of limited liquefaction or dilative type sand behaviour has been termed "phase transformation state" (Ishihara et. al., 1975). In

the former case, this state apears as an elbow on an effective stress path diagram (see Figure 2.1(b)). The friction angle at phase transformation state has been shown to be unique for a given sand (Vaid and Chern, 1985). Among different sands it is dependent upon soil mineralogy (Negussey et. al., 1988). Under undrained loading, the phase transformation angle equals the friction angle mobilized at steady state and under drained loading it equals constant volume friction angle ϕ_{cv} (Vaid and Chern, 1985; Negussey et al., 1988). After passing the phase transformation state, the effective stress path moves up to and follows the undrained failure envelope that represents the line of maximum obliquity (Ishihara et. al. 1975).

2.1.3 Steady-State Concepts

If the sand shows response type 1, void ratio and undrained strength (or effective confining pressure) at steady-state are assumed uniquely related (Castro et al., 1982). This relationship between void ratio and confining pressure (or undrained strength) is called the steady-state line. The steady-state line has been used as a boundary that separates initial states of sand into regions of contractive and dilative behaviour.

Steady-state concepts were originally developed from drained triaxial tests and the concept of critical void ratio (Casagrande, 1975). The applicability of steady-state concepts to undrained loading conditions was postulated for

several years, until Castro (1969) provided the first
experimental evidence in its support from extensive
undrained compression tests on several moist tamped sands.

2.1.3.1 Critique of Steady-State Concepts

Steady-state concepts imply that a soil is either
dilative or contractive to failure, depending on the state
of the soil relative to the steady-state line. The limited
liquefaction type of soil response shows that a soil may be
both contractive and dilative, depending upon strain level.
Such behaviour cannot be explained using steady-state
concepts. For the limited liquefaction type of soil
response, one must decide which stage of the stress strain
curve is indeed defined as steady-state. Most researchers
who have used steady-state concepts have treated phase
transformation state as steady-state. This treatment adds
conservatism to slope stability analyses based on steady-
state concepts, because the effects of strength gain due to
dilation after phase transformation state are ignored.

In contrast, Castro (1982) suggests that steady-state
is only achieved after all soil dilation is complete, which
may be at very large undrained strength if a soil is
substantially dilative past phase transformation state (see
Figure 2.2). Figure 2.2 also shows that the degree of
dilation of different soils which have been strained past
phase transformation state is dependent upon soil type as
well as soil density. A soil such as Ottawa C-109 sand may
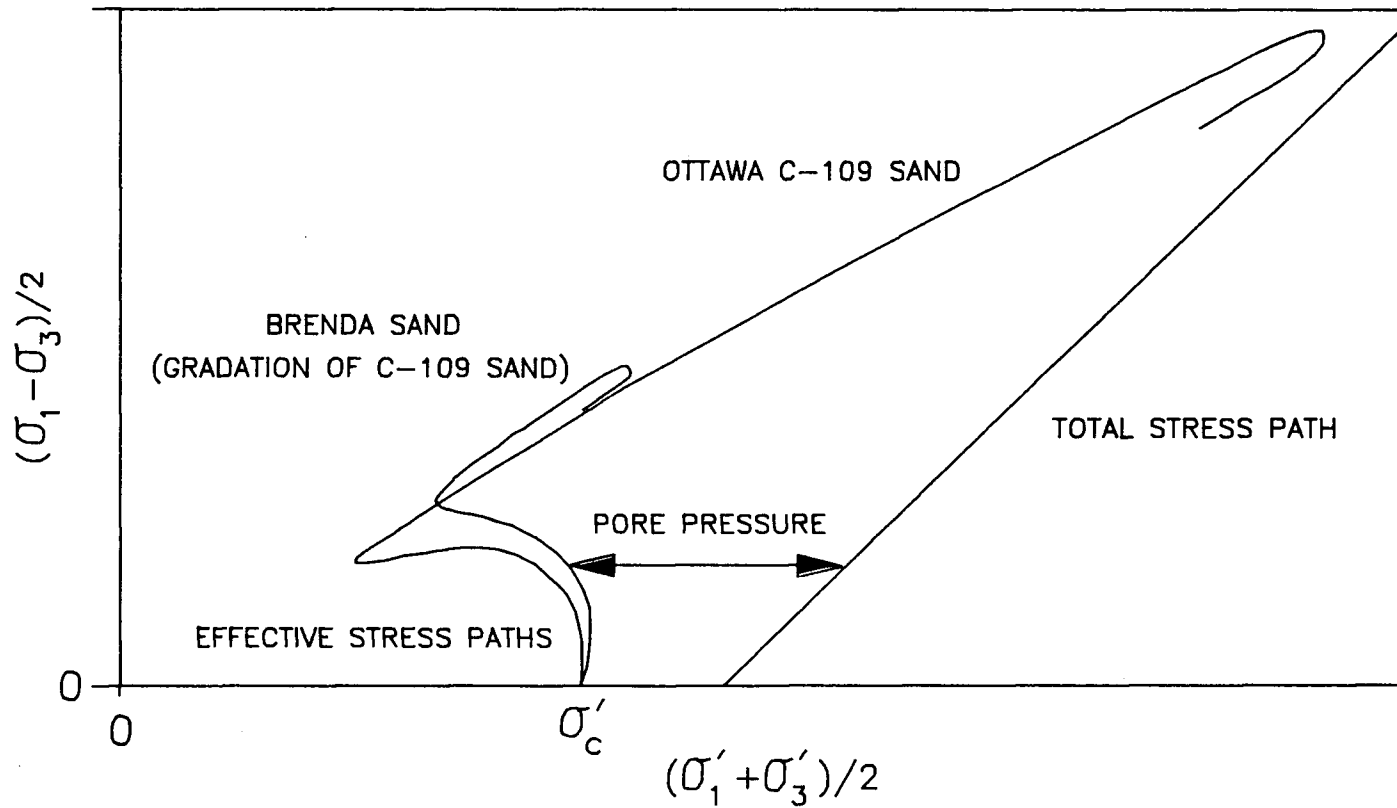
Figure 2.2 Comparison of undrained monotonic loading effective stress path response of two different loose sands

have a limited liquefaction type of response yet still have a substantially higher ultimate undrained strength than a sand such as Brenda sand, which does not show a limited liquefaction type of response.

Vaid and Chern (1985) treated both limited liquefaction and steady-state types of response within a unified framework. They considered stress conditions at phase transformation state for limited liquefaction and found a unique relationship between void ratio and effective confining stress (or undrained strength) in triaxial compression loading tests. This line also encompassed the steady-state data if the true steady-state type of response was observed in undrained loading.

Several researchers have shown that at a given void ratio and stress-state, undrained response of sand may be a function of sample fabric. Sand fabric is governed by the technique of sample formation and any strain history that may be a result of past seismic events. Miura and Toki (1982) show that there is a large difference in stress-strain response between sands prepared by 1) pluviation through air, 2) moist tamping, and 3) moist rodding. Ishihara and Okada (1978, 1982) and Chung (1985) show that undrained response is softened if the sand is pre-strained (even though reconsolidated to a lower void ratio) in a direction opposite to subsequent undrained loading. Conversely, undrained response is strengthened by initially pre-straining in the same direction of subsequent undrained

reloading (see Figure 2.3). A large pre-strain in a direction opposite to subsequent shearing may transform an initially dilative sand into a contractive sand (Chung, 1985).

The undrained response of soils is particularly sensitive to the direction of loading. This is a consequence of soils being inherently anisotropic. The degree of this anisotropy is intimately related to soil fabric. Chung (1985) shows that undrained water pluviated sand is considerably weaker in triaxial extension than in compression loading. At a given initial void ratio and stress state, compression behaviour could be dilative and extension contractive (see Figure 2.3). Miura et. al. (1982) show the effect of sample preparation technique upon the difference between triaxial extension and compression undrained loading response. The greatest difference is shown to occur in pluviated sand specimens. Undrained extension response in all cases is shown to be considerably softer and weaker than compression response. Recent research on the undrained behaviour of water pluviated sand using the hollow cylinder device shows similar dependence of undrained behaviour on the direction of loading (Symes et. al., 1985, Shibuya and Hight, 1987). Water pluviated sand is shown to be least contractive and least susceptable to liquefaction in the triaxial compression mode of loading, and most contractive or most susceptable to liquefaction in the triaxial extension mode of loading. Directional
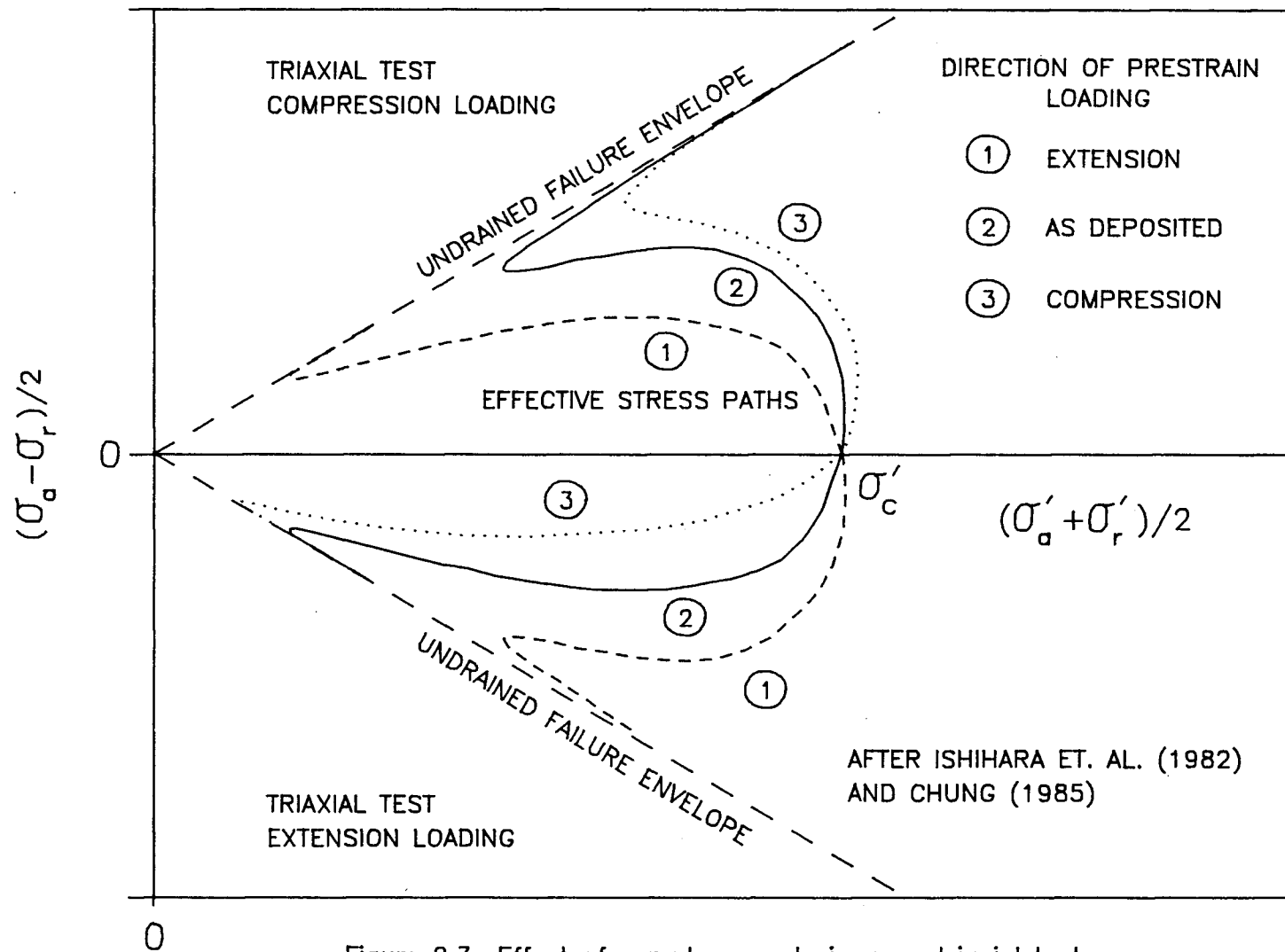
Figure 2.3 Effect of sample pre—strain upon triaxial test
undrained monotonic loading response

dependence of response may be qualitatively explained in relation to the fabric of sand.

2.2 SOIL FABRIC

Although several researchers have observed and identified the effects of soil fabric and resulting anisotropy in laboratory test results, the physical structures and mechanisms which produce and control fabric and anisotropy have been relatively inadequately described and generally only qualitatively assessed. The reasons fabric and anisotropy have been relatively neglected is that, in practice, most models treat soil as an isotropic macroscopic continuum, while fabric and anisotropy are derived from the microscopic interaction of discrete particles. Various workers in the field of particulate soil mechanics have attempted to analyze the effects of stress upon an assembly of particles (for example Rowe, 1962,1971; and Horne, 1965). Others (Oda et al., 1972,1974,1978,1985) have recognized the significant dependence of overall soil properties upon the spacial arrangement of particles. Workers such as Nemat-Nasser (1980), Matsuoka et al. (1980) and Mehrabadi et al. (1982) have attempted to formulate statistical analytical methods based on simple particulate models to relate macroscopic behaviour to the mechanics of particles.

Of all the particulate soil models described in the past, the simplified physical model described by Rowe (1962,1971) and Horne (1965) provides perhaps the best physical description of the factors which contribute to sand fabric. The particulate model described by Rowe forms the basis for his stress-dilatancy theory. A mathematical representation of the physical particulate model is used in a work function to derive the stress-dilatancy equation $R = KD$, where R is the principal effective stress ratio, K is a constant which is dependent upon the intrinsic angle of friction of the surface of individual soil particles, and D is the dilatancy produced by application of the stress ratio R ($D = -2d\epsilon_3/d\epsilon_1$ for triaxial compression loading). The stress-dilatancy equation has been shown to adequately represent the mono-directional drained loading behaviour of a large number of different particulate materials. The equation has also been shown to be independent of soil fabric, anisotropy, or principal stress direction (Oda, 1972b). Although the stress dilatancy equation is independent of soil fabric for drained test results, this does not imply that stress-strain behaviour is independent of direction of loading. Drained stress-strain response has been shown to be a function of principal stress direction which implies soil anisotropy (Oda, 1972b,1981; Arthur and Menzies, 1972; Negussey, 1984). This apparent conflict of the non-dependence of the stress dilatancy equation yet the dependence of stress-strain response upon soil anisotropy is

due to the fact that the stress dilatancy equation is based upon stress and strain ratios, not the magnitude of principal stresses and strains. Although incremental strain magnitudes at a given stress ratio may be considerably different under different directions of loading, the incremental strain ratio is shown to be independent of direction of loading.

The physical model which Rowe used to derive the stress dilatancy equation may be used to explain why stress-strain behaviour is dependent upon soil anisotropy and principal stress direction, although the model was not originally derived nor employed to explain soil anisotropy. The basic ideas behind the model are summarized in the following section. The model is used to explain factors and mechanisms which control soil anisotropy, and is subsequently used to explain and interpret observed test results.

2.2.1 Rowe's Soil Particle Interaction Model

A soil sample is idealized as an assemblage of uniformly shaped particles in contact with one another, as shown in Figure 2.4. The externally applied stress ratio (R) required to cause movement on contact planes and thus strain in the two dimensional model is derived from: (1) the dimensions of the idealized soil structure (Figure 2.4); (2) the internal stress level on particle contacts; and (3) Mohr's diagram for stress conditions on a contact plane

(a) Idealized soil structure

(b) Single repetitive element
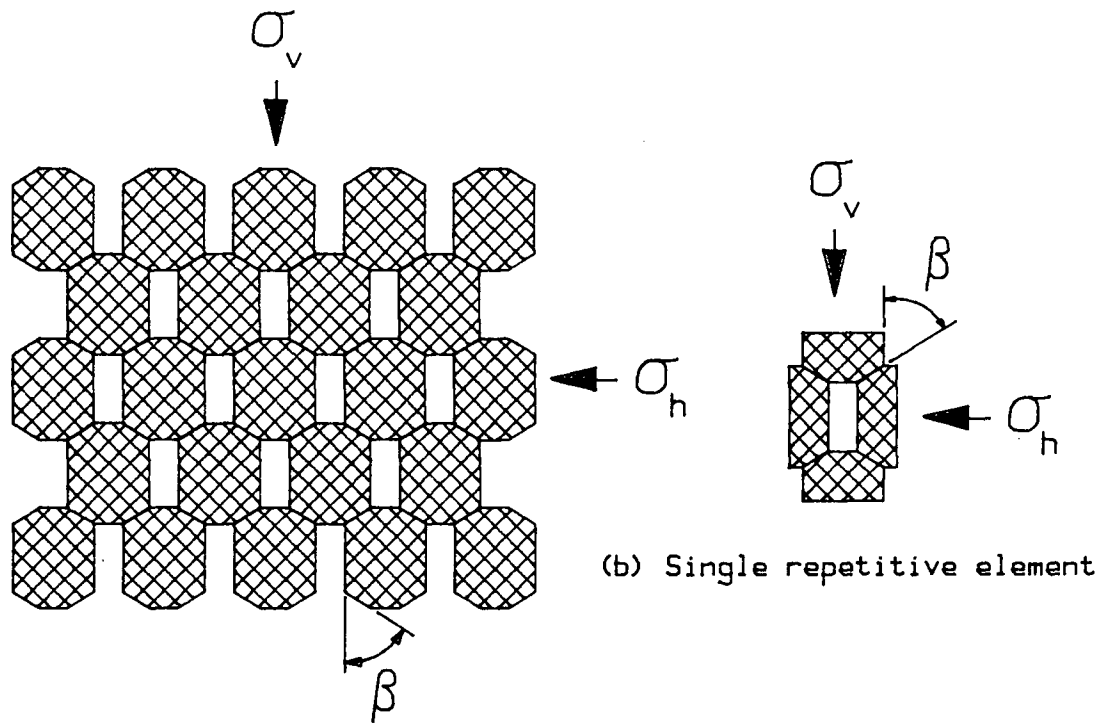
(c) Elemental free body diagram

β = Interparticle contact angle

α = Structure dimension factor

σ = Principal stress

δ = Deformation

ε = Strain

ϕ_μ = Intrinsic angle of friction

ϕ_m = Mobilized friction angle
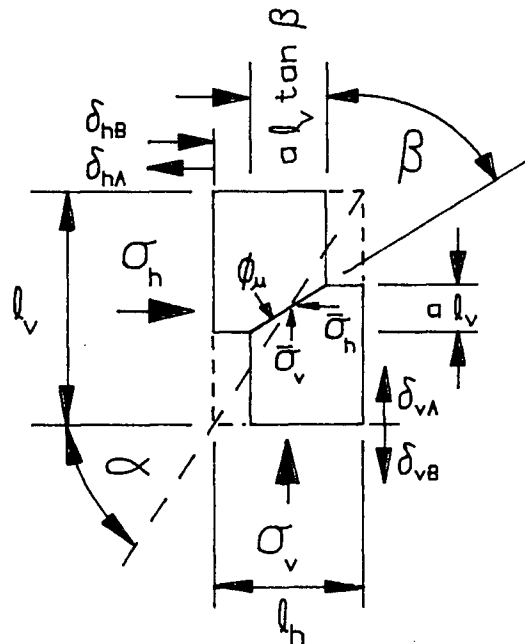
Figure 2.4   Stress-strain mechanisms in an idealized
two dimensional soil structure
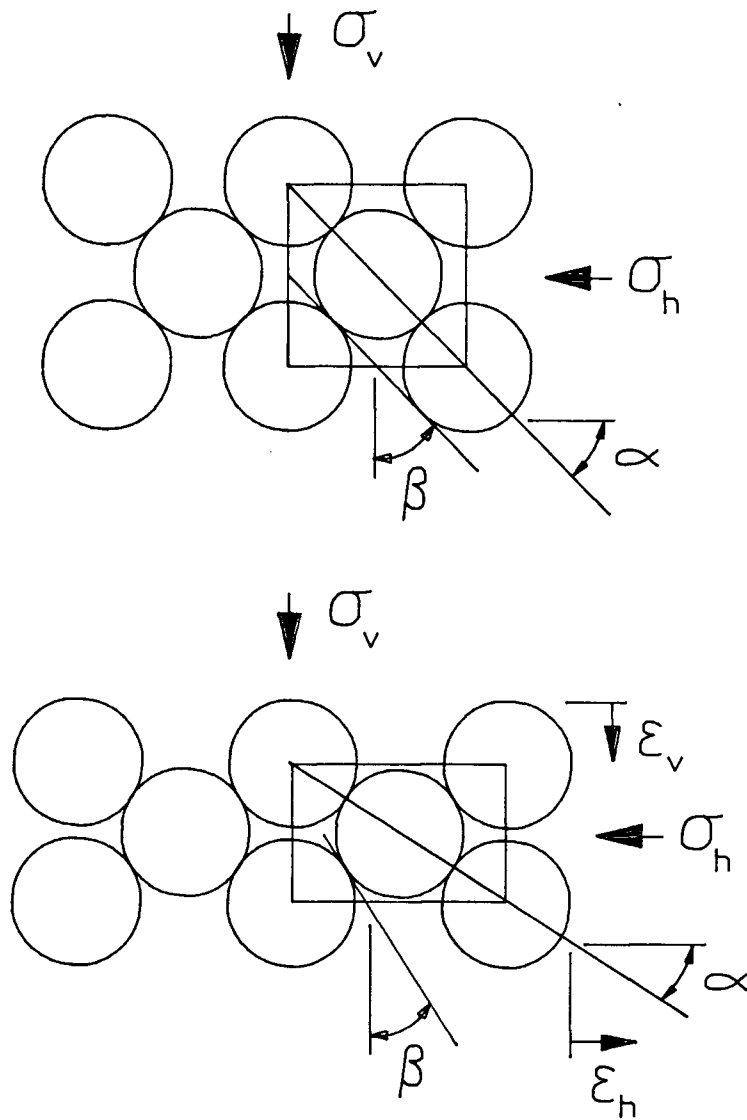
Increasing strain in one direction of loading initially
produces a decrease in both ∝ and β parameters.

Figure 2.4 (d)   Variation of ∝ and β parameters with
                 strain level

(Figure 2.5). The structure may be defined by two parameters; the inclination of the particle contact plane, β, and the shape of a single repetitive element, defined by the structure dimension factor α.

The model may undergo slip in only two modes. The first mode (Mode A) was analyzed by Rowe and other workers, and involves movement in the direction of maximum principal stress (Figure 2.4c). The second mode of movement (Mode B) has not been previously identified; this is probably because it involves movement against the direction of maximum external principal stress. Mode B movement is only possible for those combinations of particle dimension factor α and particle contact angle β where the maximum internal principal stress direction at a contact plane is opposite to the external maximum principal stress direction.

The mathematical representation of the stress ratio required to cause strain in the two dimensional model is derived in Section 2.2.1.1.

2.2.1.1 Mathematical Representation of Stress–Strain Behaviour in Rowe's Two Dimensional Particulate Structure

From particle dimensions shown in Figure 2.4:

$$\bar{\sigma}_v = \sigma_v \ell_h / (a\, \ell_v \tan(\beta)\,) \qquad \bar{\sigma}_h = \sigma_h \ell_v / (a\, \ell_v)$$

$$\frac{\ell_v}{\ell_h} = \tan \alpha \qquad \frac{\delta_v}{\delta_h} = \frac{1}{\tan \beta} \qquad \mathcal{E}_v = \frac{\delta_v}{\ell_v} \qquad \mathcal{E}_h = \frac{\delta_h}{\ell_h}$$

$$\frac{\bar{\sigma}_v}{\bar{\sigma}_h} = \frac{\sigma_v \, \ell_h}{\sigma_h \, \ell_v \tan(\beta)} = \frac{\sigma_v}{\sigma_h \tan(\alpha)\tan(\beta)}$$

MODE A DEFORMATION:

δ_{vA} and δ_{hA} directions, δ_{vA} strain in same direction as σ_v (see Figure 2.4)

Figure 2.5a   Mohr's circle for stresses required to cause slip on a particle contact plane and produce MODE A deformation
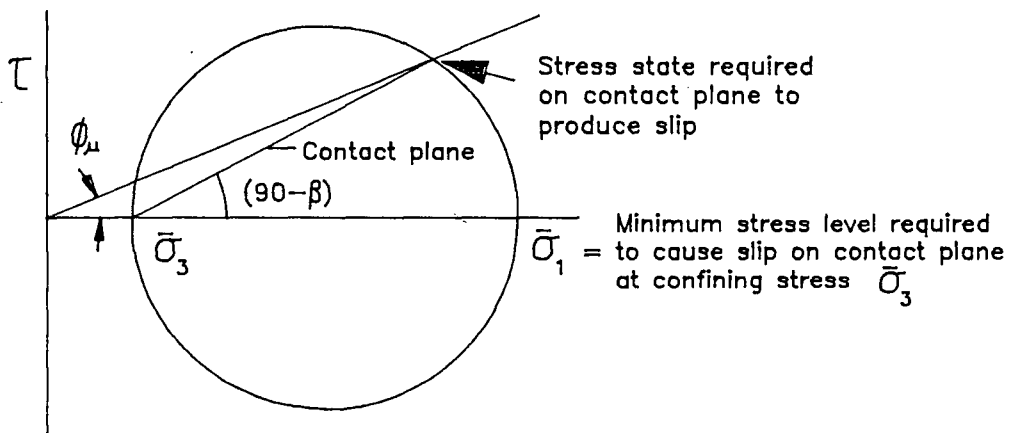
$$\frac{\bar{\sigma}_1}{\bar{\sigma}_3} = \frac{\bar{\sigma}_v}{\bar{\sigma}_h} = \frac{\tan(\beta + \phi_\mu)}{\tan(\beta)} = \text{Minimum stress ratio required to cause slip}$$

CRITERION FOR MODE A DEFORMATION: $\qquad \bar{\sigma}_v > \bar{\sigma}_h$

If $\qquad \dfrac{\bar{\sigma}_v}{\bar{\sigma}_h} < \dfrac{\tan (\beta + \phi_\mu)}{\tan (\beta)} \qquad$ no slip

If $\qquad \dfrac{\bar{\sigma}_v}{\bar{\sigma}_h} \geq \dfrac{\tan (\beta + \phi_\mu)}{\tan (\beta)} \qquad$ slip

$$\dfrac{\bar{\sigma}_v}{\bar{\sigma}_h} = \dfrac{\sigma_v}{\sigma_h \, \tan(\alpha) \, \tan(\beta)}$$

If $\qquad \dfrac{\sigma_v}{\sigma_h} < \tan (\beta + \phi_\mu) \, \tan (\alpha) \qquad$ no slip $\qquad$ Eqn. 2.1a

If $\qquad \dfrac{\sigma_v}{\sigma_h} \geq \tan (\beta + \phi_\mu) \, \tan (\alpha) \qquad$ slip $\qquad$ Eqn. 2.1b

$$\text{Sin } \phi_m = \dfrac{\tan (\beta + \phi_\mu) \, \tan \alpha - 1}{\tan (\beta + \phi_\mu) \, \tan \alpha + 1} \qquad\qquad \text{Eqn. 2.2}$$

$$\dfrac{\varepsilon_v}{\varepsilon_h} = \dfrac{-1}{\tan \beta \, \tan \alpha} \qquad\qquad \text{Eqn. 2.3}$$

MODE B DEFORMATION:

δ_{vB} and δ_{hB} directions, δ_{vB} strain against direction of σ_v (see Figure 2.4)

Figure 2.5b Mohr's circle for stresses required to cause slip on a particle contact plane and produce MODE B deformation
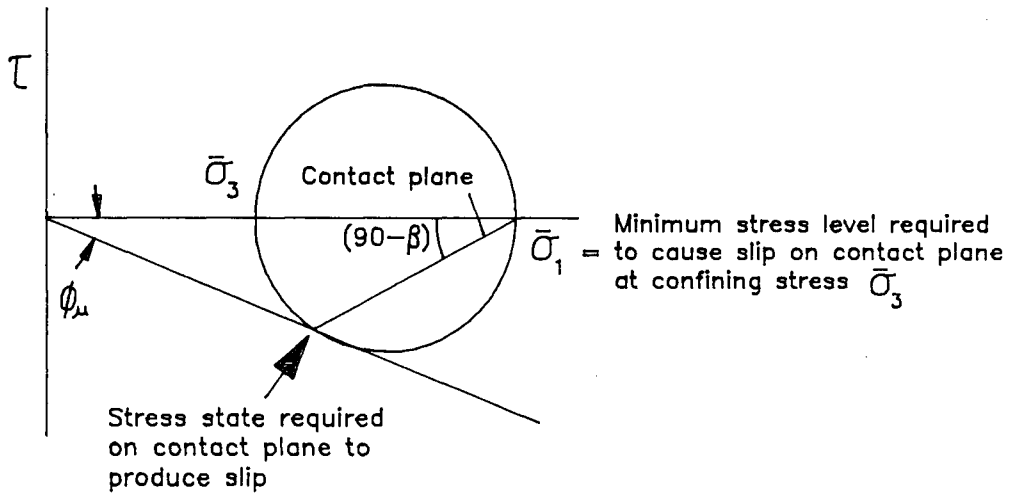
$$\frac{\bar{\sigma}_1}{\bar{\sigma}_3} = \frac{\bar{\sigma}_h}{\bar{\sigma}_v} = \frac{\tan(\beta)}{\tan(\beta - \phi_\mu)} = \text{Minimum stress ratio required to cause slip}$$

CRITERION FOR MODE B DEFORMATION: $\bar{\sigma}_v < \bar{\sigma}_h$

If $\dfrac{\bar{\sigma}_h}{\bar{\sigma}_v} < \dfrac{\tan(\beta)}{\tan(\beta - \phi_\mu)}$ no slip

If $\dfrac{\bar{\sigma}_h}{\bar{\sigma}_v} \geq \dfrac{\tan(\beta)}{\tan(\beta - \phi_\mu)}$ slip

$$\frac{\bar{\sigma}_v}{\bar{\sigma}_h} = \frac{\sigma_v}{\sigma_h \tan(\alpha) \tan(\beta)}$$

$$\text{If} \quad \frac{\sigma_v}{\sigma_h} > \tan(\beta - \phi_\mu)\ \tan(\alpha) \qquad \text{no slip} \qquad \text{Eqn. 2.4a}$$

$$\text{If} \quad \frac{\sigma_v}{\sigma_h} \leq \tan(\beta - \phi_\mu)\ \tan(\alpha) \qquad \text{slip} \qquad \text{Eqn. 2.4b}$$

$$\text{Sin}\ \phi_m = \frac{\tan(\beta - \phi_\mu)\ \tan\alpha\ -\ 1}{\tan(\beta - \phi_\mu)\ \tan\alpha\ +\ 1} \qquad \text{Eqn. 2.5}$$

$$\frac{\varepsilon_v}{\varepsilon_h} = \frac{-1}{\tan\beta\ \tan\alpha} \qquad \text{Eqn. 2.6}$$

Equations 2.1 and 2.4 are plotted as constant stress ratio contours in Figure 2.6. The contours segregate an inner zone of stable particle contact population from outer zones of unstable particle contact populations. Equation 2.6 which defines the strain ratio derived from slip under either MODE A or MODE B deformation is plotted in Figure 2.7. Although strain ratio is not a function of mode of deformation (MODE A and MODE B), the degree of volume change or dilatancy is a function of mode of deformation. When MODE A deformation is contractive, MODE B deformation is dilative, and when MODE A deformation is dilative, MODE B deformation is contractive at a given strain ratio, unless strain ratio equals −1.0, in which case no volume change occurs under any mode of deformation.

Figure 2.6   Stability contours for Rowe's particulate model as a function of particle dimension factor α and interparticle contact angle β

ZONE OF MODE B SLIP WHEN
$$\sigma_v/\sigma_h \leq \tan(\beta - \phi_\mu) * \tan(\alpha)$$

ZONE OF MODE A SLIP WHEN
$$\sigma_v/\sigma_h \geq \tan(\beta + \phi_\mu) * \tan(\alpha)$$

SLIP MODE A = SLIP IN DIRECTION OF
            MAXIMUM PRINCIPAL STRESS

SLIP MODE B = SLIP AGAINST DIRECTION OF
            MAXIMUM PRINCIPAL STRESS

$\sigma_v/\sigma_h = 1.0$

$\phi_\mu = 25°$
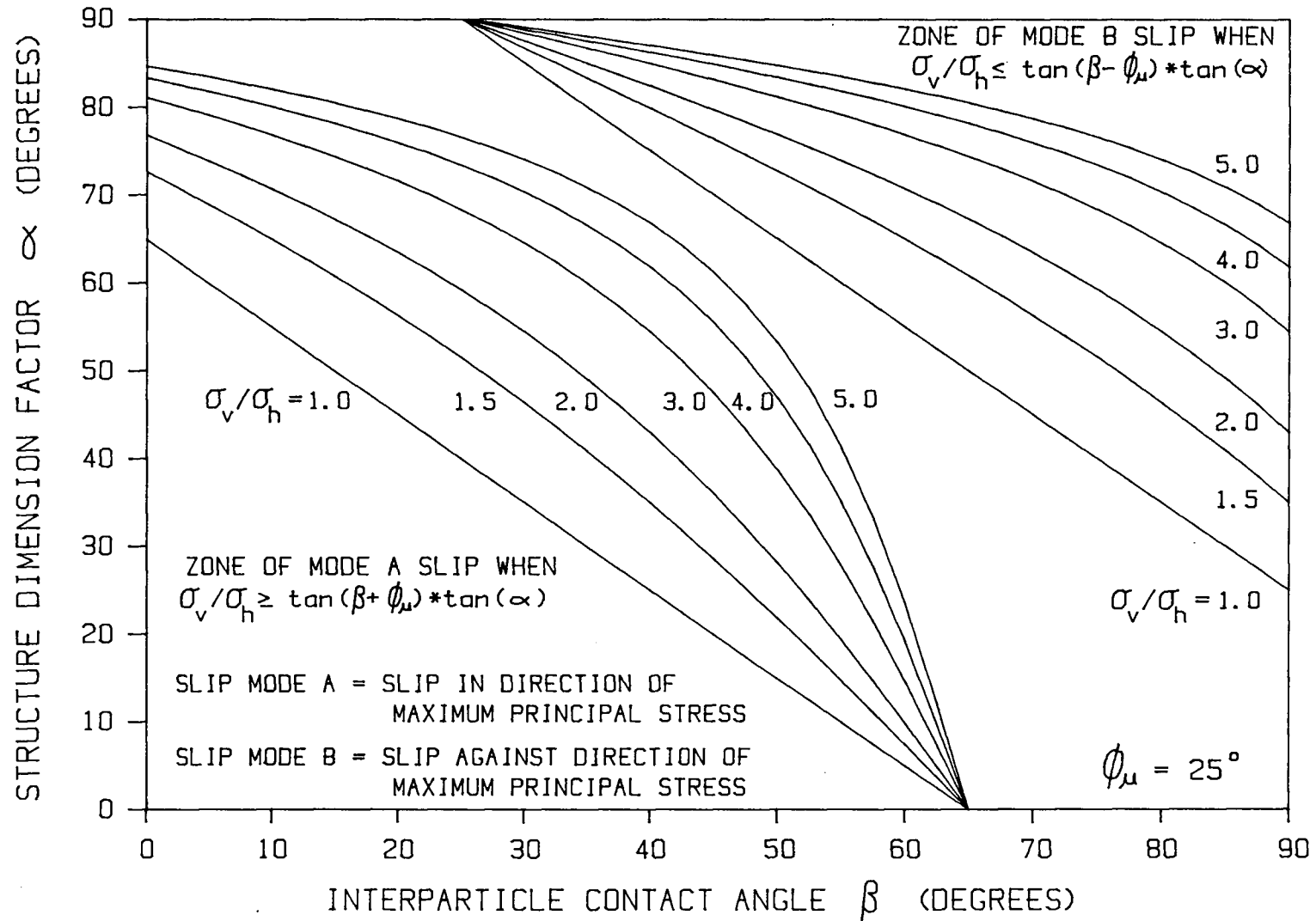
Fig. 2.7 Constant incremental strain ratio contours for Rowe's particulate model as a function of particle dimension factor α and interparticle contact angle β
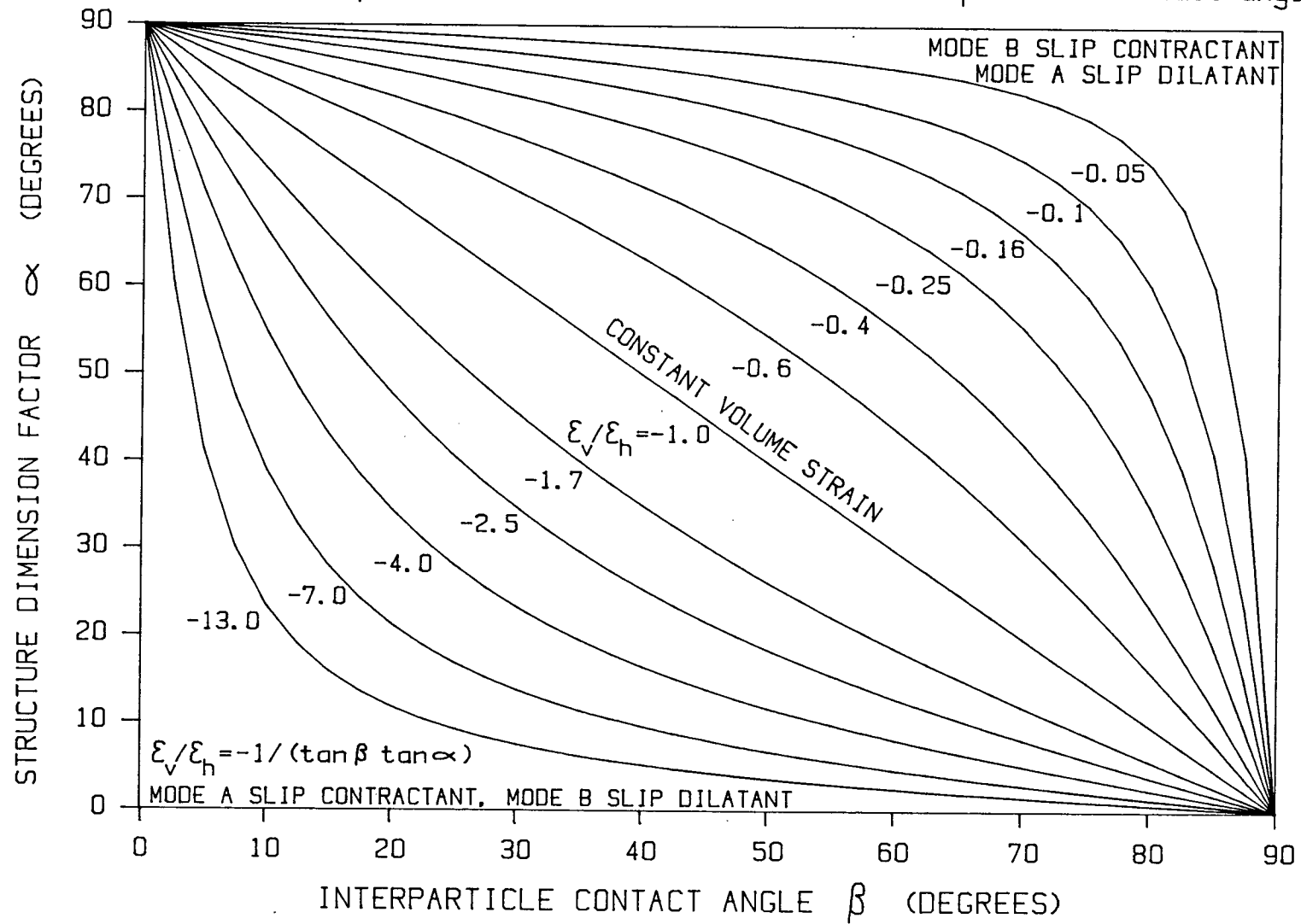
2.2.1.2 Discussion of Rowe's Particulate Model

Equation 2.1 and Equation 2.4 show that the stress ratio required to cause Mode A and Mode B strain respectively within the model particulate structure of Figure 2.4(a) is a function of angle of particle contact β, and structure dimension factor α. Within the idealized model, α is a function of particle dimensions and strain level. If particles were rounded in nature (Rowe's original analysis assumed spherical particles as shown in Figure 2.4d), particle contact angle β could also vary with strain level. Since the developed friction angle of the material is calculated from the stress ratio required to cause slip, the developed friction angle is also shown to be a function of particle contact angle β and structure dimension factor α (see Equation 2.2 and Equation 2.5). Thus developed friction angle is also affected by particle dimensions and strain level.

Figure 2.6 shows that the external stress ratio required to cause slip in the idealized model may range from 1.0 (which implies slip along contact surfaces under isotropic external stress, or a developed friction angle of zero degrees) to a value of stress ratio or developed friction angle much greater than the intrinsic angle of friction between particles, depending upon the values of α and β. The stress ratio contours shown in Figure 2.6 separate stable from unstable particle contact populations at a particular stress ratio level. The middle zone between

two similar stress ratio contours, of Mode A and B strain respectively, represents a stable particle contact population under the specified external stress ratio. The outer zone towards $\alpha = 0$, $\beta = 0$ represents an unstable particle population with strain type A. The outer zone towards $\alpha = 90$, $\beta = 90$ represents an unstable particle population, with strain type B. The middle zone of stable particle contacts is shown to be a function of external stress ratio. In the idealized model, if a particle structure with a specific stable combination of α and β under isotropic stress is subjected to increasing stress ratio, no strain is induced until the particle contact combination of α and β is subjected to an unstable stress ratio. Figure 2.4(d) suggests that the strain induced in the structure at an unstable stress ratio may cause a reduction in α and β values, which may cause large strains or a collapse in the structure until a stable combination of α and β is induced by strain.

The two dimensional model also shows how dilatancy or volume change during shear may be affected by particle contact structure. The principal strain ratio for both Mode A and Mode B strain may be calculated using Equation 2.3 or 2.6. If the principal strain ratio equals -1.0, there is no change in volume during shear. If the strain ratio is less than -1.0, then the structure contacts in volume during shear under Mode A strain, but dilates in volume under Mode B strain. When the strain ratio is greater than -1.0, the

structure expands in volume under Mode A strain, but contracts under Mode B strain. Constant strain ratio contours calculated from Equation 2.3 are shown in Figure 2.7. This figure shows how both strain ratio and dilatancy are a function of α and β population. The strain induced by a change in stress ratio is dependent upon the population of α and β which was previously within the stable zone but is now exposed to an unstable zone as stress ratio is changed.

In order to maintain a stable structure under increasing stress ratio, the strain induced by an increase in stress ratio must push unstable α and β value combinations of particle contacts into the stable zone. This may not occur in an incremental fashion in the two structurally homogeneous models shown in Figure 2.4, but could be expected in a variably sized, variably shaped particulate material such as sand.

The two particulate structures in Figure 2.4 can be shown to have an anisotropic or variable response to different directions of loading. If stress directions are reversed or principal maximum and minimum stresses are interchanged, the previous combination of α and β particle contact values would become $\alpha' = (90-\alpha)$ and $\beta' = (90-\beta)$. This change in α and β values for the same particle contact configuration would tend to make a previously more stable structure considerably less stable, or a previously less stable structure considerably more stable under the new direction of loading. The stress-strain response observed

under the reversed direction of loading could be substantially different from that which may have been observed under the previous loading conditions.

Although the structures shown in Figure 2.4 are not a true representation of the structure of sand, they do show that the structure of a particulate material controls stress-strain and dilatancy behaviour under loading. The models also show that loading response is a function of stress direction and strain level.

The two dimensional structure shown in Figure 2.4 can not model all the mechanisms which affect shear resistance of particulate soils, but the model does provide insight into some of the factors which control shearing resistance, and how these factors may contribute to directional soil behaviour. Some key points to consider are: 1) frictional resistance of soil is not only governed by the intrinsic friction angle of the particles which make up the soil, but also by the spacial relationship between particles which may be described as soil structure or soil fabric; 2) a random assemblage of soil particles may have a complex distribution of interparticle contact angles and soil particle orientations; 3) the factors which make up cohesionless soil fabric, such as interparticle contact angle, spacial orientation, and position of particles, can be easily altered by a change in method of placement or by induced strains; 4) dilatancy is governed by soil structure; and 5)

a soil may show different dilatancy response when subjected to different directions of loading.

In a natural soil structure there is a complex distribution of contact angles and particle orientations. Slip is generally more likely to occur on particular particle contacts which are preferentially oriented with respect to the direction of loading. Particle contacts which slip during loading may be reoriented to develop a more stable fabric that is able to support greater applied load, or alternatively disturb other parts of the soil fabric to reduce strength.

2.3 CYCLIC LOADING BEHAVIOUR

There are many simularities between cyclic and monotonic loading behaviour (Castro, 1982; Vaid and Chern, 1985; Chung, 1985). Both steady-state and critical stress ratio lines are independent of the mode of loading, monotonic or cyclic. Many researchers have found that a soil which is dilative and develops only limited strain under monotonic loading may develop large strains when subjected to cyclic loading. This is a consequence of the development of cyclic mobility.

Cyclic loading leads to a gradual softening of response as pore pressure and shear strain develop. In general, very low shear strain occurs until a pore pressure in excess of about 60% of the initial effective stress has developed

(Seed, 1979). Strain development during cyclic loading may be due to: 1) steady-state or limited liquefaction (classed together as contractive deformation), or 2) cyclic mobility (Castro, 1969; Seed, 1979). The development of cyclic mobility strain is represented on the effective stress path diagram by movement up and down the undrained friction envelope in both compression and extension phases of loading (see Figure 2.9). A transient state of zero effective stress occurs at the point when the shear stress is zero. The magnitude of cyclic mobility strain developed during cyclic loading is governed by relative density. If a sand is dense it may develop only limited cyclic mobility strain. In contrast, a looser sand may develop very large cyclic mobility strain, even if it is dilative under monotonic loading. Cyclic mobility strain may develop without the occurrence of limited liquefaction, or following the occurrence of limited liquefaction (see Figure 2.8).

Due to the various mechanisms which are responsible for strain development during cyclic loading (i.e. steady-state liquefaction, limited liquefaction, or cyclic mobility), the results of cyclic loading are generally assessed in terms of a strain criterion. The cyclic strength or resistance of a sample is defined as the cyclic stress amplitude required to cause a specified level of strain (2, 5, or 10%) in a fixed number of load cycles.
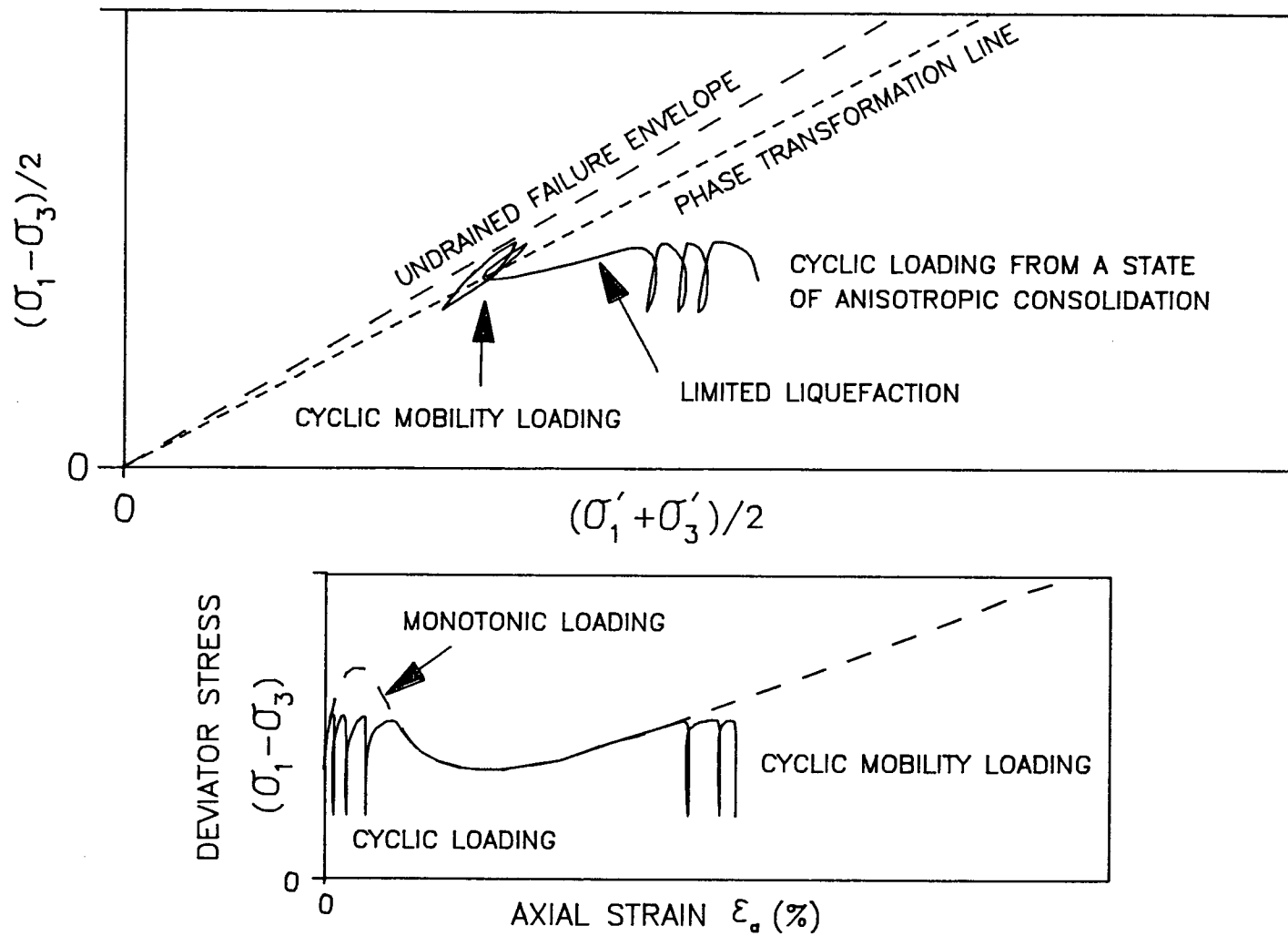
Figure 2.8 Undrained cyclic loading response of an anisotropically consolidated sandy soil subject to limited liquefaction

Figure 2.9 Typical undrained cyclic loading response of an isotropically consolidated sandy soil triaxial test sample
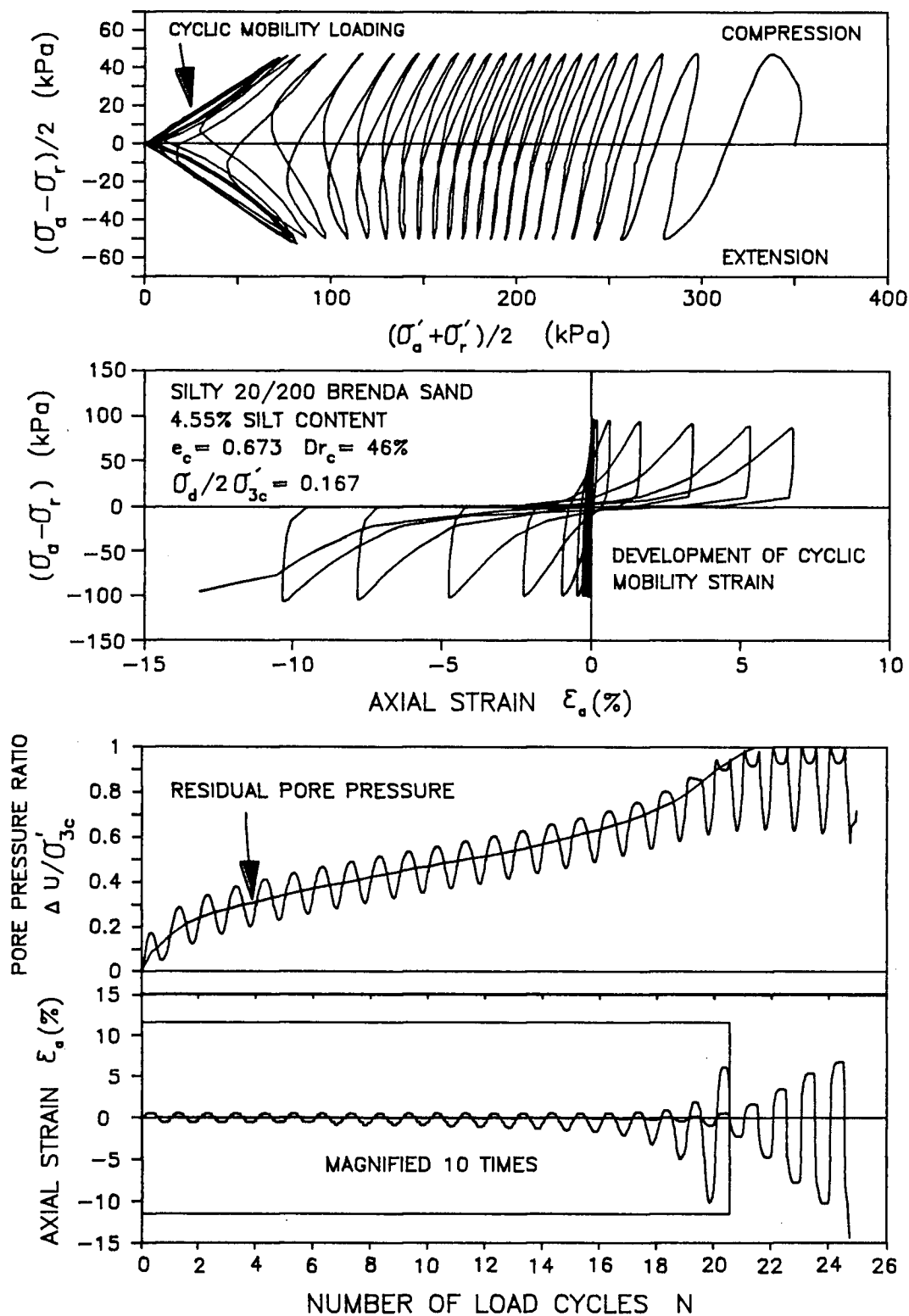
2.4 **THE EFFECT OF GRADATION AND FINES CONTENT ON THE UNDRAINED LOADING RESPONSE OF SAND**

Few studies have been conducted to determine the effect of gradation and fines content on the undrained loading response of sand. This is primarily due to the difficulty of preparing homogeneous test specimens. Homogeneous well mixed laboratory soil specimens are required for the determination of elemental soil properties. Most researchers who have studied the strength properties of silty sand have employed moist tamping or air pluviation techniques for the preparation of test specimens. Many well-graded and silty sands found in the field are deposited by settlement within water. A fundamental question which must be addressed in the evaluation of well-graded and silty sand properties is how does the method of sample preparation affect soil response.

Castro and Poulos (1976) studied the effect of gradation upon steady-state behaviour of sand using samples prepared by moist tamping. When compared in terms of relative density, gradation is shown to have the same magnitude of effect upon steady-state line as changes in mineralogy and angularity. Sands with generally more well rounded grains or higher C_u show a general trend towards lower steady-state void ratios. Absolute trends are difficult to identify.

Ishihara et al. (1980) present the results of an undrained cyclic triaxial test program conducted to

investigate the cyclic resistance of various types of mine tailings sands and slimes. Sand samples were air pluviated and either tamped or vibrated to the required density before saturation with water. Slimes samples were consolidated from slurry. When compared in terms of void ratio, various gradations of mine tailings sands are shown to have similar or slightly lower cyclic strength than clean poorly-graded sands. Slurry reconstituted cohesionless slimes are shown to have cyclic resistance similar to that of cohesionless tailings sands, while cohesive slimes are shown to have generally greater cyclic resistance than either tailings sands or non-cohesive slimes.

Lee and Fitton (1969) show that well-graded sands have cyclic strengths similar to those of poorly-graded sands of the same relative density. Samples were prepared by both pluviation in air and in water. The undrained loading response of well-graded but non-homogeneous segregated water pluviated sand is compared with that of less segregated air pluviated sand. It is shown that water pluviated segregated sand has a higher cyclic strength than unsegregated sand. The cyclic strength of silty sands tested by Lee and Fitton (1969) is similar to that of clean sands at the same relative density, although the data set shown is too limited to make broad generalizations.

Sladen et. al. (1985) have also used the moist tamping technique of sample preparation to determine the effect of silt content upon steady-state strength in triaxial

compression loading. Test results were used to back-analyse the failure of hydraulically placed silty sand in the Nerlerk berm island in the Canadian Beaufort sea. Silt content is shown to reduce steady-state strength considerably at a given void ratio, leading Sladen et. al. to the conclusion that silty sands are always more susceptible to liquefaction than clean sands. Troncoso and Verdugo (1985) derive similar conclusions for silty Chilean tailings sands. Their samples were also prepared by moist tamping. From results of static and cyclic triaxial tests on isotropically consolidated samples at the same void ratio, Troncoso and Verdugo show: 1) drained friction angle decreases with increasing silt content; 2) higher silt content makes the sand less dilative during drained loading; 3) undrained dynamic shear modulus as a function of strain level decreases with increasing silt content; 4) pore pressure generation during cyclic undrained loading occurs more easily in sands with a higher silt content; and 5) cyclic strength decreases substantially with increasing silt content.

Many of the conclusions described above concerning the effect of gradation and fines content upon soil behaviour under static and cyclic loading are conflicting. This may be due to the following factors: 1) differences in soil types tested; 2) differences in method of sample preparation; and 3) differences in method of soil density comparison, for example constant void ratio versus constant

relative density versus constant compactive effort applied during sample preparation.

The method of sample preparation and the resulting soil fabric have been shown to have a great influence upon the undrained behaviour of sand (see Sections 2.1 and 2.2). Ladd (1974) shows the extent of the effect of sample preparation technique on the behaviour of silty well-graded sand. The undrained cyclic strength of well-graded silty sands prepared by both pluviation in air and moist tamping was compared. Sample preparation method is shown to have a large effect on cyclic strength at a given void ratio. Air pluviated sand is shown to be up to 50% weaker than comparable moist tamped sand. Mulilis et al. (1977) show similar test results.

In the interpretation of the effect of gradation and fines content upon soil behaviour one must recognize the effect of sample preparation technique. If test results are to be meaningful, simulation of the fabric of the field soil to be modelled must be ensured. Since many well-graded and silty sands of interest in field investigations are deposited through water, such as in hydraulic fill or fluvial deposits, it is imperative to reproduce similar fabric in laboratory samples. It is also important to know the expected range of density and stress path dependent behaviour possible within a hydraulic fill or fluvial field deposit. This can only be achieved by simulating closely the expected method of field deposition in the preparation

of laboratory samples and by subjecting samples to the range of loading paths anticipated in the field. Unfortunately, simple water pluviation of sand, which is thought to best simulate the fabric of sand deposited in water, results in segregated well-graded samples (Lee and Fitton, 1969). They can not be considered homogeneous or repeatable, a necessary condition for a fundamental and systematic assessment of element properties in controlled laboratory tests.

CHAPTER 3

EXPERIMENTAL WORK

This chapter describes 1) the apparatus used for undrained monotonic and cyclic triaxial loading, 2) the materials used in the test program, 3) the sample preparation technique developed to produce homogeneous soil specimens for testing purposes, and 4) the objectives of the test program.

3.1 TESTING APPARATUS

Triaxial specimens were approximately 12.7 cm high and 6.4 cm in diameter. Tests were conducted using the triaxial apparatus and loading system described by Chern (1985). A schematic diagram of the equipment is shown in Figure 3.1. Axial load, confining cell pressure, pore pressure and axial displacement were measured using electronic transducers coupled to a data acquisition system interfaced with a microcomputer. Volume changes were measured with a pipette.

3.1.1 Load Controlled System
3.1.1.1 Consolidation

Samples were isotropically consolidated by stepwise increasing cell pressure in reservoir A and using a back pressure of 100 kPa (valves 1, 3 and 6 open and 7 closed). Anisotropic consolidation requires that cell pressure and
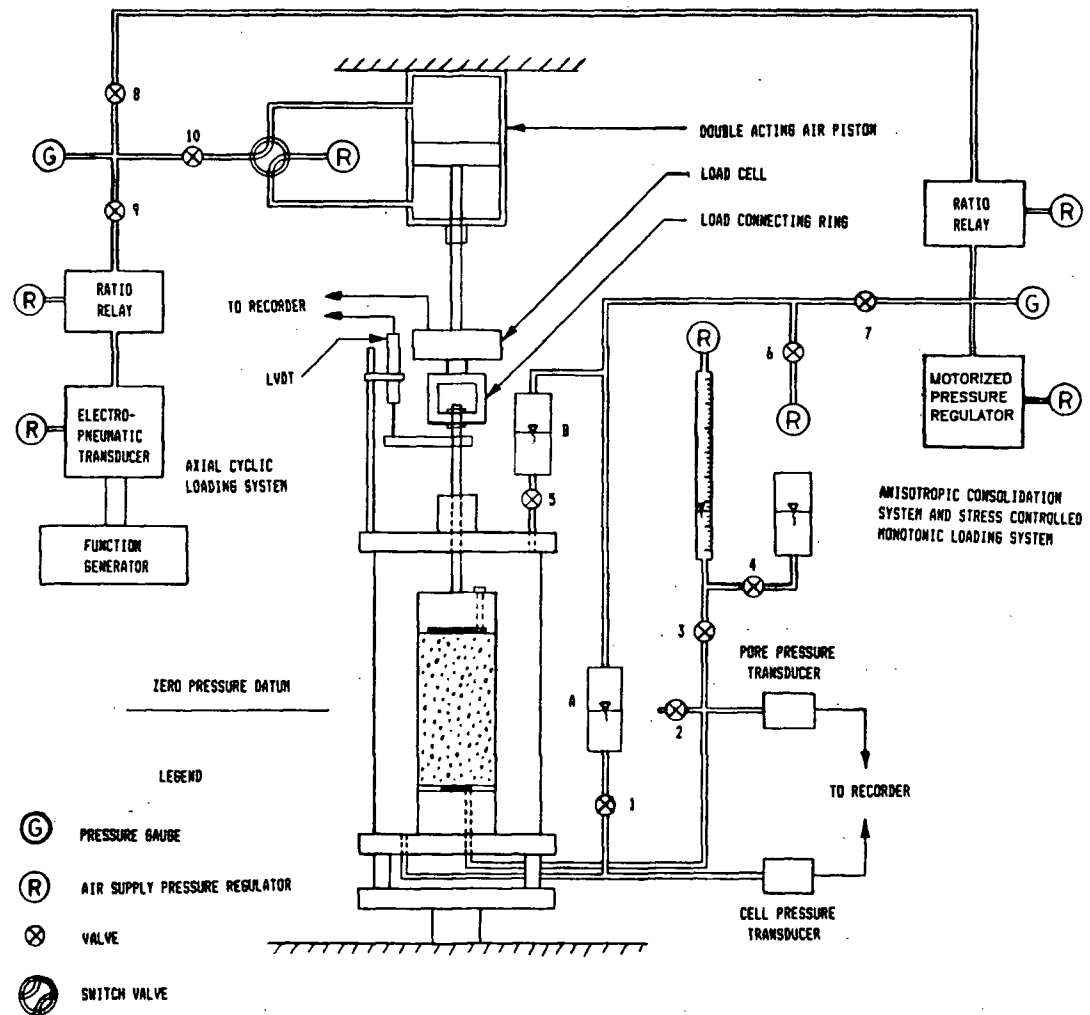
Figure 3.1 Schematic layout of load controlled monotonic and cyclic triaxial testing system

axial stress be increased simultaneously in a predetermined ratio. This was accomplished by feeding cell pressure as a signal to a ratio relay and the output of the relay to the upper chamber of the double acting air piston (valves 7, 8 and 10 open and 6, 9 closed). The cell pressure was increased by the motorized regulator. Prior to initiating anisotropic consolidation, both chambers of the piston were pressurized to an approximate equal base pressure, the difference serving to compensate the uplift on the loading ram during setting up of back pressure.

3.1.1.2 Monotonic Loading System

Monotonic shear tests were conducted by increasing or decreasing the air pressure in one of the chambers of the double acting air piston by the motorized pressure regulator. Vertical load is increased to achieve monotonic compression loading, or decreased to achieve monotonic extension loading at constant cell pressure.

3.1.1.3 Cyclic Loading

Cyclic loading is applied by means of an electropneumatic transducer driven by a function generator. After consolidation, valve 8 is closed and valve 9 opened to the cyclic loading system in which a pressure equal to the current piston pressure is preset by the D.C. offset on the function generator. The low pressure output from the electro-pneumatic transducer is amplified by a ratio relay

before admission to one chamber of the double acting air piston. A sinusoidal cyclic load pulse was applied at 0.1 Hz and calibrated prior to setting up of the test specimen by use of a dummy rod in place of the soil sample.

A 0.1 hz cyclic loading rate is generally slower than anticipated in most earthquake loading conditions. However, the slower rate of loading was chosen for a better resolution of measurements with the data acquisition system.

During cyclic loading, cell pressure was maintained through reservoir B rather than reservoir A. This provided a large bore convection to the cell water and thus prevented any fluctuations in cell pressure due to the displacement of water by the loading ram moving in and out of the cell when large deformations developed.

3.1.2 Strain Controlled Testing System

This was done using a simple Wykeham Farrance Eng. Ltd. (Slough, England) strain controlled loading machine. Tests were conducted at an axial strain rate of 0.5 percent per minute to ensure confident measurement of pore water pressures in silty sand specimens. Strain controlled tests provide a better record of stress-strain and pore pressure response than load controlled triaxial tests, especially if the soil tested is subject to limited liquefaction or liquefaction. The undrained response may differ with rate of loading due to soil creep. However, several workers (Chang et. al., 1982; Castro et. al., 1982; Chern et. al.,

1985) report that undrained shear properties of sand are relatively unaffected by the rate of loading.

3.1.3 Resolution of Measurement

The measured stresses were generally accurate to 0.4 kPa. Axial stress was corrected for: 1) membrane loads, as described in Appendix B, 2) uplift force on the upper loading platen due to cell pressure which does not act on sample cap rod area, 3) friction on the rod, depending on strain direction (see Appendix B), 4) buoyant weight of loading rod and top cap, 5) LVDT spring force on sample, and 6) 1/2 total weight of the sample. Cell pressure, pore pressure and axial stress measurements were referenced to mid sample height, as shown in Figure 3.1. The resolution of vertical and volumetric strains was 0.01%.

3.2 MATERIALS TESTED

Ottawa sand (ASTM-C-109) and Brenda mine tailings sand were used in the testing program. The triaxial behaviour of water pluviated Ottawa sand has previously been studied by Chern (1984), Chung (1985) and others. The triaxial loading behaviour of a poorly-graded water pluviated Brenda sand has been studied by Chern (1984). In this study, various mean grain sizes and gradations of clean Brenda tailings sand were tested in order to investigate the effect of grain size and gradation upon undrained behaviour. Kamloops silt was

mixed with Brenda sand to generate silty sands and thus examine the effect of silt content on the undrained monotonic and cyclic loading response of sand. The materials tested are fully described in the following sections.

3.2.1 General Description of Materials Tested

3.2.1.1 Ottawa Sand ASTM-C-109

Ottawa sand (ASTM designation C-109-69) is a subrounded medium quartz sand from Ottawa, Illinois. The standard test sand is used to calibrate both the testing equipment and the sample preparation technique used in the test program. The particle size distribution of Ottawa sand is shown in Figure 3.2.

3.2.1.2 Brenda Tailings Sand

Brenda tailings sand was obtained from the Brenda copper and molybdenum mine situated in the Okanogan area, British Columbia (Soregaroli, 1974). The tailings sand is coarse to very fine grained, salt and pepper colored angular sand derived from mechanically crushed unweathered granodiorite rock. The mineralogy of the tailings sand is shown in Table 3.1.

Figure 3.2 Gradation of Ottawa C–109 sand

M.I.T GRAIN SIZE CLASSIFICATION

SAND			SILT		
COARSE	MEDIUM	FINE	COARSE	MEDIUM	FINE

OTTAWA C–109 SAND

U.S.B.S. SIEVE SIZE

PERCENTAGE FINER BY WEIGHT

GRAIN SIZE (mm)
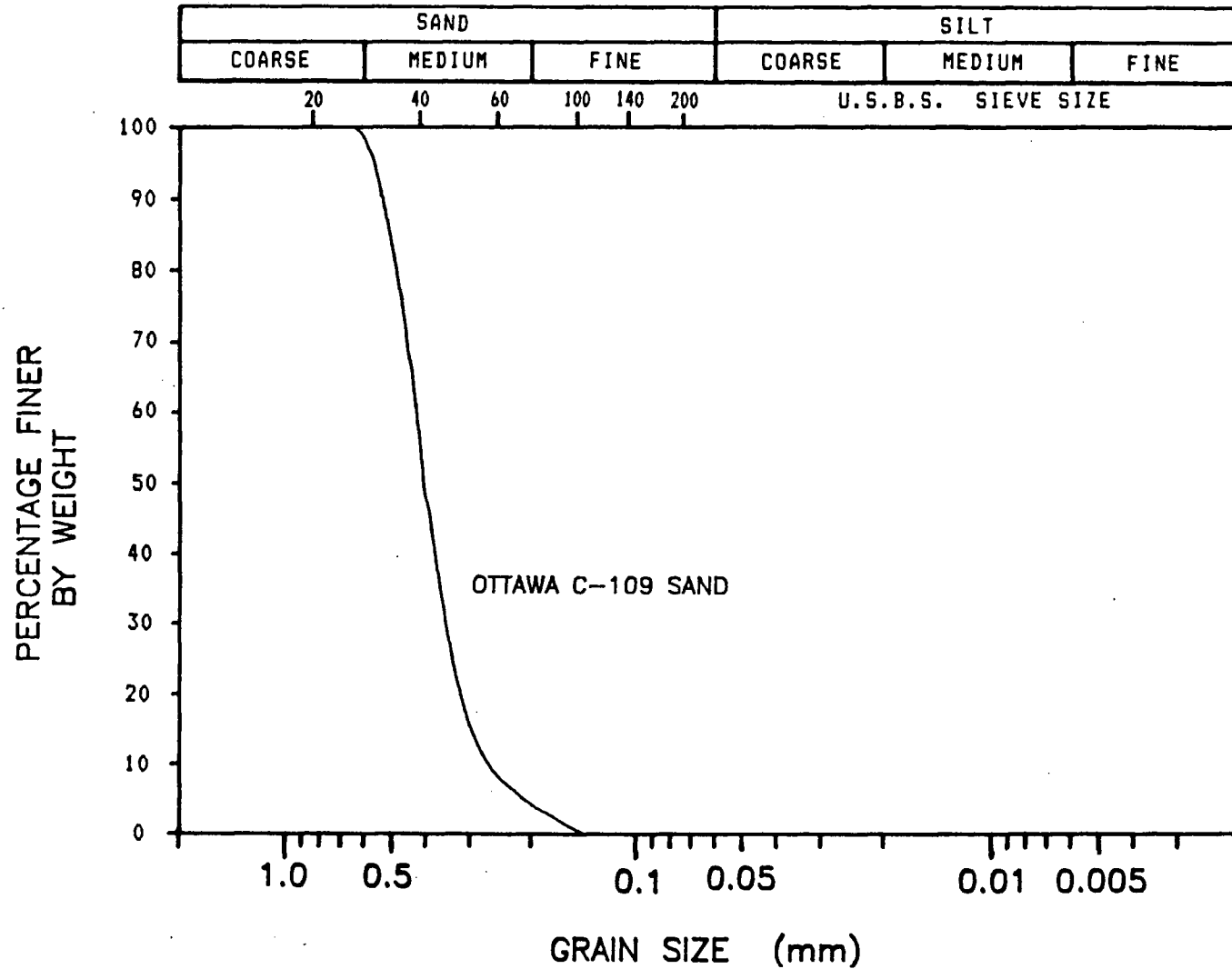
Table 3.1 Mineralogy of Brenda Mine Tailings Sand

(determined by examining grains passing #20
and retained on #40 sieves)

Plagioclase Feldspar	41%
Potassium Feldspar	20%
Quartz	27%
Biotite Mica	6%
Hornblende	4%
Heavy Minerals	2%
magnetite,pyrite	

In order to formulate a specific gradation of tailings sand, oven dried tailings which had been sieved through a set of U.S. standard #20, #40, #60, #100, #140 and #200 sieves for twenty minutes were taken from storage jars, weighed to 0.01 g accuracy, and independently remixed for each sample. Three types of poorly-graded sand samples were prepared; the first obtained from sand passing the number 20 and retained on the number 40 sieve (called 20/40 sand), the second obtained from sand passing the number 60 and retained on the number 100 sieve (called 60/100 sand) and the third obtained from sand passing the number 100 and retained on the number 140 sieve (called 100/140 sand). A well-graded sand with a grain size distribution from coarse to fine grained sand was also prepared (called 20/200 sand). Grain size distributions of various Brenda sands tested are shown in Figure 3.3.

3.2.1.3 Kamloops Silt

Kamloops silt was obtained from an approximately 10,000 year old glacial lake deposit which occupies the valley

Figure 3.3 Gradations of Kamloops silt and various clean Brenda tailings sands tested
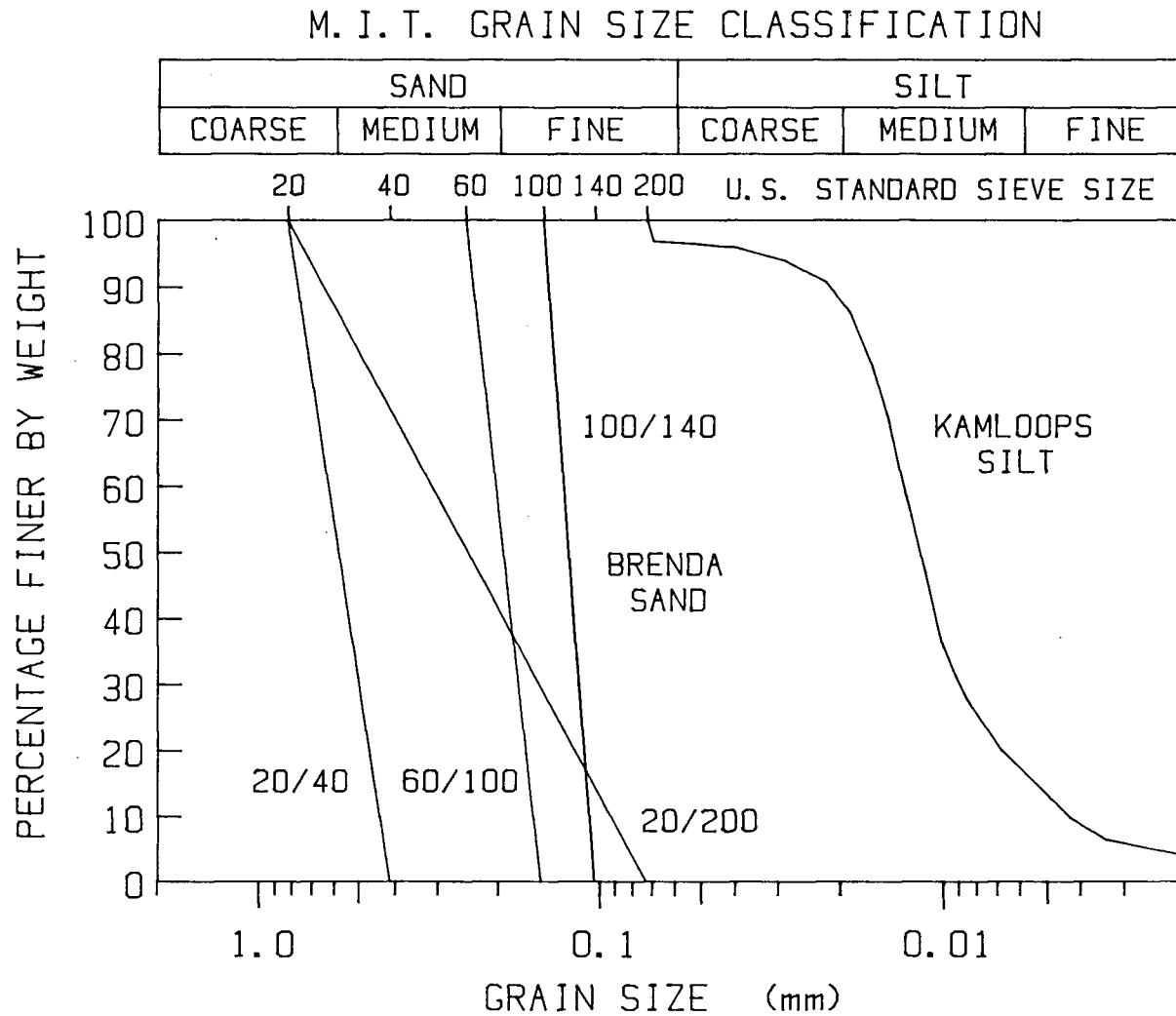
surrounding the city of Kamloops, British Columbia. Kamloops silt is brownish grey colored medium grained non-cohesive inorganic silt. A grain size distribution curve for Kamloops silt obtained using the hydrometer test (Lambe, 1951) is shown in Figure 3.3. During the testing program, previously used silt was washed to remove fine sand derived from minor particle crushing during testing, and oven dried before reuse in a new soil sample.

Various amounts of silt were mixed with Brenda 20/200 sand samples (as described in Section 3.3.2) to obtain target silt contents of approximately 4.3%, 7.5%, 14%, and 21% by weight of solids. The grain size distributions of resulting silty sands are shown in Figure 3.4. The range of silt content in silty sands tested is probably representative of that found in homogeneous natural and hydraulic fill sands, where sand has been deposited rapidly through a silty slurry. Higher average silt contents which may be found in sandy field soils are probably due to non-homogeneous silt lenses within sand, produced by intermittent deposition of coarser and finer grained particles. Material properties of such a non-homogeneous soil are difficult to measure or quantify, as such soil is a stratified assemblage of less well-graded soil layers.

3.2.2 Physical Properties of the Materials Tested

Table 3.2 presents a summary of the physical properties of the materials tested. The physical properties of the

Figure 3.4 Gradations of silty 20/200 Brenda tailings sands tested

M. I. T. GRAIN SIZE CLASSIFICATION

SAND			SILT		
COARSE	MEDIUM	FINE	COARSE	MEDIUM	FINE
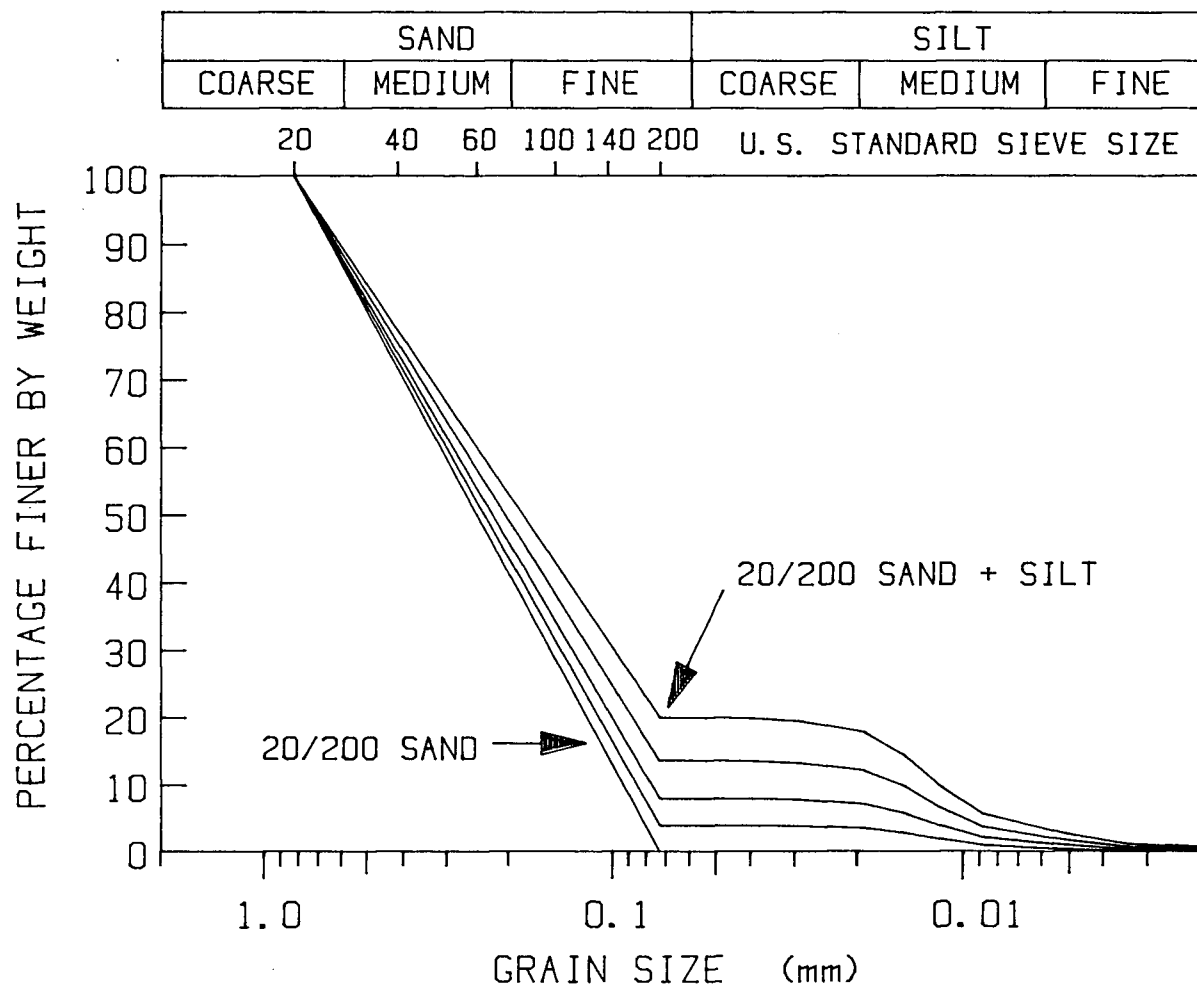
TABLE 3.2 Physical properties of materials tested

MATERIAL	Gs	ASTM VOID RATIO (DRY)		MAXIMUM SLURRY VOID RATIO		GRAIN SIZE (mm)		Cu	MEMBRANE PENETRATION FACTOR m (cm) (see Appendix A)
		MAXIMUM	MINIMUM	DRY	SATURATED	D50	D10		
OTTAWA C-109 SAND	2.67	0.760	0.50	0.770	0.770	0.4	0.25	1.64	0.0048
BRENDA TAILINGS SAND									
20/40	2.68	1.1370	0.7734	1.1618	1.1576	0.595	0.447	1.41	0.00566
40/60	2.68					0.323	0.264	1.29	
60/100	2.689	1.1850	0.7899	1.1977	1.1323	0.192	0.157	1.29	0
100/140	2.705	1.1947	0.7765	1.2017	1.1504	0.125	0.109	1.19	0
140/200	2.705					0.088	0.076	1.20	0
20/200	2.689	0.8643	0.5180		0.890	0.25	0.093	3.44	0.00078
KAMLOOPS SILT	2.67			2.67	1.447	0.012	0.0043	3.09	0

materials shown in Table 3.2 are discussed and compared in the following sections.

3.2.2.1 Specific Gravity

The specific gravity of Brenda sand is higher than that of Ottawa sand due to mafic and minor heavy minerals in Brenda sand. The specific gravity of Brenda sand is fairly constant, although it increases slightly with decreasing grain size due to a higher percentage of heavy minerals such as magnetite in finer grained Brenda sand.

3.2.2.2 ASTM Standard Void Ratios

ASTM standard maximum and minimum dry void ratios were determined for all sands tested. Maximum void ratios obtained by slurry deposition method (see Section 3.3) are also shown in Table 3.2 for comparison. They are in general slightly larger than the maximum ASTM void ratios. This is due to the lower energy of deposition obtained using the slurry deposition method. Grains are deposited from essentially zero drop height, when deposited in a slurry, while ASTM maximum void ratio samples are deposited from a one inch drop height. Maximum void ratios achieved by simple water pluviation of sand are approximately equal to those obtained by the ASTM maximum void ratio method.

The various poorly-graded Brenda sand gradations tested have similar maximum and minimum void ratios. ASTM maximum and minimum void ratios of well-graded 20/200 sand are much

lower than those of poorly-graded sands, due to smaller particles filling void space between larger particles. The difference between maximum and minimum ASTM void ratios obtained for each sand gradation tested is similar. Rounded Ottawa C-109 sand on the other hand has much lower maximum and minimum void ratios than angular tailings sand.

3.2.2.3 Maximum Silt Void Ratio

Kamloops silt was pluviated through both air and water to determine maximum dry and saturated void ratios. Maximum dry void ratio was found to be 2.67, almost twice the maximum water pluviated void ratio of 1.447. One might expect dry maximum void ratio to be smaller than water pluviated maximum void ratio for the following reasons: 1) dry silt is deposited in air with a higher energy of deposition; 2) oven dried silt must be sifted to segregate silt particles, thus silt particles which remain unsegregated by sifting would tend to produce a lower dry state maximum void ratio; and 3) silt pluviated through water tends to segregate according to grain size, which would tend to increase maximum void ratio. Thus there must be a fundamental difference in silt particle interaction in air and water deposition environments which produces the large difference between dry and saturated state maximum void ratio.

During the determination of maximum ASTM dry void ratios for fine sands it was observed that particles carry a

static charge which in some cases was large enough to expel some highly charged particles from the container into which they were being poured. Similarly, the excessively large dry maximum void ratio of 2.67 of silt is probably due to the repulsion of electrically charged dry silt particles. In the saturated state, electrical charges may be somewhat neutralized by water, enabling particles to settle into a much denser structure in a manner similar to that of coarser grained sand.

3.2.2.4 Maximum and Minimum Void Ratios of Silty Sand

Figure 3.5 shows how maximum and minimum dry ASTM void ratios and maximum slurry deposition void ratios of silty well-graded 20/200 Brenda sand vary with silt content. The standard ASTM maximum and minimum density tests are not generally considered applicable to soils with greater than 12% fines (passing the number 200 sieve). Nevertheless, ASTM maximum and minimum void ratios have been included to show the difference in void ratios attained by air pluviation in the dry state and by pluviation through water.

From Figure 3.5 it is clear that pluviation of silty sand through water yields a considerably different material than pluviation through air. Air pluviation of silty sand yields much higher void ratios than pluviation through water, although in both cases particle size segregation is a minimum. The observed behaviour of silty sand is similar to that of pure silt, where the maximum void ratio obtained by

Fig. 3.5 Comparison of ASTM dry maximum and minimum void ratios and slurry deposition maximum void ratios of silty 20/200 Brenda sand
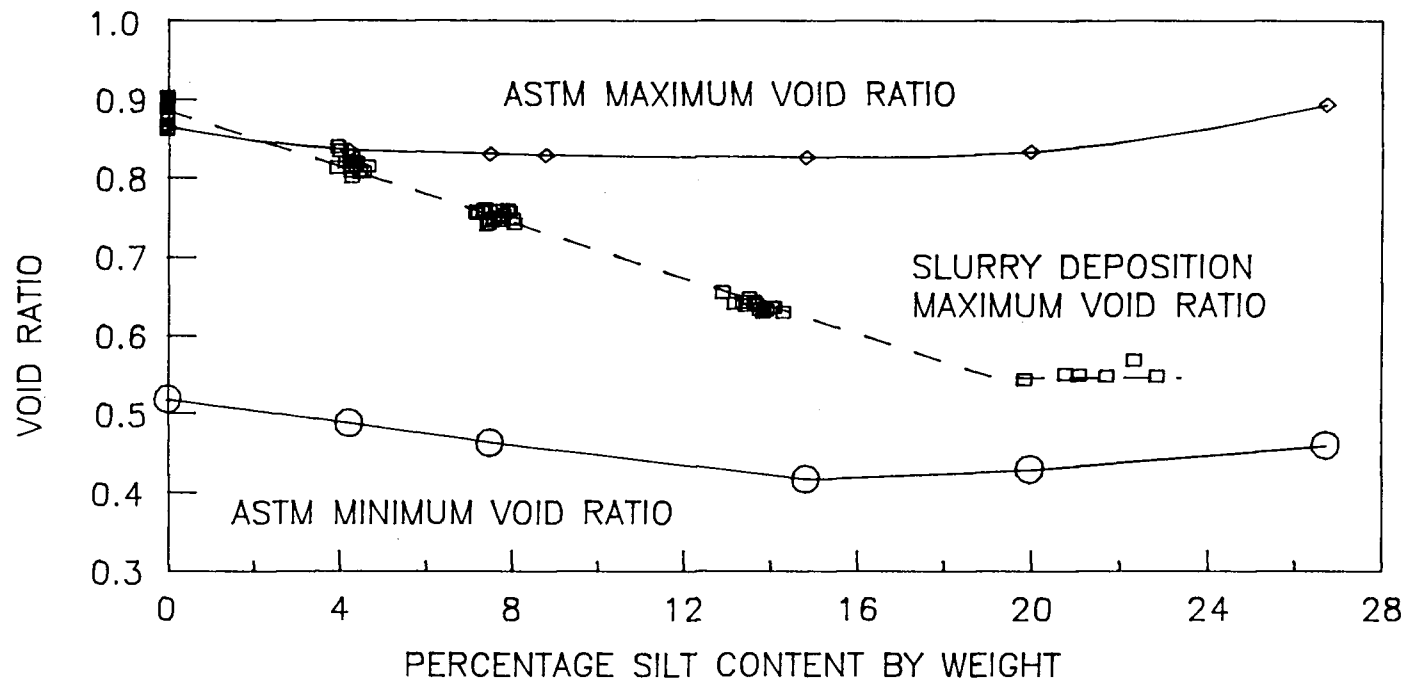
pluviation of silt through air (e = 2.67) is much larger than that obtained by pluviation through water (e = 1.447). The mechanisms which control the large difference in maximum void ratios obtained by pluviation in dry versus saturated state are probably similar in silt and silty sands.

A major reason for the difference in maximum void ratios obtained by air versus water pluviation of silty sands is that sand has a much higher terminal velocity of settlement through water than silt. When sand is deposited through a silty slurry, the sand fraction settles through the slurry water much faster than the silt fraction. One could expect the sand to pluviate through a silty slurry in much the same manner as through clean water, unless the slurry is very thick and viscous with a large fines content. Consequently, one would expect the maximum void ratio of the sand fraction of a water pluviated silty sand to vary little with increasing silt content, on the postulate that the fines fraction effectively fills void space between sand particles. Mechanical properties of water pluviated silty sand might also be essentially controlled by the density of the sand fraction, or sand skeleton void ratio, which may be calculated using Eqn. 3.1:

$$e_{skeleton} = [V_T G_s \rho_w / (M - M_{silt})] - 1 \qquad (3.1)$$

where:

V_T = total volume of the specimen

G_s = specific gravity of sand

ρ_w = density of water

M = total mass of soil solids in the specimen

M_{silt} = mass of silt in the specimen

$e_{skeleton}$ = sand skeleton void ratio

Figure 3.5 is replotted with respect to sand skeleton void ratio as Figure 3.6. It may be seen that the maximum sand skeleton void ratio of unsegregated slurry deposited silty 20/200 sand is in fact essentially constant with increasing silt content until the silt content exceeds about 20% by weight. At large silt contents, the silty slurry through which the sand is pluviating is very thick and viscous, and apparently increases maximum sand skeleton void ratio.

Figure 3.6 also shows the variation of sand skeleton void ratios calculated from ASTM maximum silty sand void ratios. The ASTM maximum sand skeleton void ratio curve shows that an increase in silt content bulks the sand structure during air pluviation. This bulking effect contrasts radically with only minor influence of silt content upon sand structure produced by pluviation of silty sand through water.

The change in ASTM minimum void ratio with silt content shown in Figure 3.5 indicates that it becomes more difficult to compact a dry sand skeleton by vibration as silt content is increased. In contrast, a slurry deposited sand with 20%

Fig. 3.6   Comparison of maximum void ratios obtained by air pluviation and
slurry deposition of silty 20/200 Brenda sand
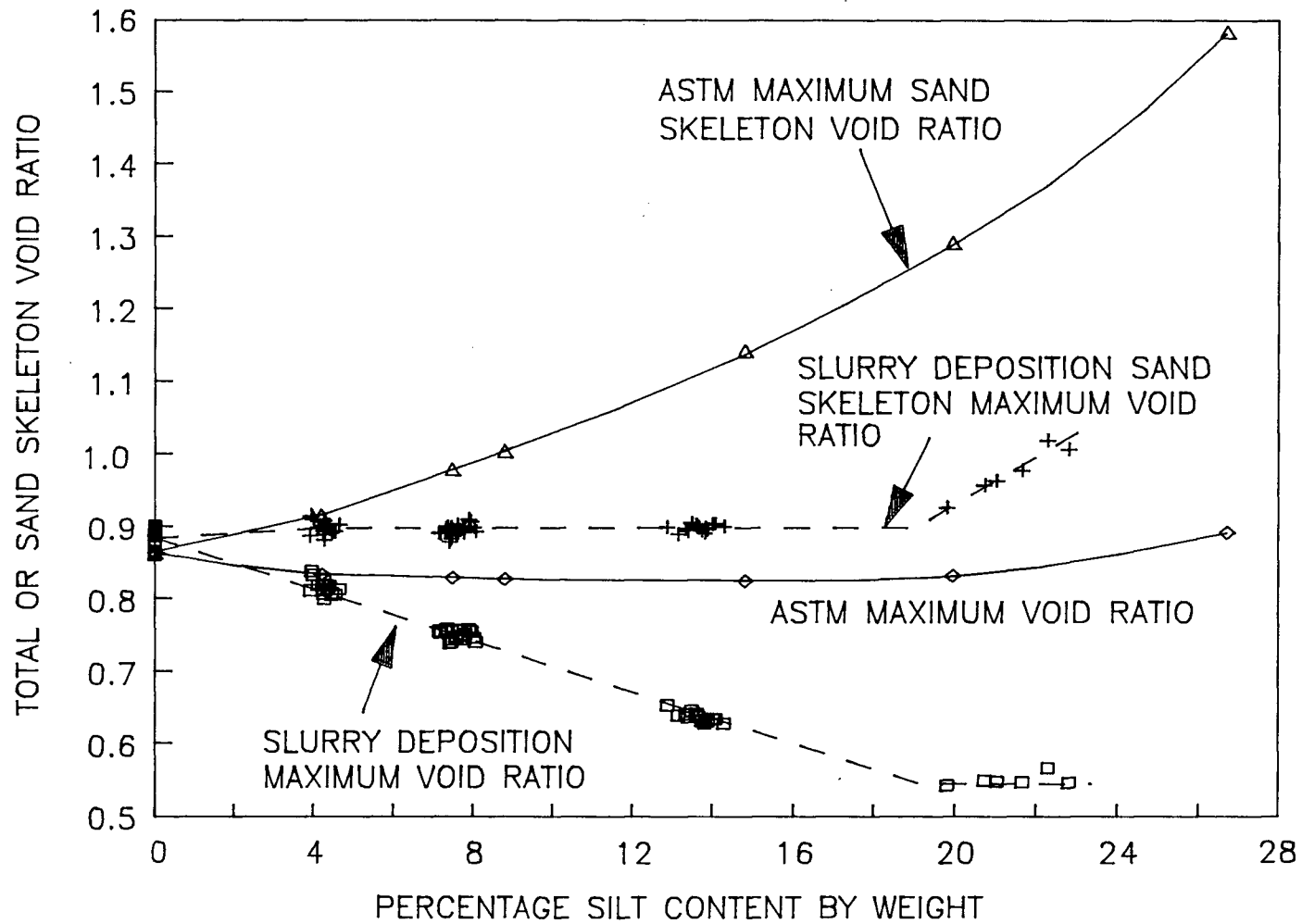
silt content is found to have a 100% ASTM relative density when consolidated to 350 kPa isotropic effective stress from an initially loosest state of slurry deposition. Silty sand is thus much more compressible when deposited in a saturated state than in a dry state.

The conclusion that may be drawn from Figures 3.5 and 3.6 is that ASTM maximum and minimum void ratio specifications provide a rather poor basis for the classification of hydraulic fill silty sand behaviour. One may also conclude that the method of preparing silty sand samples may severely affect soil fabric and measured soil properties.

3.2.2.5 Coefficient of Uniformity

Table 3.2 provides a summary of the coefficients of uniformity of the sands tested. Coefficient of uniformity of silty sand shows an abrupt jump from 3.7 to 19 as silt content increases from 7.5% to 14.8%. This indicates that coefficient of uniformity provides a rather poor basis for the classification of silty sand gradation or its behaviour.

3.2.2.6 Membrane Penetration Factors

Membrane penetration corrections for the sands tested were calculated from load-unload isotropic consolidation test results, according to the method described by Vaid and Negussey (1984). Membrane penetration factor calculations are summarized in Appendix A and the correction factors 'm'

at loosest density state for the various sands tested are shown in Table 3.2.

Membrane penetration effects are small for the well-graded 20/200 sand, zero for fine sands with D50 less than 0.2 mm (grain size less than approximately half the membrane thickness), and fairly large for coarse grained Brenda 20/40 and Ottawa C-109 sands.

3.2.3 Criteria for Choosing Test Soils

Ottawa sand was chosen as a control sand to show that the testing equipment and the slurry deposited sample produce test results similar to those obtained for water pluviated Ottawa sand by previous workers. Tests on rounded Ottawa sand also enabled comparison with the behaviour of angular Brenda sand.

Brenda sand was selected for the study of the effect of silt content upon sand behaviour because well-graded soils generally have more angular particles, especially in seismically active areas which are generally mountainous and close to the source of well-graded sediments. The composition of Brenda sand is fairly uniform across all grain sizes. The sand is made up of only a few common minerals such as quartz, feldspar, and mica. Since various gradations selected have the same mineralogy, the effect of gradation upon material behaviour may be systematically assessed. Brenda sand is from a tailings dam, so there is a direct applicability of test results to the practical

problem of designing and assessing the stability of a hydraulic fill dam composed of well-graded sand.

Kamloops silt was selected for the study of the effect of silt content upon soil behaviour because it is inorganic, and was obtained from near the source of Brenda sand. It has a similar composition as Brenda sand or Brenda tailings slimes. The silt is probably representative of fines commonly found within well-graded fluvial deposits in seismically active areas.

3.3 SAMPLE PREPARATION - THE SLURRY DEPOSITION METHOD

Testing of homogeneous (uniform) samples under uniform states of stress and strain is required for fundamental studies of soil property characterization. It is also necessary to be able to precisely replicate several homogeneous specimens for such studies. These requirements have promoted the use of reconstituted soils in preference to natural materials for fundamental investigations of soil behaviour. Each reconstituted cohesionless soil specimen must be individually prepared. This makes the control of uniformity and the ability to replicate several specimens considerably more difficult.

The technique for reconstituting sand samples must fulfill the following criteria: 1) the method must produce loose to dense samples in the density range expected within an insitu soil deposit; 2) the samples must have a uniform

void ratio throughout; 3) the samples must be fully saturated, particularly for undrained testing; 4) the samples should be well mixed without particle size segregation regardless of particle size gradation or fines content; and 5) the sample preparation method should simulate the mode of soil deposition commonly found in the soil deposit being modelled.

Several different methods of sample preparation which have been used in the past are first discussed. The slurry deposition method of sample preparation which models hydraulic fill or fluvial deposition and which meets the above criteria is then described. The success of the proposed method is evaluated by a series of tests to determine the homogeneity and monotonic undrained strength of poorly-graded and well-graded sand with and without fines.

3.3.1 Summary of Techniques Used for Sand Sample Preparation

Since the first laboratory studies of sand liquefaction behaviour conducted by Casagrande (1936), a major problem has been to produce sand samples with a low enough density so as to be susceptible to liquefaction. Numerous sand bulking techniques designed to increase susceptibility to liquefaction have been described in soil mechanics literature. The most effective sand bulking technique is sample preparation in a moist state where water tension forces between particles tend to expand the soil matrix. Many preparation techniques specify a minimum of

depositional energy to achieve a loose state. This may be done by reducing particle drop height, or pluviating sand through water. Sand may also be bulked after deposition by drawing a sieve mesh through it or by applying an upward seepage gradient sufficient to induce and maintain a uniform quick sand condition.

An important factor to consider in laboratory studies is whether the fabric of sand sample produced by the method of preparation is similar to that found within the soil deposit being modeled. Numerous studies have shown that soil behaviour is highly dependent upon laboratory sample preparation technique (for example Mulilis et. al., 1977, and Miura et. al., 1982).

3.3.1.1 Moist Tamping

The oldest technique for preparing reconstituted sand samples in the laboratory is moist or dry tamping of soil in layers (Lambe, 1951). The technique consists of pouring consecutive soil layers of specified thickness into a sample former tube, and tamping each layer flat with a specified force and frequency of tamping before the next layer is placed. The moist tamping method best models the soil fabric of rolled construction fills, for which the method was originally designed.

The moist tamping method produces very loose to dense partially saturated samples which may be somewhat non-uniform with respect to density or particle size gradation.

Several studies have been conducted to assess the uniformity of samples prepared by moist tamping, often with conflicting conclusions as to the success of the method (Castro, 1969,1982). Miura et. al., (1984) compare miniature cone penetration resistance within triaxial samples prepared by various methods. It is shown that a high degree of sample uniformity may be achieved by air pluviation while tamping results in considerable non-uniformity in cone penetration resistance.

Due to water tension forces between grains, sand samples prepared by the moist tamping method may be prepared at much larger void ratios than possible in a dry or saturated state. Casagrande (1976) suggests that sand dumped in a moist state is particularly prone to liquefaction due to a "honeycomb structure because of capillary forces between moist grains"; Casagrande states that moist dumped sand remains a "bulked sand when saturated". Water tension forces between grains are larger in finer grained material, thus finer grained soil is more susceptible to bulking by water tension forces than coarse grained sand. It has been observed that fine grained sand samples prepared by the moist tamping method may be assembled in such a loose state that they may undergo large strains during the saturation process due to the removal of water tension forces between grains. Other workers have observed similar large strains in moist tamped silty sands

during the saturation process (Marcuson et. al., 1972, Chang et. al., 1982, Sladen et. al., 1985).

If a moist tamped soil specimen can be saturated with minor induced strain, it is often considerably less compressible during consolidation than a comparable water pluviated specimen, and thus may be consolidated to much larger void ratios. Such incompressible specimens are often metastable and more susceptable to liquefaction in monotonic loading.

3.3.1.2 **Air Pluviation**

The major factors that affect relative density of air pluviated sands are height of particle drop (Vaid and Negussey, 1986) and rate of deposition (Miura et. al. 1982). A higher drop height or a higher rate of deposition results in a higher energy of deposition and thus a denser soil specimen. Numerous workers who have used air pluviation have attempted to restrict drop height and thus produce very loose sand samples.

The air pluviation technique produces fairly uniform specimens depending upon the technique used (Mulilis et. al., 1975, Miura et. al., 1982, 1984). Air pluviation best models the natural deposition process of wind blown aeolian deposits, which generally consist of either well-sorted sand or well-sorted silt.

Air pluviation of well-graded sand is not as successful as air pluviation of well-sorted sand. Well-graded sand may

become segregated when deposited by pluviation through air, especially if it has a considerable fines content. The process of sample saturation may disrupt initial sand fabric, and produce some soil segregation due to washing out of fines from the sample.

Air pluviated dry silty sands which have a large fines content are prone to bulking due to the fines content. The extent of this bulking is illustrated in Figure 3.6 for silty 20/200 Brenda sand. The figure shows that the ASTM maximum void ratio obtained by air pluviation is virtually unaltered with silt content up to about 20%. The maximum void ratio obtained by the proposed slurry deposition method, on the other hand, decreases substantially with increases in silt content up to about 20%. Air pluviation of silty sand would neither simulate the deposition process nor the range of void ratios possible in hydraulic fills or fluvial deposits which are often comprised of silty sands.

Figure 3.6 also shows the variation of sand skeleton void ratio of silty sand in the loosest state. By slurry deposition this void ratio may be noted to remain essentially constant with increasing silt content despite decrease in overall void ratio. This shows that sand deposits through a silty slurry in much the same manner as it does through clean water due to the large difference in settlement velocity of finer silt and coarser sand through water. Air pluviation on the other hand causes a radical increase in the void ratio of the sand skeleton with

increasing silt content, thus demonstrating large bulking of the sand matrix.

Air pluviated silty sand which is bulked would tend to be metastable and undergo very large strains similar to those found in moist tamped silty sands during saturation and consolidation. Large strains induced within a sample during the preparation stage impart a strain history to the soil that is much different from that produced in a loose natural silty sand which is invariably deposited through water and not appreciably bulked by silt content. Non-standardization of initial strain during sample preparation has been identified by Tatsuoka et. al. (1986) as one reason for the variation in triaxial behaviour of sand among various soil laboratories. Very loose air pluviated silty sands bulked by silt content would tend to be more susceptible to liquefaction under monotonic or cyclic loading than clean well-sorted sands at the same void ratio.

Numerous studies have been conducted to explore the effect of sample preparation technique and the influence of sand fabric upon undrained behaviour. Laboratory tests conducted by Miura and Toki (1982) indicate that there is a large difference in behaviour of clean sands prepared by pluviation through air and by moist tamping or moist rodding. Tatsuoka et. al. (1986) report similar results, and find that air pluviated and water pluviated clean sands have fairly similar cyclic strength which is generally lower

than the cyclic strength of comparable moist tamped or vibrated sand at the same void ratio.

3.3.1.3 Water Pluviation

Sample preparation by the water pluviation technique has been described by several researchers, including Lee and Seed (1967), Finn et. al. (1971), Chaney et. al. (1978), and Vaid and Negussey (1984). The water pluviation technique ensures sample saturation. The terminal velocity of sand falling through water is lower than that of sand falling through air. This leads to a lower energy of deposition in water pluviated samples and hence a looser deposit, as long as sedimentation currents are not set up within the water in the deposition mold.

The water pluviation technique simulates the deposition of sand through water found in many natural environments and mechanically placed hydraulic fills. Oda et. al. (1978) report that natural alluvial sands and water pluviated sands have similar fabric and thus similar stress-strain and strength behaviour.

The water pluviation technique produces uniform samples of poorly-graded sand (Vaid and Negussey, 1984), but particle size segregation is a problem in water pluviation of well-graded or silty sands. Since laboratory tests such as the triaxial test are designed to model the stress conditions which exist at a point and thus require uniform samples to ensure uniform stresses and strains, the water

pluviation technique should only be used to test poorly-graded sands. When a well-graded soil is subjected to grain size segregation during pluviation, the segregated soil generally has a larger average maximum void ratio than that of the unsegregated soil, and its mechanical properties are similar to that of a more poorly-graded soil.

The maximum possible void ratio after consolidation to a given stress state of a water pluviated sand is generally lower than that of dry or moist tamped sand. This is due to the effects of bulking of fines in the dry state or water tension forces in the moist state. Water pluviated sands are generally more compressible during consolidation than moist tamped sands due to the higher radial compressibility of water pluviated sand fabric (see Section 4.1.4).

3.3.2 The Slurry Deposition Method

To overcome inherent problems of the methods of preparing reconstituted sand samples described in Section 3.3.1 (especially the problem of particle segregation in poorly-graded or silty sand samples) a new technique called the slurry deposition method was developed. The slurry deposition method used in the preparation of 63 mm diameter triaxial specimens is described in the following paragraphs.

3.3.2.1 Preparation of Sand

A mass of test sand sufficient to fill the sample preparation mold at minimum density is poured into a flask

with sufficient water (see Figure 3.7(a)) and boiled for fifteen minutes to de-air the mixture. After cooling, more de-aired water is added to the flask to fill it completely. If the test sample is to contain silt or clay fines, a separate flask is filled with the fines and a volume of water approximately 60% of the final sample volume. The fines slurry is also boiled to de-air and allowed to cool.

3.3.2.2 Sample Preparation Mixing Tube

The sample preparation tube is a clear plexiglass cylindrical tube (see Figure 3.7(b)) 22.5 cm long, 6 cm in diameter and with walls 5 mm thick. The preparation tube has a rubber membrane gasket seal glued to one end, and a number 11.5 rubber stopper which is used to seal the other end.

The fines fraction slurry is poured into the sample preparation tube and topped up with the de-aired water used to flush clean the fines slurry flask. The fines slurry within the preparation tube is allowed to settle to the bottom of the tube before the sand fraction of the soil sample is pluviated into the tube. For clean sand samples the preparation tube is simply filled with de-aired water. The sand flask opening is constricted with a tapered rubber stopper which aids in pluviation of the sand through water from the flask to the preparation tube. Thus sample saturation is maintained during all stages of preparation. Some slurry fines which may move up into the sand flask

(a)

SAND BOILED IN WATER TO DE-AIR;
SILT OR CLAY SLURRY BOILED SEPARATELY

(b)

SILT SLURRY OR CLAY SLURRY OR WATER POURED
INTO TRANSPARENT PLASTIC MIXING TUBE;
SAND PLUVIATED INTO MIXING TUBE; SILT OR
CLAY SLURRY LOST DURING SAND PLUVIATION IS
COLLECTED TO BE WEIGHED

RUBBER MEMBRANE SEAL GLUED TO
TOP OF MIXING TUBE

4.8 mm

22.5 cm

PLASTIC MIXING TUBE

RUBBER STOPPER

6.0 cm

RUBBER MEMBRANE
WHICH SEALS END
DISK ASSEMBLY

TOP SEALED WITH METAL PLATE

(c)

PORDUS DISK

SAMPLE SEALED IN MIXING
TUBE IN WATER BATH

WATER BATH

BOTTOM SEALED; WATER TENSION
MAINTAINS SATURATION AND
RETAINS POROUS DISK

(d)

SAND MIXED THOROUGHLY IN
LEAN SLURRY FORM;

BOTTOM METAL PLATE IS
REMOVED BEFORE PLACEMENT
OF TUBE AND POROUS DISK
ONTO BASE PLATEN OF
TRIAXIAL TEST APPARATUS

FIGURE 3.7

SCHEMATIC DRAWING OF SLURRY DEPOSITION METHOD FOR
PREPARATION OF WELL GRADED SILTY OR CLAYEY WELL
MIXED SATURATED LOOSE TRIAXIAL TEST SAND SPECIMENS

(e)

(f)

(g)
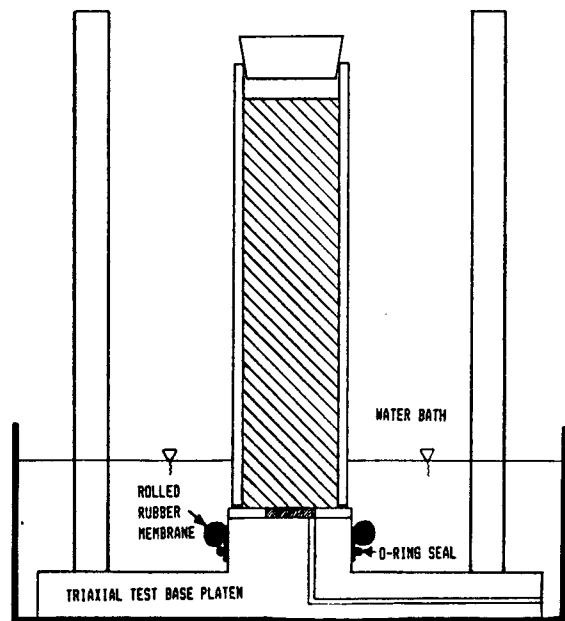
MIXING TUBE PLACED UPON TRIAXIAL TEST APPARATUS BASE
PLATEN IN WATER BATH; RUBBER MEMBRANE IS ROLLED UP
SIDES OF MIXING TUBE
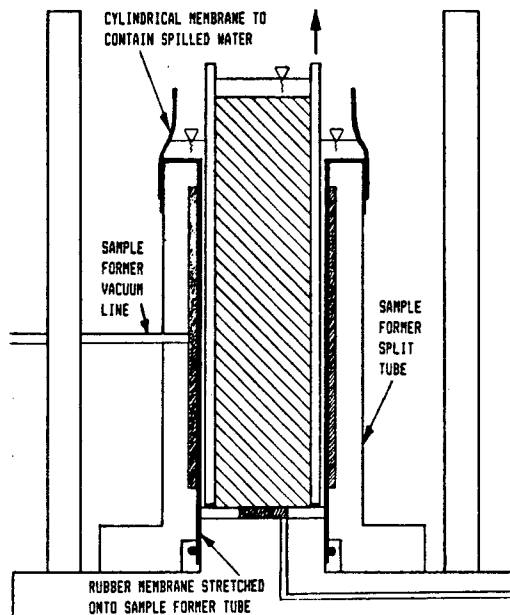
SAMPLE FORMER TUBE ASSEMBLED AROUND MIXING TUBE; SAMPLE
MEMBRANE STRETCHED OVER SAMPLE FORMER TUBE; APPLICATION
OF VACUUM TO FORMER TUBE EXPANDS MEMBRANE AND DRAWS IN
RESERVOIR WATER FROM ABOVE, MAINTAINING SATURATION
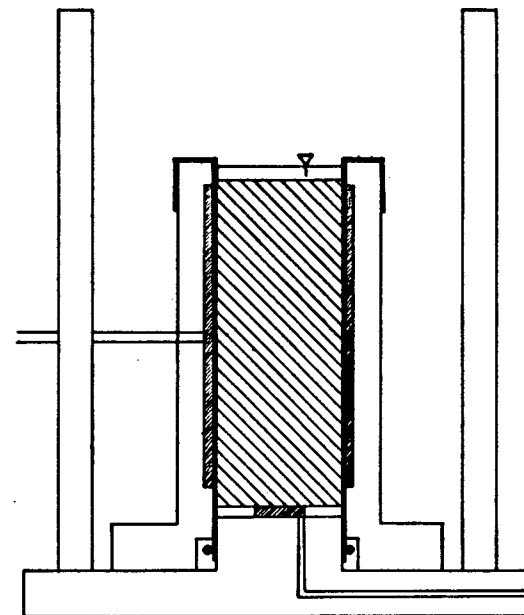
MIXING TUBE WITHDRAWN LEAVING LOOSE SATURATED UNIFORMLY
MIXED SAMPLE IN FORMER TUBE; TOP OF SAMPLE CAREFULLY
FLATTENED; EXCESS SILTY SLURRY REMOVED AND WEIGHED

FIGURE 3.7 (continued)
SCHEMATIC DRAWING OF SLURRY DEPOSITION METHOD FOR
PREPARATION OF WELL GRADED SILTY OR CLAYEY WELL
MIXED SATURATED LOOSE TRIAXIAL TEST SAND SPECIMENS

73

(h)

(i)

(j)
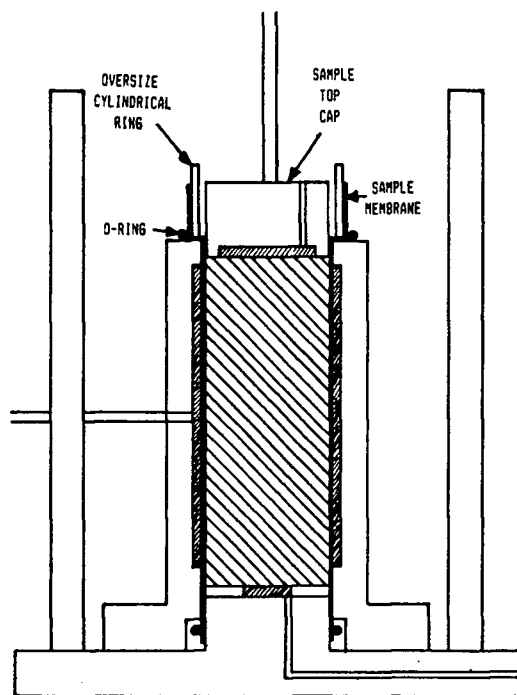
TOP CAP APPLIED CAREFULLY TO TOP OF SAMPLE; OVERSIZE
CYLINDRICAL RING PLACED AROUND TOP CAP ONTO TOP OF
FORMER TUBE. SAMPLE MEMBRANE PULLED UP OVER CYLINDRICAL
RING; RUBBER O-RING ROLLED OVER RUBBER MEMBRANE AND
CYLINDRICAL RING. EXCESS RUBBER MEMBRANE ROLLED DOWN
TO O-RING TO ALLOW REMOVAL OF CYLINDRICAL RING AND
ACHIEVE UNDISTURBED SEALING OF TOP CAP WITH O-RING
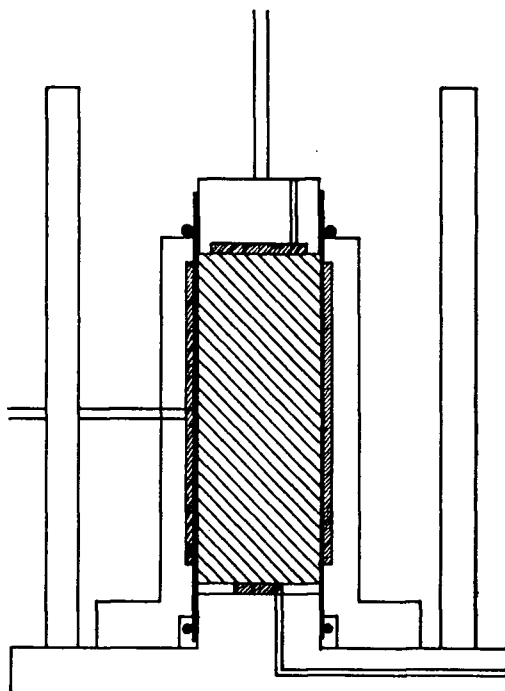
FIGURE 3.7 (continued)

SCHEMATIC DRAWING OF SLURRY DEPOSITION METHOD FOR
PREPARATION OF WELL GRADED SILTY OR CLAYEY WELL
MIXED SATURATED LOOSE TRIAXIAL TEST SAND SPECIMENS
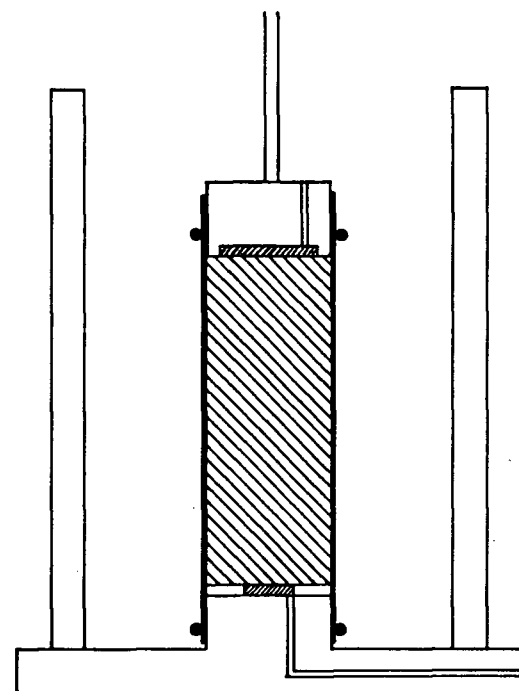
RECONSTITUTED SOIL SAMPLE MAINTAINED UNDER VACUUM
AFTER REMOVAL OF SPLIT SAMPLE FORMER TUBE

during pluviation are retained and weighed when dry to adjust the weight of fines retained within the sand sample.

3.3.2.3 Sealing of Sample Preparation Mixing Tube

To mix the sand slurry within the sample preparation mixing tube, the tube is sealed in the following manner. A thin 2 inch diameter rubber membrane is rolled onto the outside of the open end of the mixing tube and the tube is placed in a water bath as shown in Figure 3.7(c). A boiled and de-aired porous disk, which is the bottom platen of the triaxial test apparatus upon which the finished sample will be seated, is placed upon the open end of the mixing tube within the water bath, maintaining saturation of the porous disk within the water bath.

The rubber membrane around the end of the mixing tube is pulled over the porous disk assembly, sealing the sides of the disk assembly. A thin round metal plate approximately the same diameter as the porous disk assembly is placed upon the disk assembly and rubber membrane which seals it, thus completely sealing the end disk assembly and sample mixing tube.

The mixing tube is then withdrawn from the water bath while maintaining a firm finger pressure upon the end disk assembly to keep it sealed. The slurry within the sample mixing tube is then mixed by vigorously rotating the mixing tube (see Figure 3.7(d)). The progress of sample mixing may be observed through the clear plastic tube. Twenty minutes

of mixing was found sufficient to obtain completely homogeneous samples.

3.3.2.4 Placement of Mixing Tube Onto Triaxial Base Platen

Before the sand sample is prepared in the mixing tube, the triaxial test base platen is assembled within a water bath as shown in Figure 3.7(e). A rubber membrane (generally 0.3 mm thickness, 59 mm diameter and 20 cm long) is rolled onto the base platen of the test apparatus and sealed to the platen with a rubber o-ring. Once the sand slurry in the mixing tube has been mixed thoroughly as discussed in the previous section, the tube is held vertically with the porous disk assembly downwards, and the slurry is allowed to settle. After the slurry has sedimented to its loosest stable state, the basal metal plate is removed from the disk assembly and the rubber membrane which holds the disk assembly is pulled back to the sides of the porous disk which is now held by water tension and the membrane on the sides of the porous disk. The porous disk end of the mixing tube is then carefully placed upon the triaxial test base platen as shown in Figure 3.7(e). The rubber membrane which seals the porous disk is now rolled up off the mixing tube.

The sample rubber membrane is rolled up from the base platen and o-ring seal which retains one end, over the porous disk and mixing tube towards the rubber stopper which seals the upper end of the mixing tube. The mixing tube is

thus sealed to the base platen and the whole apparatus may be removed from the water bath and taken to the final sample assembly station.

3.3.2.5 Deposition of Sand Sample

A split sample former tube is assembled around the base platen and sample mixing tube (see Figure 3.7(f)). The soil rubber membrane is pulled radially outwards from the top of the sample mixing tube and folded over the top of the former. At this point the split former completely seals the outside of the sample membrane.

A cylindrical rubber membrane (75 mm diameter by 100 mm height, see Figure 3.7(f)) is stretched over the top of the split sample former and the top of the sample membrane. Water is poured into the cylindrical membrane to form a water bath above the split former. A vacuum applied to the inside of the former withdraws the sample membrane to the former walls and also draws water down from the membrane water bath above. The inside of the sample membrane is now ready to accept the sand slurry.

The rubber stopper which plugs the end of the sample mixing tube is removed. Excess slurry fines or water are withdrawn from within the top of the sample mixing tube and are weighed later when oven dry to determine the exact fines content in the sand sample. The mixing tube is then carefully and steadily withdrawn to deposit the sand slurry

within the membrane in a very loose, homogeneous saturated state.

The top of the sample is carefully leveled, excess fines slurry or water are withdrawn from the membrane water bath (to be weighed dry) and the water bath membrane is removed from the top of the sample former tube (Figure 3.7(g)).

3.3.2.6 Application of Sample Top Cap

The upper triaxial test platen is carefully placed on the top surface of the sand sample. A small circular bubble level placed upon the top of the platen is used to keep it level at all times during placement.

The slightest pressure upon or vibration of the upper platen causes settlement of the loose sample. Therefore a special technique for sealing the upper platen was developed. A cylindrical copper ring slightly larger than the diameter of the platen (see Figure 3.7(h)) is placed upon the top of the sample former. While pressure is applied to the top of the copper ring to hold the sample membrane in place against the top of the former, the folded portion of the membrane is pulled up off the split former and onto the sides of the copper ring. A rubber o-ring is rolled downwards over the rubber membrane which covers the copper tube until the o-ring touches the top of the sample former. The excess rubber membrane which covers the copper tube is rolled down on top of the o-ring, and held down

firmly while the copper ring is withdrawn. The o-ring snaps onto the top platen and over the sample membrane, sealing the sample with no disturbance.

The top cap placement method described has been found to be very effective in the assembly of as deposited sand specimens of initially loosest density. Once the sample has been sealed in its rubber membrane, a 20 kPa vacuum is applied to the pore pressure line in order to confine the specimen. After consolidation under the applied vaccuum the split former is dismantled, and triaxial cell assembly completed in the manner described in Section 3.4.

3.3.2.7 Preparation of Densified Sand Samples

Densified sand samples are prepared by placing the top platen upon the soil sample, applying a slight pressure upon the platen, and vibrating the base of the triaxial cell with a mechanical vibrator or soft hammer until the desired relative density is attained. Excess pore pressures caused by vibration are allowed to dissipate through top and bottom drainage lines. This technique yields samples of uniform density throughout (Vaid and Negussey, 1986). Densified soil samples are finally sealed and confined in the same manner as loose samples (see Section 3.3.2.6).

3.3.3 Evaluation of Slurry Deposition Method

The attractive features of the slurry deposition method are as follows: 1) a sand sample remains fully saturated

within de-aired water during preparation; 2) sample preparation is normally completed within about 1.5 hours; 3) a sample is mixed thoroughly as a lean saturated slurry with little excess pore water so as to minimize height of particle drop through water during deposition and thus control sedimentation currents and particle size segregation during deposition; 4) the method forms initially loose samples (poorly-graded unsegregated sand obtained by simple pluviation through water is generally slightly denser than slurry deposited sand) which may be uniformly densified by mechanical vibration; 5) samples are exceptionally homogeneous with respect to void ratio and particle size gradation, regardless of gradation and fines content; and 6) the deposition method models the soil fabric found within natural fluvial deposits or hydraulic fills.

3.3.3.1 Sample Homogeneity

To test the uniformity of sand samples prepared using the slurry deposition method, identical samples of well-graded 20/200 Brenda sand were prepared in a loose state using the slurry deposition method and the water pluviation method. The samples were set in a 2.5% gelatin solution under a confining pressure of 20 kPa (using the procedure described by Emery et.al., 1973). When solidified, the membrane was removed and the sample cut into four equal horizontal slices. Grain size distribution and void ratio

of each slice was then measured. The test results are shown in Figure 3.8 and Figure 3.9.

The slurry deposited sample may be seen to be homogeneous with respect to particle size gradation (Figure 3.9). In contrast, the water pluviated sample shows considerable particle size segregation (Figure 3.8). Both water pluviated and slurry deposited samples appeared visually quite uniform, although water pluviated samples may have visible layers of finer and coarser grained soil if insufficient care is taken to maintain visual sample homogeneity. Void ratio distribution with sample height of both water pluviated and slurry deposited samples is fairly uniform, although a tendency toward a slightly better uniformity may be noted in slurry deposited samples. The water pluviated specimen deposited at a slightly looser state due to particle segregation during deposition (compare void ratios in Figures 3.8 and 3.9). In contrast, poorly-graded sand, which by definition cannot segregate, was found to be slightly denser when deposited by pluviation than when deposited by slurry deposition.

The results of a similar test to determine the uniformity of a slurry deposited silty sand specimen with 14% silt content are also illustrated in Figure 3.9. It may be noted that the silty sand specimen is remarkably homogeneous with respect to particle size gradation over its entire height, even though it has previously been densified and cyclically loaded to initial liquefaction.

Figure 3.8 Grain size distribution curves for horizontally
            quartered sections of a water pluviated sand sample

M. I. T. GRAIN SIZE CLASSIFICATION

SAND			SILT		
COARSE	MEDIUM	FINE	COARSE	MEDIUM	FINE

VOID RATIO DISTRIBUTION
(BRENDA 20/200 SAND)

SECTION		VOID RATIO
1	O	0.893
2	□	0.892
3	△	0.908
4	*	0.924
TOTAL		0.904

CLEAN WELL-GRADED WATER
PLUVIATED 20/200 BRENDA
SAND (LOOSEST STATE)

σ'_c = 20 kPa
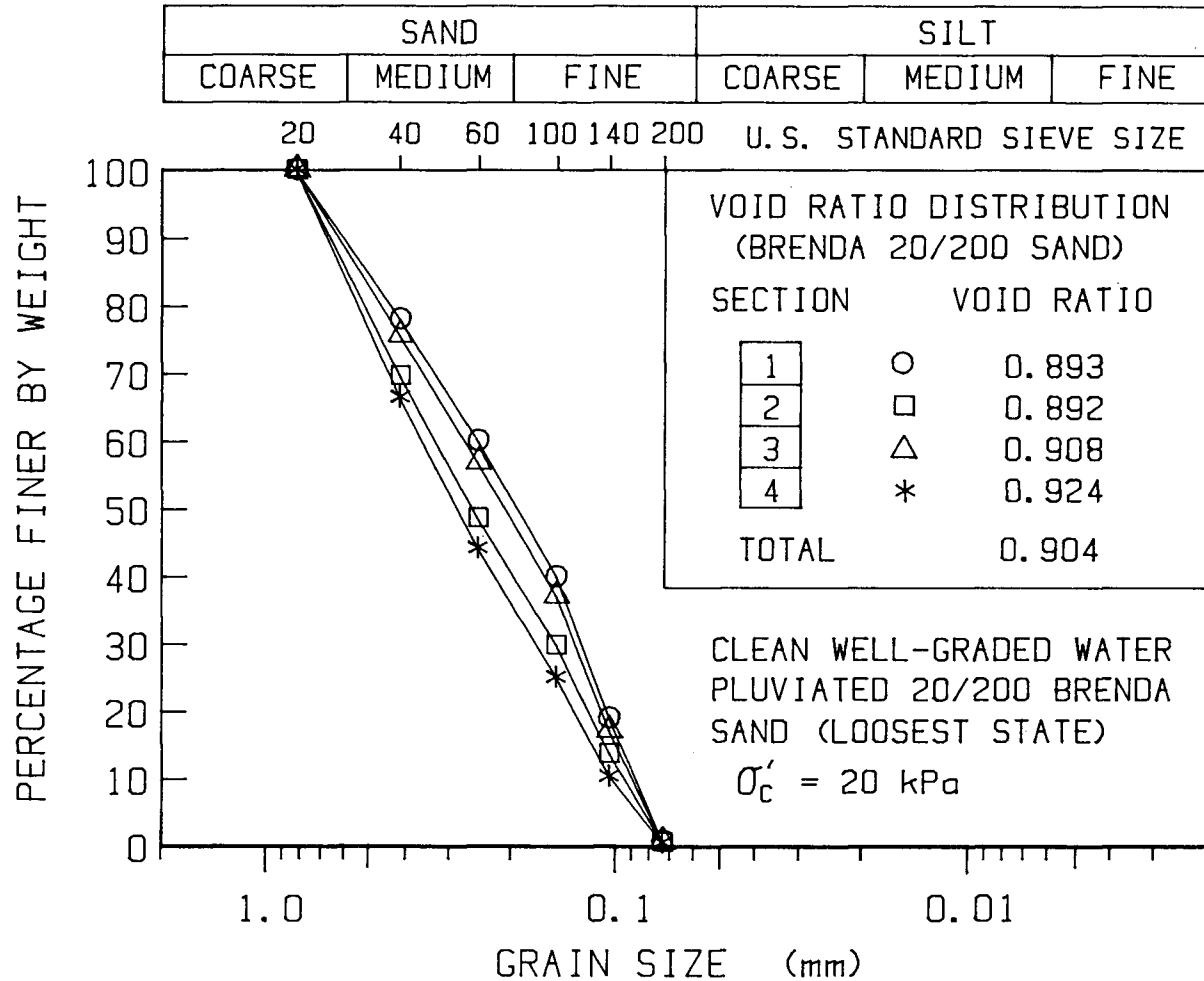
Figure 3.9   Grain size distribution curves for horizontally
quartered sections of slurry deposited sands
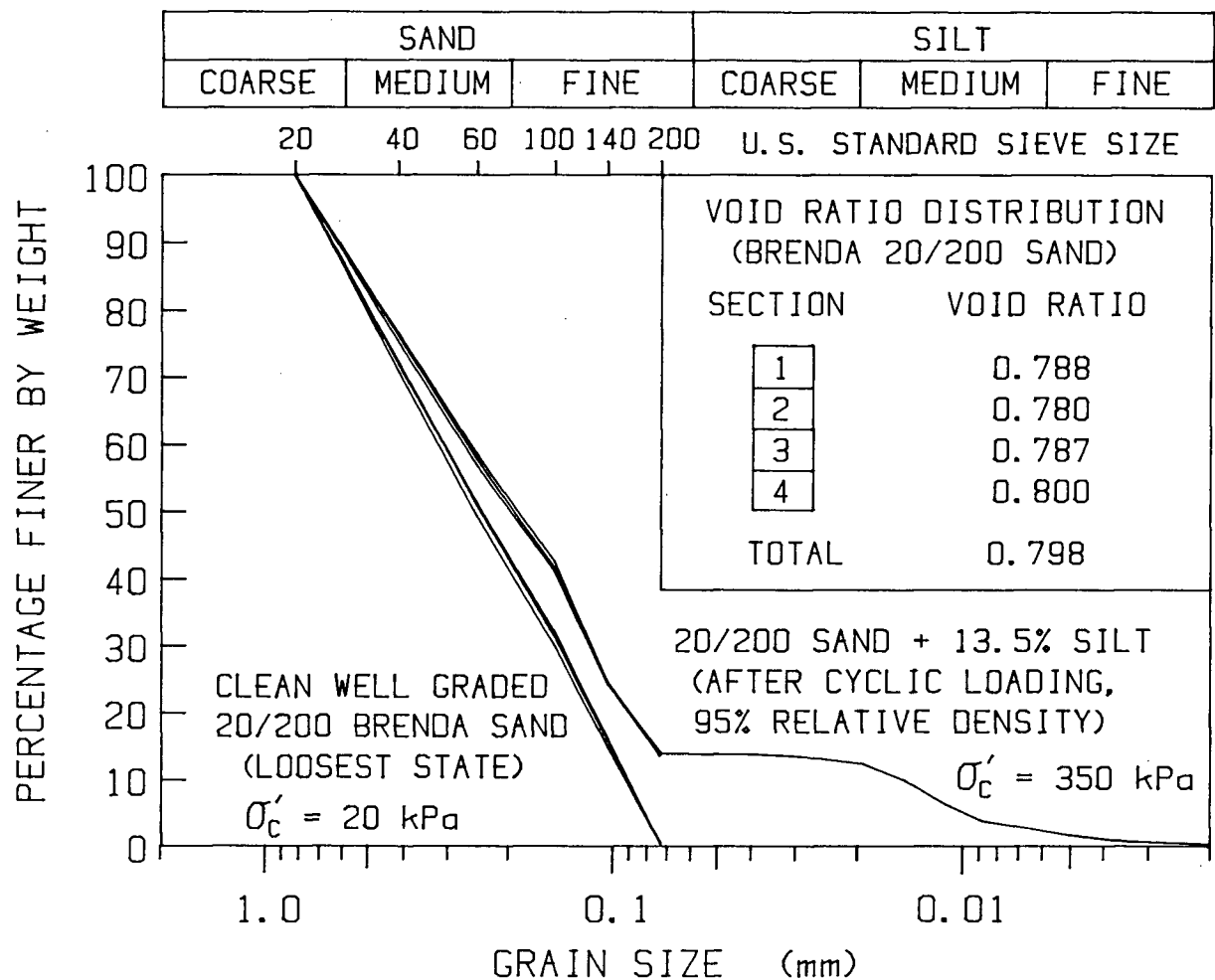
A major advantage of the slurry deposition method is that regardless of size gradation, the method produces homogeneous well mixed samples. The extent of sample mixing obtained in the sample mixing tube controls sample homogeneity (see Figure 3.7(d)). This may be controlled by the skill and experience of the researcher. It was found that the slurry deposition method produces homogeneous samples with repeatable results if the sand slurry is mixed for at least twenty minutes for the sample size used. The homogeneity of silty sand specimens was more easily controlled because the well-graded material had to be completely mixed before a uniform slurry consistency and color were obtained.

Four factors affect the choice of dimensions for the slurry deposition method mixing tube: 1) soil specimen dimensions at the loosest state of deposition, 2) mixing tube diameter should be only slightly smaller than the diameter of the completed soil specimen to maintain homogeniety of the soil in the original well mixed state during the transfer process, 3) the slurry within the mixing tube should have a high enough water content to allow mixing, and 4) the slurry should have a low enough water content such that particle settlement distance is kept to a minimum and sedimentation currents do not segregate the soil during sedimentation. A mixing tube volume which is 5 to 10% larger than the volume of sand deposited in the loosest state was found to be most effective. The dimensions of the

slurry mixing tube used for this study are shown in Figure 3.7(b). A longer mixing tube was used to deposit well-graded sand with 20 percent silt content because of the higher viscosity and larger segregated volume of the silty sand.

Better sample homogeneity and perhaps looser fine grained samples might be attained if the sand slurry were mixed directly within the sample former and deposited directly within the sample membrane without the need for a transfer from the mixing tube. This is because slight densification or segregation may occur during transfer from the mixing tube. Such a method would require construction of a specialized mixing apparatus.

3.3.3.2 Replication

The degree to which the slurry deposition technique is able to replicate specimens at a desired density is illustrated in Figure 3.10. Results of monotonic undrained compression response of two identical specimens of uniform 20/40 Brenda sand isotropically consolidated to 200 kPa are shown. Excellent repeatability may be noted in the test results.

Similar replication of specimens was possible with silty sands using up to 20% silt content. For a given silty sand, the same loosest state void ratio was obtained following slurry deposition. Since the uniformity of specimens was insured by the deposition technique,

Figure 3.10 Repeatability of slurry deposited Brenda sand test results

98
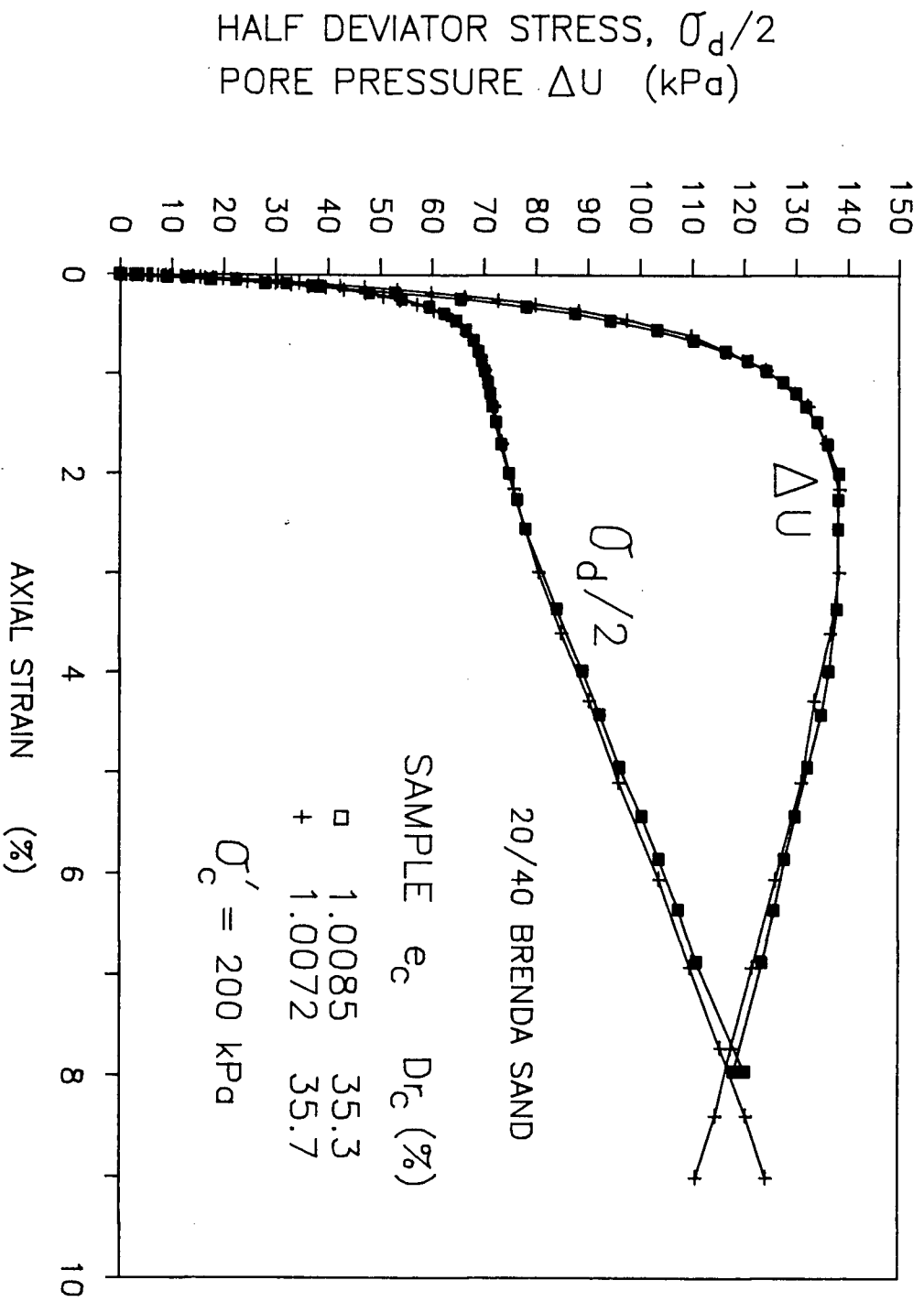
replication of specimens was easily attained at any targeted density.

3.3.3.3 Sand Fabric

Since water pluviated sands have been shown to possess fabric similar to natural fluvial sands (Oda, 1978), it is necessary to evaluate if the slurry deposition technique also gives rise to a similar fabric. This evaluation was done by comparing undrained monotonic response of specimens of Brenda 20/40 sand at identical density, one prepared by water pluviation and the other by slurry deposition technique. The results illustrated in Figure 3.11 show that water pluviated and slurry deposited loose sands (near the loosest state possible by water pluviation and slurry deposition methods) have similar triaxial monotonic loading response. Both deposition methods produce considerably more dilative response in triaxial compression than in extension loading. This is typical of air or water pluviated sands (Miura and Toki, 1982) and undisturbed natural sands (Miura and Toki, 1984).

A similar comparison of water pluviated and slurry deposited ASTM Ottawa C-109 sand is shown in Figure 3.12. Sample preparation technique may be seen to affect behaviour of Ottawa C-109 sand shown in Figure 3.12 more than that of poorly-graded Brenda 20/40 sand illustrated in Figure 3.11. The greater degree of variation is probably due to the fact that Ottawa sand, though considered uniform (Cu = 1.5), is

Figure 3.11 Comparison of test results for slurry deposited and water
pluviated 20/40 Brenda sand
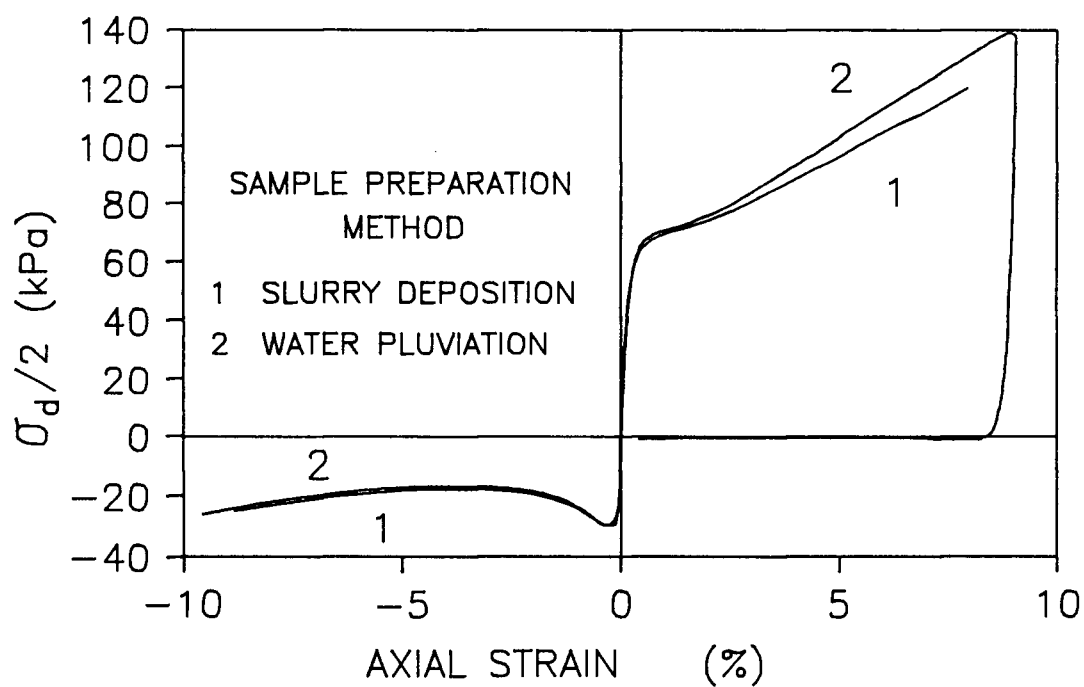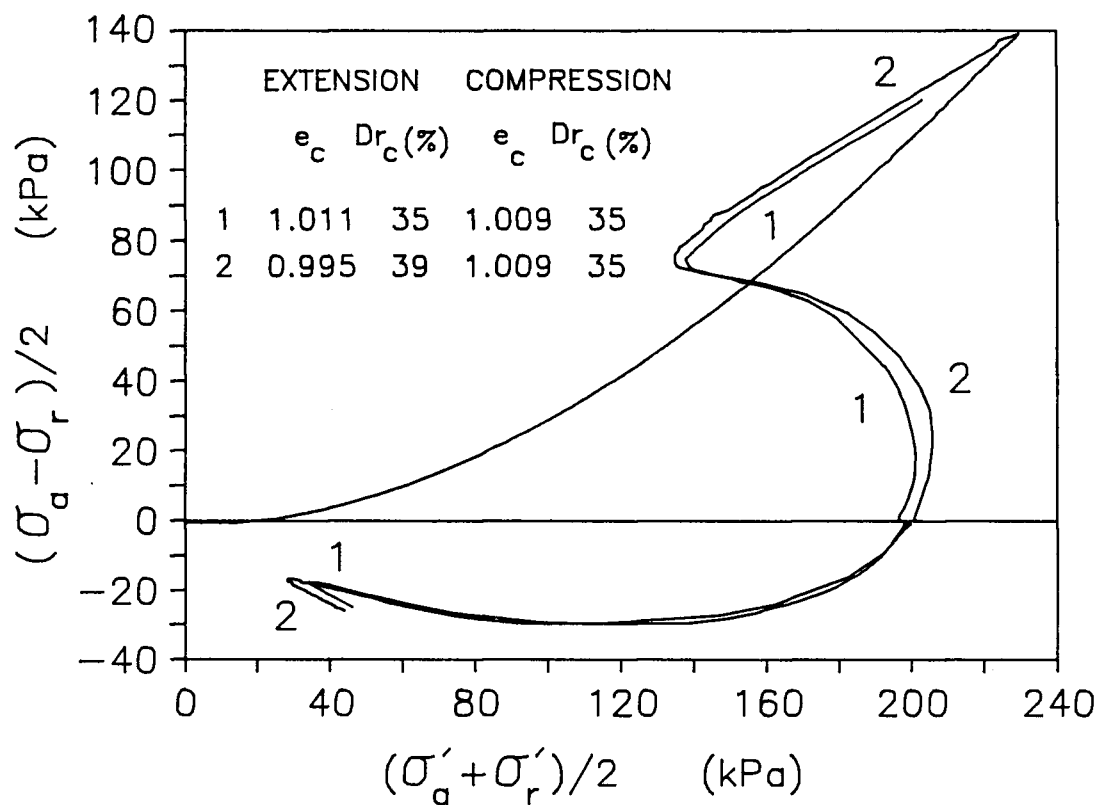
Fig. 3.12 Comparison of undrained response of slurry deposited and water pluviated Ottawa C−109 sand
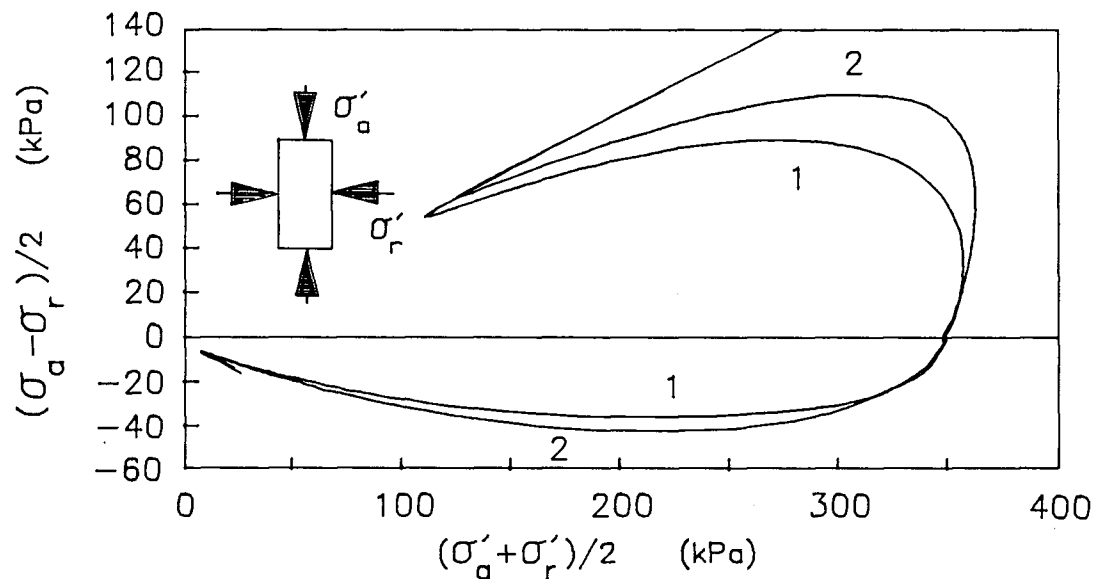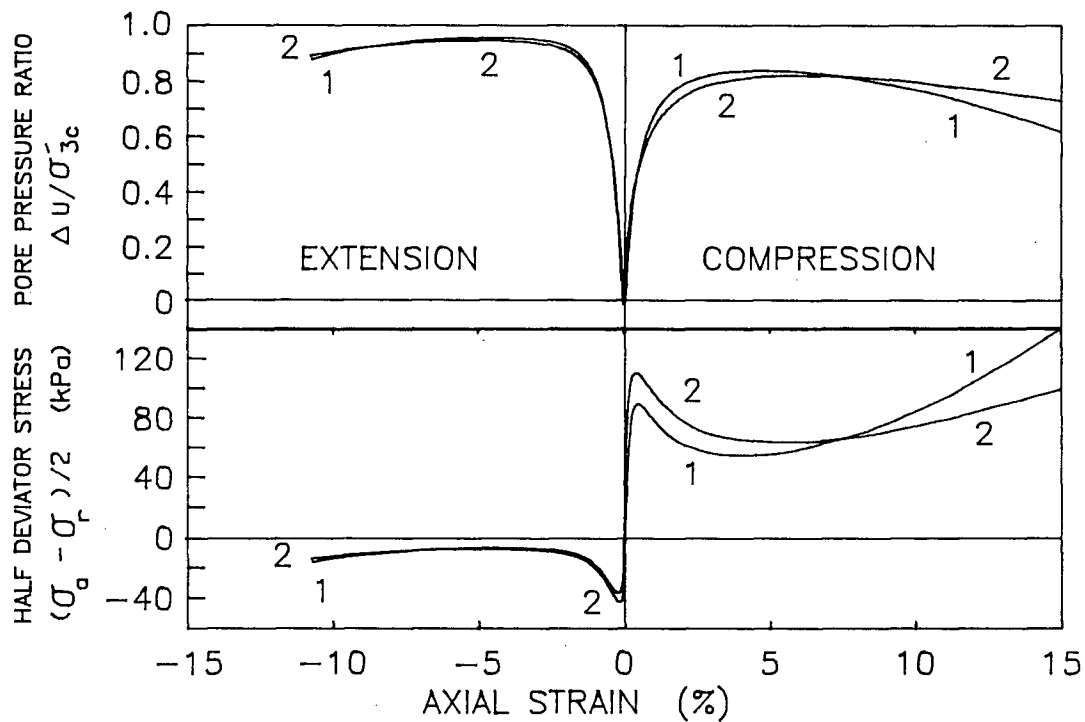
more well-graded than Brenda 20/40 sand and thus is more subject to size segregation during pluviation through water than Brenda 20/40 sand. Grain size segregation was visually observed on water pluviation of Ottawa sand. Apparently, grain size segregation produced by pluviation through water makes a more well-graded sand initially stiffer or more dilative at low strain level, such that it behaves as if it were a more poorly-graded material (see Section 5.2). In contrast, at larger strain level, water pluviated segregated sand is apparently less dilative than slurry deposited well mixed sand.

3.3.4 Summary of Slurry Deposition Method

To overcome inherent problems of reconstituted sand sample preparation methods a new technique called the slurry deposition method has been developed.

Slurry deposition sand samples are prepared in a fully saturated state within de-aired water to ensure full saturation. Samples are mixed thoroughly as a saturated slurry with little excess pore water so as to minimize height of sand particle drop through water during deposition and thus control sedimentation currents and particle size segregation during deposition. Samples are formed in an initially loose state with an initial void ratio which is generally larger than that obtained in a comparable unsegregated water pluviated sand. Initially loose samples

may be uniformly densified by mechanical vibration to obtain a desired void ratio.

Slurry deposited samples are exceptionally homogeneous with respect to void ratio and particle size gradation, regardless of gradation and fines content. The slurry deposition method simulates well the soil fabric found within a natural fluvial or hydraulic fill deposit, yet creates homogeneous samples that can be easily replicated as required in laboratory tests for fundamental studies of material behaviour.

3.4 ASSEMBLY OF TRIAXIAL TEST APPARATUS

Once the sample has been deposited within the split former and the top platen positioned, initial sample height is recorded to determine maximum slurry deposition void ratio. Sample height is again recorded once the top platen is sealed with the sample membrane. The former vacuum is removed and a 20 kPa vacuum is applied to the pore pressure line to confine the soil specimen. The volume change during consolidation under this 20 kPa effective stress is recorded together with sample height and circumference after removal of the sample former, to determine initial dimensions and void ratio.

The triaxial cell is then assembled and an LVDT reaction bar bolted to the top platen loading rod (see Figure 3.1) before the final sample height and volume change

data are recorded and the pore pressure line closed to seal the consolidation vacuum. The triaxial cell is filled with de-aired water and transfered to the loading frame.

Transducers for the determination of axial load, pore pressure, cell pressure, and axial deformation are then set to their initial zero levels, and data zeros for all transducers are recorded by strip chart or computerized data acquisition system.

The cell pressure line is attached to the triaxial cell and cell pressure increased to 20 kPa to bring the sample pore pressure to zero. The pore pressure line is now attached to the sample, and the cell pressure applied undrained in 25 kPa increments to 120 kPa. Increase in pore pressure is recorded to evaluate and thus check for saturation. The sample is then consolidated incrementally to the desired effective stress state isotropically or anisotropically as described in Section 3.1.1.1. A back pressure of 100 kPa was used during consolidation. Each consolidation increment was maintained for ten to twenty minutes in order to allow most of the secondary consolidation to be completed (Negussey, 1984; Mejia et al., 1988).

3.5 UNIFORMITY OF SAMPLE STRAIN DURING MONOTONIC AND CYCLIC LOADING

Strain during undrained triaxial compression and extension loading was observed to be uniform for axial

strain levels below 10 to 15%, as shown in Figure 3.13. At strain levels greater than 10 to 15%, samples loaded in compression developed a uniform bulge at the mid section followed by the development of shear planes at very large strain. Samples loaded in extension developed thinning of the x-sectional area at a random height within the sample, which led to the evolution of conjugate shear planes and radical sample necking. Often sample strain uniformity is better maintained in extension loading than compression loading due to reduced end effects in extension loading. Only test results from the uniform region of strain have been included in this thesis. Results from the region of large non-uniform strain have been excluded.

3.6 TEST PROGRAM

The range of undrained monotonic loading behaviour of several Brenda sand types was determined over a range of confining stresses. Both monotonic compression and extension tests were conducted. Several poorly-graded sands, a well-graded sand, a poorly-graded silty sand, and a well-graded silty sand were tested. All samples were consolidated from loosest state of slurry deposition, to determine the range of maximum contractive response for the various sands tested. Consolidation from loosest state of slurry deposition was also chosen as a reference density to provide a method of comparing different sand properties

94

SAMPLE SHAPE UP TO 10 TO 15% STRAIN
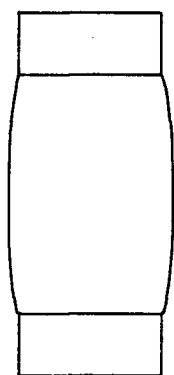
COMPRESSION   EXTENSION
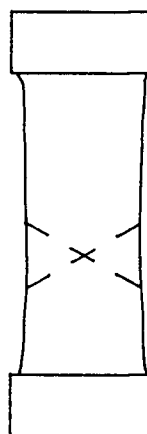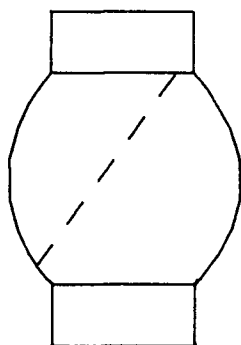
DEVELOPMENT OF NON—UNIFORM STRAIN AT
LARGE STRAIN LEVEL > 15%

Figure 3.13 Uniformity of sample strain during loading

which takes into account the origin of the soil deposit. The concept of relative density attempts to classify soil density as a state between extremes of loosest and densest state obtained by standard laboratory test techniques. This may not reflect the mechanism of placement of field soils. When test results are compared at loosest state of consolidation after slurry deposition, two factors are automatically considered: (1) various soil gradations undergo the same deposition and loading history as would be expected to occur in a fluvial or hydraulic fill deposit; and (2) because samples are at loosest possible slurry deposited state, the maximum possible contractive behaviour of sand deposited within water can be assessed.

In summary, the objectives of the monotonic loading test program are as follows:

(1)   To determine the effect which soil gradation and silt content have upon the undrained loading response of Brenda sand consolidated from loosest slurry deposition state;

(2)   To determine the effect which soil gradation and silt content have upon the difference between extension and compression loading response;

(3)   To determine the effect which soil gradation and silt content have upon the variation of undrained response with consolidation stress level.

Consolidation data from all tests was compiled to determine the effect which soil gradation and silt content have upon the range of void ratio, relative density, sand skeleton relative density, and consolidation strains obtained during consolidation from loosest state of slurry deposition.

A series of undrained cyclic triaxial tests were conducted on isotropically consolidated samples of: (1) poorly-graded silty sand; and (2) well-graded silty sand. Silty sand samples were prepared in a very loose to dense state. Cyclic tests were conducted to determine the effect of silt content upon the following features of sand cyclic loading behaviour: (1) stress-strain response; (2) pore pressure generation; (3) variation of cyclic strength at constant void ratio, relative density, and sand skeleton relative density; and (4) variation of cyclic strength after consolidation from loosest state of slurry deposition.

CHAPTER 4

TRIAXIAL TEST CONSOLIDATION RESULTS

4.0 INTRODUCTION

The following sections present isotropic consolidation data for the various sand materials tested. Differences and similarities in consolidation behaviour are discussed, including 1) void ratios and relative densities at loosest state of slurry deposition and subsequent consolidation, 2) compressibility and bulk modulus during consolidation, 3) strain paths during consolidation, and 4) incremental strain ratios to demonstrate inherent anisotropy during isotropic consolidation.

4.1 ACCURACY OF CONSOLIDATION DATA

Inaccuracies in calculated volumetric strains result mainly from membrane penetration effects. Measured volume chnages were therefore corrected for membrane penetration according to method 2 described by Vaid and Negussey (1984) (see Appendix A).

Two sands (Brenda 60/100, 100/140 gradations) required no membrane penetration correction to measured volume changes. This was consistent with the criterion that membrane penetration effects are minimal if average particle size is less than half the membrane thickness. Well-graded

20/200 sand samples required a small correction, while coarse grained 20/40 Brenda sand and Ottawa C-109 sand required relatively large membrane penetration corrections (see Table 3.2).

Although the consolidation data presented is considered reliable, samples consolidated from as deposited loosest state were generally subject to greater variation in consolidation response. The difference in consolidated density between directly comparable tests, such as complementary compression and extension tests, on the same sand at identical consolidation stress was kept to a minimum, and was generally less than 0.01 void ratio or 2% relative density.

4.2 VOID RATIO AND RELATIVE DENSITY DURING CONSOLIDATION

Figure 4.1 to Figure 4.4 display consolidation data (void ratio versus logarithm of effective confining stress) for the various Brenda clean and silty sands. As shown in these diagrams, the void ratio attained by clean sands after slurry deposition and after placement of the top platen (nominal consolidation stress of 1 kPa) is approximately equal to the maximum void ratio attained by ASTM standard minimum density tests (see Table 3.2).   All loosest deposited sands possess similar consolidation curves although there is a large variation in absolute void ratio among various sand gradations, especially between the

FIGURE 4.1   TRIAXIAL TEST ISOTROPIC CONSOLIDATION RESULTS FOR
LOOSE COARSE GRAINED 20/40 BRENDA TAILINGS SAND
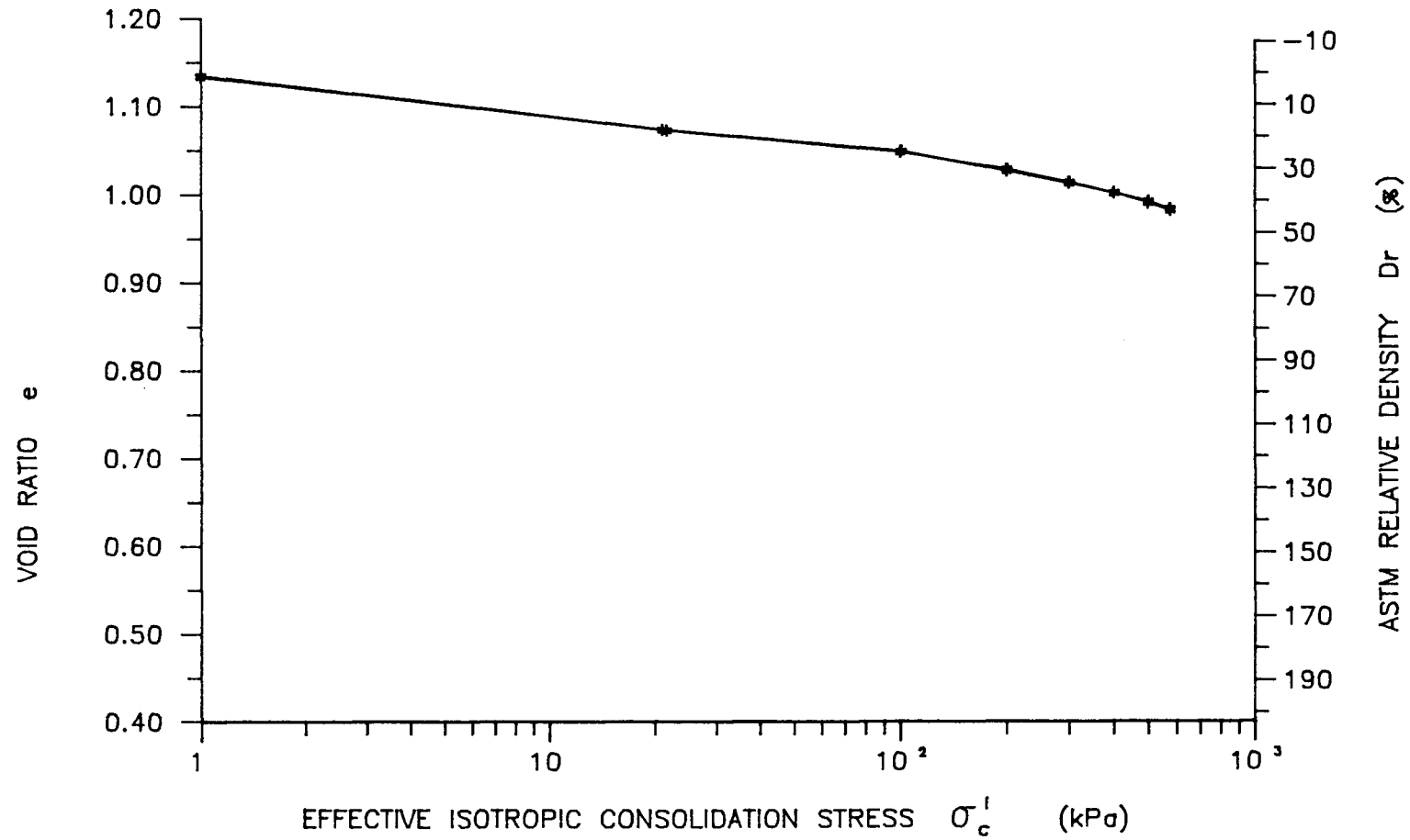
FIGURE 4.2   TRIAXIAL TEST ISOTROPIC CONSOLIDATION RESULTS FOR
LOOSE MEDIUM GRAINED 60/100 BRENDA TAILINGS SAND

EFFECTIVE ISOTROPIC CONSOLIDATION STRESS σ_c^1 (kPa)
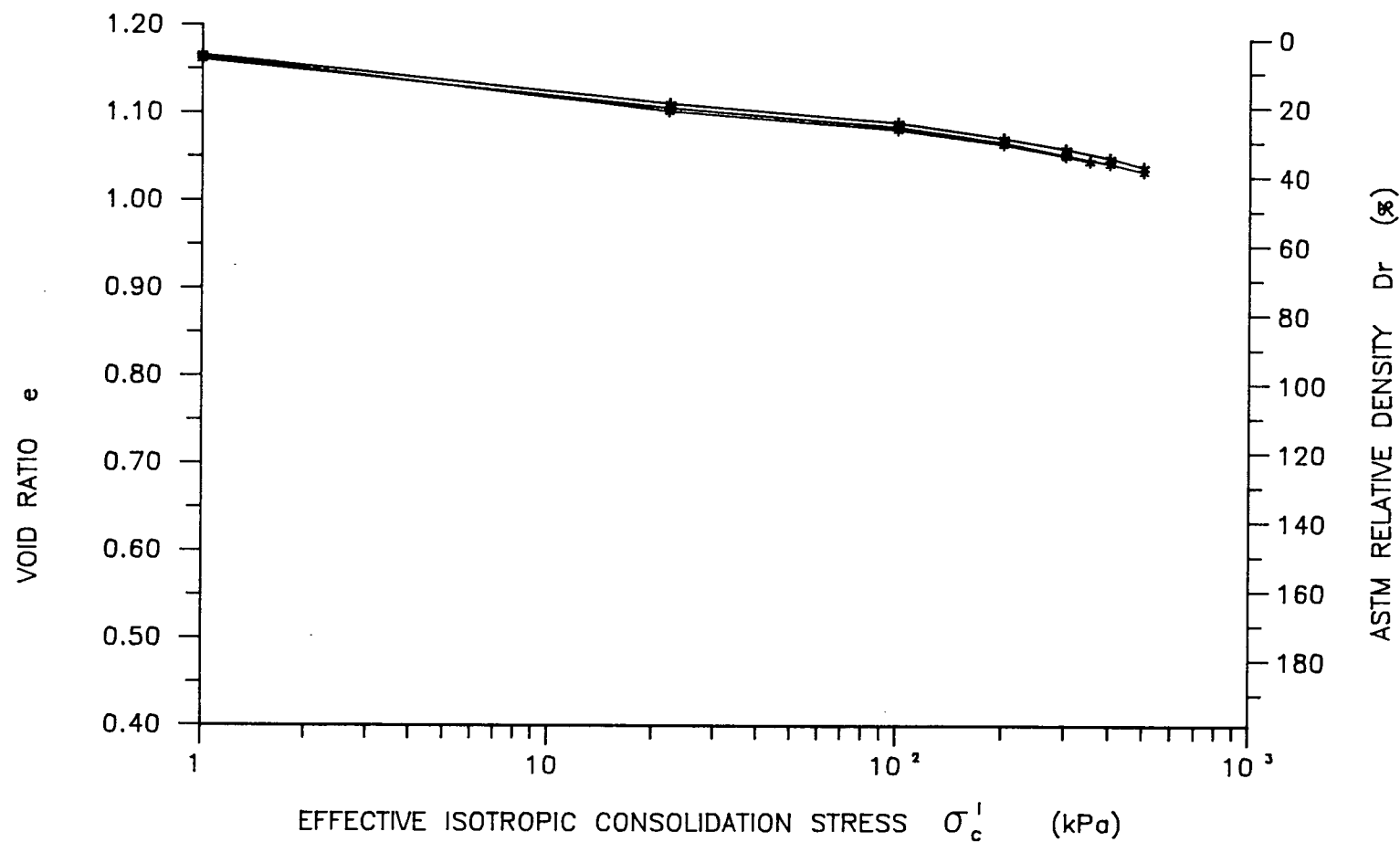
FIGURE 4.3 TRIAXIAL TEST ISOTROPIC CONSOLIDATION RESULTS FOR LOOSE UNIFORM FINE GRAINED 100/140 BRENDA TAILINGS SAND
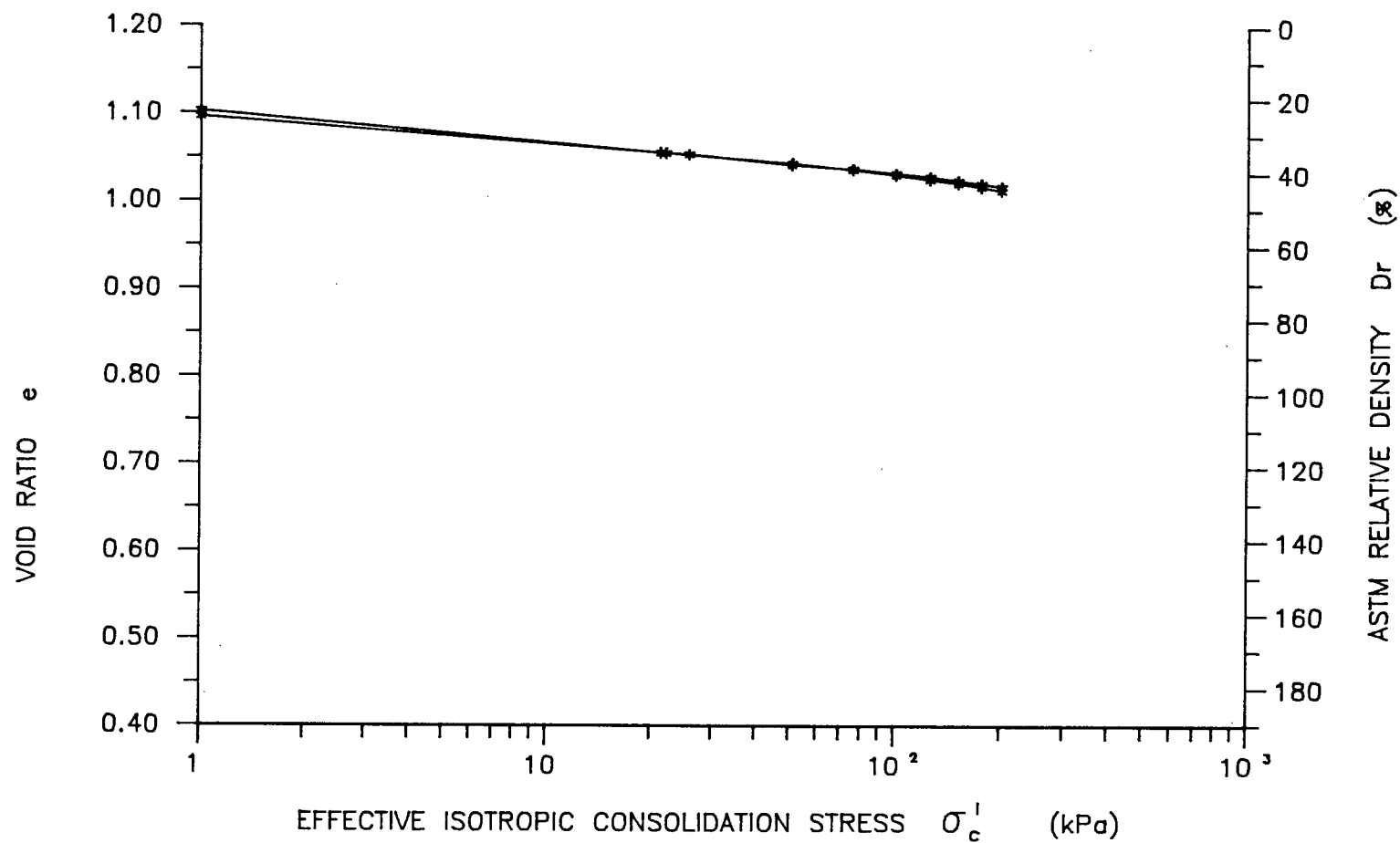
FIGURE 4.4   TRIAXIAL TEST ISOTROPIC CONSOLIDATION RESULTS FOR
SILTY WELL—GRADED 20/200 BRENDA TAILINGS SAND
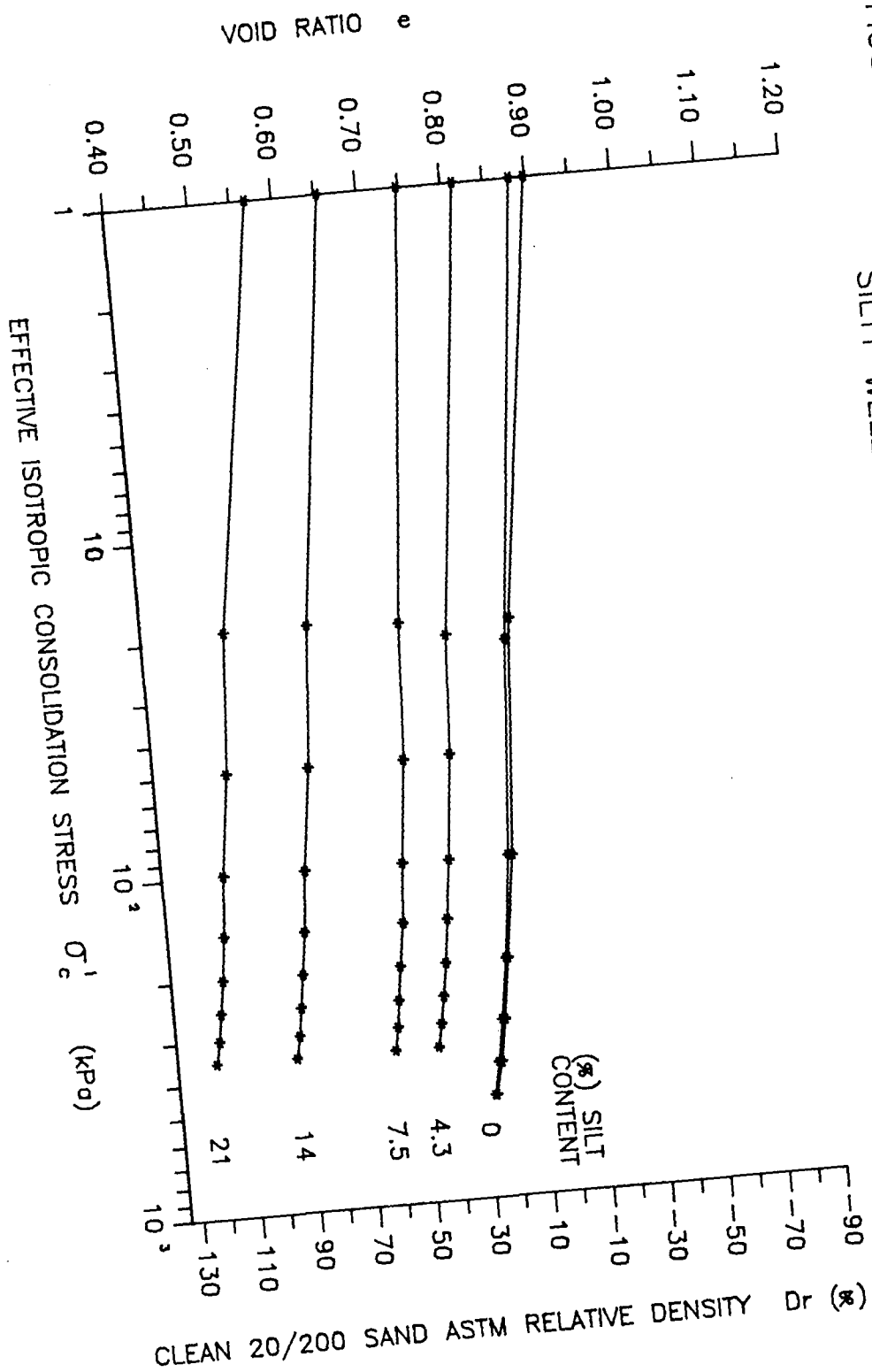
uniform sands (Figure 4.1 through Figure 4.3) and the well-graded sand (Figure 4.4). The relatively low maximum void ratio of the well-graded sand is interpreted to be the result of finer particles filling voids between coarser particles in the well mixed well-graded sand.

4.3 VOLUMETRIC STRAIN DURING CONSOLIDATION

Figure 4.5 displays how volumetric strain changes with confining stress level for the various clean sands consolidated from loosest slurry deposition state. It is interesting to note that the various Brenda sands tested show little difference in volumetric compressibility with change in gradation or mean grain size, even though, as noted in Section 4.2, there is a large difference in their absolute void ratios. This similarity in volumetric compressibility between the various gradations of Brenda sand may be a consequence of their similar fabric in the loose state.

The compressibility of loose Ottawa sand is also shown in Figure 4.5 for comparison purposes. This rounded sand may be seen to be considerably less compressible than the angular tailings sand, even though both sands were initially at their loosest slurry deposition state.

Figure 4.6 shows compressibility of loose silty 20/200 sand. The test results indicate that silt content has little effect on the compressibility of sand prepared at the

Figure 4.5 Volumetric strains of various clean sands during isotropic consolidation from loosest state of slurry deposition

ISOTROPIC CONSOLIDATION CHARACTERISTICS
FROM LOOSEST STATE OF SLURRY DEPOSITION

POORLY GRADED 60/100
BRENDA SAND

POORLY GRADED 20/40
BRENDA SAND

WELL GRADED 20/200
BRENDA SAND

POORLY GRADED 100/140
BRENDA SAND

OTTAWA C-109 SAND,
NORMAL PREPARATION

VOLUMETRIC STRAIN ε_v

EFFECTIVE CONFINING STRESS σ_c' (kPa)
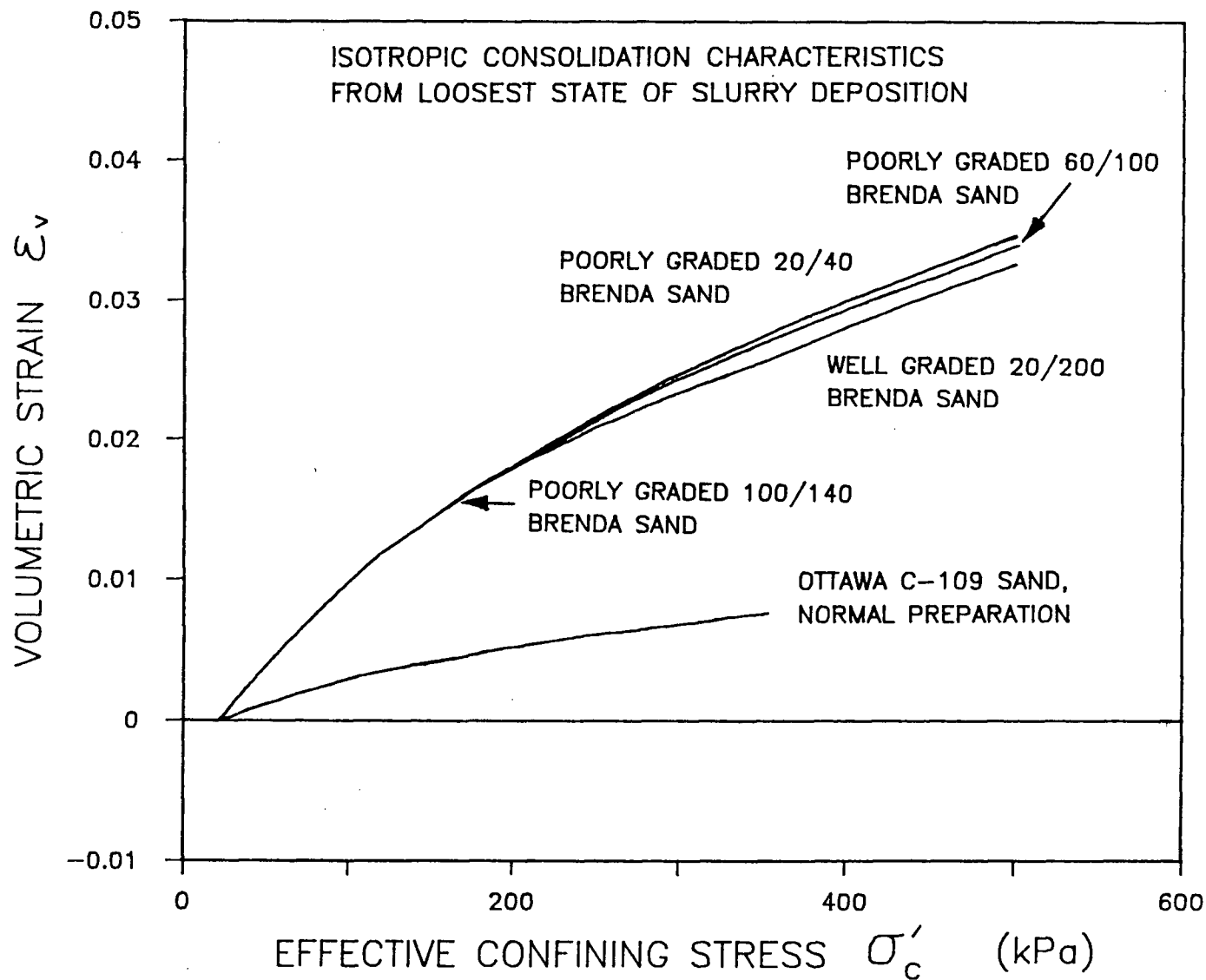
Figure 4.6 Volumetric strains of silty 20/200 Brenda sand during isotropic consolidation from loosest state of slurry deposition
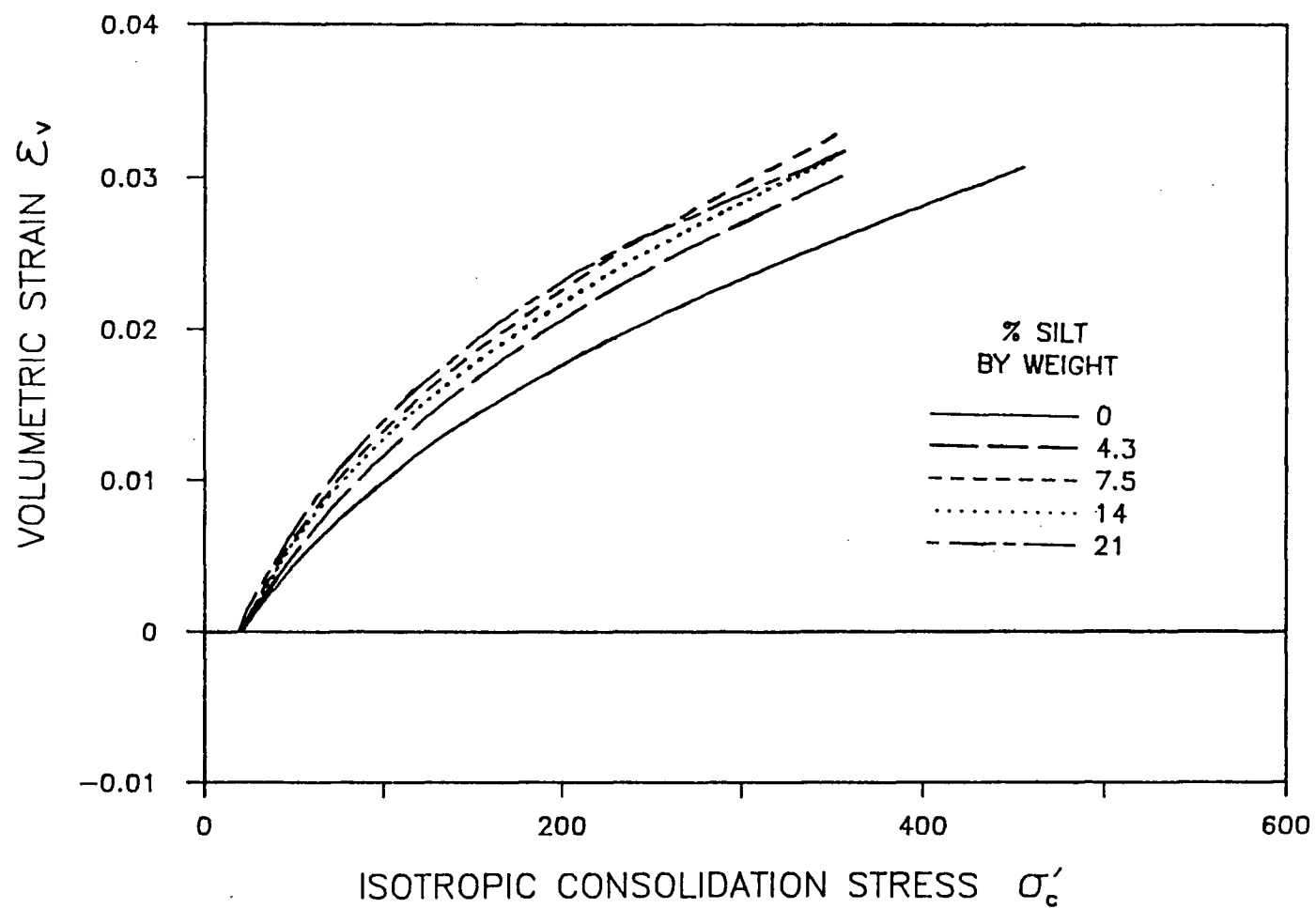
loosest state of slurry deposition, even though absolute void ratio undergoes a drastic reduction with an increase in silt content as shown in Figure 4.4. This is clearly a consequence of essentially constant sand skeleton void ratio regardless of silt content.

Figure 4.7 displays the variation of bulk modulus with isotropic consolidation stress for various clean tailings sands. Bulk modulus is seen to increase linearly with confining stress for each gradation of sand tested, with a slight variation in slope for each type of sand. This is in contrast with the more commonly quoted linear variation with square root of confining stress. The initial bulk modulus of each sand is approximately the same with B_0 = 4.5 MPa.

A similar variation in bulk modulus with stress level was found for silty well-graded 20/200 sand at several deposition relative densities (see Figure 4.8). A summary of compressibility characteristics of silty 20/200 sand and its variation with silt content and sand skeleton relative density is shown in Figure 4.9 and Figure 4.10. The figures show how the parameters B_0 and K_B in the bulk modulus expression $B = B_0 + K_B \sigma_3'$ vary with silt content and sand skeleton relative density. The test results show that silt content has little effect upon the compressibility of silty sand, although silt content drastically reduces absolute void ratio. The bulk modulus of very silty sand or silty sand at larger sand skeleton relative density may be seen to increase slightly with increasing silt content.

Figure 4.7 Bulk modulus of various clean Brenda sands during isotropic consolidation from loosest state of slurry deposition

WELL GRADED 20/200 BRENDA SAND

POORLY GRADED 60/100 BRENDA SAND

POORLY GRADED 100/140 BRENDA SAND

POORLY GRADED 20/40 BRENDA SAND

$$\text{BULK MODULUS} \quad B = \frac{\Delta \sigma_3'}{\Delta \varepsilon_v}$$

ISOTROPIC CONSOLIDATION CHARACTERISTICS
FROM LOOSEST STATE OF SLURRY DEPOSITION

BULK MODULUS B (MPa)

EFFECTIVE CONFINING STRESS σ_c' (kPa)
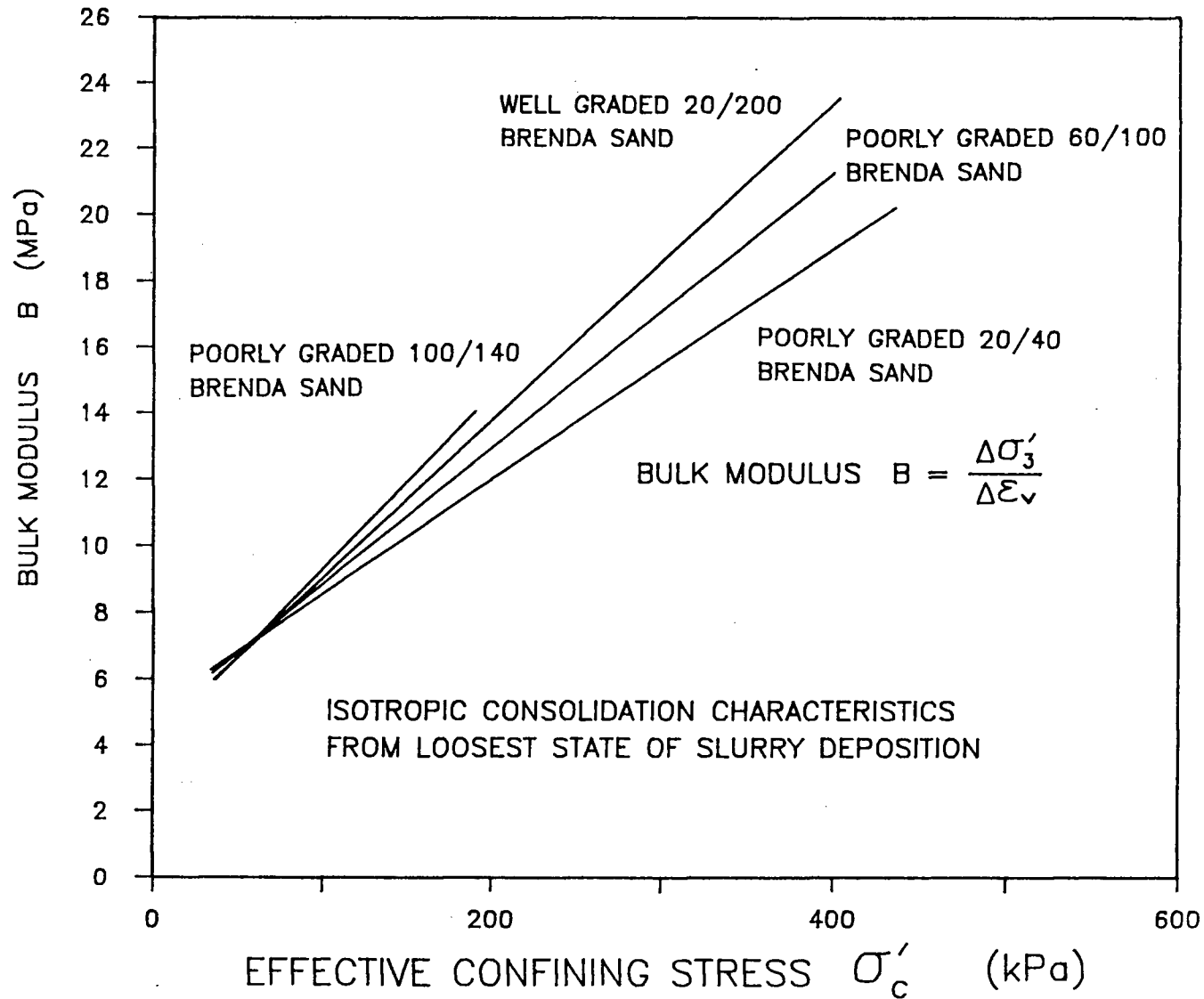
Figure 4.8 Bulk modulus of silty 20/200 Brenda sands during isotropic consolidation from loosest state of slurry deposition

13.33$\pm$.15% SILT

$e_C = 0.442\pm.002$

$Dr_C = 94.9\pm0.6\%$

Dr_C (skel) $= 57.5\pm0.1\%$

13.67$\pm$.14% SILT

$e_C = 0.488\pm.001$

$Dr_C = 83.1\pm0.3\%$

Dr_C (skel) $= 40.0\pm0.5\%$

13.94$\pm$.13% SILT

$e_C = 0.534\pm.007$

$Dr_C = 71.0\pm2\%$

Dr_C (skel) $= 20.0\pm2\%$

BULK MODULUS B (MPa)

ISOTROPIC CONSOLIDATION STRESS σ'_c
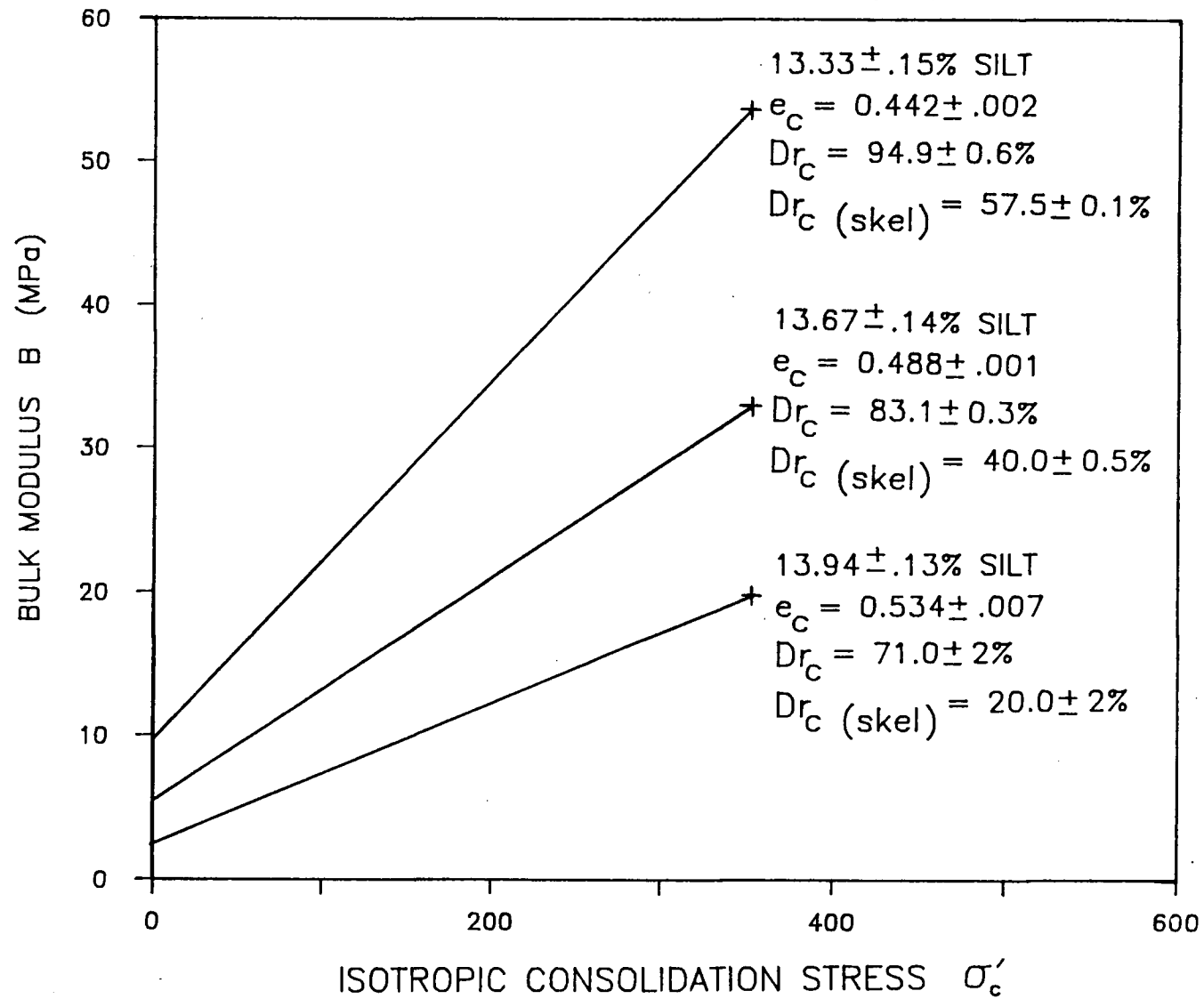
FIGURE 4.9 SUMMARY OF COMPRESSIBILITY CHARACTERISTICS OF SILTY WELL—GRADED 20/200 BRENDA TAILINGS SAND

INITIAL SAND SKELETON VOID RATIO e_i (skel)

BULK MODULUS $B = \dfrac{\Delta \sigma_3'}{\Delta \mathcal{E}_v} = K_B \sigma_3' + B_0$

e_i (skel), Dr_i (skel) taken at 20 kPa effective stress after sample preparation.

% SILT BY WEIGHT

* 0
× 4.3
+ 7.5
□ 14
△ 21

BULK MODULUS MULTIPLICATION FACTOR K_B

INITIAL SAND SKELETON RELATIVE DENSITY Dr_i (skel)
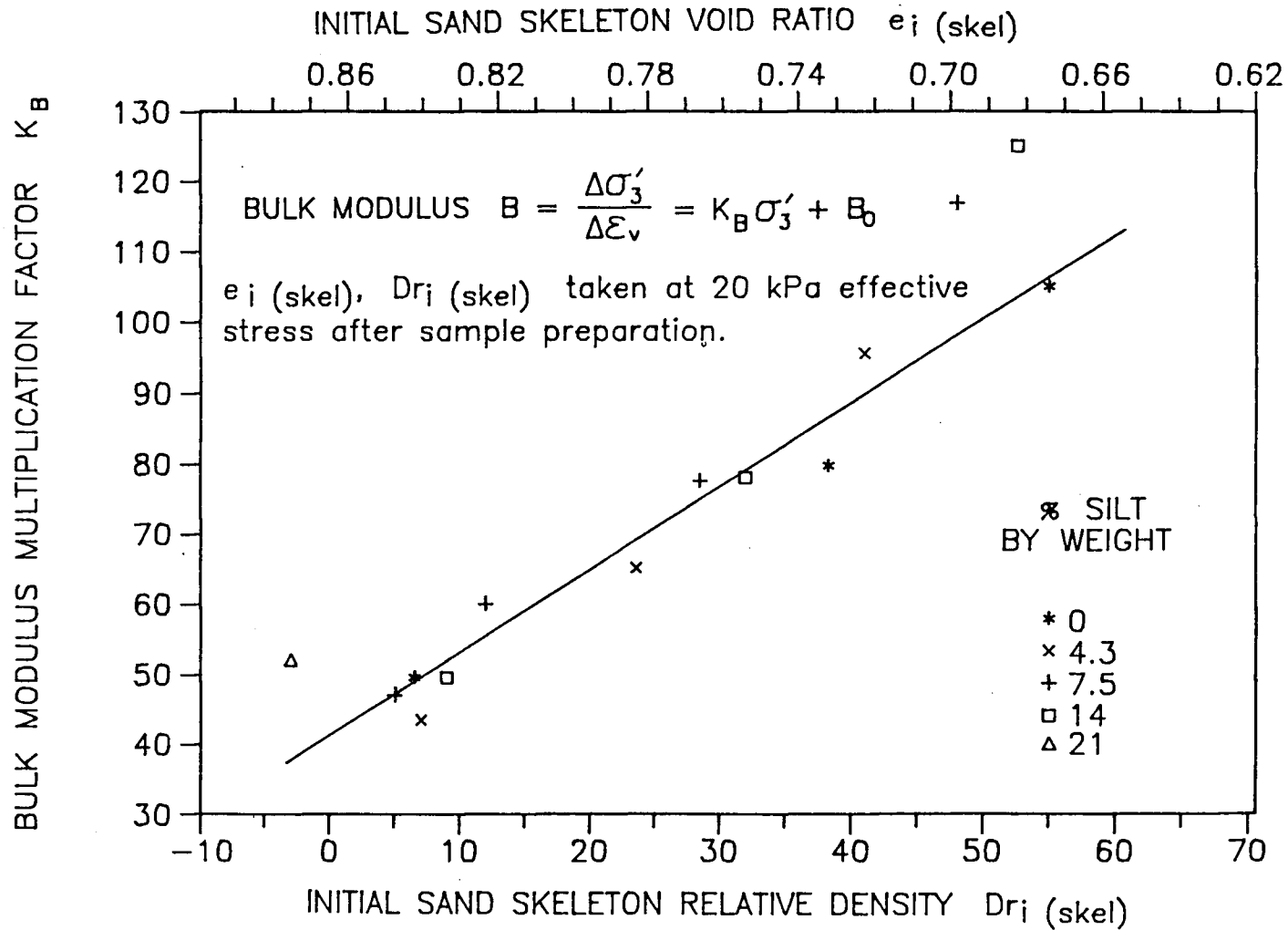
FIGURE 4.10   SUMMARY OF INITIAL COMPRESSIBILITY CHARACTERISTICS
OF SILTY WELL—GRADED 20/200 BRENDA TAILINGS SAND

INITIAL SAND SKELETON VOID RATIO e_i (skel)

BULK MODULUS $B = \dfrac{\Delta \sigma_3'}{\Delta \mathcal{E}_v} = K_B \sigma_3' + B_0$

% SILT
BY WEIGHT

* 0
× 4.3
+ 7.5
□ 14
△ 21

e_i (skel), D_{r_i} (skel) taken at 20 kPa effective
stress after sample preparation.

INITIAL SAND SKELETON RELATIVE DENSITY D_{r_i} (skel)
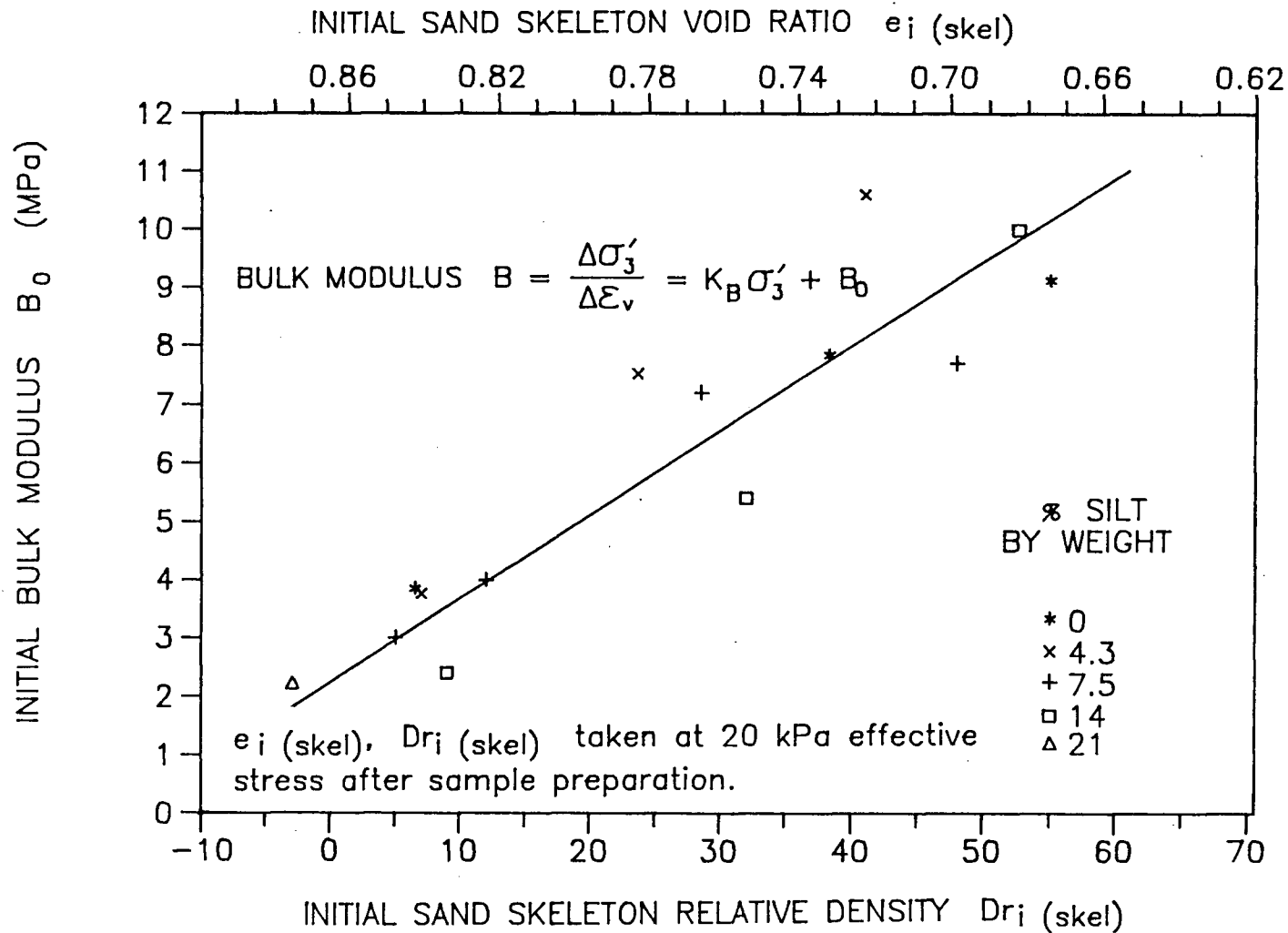
4.4 AXIAL AND RADIAL STRAIN DURING CONSOLIDATION

Although the magnitude of volumetric strain during consolidation is similar for the various loose clean tailings sands tested, there is a large variation in the distribution of axial versus radial strain for each sand, as shown in Figure 4.11. All sands prepared using the slurry deposition or water pluviation technique show much greater radial strain than axial strain during isotropic consolidation. This indicates that these reconstitution techniques give rise to a fabric that is inherently more compressible in the horizontal than in the vertical direction. This type of behaviour has been observed by other workers including Negussey (1984), Ishihara and Okada (1982), and has been suggested as a method for the measurement of inherent anisotropy by El-Sohby (1969).

The slope of the consolidation strain path (incremental strain ratio, see Figure 4.12) may be used as an indicator of the difference between radial and vertical compressibility of a sand sample. If axial strain equals radial strain during isotropic consolidation, the incremental strain ratio would be 1.0 and sand compressibility would be isotropic. If the incremental strain ratio is not equal to 1.0, the compressibility of sand would be anisotropic. It is important to note that

Figure 4.11 Strain paths of various clean sands during isotropic consolidation from loosest state of slurry deposition

60/100

20/40

20/200

WELL GRADED
BRENDA SAND

100/140

$$\mathcal{E}_a = \mathcal{E}_r$$

ISOTROPIC CONSOLIDATION CHARACTERISTICS
FROM LOOSEST STATE OF SLURRY DEPOSITION

OTTAWA C-109 SAND

RADIAL STRAIN $\mathcal{E}_r$

AXIAL STRAIN $\mathcal{E}_a$
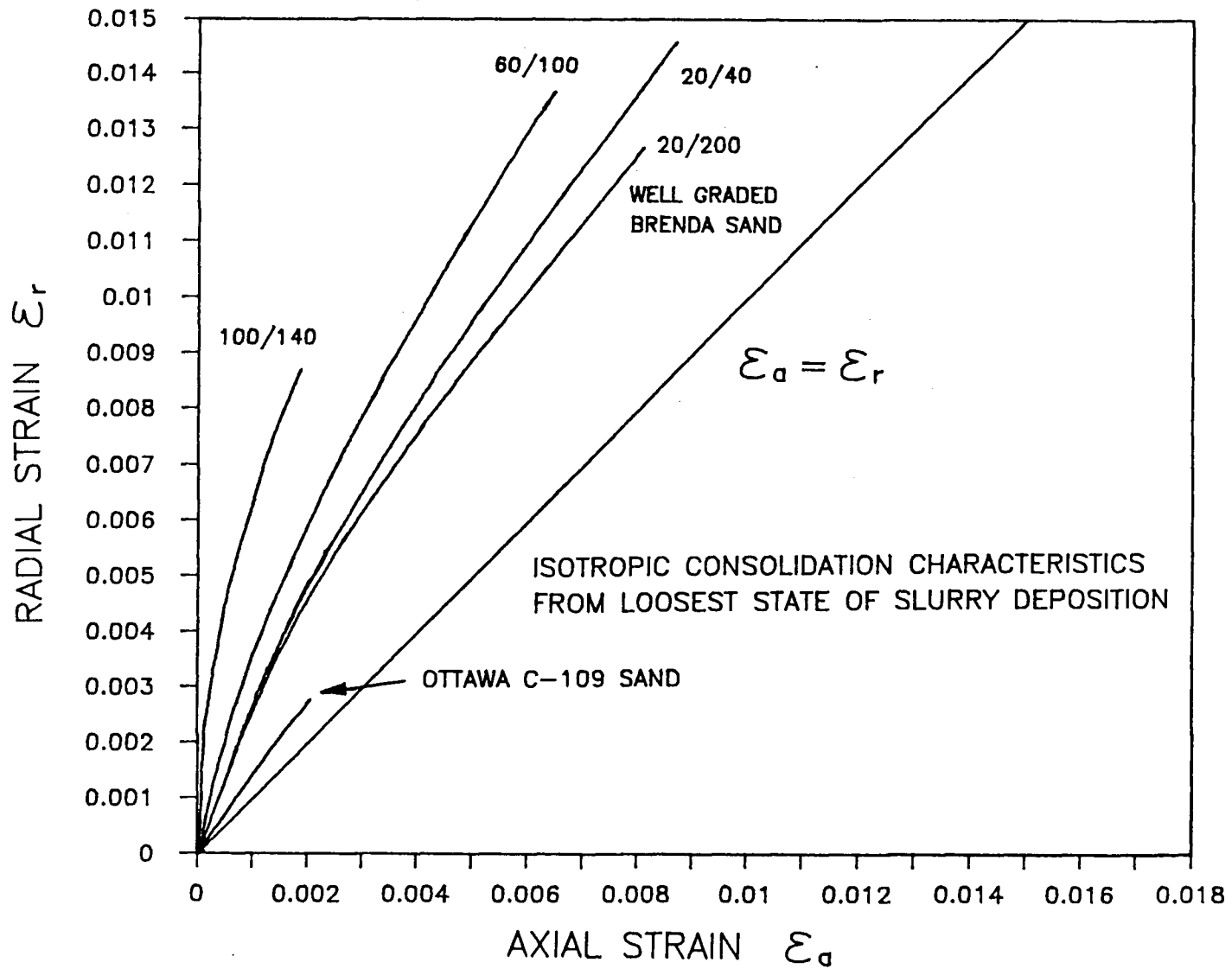
Figure 4.12 Incremental strain ratios of various clean sands during isotropic consolidation from loosest state of slurry deposition

WELL GRADED 20/200 BRENDA SAND

OTTAWA C-109 SAND

20/40

POORLY GRADED 60/100 BRENDA SAND

POORLY GRADED 100/140 BRENDA SAND

ISOTROPIC CONSOLIDATION CHARACTERISTICS FROM LOOSEST STATE OF SLURRY DEPOSITION

INCREMENTAL STRAIN RATIO $\dfrac{\Delta \varepsilon_a}{\Delta \varepsilon_r}$

EFFECTIVE CONFINING STRESS σ'_c (kPa)
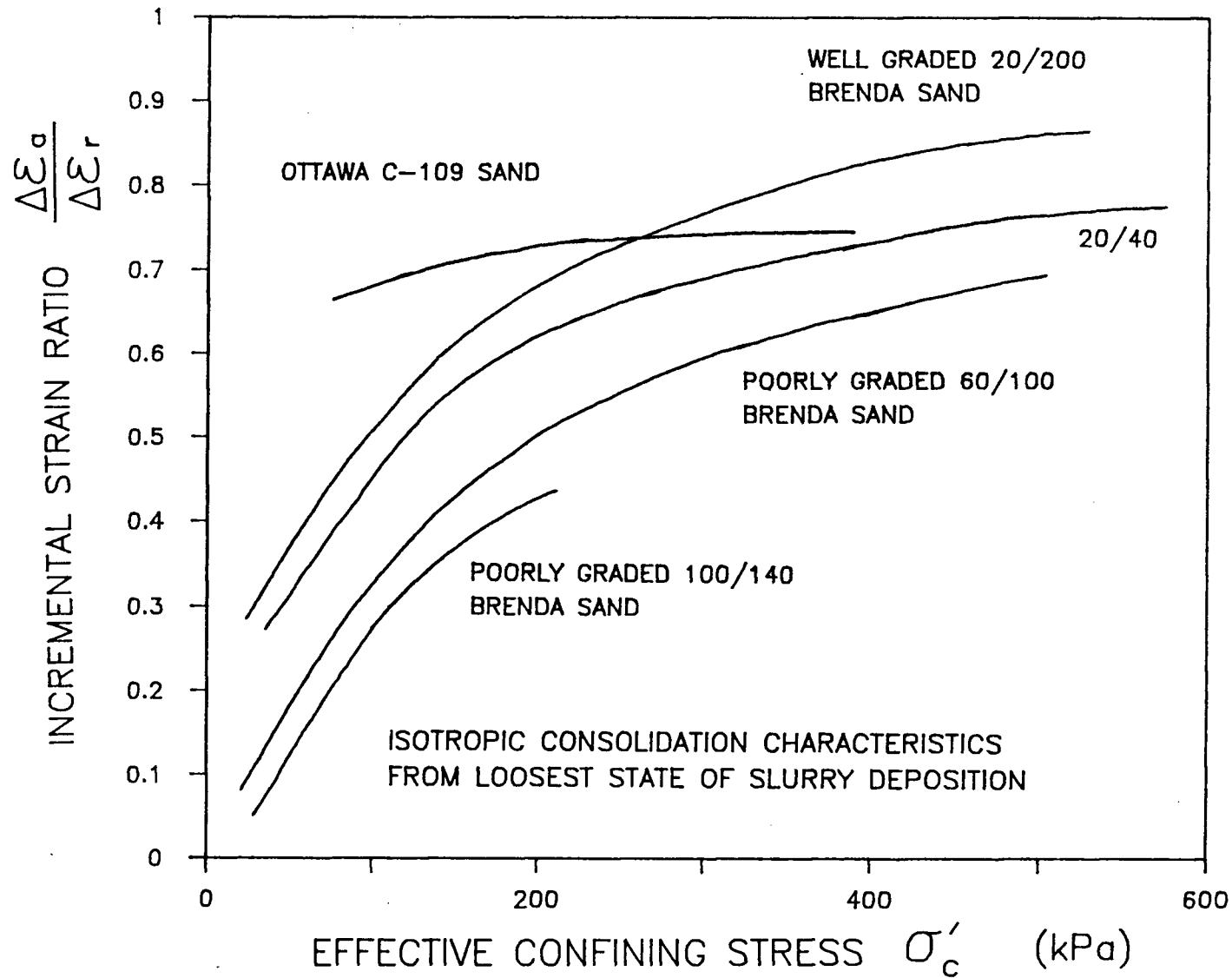
isotropic strain ratios do not ensure isotropic monotonic loading response.

The incremental strain ratio of loose Ottawa sand is shown to be essentially constant with increasing consolidation stress, as was also observed by Negussey (1984). Various gradations of clean tailings sand show a consistent variation of incremental strain ratio with consolidation stress. At low consolidation stess levels, incremental strain ratio is low, indicating that vertical compressibility is much lower than radial compressibility. With increasing consolidation stress, incremental strain ratio increases to an essentially constant value. Apparently, the process of isotropic consolidation alters the anisotropic compressibility properties of tailings sand samples, when consolidated from a very loose state.

Figure 4.12 shows that fine poorly graded tailings sand (100/140 gradation) has the greatest anisotropy in compressibility, while well-graded tailings sand (20/200 gradation) shows the least anisotropy in compressibility.

A large difference between axial and radial strains occurs only during virgin consolidation. If the sand is isotropically unloaded and reloaded after virgin consolidation, the strain path reflects isotropy (axial strain = radial strain) below the maximum past pressure. This feature has been used to estimate membrane penetration correction (Vaid and Negussey, 1984, Method 2). Researchers who use dry or moist tamping to prepare sand samples, which

must be saturated after deposition, generally observe essentially isotropic behaviour during virgin consolidation following saturation (Miura and Toki, 1982). It has also been observed that sands which are saturated after deposition are much less compressible during virgin consolidation than water pluviated sands. One may conclude that sands which are prepared in a moist or dry state and must be resaturated display a form of overconsolidation behaviour.

Consolidation strain paths shown in Figure 4.11 are dependent upon many factors, including void ratio, stress level, strain history, time dependent creep behaviour, and perhaps most importantly the fabric that results from sample preparation technique. The strain paths shown in Figure 4.11 are average results for several tests performed on each sand type.

CHAPTER 5

UNDRAINED MONOTONIC LOADING BEHAVIOUR

5.0   INTRODUCTION

The results of undrained monotonic loading tests on clean and silty Brenda sands are presented and compared. Tests were conducted on poorly-graded sands with different D_{50} (gradations 20/40, 60/100 and 100/140), a well-graded sand (20/200) with a D_{50} similar to that of 60/100 poorly-graded sand, and well-graded 20/200 sand which contained various amounts of silt (see Section 3.2.1.2 for grain size distributions). Samples of each sand were prepared at loosest state of slurry deposition. Consolidation from this state yields soil which displays the most contractive undrained loading response expected for each water deposited material. Samples were isotropically consolidated. Both triaxial compression and extension test were performed over a range of confining stresses. Samples were tested from an initial state of isotropic consolidation in order to emphasize the effects which direction of loading have upon soil behaviour. The effects of inherent anisotropy in water pluviated sand are identified in test results. Soil properties specific to water pluviated sand are identified and discussed, and various methods of sand behaviour categorization are assessed.

5.1 UNIQUENESS OF UNDRAINED RESPONSE

For saturated soil at a given consolidation and density state, the undrained stress-strain response and effective stress path are unique regardless of the total stress path, as long as the direction of major principal stresses remains the same in relation to the sand deposition direction (Bishop and Wesley, 1973; Vaid et al., 1988). This is shown in Figure 5.1 for coarse-grained Brenda 20/40 sand in compression loading by two different total stress paths (denoted A and B). Results of a conventional triaxial compression test (with radial total stress constant) and an active triaxial test (with axial total stress constant) are shown. Essentially identical stress-strain response and effective stress path may be noted for the two tests. The undrained extension response is also unique, although the extension effective stress path is in general not identical to compression path, as discussed in Section 2.1.3.1. At a given confining pressure, undrained effective stress path depends on void ratio, but it may also be affected at the same void ratio by (1) prestrain history (Finn et al., 1970; Seed et al., 1975; Ishihara et al., 1978, 1982), (2) membrane penetration, and (3) sample preparation method (Mulilis et al., 1975; Marcuson and Townsend, 1974; Tatsuoka et al., 1986).

Uniqueness of effective stress path for a given loading mode requires that pore pressure generated during undrained

Figure 5.1 Verification of independence of effective stress path from total stress path in undrained monotonic compression loading of Brenda 20/40 sand
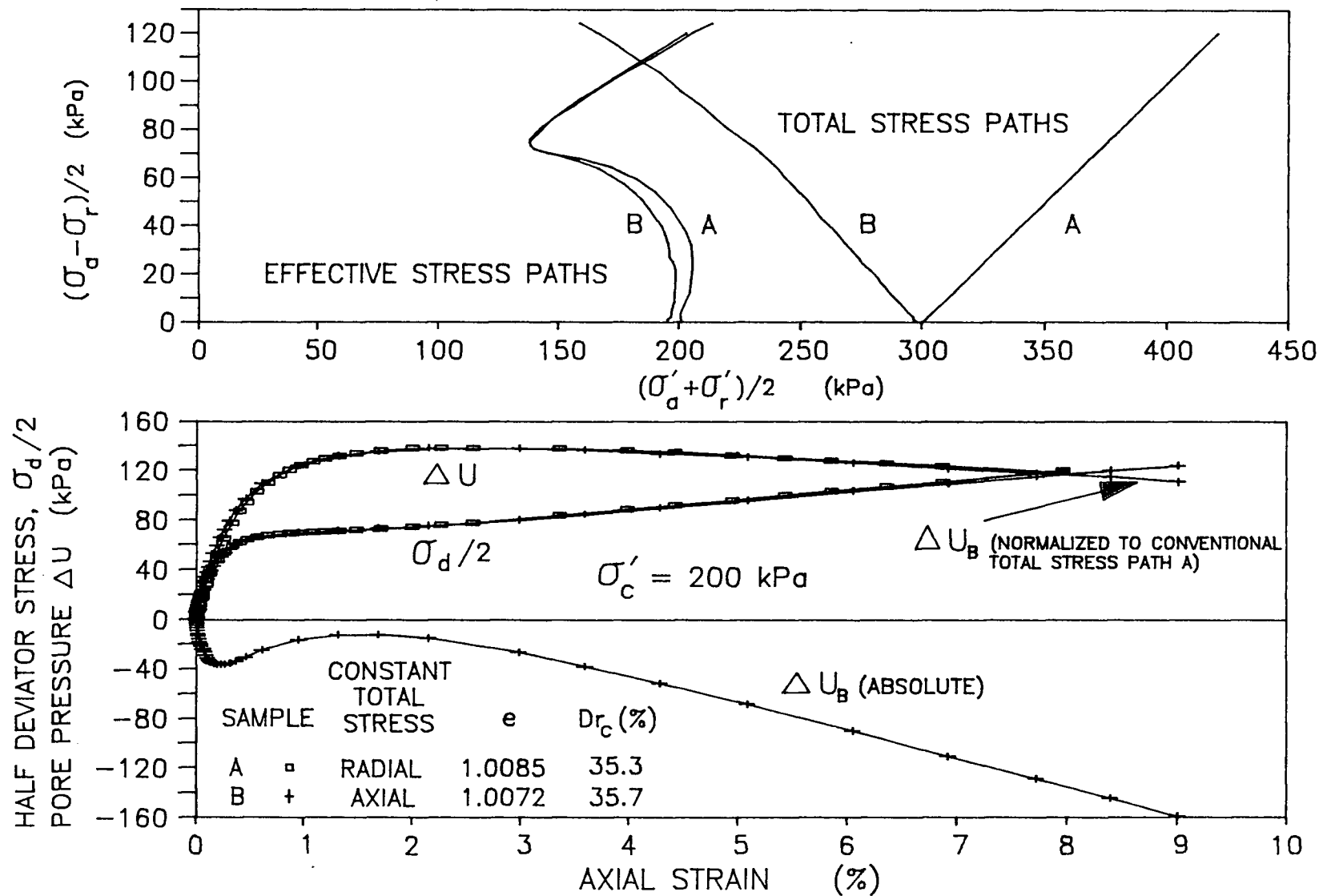
loading be dependent upon total stress path. This is shown for compression test A and B in Figure 5.1. Absolute pore pressure response is clearly not unique. The fact that pore pressure response is not unique makes it a rather poor index property for the comparison of soil behaviour subject to different modes of loading.

5.2 BEHAVIOUR OF CLEAN SANDS

Figure 5.2 through Figure 5.4 display the monotonic loading behaviour of various clean Brenda sand gradations. The sands were consolidated from loosest state of slurry deposition, to various levels of consolidation stress. For comparison purposes, the response of clean sands at 200 kPa consolidation stress has been summarized in Figure 5.5.

5.2.1 Stress-Strain Response

The results presented in Figure 5.2 through 5.5 show typical undrained stress-strain response of Brenda sand. All gradations show a considerable difference or anisotropy between extension and compression loading response. This sort of anisotropy in soil behaviour has been observed for natural and reconstituted sands by several workers, including Ishihara et al. (1978,1982), Chang et al. (1982), Miura and Toki (1982), and Chung (1985). Test results show that anisotropy in undrained response is affected by both grain size and gradation. Poorly-graded gradations of sand

Figure 5.2   Undrained monotonic triaxial test results for 20/40 Brenda sand
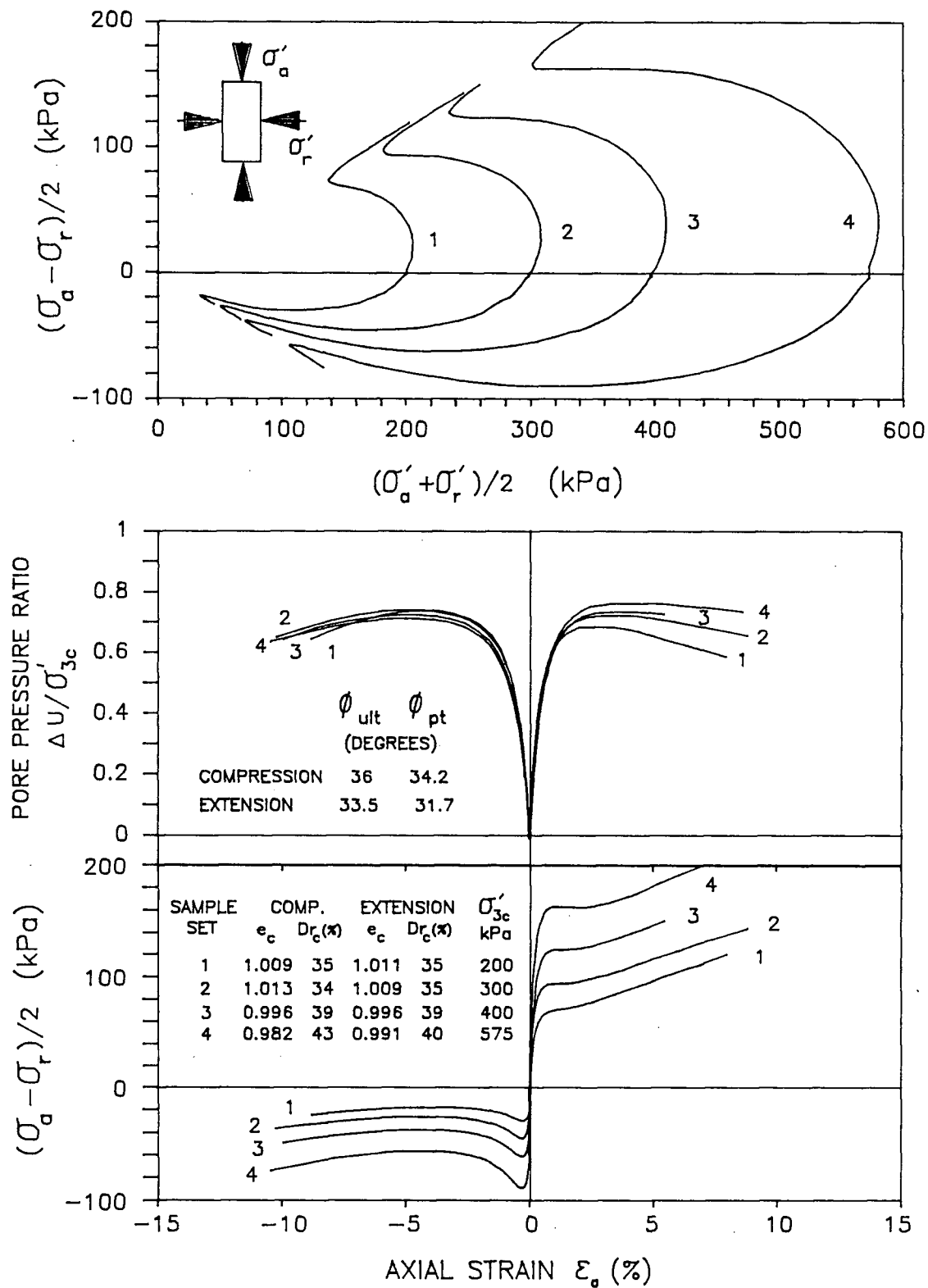
Figure 5.3 Undrained monotonic triaxial test results for 60/100 Brenda sand
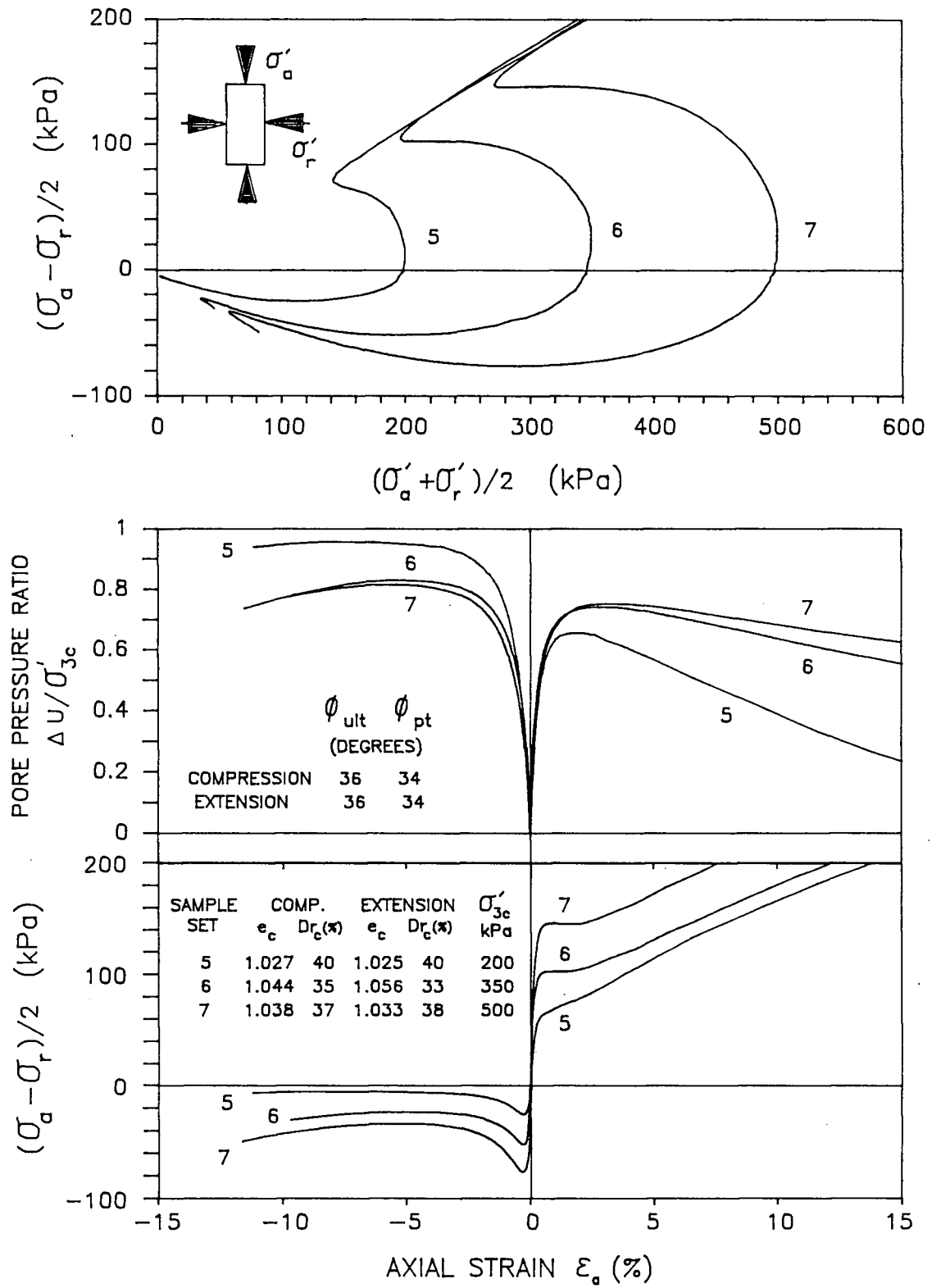
Figure 5.4   Undrained monotonic triaxial test results for 20/200 Brenda sand

SAMPLE	COMP.		EXTENSION		σ'_{3c}
SET	e_c	$Dr_c(\%)$	e_c	$Dr_c(\%)$	kPa
8	0.767	28	0.768	28	200
9	0.763	29	0.765	29	350
10	0.770	27	0.771	27	500

	ϕ_{ult}	ϕ_{pt}
	(DEGREES)	
COMPRESSION	36	33.9
EXTENSION	33.6	31.4
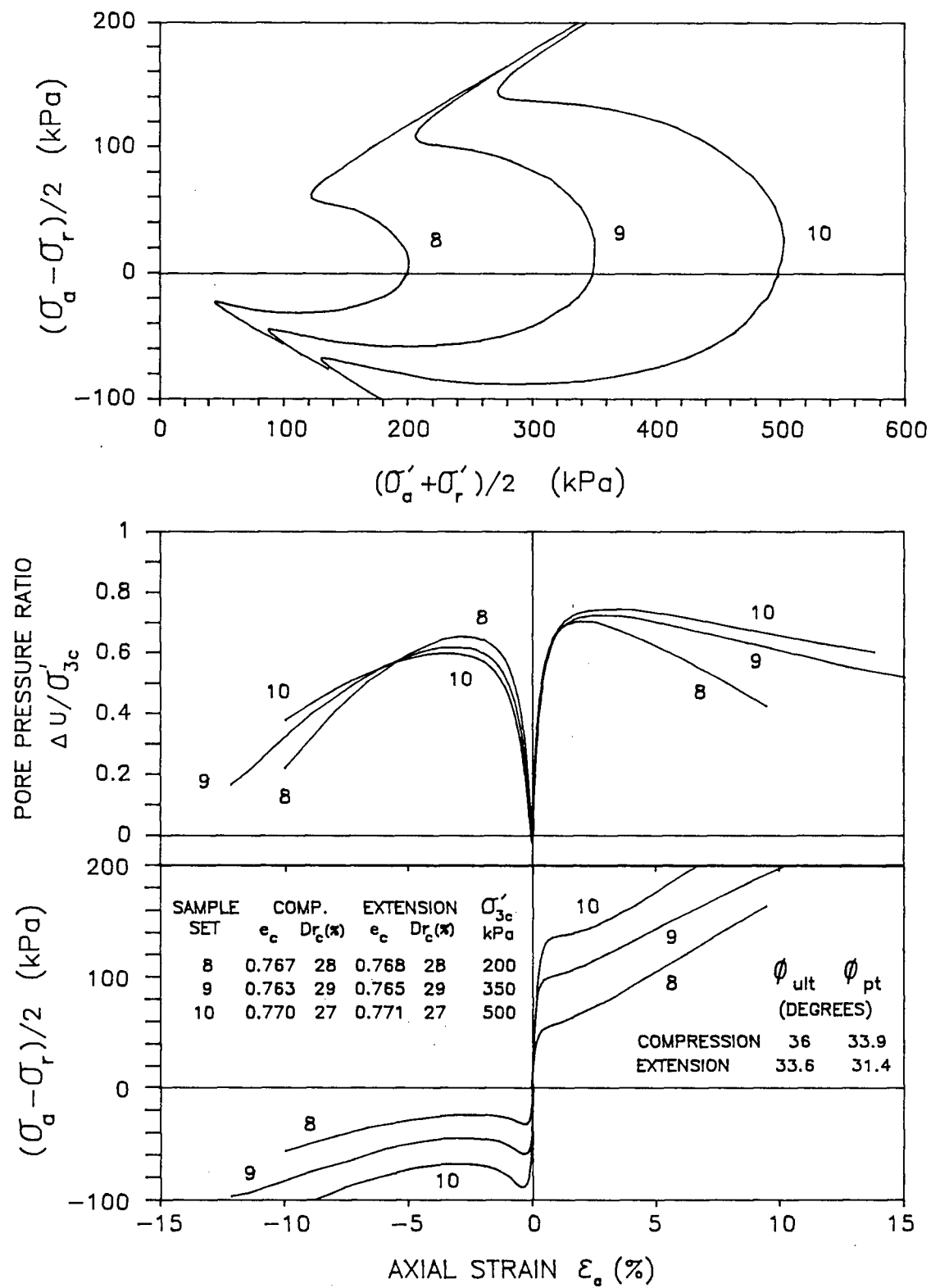
Figure 5.5   Undrained monotonic triaxial test results for various sand gradations
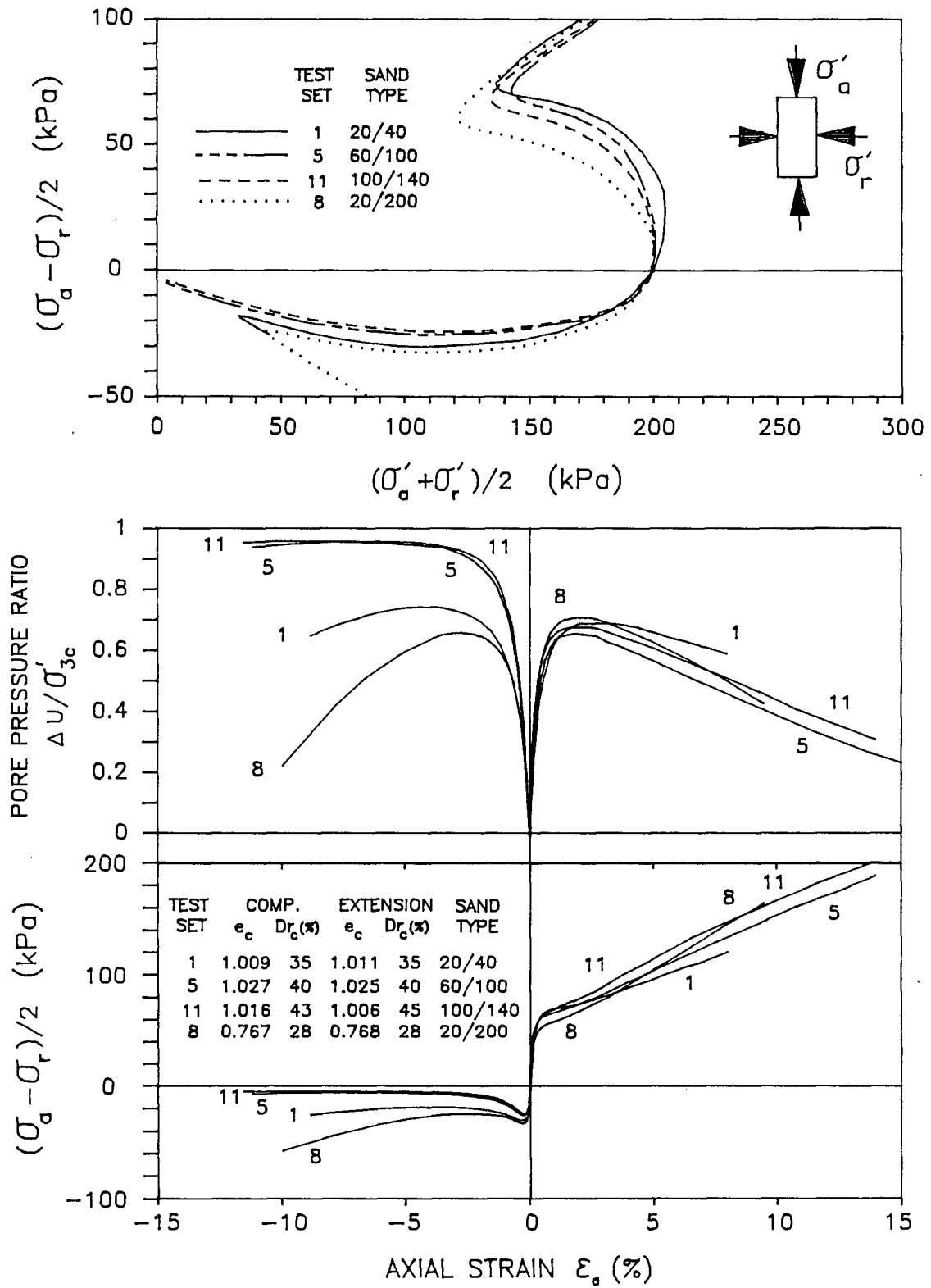
(20/40, 60/100 and 100/140) exhibit considerably more anisotropy than the well-graded 20/200 sand. Finer grained uniform 60/100 and 100/140 sands have typically dilative soil response in compression loading, yet almost steady-state liquefaction response in extension loading. Well-graded 20/200 sand has limited liquefaction response in extension loading, with larger strength at phase transformation state than observed in any of the poorly-graded sands.

The various Brenda sands which have been consolidated from loosest state of slurry deposition show similar behaviour in compression loading but rather different behaviour in extension loading. These results suggest that although the behaviour of different soils in one particular mode of loading may be similar, this does not ensure similar behaviour in other modes of loading. These results also suggest that soils with different fabrics may have either different or similar soil properties. It is suggested that compression loading test results are similar only because each soil was deposited at loosest slurry deposition state. The density of sands deposited by vertical settlement through water is governed by the vertical load bearing capacity of the material at low stress level. Apparently the loosest state vertical compressibility properties of the various soil gradations is similar, with this similarity being maintained at higher consolidation stress level.

5.2.2 Effective Stress Path Response

The various effective stress path responses shown in Figures 5.2 through 5.5 emphasize the effect of mode of loading on undrained behaviour. Figure 5.5 shows that uniform fine grained sands (60/100 and 100/140) have similar behaviour, which is considerably different from that of either coarse grained 20/40 sand or well-graded 20/200 sand. The effective stress path of coarse grained 20/40 sand is probably affected by membrane penetration. Membrane penetration causes a characteristic stiffening of undrained response due to lower induced pore pressures. Membrane penetration effects during undrained loading are believed to be minor for the finer grained sands tested (see Table 3.2).

A peculiar feature of the compression loading response of the well-graded 20/200 sand shown in Figure 5.5 is that at low deviator stress and strain level, this sand is slightly softer than poorly-graded sand, yet at high deviator stress and strain level, well-graded sand is slightly stiffer than poorly-graded sand. This behaviour is probably a result of the difference in fabric within well-graded and poorly-graded water-pluviated sands.

Effective stress path plots show quite clearly that well-graded sand behaviour is less anisotropic than poorly-graded sand behaviour.

5.2.3 Pore Pressure Response

As described in Section 5.1, pore pressure response is not unique, but dependent upon total stress path. Pore pressure data shown in Figures 5.2 through 5.5 reflects the influence of total stress path and mode of loading. Direct comparison of pore pressures generated in compression and extension loading may lead to unrealistic conclusions, due to the difference in total confining stress between compression and extension modes of loading.

To separate shear induced pore pressure from changes in pore pressure induced by changes in mean normal stress, pore pressure data has been plotted using Henkel's (1960) pore pressure parameter 'a' (see Figure 5.6). Figure 5.6 shows clearly that shear induced pore pressures generated in extension loading are considerably larger than those generated in compression loading for all sand types tested. Fine grained uniform sands are shown to have the greatest anisotropy in loading response, while well-graded sand is shown to have the least anisotropy in loading response.

Pore pressure parameter 'a' curves are normalized with respect to consolidation stress. The curves show that anisotropy in soil response is reduced by increasing isotropic consolidation stress. There is a general trend towards larger 'a' parameters in compression loading and smaller 'a' parameters in extension loading, at higher isotropic consolidation stress. There is also a general

Figure 5.6 Plot of Henkel's pore pressure parameter 'a' versus strain for various gradations of undrained Brenda sand
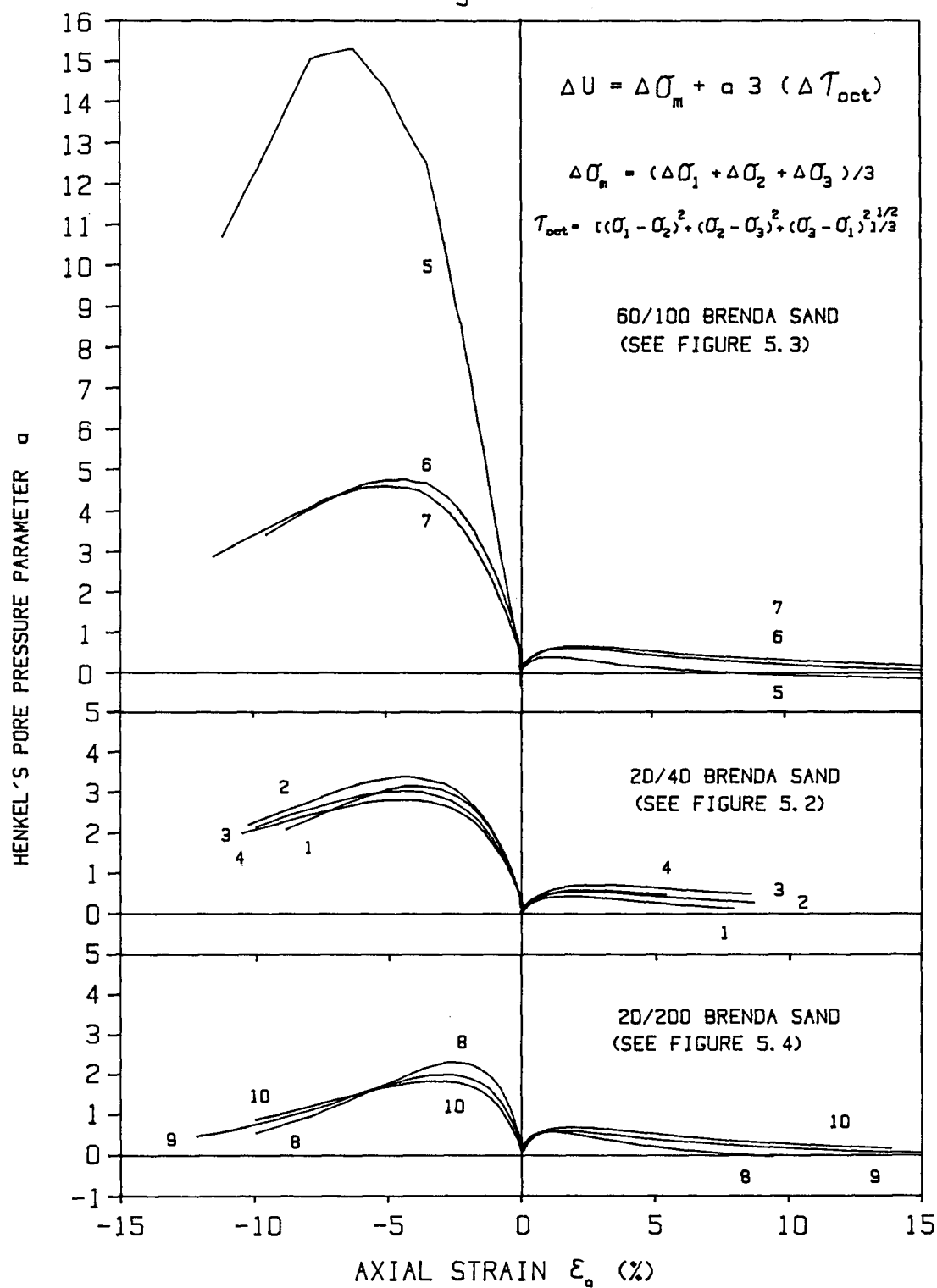
trend toward smaller variation in 'a' parameter with variation in strain level at higher consolidation stress.

5.2.4 Effect of Consolidation Stress

An increase in isotropic consolidation stress affects extension and compression loading response differently. All sand types show a tendency toward more contractive response in compression loading at higher consolidation stress. This contrasts significantly with a tendency toward more dilative response in extension loading at higher consolidation stress. There is a trend towards lessening difference between compression and extension response with increasing consolidation stress. This implies a change in the nature of inherent anisotropy with changing level of consolidation stress. The observed tendency towards more isotropic behaviour at higher consolidation stress is similar to that observed in consolidation strain data (see Section 4.4). Consolidation stress level is observed to have less of an effect upon sample anisotropy than soil gradation.

The observed increase in dilatancy of extension loading response with increasing isotropic consolidation stress may only be characteristic of lower stress range behaviour of water pluviated sand, due to the highly anisotropic nature of water pluviated sand after deposition. Different behaviour may be observed at much larger consolidation stress, or under anisotropic consolidation stress conditions. Anisotropic consolidation with vertical stress

larger than horizontal stress has been observed to decrease dilatancy and strength in extension loading.

5.2.5 Effect of Grain Size and Gradation

For loosest state slurry deposited sands, compression loading response is similar regardless of gradation, while extension loading response is apparently quite dependent upon gradation. The observed trend toward more dilative behaviour in extension loading in more well-graded sand could be explained by the trend toward lower absolute void ratio within more well-graded sand. This explanation is not completely convincing because it cannot explain the small difference in compression loading response between the various sands tested. Consolidation from loosest state of slurry deposition is observed to produce variable relative densities, although all sands consolidated from loosest slurry deposition state have similar bulk modulus or volume change characteristics (see Section 4.3). There does not appear to be a simple relationship between the relative density of soil and its undrained loading response. The differences between responses of different soil gradations can be best explained as differences in soil fabric and inherent anisotropy which are the result of differences in soil gradation. Uniform sands show the greatest degree of anisotropy, while well-graded sands show a tendency toward more isotropic behaviour. Coarse grained 20/40 sand shows a slightly more dilative response than other uniform sands,

which could be a consequence of membrane penetration effects. Membrane penetration effects are believed to be negligible for other sands tested.

5.3 MATERIAL PARAMETERS

Various material parameters, such as critical stress ratio, phase transformation angle, ultimate friction angle (or friction angle at maximum obliquity), and steady-state concepts have been used by various researchers (see Section 2.0) to characterize undrained behaviour, with the assumption that the material parameters are constant for a specific type of sand. Test results of Brenda tailings sand indicate that sand material parameters such as phase transformation angle and friction angle at maximum obliquity are indeed fairly consistent between various test samples and stress paths, while other parameters such as critical stress ratio and steady-state concepts are not generally applicable. Table 5.1 presents a summary of the material properties.

5.3.1 Ultimate Failure Envelope

Friction angle at maximum obliquity (Ishihara et. al., 1975), or boundary surface friction angle (Chang et. al., 1982), has been shown to be fairly constant for various types of sands tested using the undrained triaxial test. This angle has a general dependence upon soil mineralogy and

Table 5.1 Sand sample undrained friction angles

Undrained friction angle (Degrees)

	Compression			Extension		
	ϕ_{ult}	ϕ_{pt}	ϕ_{CSR}	ϕ_{ult}	ϕ_{pt}	ϕ_{CSR}
Brenda Sand Gradation						
20/40 WP	37.5	35.2		37.5	34.5	18
20/40 SD	35.6	34.2	26.4	33.0	31.7	17.0
60/100 SD	36.0	34.0	26.4	36.0	34.0	16.1
100/140 SD	35.3	33.0				12.0
20/200 SD	36.0	33.9		34.0	31.4	19.0
C−109 (Chern, 1985)	38.2	36.5	25.1			
Ottawa C−109 Sand						
SD	30.6	29.5	20.0			9.1
WP	30.9	30.1	21.5	31.5	29.5	10.7
(Chern, 1985)	31.5	29.5	23.5			
(Chung, 1985)	31.5	29.5	23.0	31.5	29.5	13.5

WP = Loosest state water pluviated sand

SD = Loosest state slurry deposited sand

the intrinsic angle of friction between mineral grains. Some researchers have found slight variations in this angle for a single type of sand material as follows: (1) some variation with stress and strain level, first increasing with increasing strain and then decreasing to phase transformation angle at very large strain (Castro et. al., 1982, see Figure 2.2), (2) some increase with an increase in relative density (Chang et. al., 1982, Miura and Toki, 1982), (3) some variation between triaxial extension and compression tests (Chang et. al., 1982, Miura and Toki, 1982), and (4) some variation with sample preparation technique or sand fabric (Miura and Toki, 1982).

As shown in Table 5.1, a friction angle at maximum obliquity of 36 degrees is fairly consistent for all Brenda sand gradations tested in compression loading. Extension loading results are not as consistent as compression results, varying from 36 degrees for 60/100 sand to 34 degrees for 20/200 sand and 33 degrees for 20/40 sand. The slight variations in extension friction angles at maximum obliquity could be due to several factors, including the following: (1) variation with effective stress level, as extension loading stress paths reach ultimate failure at much lower effective confining stress than compression loading stress paths, (2) some natural variation in material properties between extension and compression loading for different sand gradations, (3) incomplete development of

ultimate friction angle in the stress and strain range tested.

Some extension test results show a marked decrease in maximum obliquity friction angle at large strain (greater than 10 to 15%) due to the development of conjugate extension failure planes. The development of non-uniform strains in extension test results can be easily identified by this marked decrease in boundary envelope friction angle. The test data derived from strain ranges which are non-representative of elemental soil behaviour have been omitted.

It may be that friction angles at maximum obliquity of various sand gradations in compression loading are similar because stress-strain behaviour in compression loading is similar (see Figure 5.5). Stress-strain behaviour in extension loading is considerably different for the various gradations of loose sands tested. Sand fabric effects which produce the variation of stress-strain behaviour in extension tests may also account for the variation in ultimate friction angles in extension loading (see Section 2.1 and 2.2).

5.3.2 Angle of Phase Transformation

Phase transformation angles for the various sands tested are summarized in Table 5.1. Sand samples prepared by slurry deposition have similar phase transformation angles as samples prepared by water pluviation. Extension

phase transformation angles generally show greater variation with sand gradation than compression angles. Phase transformation angles are consistently 1 to 2 degrees less than the angles of maximum obliquity. As with ultimate friction angles described in the previous section, extension phase transformation angles may be slightly different between different gradations due to differences in sand fabrics.

5.3.3 Critical Stress Ratio

Critical stress ratios of Brenda sand (see Section 2.1.1) are quite variable between compression and extension loading (Table 5.1), thus CSR values may be assumed to be a function of mode of loading. Compression loading CSR-friction angle values (obtained in higher consolidation stress samples only) are fairly constant at 26 degrees. Extension loading CSR values are much lower and have been shown to vary with (1) initial sample preparation relative density before consolidation (Chung, 1985), and (2) factors such as sample preparation technique or sample strain history (see Section 2.1). Table 5.1 indicates that critical stress ratio in extension loading also varies with soil gradation when consolidation from loosest state of slurry deposition is used as a soil density reference. Extension CSR values for a specific sand gradation and initial preparation density are found to be constant with increasing confining stress over the consolidation stress

range tested, as has been found for Ottawa C-109 sand which is isotropically consolidated to various stress levels from the same initial preparation density (Chung, 1985). As a generalization, one may state that more anisotropic poorly-graded sands are more likely to have lower CSR values than well-graded sands.

From test results, one may conclude that a compression loading CSR-friction angle value of 26 degrees is a maximum value for Brenda sand, because it is observed in samples which have only minor limited liquefaction behaviour and are generally dilative in triaxial compression loading. Lower CSR values are possible and depend upon the factors described above. Thus it may be unconservative to assume a design CSR value based upon compression loading test results, as lower CSR values are possible and indeed likely in some field loading conditions. Sand micro-fabric factors which determine CSR values in undrained loading are probably different in compression and extension loading (see Section 2.2 and Section 7.0). Generalizations made about compression loading CSR values (Castro, 1982, Sladen et. al., 1985, Mohamad and Dobry, 1986) may not apply to extension loading CSR values, CSR values determined from loading conditions other than the triaxial compression test, or CSR values determined from samples which are prepared in a different manner or have a strain history which differs from that used in the test series upon which the generalizations are based.

5.3.4 Steady-State Concepts

The triaxial test results show clearly that steady state concepts (Castro et al., 1982) do not apply to the undrained loading response of Brenda sand. Steady state concepts imply that undrained strength is solely a function of soil void ratio, and is not dependent upon the direction of loading or the type of test performed. Undrained tests performed on water pluviated Brenda sands clearly do not fit these criteria (Chung, 1985 shows a similar dependence of undrained strength upon direction of loading in water pluviated Ottawa C109 sand). If only compression test results up to 600 kPa effective confining stress are considered, Brenda sand is found to be non-susceptible to liquefaction or limited liquefaction. If extension behaviour is considered, Brenda sand is found to be highly contractive and susceptible to liquefaction, especially at low consolidation stress levels. Such dependence of soil dilatancy and undrained strength on direction of loading would have serious implications in the use of steady state concepts of design (Castro et al., 1982), wherein a unique steady state line obtained from compression tests is the key assumption. It would be negligent not to consider triaxial extension test results in an analysis of sand liquefaction resistance.

The difference in the observed compression versus extension response of water pluviated sand is a reflection of the inherent anisotropy of the material with respect to

the direction of maximum principal stress of loading. The angle between the maximum principal stress and the deposition direction (vertical under gravity) is designated α. Compression mode corresponds to $\alpha=0^{\circ}$ while the extension mode corresponds to $\alpha=90^{\circ}$. Softer response under horizontal loading (as also noted in consolidation strain data, Section 4.4) is mainly responsible for contractive behaviour in extension but dilative behaviour in compression loading. A similar difference in triaxial compression and extension undrained response has been reported by others (Bishop, 1971; Miura and Toki, 1982; Hanzawa, 1980; Chang et al., 1982; Chung, 1985). Recent undrained testing using the hollow cylinder test apparatus which may induce a full range of variation of maximum principal stress direction from $\alpha=0$ to $\alpha=90$ degrees shows that water pluviated sand undergoes systematic weakening under increasing α (Symes et al., 1985; Shibuya and Hight, 1987). These test results indicate that water pluviated sand is most contractive under a triaxial extension mode of loading, and least contractive or most dilative under a triaxial compression mode of loading.

The nature of inherent anisotropy in moist tamped specimens appears to be similar but possibly not as pronounced as that in water deposited sands (Hedberg, 1977). This could be attributed to one-dimensional vertical compression in the forming mold similar to that which occurs during water deposition. Consequently, moist tamped materials would also show directional variation in undrained

behaviour. It is surprising that researchers engaged in the development and application of steady state concepts have remained oblivious to path dependence of undrained response, when such a dependence in clay has been routinely considered since the pioneering work of Bjerrum (1972).

Although the undrained strengths at phase transformation or steady state in compression and extension are different, the friction angle is essentially identical. Therefore, the phase transformation or steady state line for contractive response in void ratio stress space (Vaid and Chern, 1985) is not unique, though these lines are essentially unique in effective stress space. These differences in undrained steady state or phase transformation strength are due mainly to larger pore pressures induced in extension on account on greater horizontal compressibility.

Under field loading conditions, one could expect a large variation in principal stress directions, even within a simple soil embankment or foundation. Thus it is important that a directional dependence of soil strength be considered in the stability assessment of soil structures.

5.4 EFFECT OF SILT CONTENT UPON UNDRAINED MONOTONIC LOADING RESPONSE

The undrained effective stress paths and stress-strain response of monotonically loaded silty well-graded 20/200 sand samples deposited at loosest state by the slurry

deposition method and isotropically consolidated to 350 kPa effective stress are shown in Figure 5.7. Since the loosest state void ratio obtained by slurry deposition decreases substantially with increasing silt content (see Figure 4.4) the response shown in Figure 5.7 represents a large range of void ratios. The ASTM standard relative densities of the loosest state samples are shown to increase substantially with increasing silt content (Figure 5.7), from 29% at zero silt content to 98% at 22.3% silt content. The sand skeleton void ratio of the samples (see Section 3.2.2.4 for a definition of sand skeleton void ratio) is shown to vary less with increasing silt content (Figure 5.7).

Figure 5.7 shows that the compression loading behaviour of the silty 20/200 sand is dilative with a trend towards increasing dilatancy as silt content is increased. The behaviour in extension loading is contractive with limited liquefaction, and a trend towards less contractive behaviour as silt content is increased. The compression behaviour appears to be more greatly affected by an increase in silt content than the extension behaviour.

Ishihara et. al. (1980) suggest that relative density is not a suitable index for characterizing the behaviour of silty sands. Instead they suggest the use of void ratio for comparing the behaviour of silty sands. The void ratio and relative density data shown in Figure 5.7 suggests that both relative density and void ratio are poor indices for characterizing the behaviour of silty sands, because both

Figure 5.7 Undrained monotonic triaxial test results for silty 20/200 sand
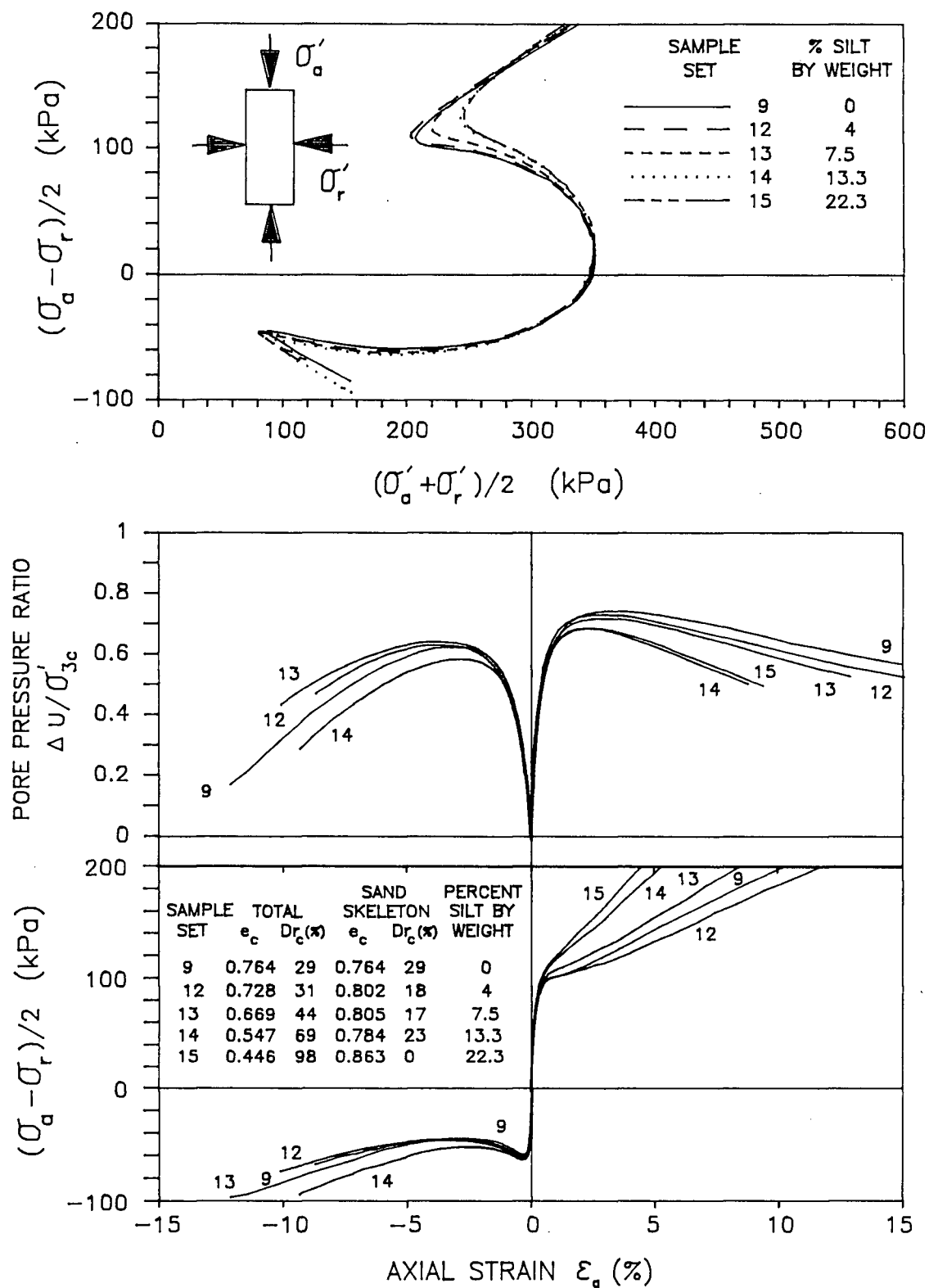
density parameters vary substantially with increasing silt content, yet soil behaviour is not observed to vary a large amount with increasing silt content.

The minor changes in soil behaviour with increasing silt content suggest that the silt within the silty sands may be occupying sand skeleton void space and for the most part have little effect upon soil behaviour. To investigate the effect of silt content upon silty sand behaviour, it is instructive to ignore the silt fraction of the soil and compare soil properties in terms of sand skeleton void ratio (see Section 3.2.2.4), as all silty 20/200 sands tested have the same gradation and thus similar sand skeletons. It may be seen that consolidation of silty 20/200 sand from loosest state of slurry deposition produces samples which have similar sand skeleton void ratios (Fig. 5.7), in contrast to total void ratios which vary considerably with silt content. This may explain the observation that the sand behaviour does not change much as silt content is increased.

Figure 5.8 shows that phase transformation and angle of maximum obliquity increase slightly (up to 2 degrees) with increasing silt content. Effective friction angles of 20/200 sand in extension and compression loading also become equal when silt is added. As described in Section 5.3, undrained friction angles have been found to vary slightly with density and sand fabric, thus it is not unexpected that they may also vary with silt content. Rowe (1962, 1971) shows test results which indicate that the friction angle of

Figure 5.8 Variation of near loosest state silty 20/200 sand undrained friction angles with silt content
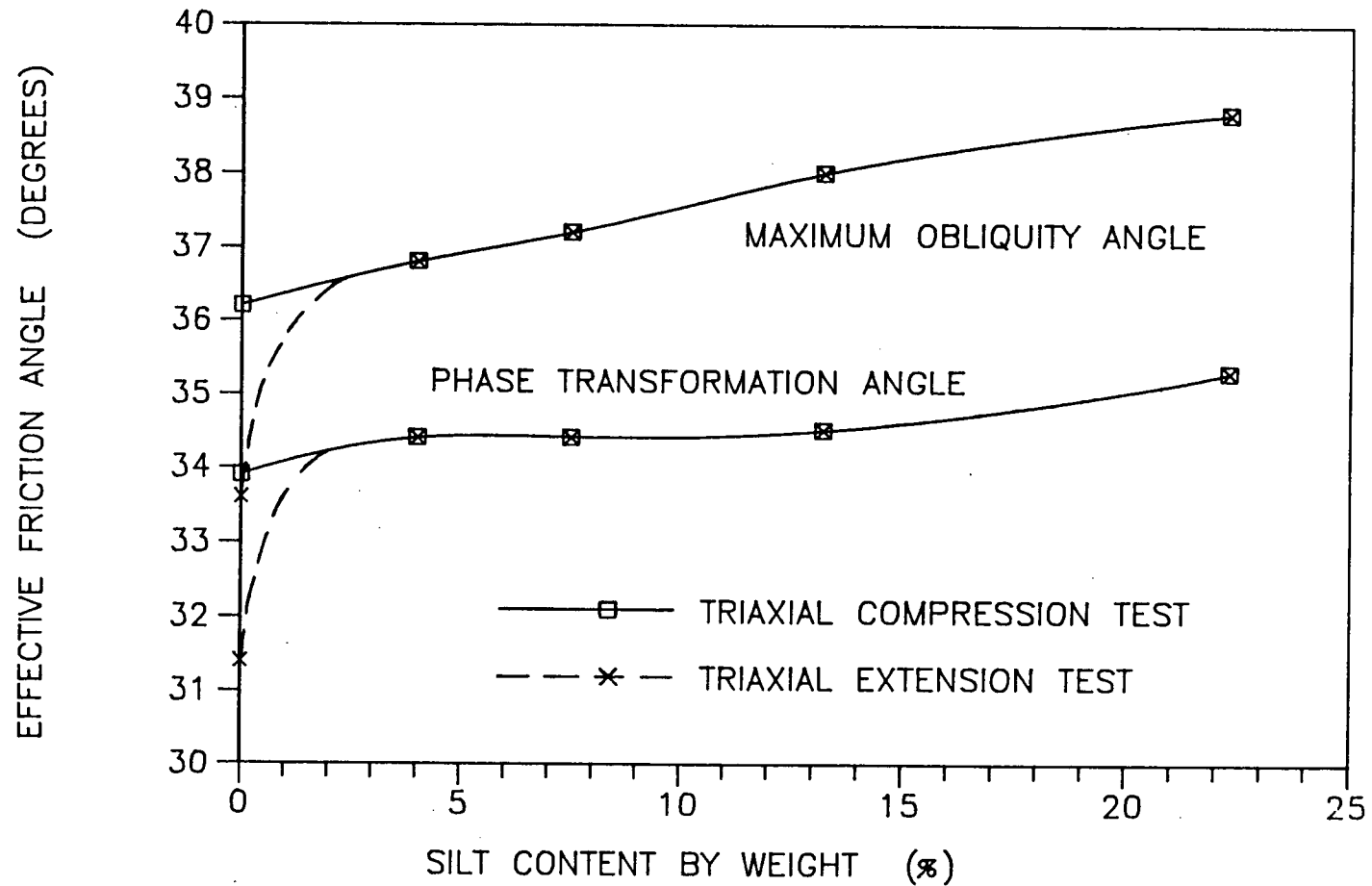
a material increases with decreasing grain size, which may account for the increase in effective friction angles of silty 20/200 sand with increasing silt content.

CHAPTER 6

CYCLIC TRIAXIAL TEST RESULTS

6.0 INTRODUCTION

Cyclic triaxial tests were conducted on samples of silty Brenda 20/40 and 20/200 sand to determine the effect of silt content upon the resistance of silty sand to liquefaction. Both poorly-graded and well-graded sands showed similar variation in cyclic strength with change in silt content. Thus only the behavior of silty well-graded 20/200 sand is discussed in detail, as natural silty sands are in general more well-graded.

Triaxial test samples were isotropically consolidated to 350 kPa effective stress. The consolidation stress used is within the range in which liquefaction of in situ soil deposits is generally encountered. Isotropic consolidation rather than anisotropic consolidation was chosen for the following reasons: (1) sample preparation is simpler, (2) the effect of anisotropic consolidation upon undrained cyclic triaxial test results is complex and not well understood, with conflicting views reported in the literature (Lee and Seed, 1967, Lee et. al. 1975, Seed et. al. 1975, Seed, 1983, Castro, 1969, 1975, Casagrande, 1976, Castro and Poulos, 1977, and Castro et. al. 1982), and (3) most correlations between field and laboratory behaviour of

soils are based upon isotropically consolidated test samples.

Anisotropic consolidation may increase or decrease the susceptibility of a triaxial specimen to liquefaction, depending upon many factors including degree of anisotropic consolidation, density, and sand type (Vaid and Chern, 1983, Mohamad and Dobry, 1986), and various factors which affect sand fabric, such as method of specimen preparation. The effect of anisotropic consolidation has also been shown to be a function of method of loading. Seed (1979) shows that anisotropic consolidation affects simple shear and triaxial test results differently.

The cyclic triaxial test does not, in general, model a specific form of field cyclic loading. An element of field soil subject to cyclic loading may have partly stress and partly strain controlled boundaries, variable mechanisms of loading (from simple shear to plane strain), and variable directions of loading, a factor which is important if soil properties are anisotropic. The question then arises as to how one may best use the triaxial test to determine cyclic strength of soil for correlation purposes. To address this question, it is instructive to consider recent research on the undrained behavior of sand using the hollow cylinder device, which can model the full spectrum of loading conditions. Using the hollow cylinder test equipment, Symes et. al. (1985) and Shibuya and Hight (1987) have shown that water pluviated sand is least contractive and least

susceptable to liquefaction in a triaxial compression mode total stress path, yet most contractive and most susceptible to liquefaction in a triaxial extension mode total stress path. These test results indicate that cyclic testing of isotropically consolidated triaxial specimens in both extension and compression phases will ensure that both most resistant and least resistant loading phases are included, such that one might hope to attain an average estimate of susceptibility to liquefaction which is useful for correlation purposes.

A factor to consider in the selection of a cyclic loading test technique is stress and strain reversal, which occurs in triaxial test loading between compression and extension phases. Stress and strain reversal has been shown by several workers (for example Vaid and Chern, 1983, Mohamad and Dobry, 1986, and others) to have a profound softening effect upon soil behavior, especially during the development of cyclic mobility due to the mechanical reorganization of soil particles. The extent to which stress reversal and cyclic mobility may occur in field loading is disputed, but recent centrifuge studies (Lee and Schofield, 1988) indicate field loading conditions may induce the cyclic fluctuation of pore pressure and directional hardening and softening of stress-strain response which is generally associated with stress and strain reversal (see Figure 6.1). Thus for correlation

Figure 6.1a Typical undrained cyclic loading response of isotropically
consolidated silty well—graded 20/200 Brenda sand
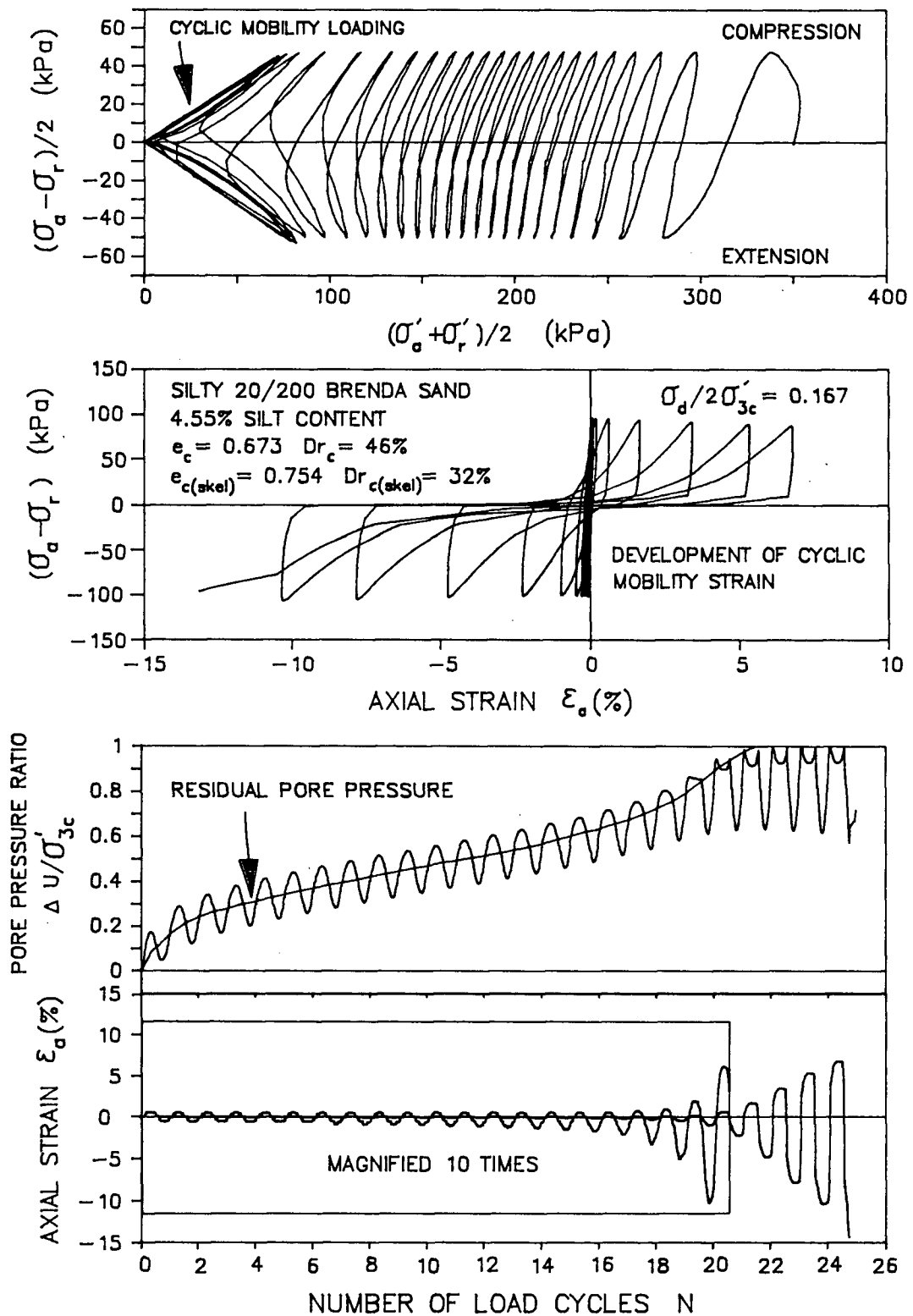
Fig. 6.1b Comparison of the typical undrained cyclic loading response of poorly—graded 20/40 and well—graded 20/200 Brenda sand (both samples prepared at loosest state)

POORLY—GRADED 20/40 SAND (analog data recorded on strip chart)

WELL—GRADED 20/200 SAND (digital data recorded by computer)
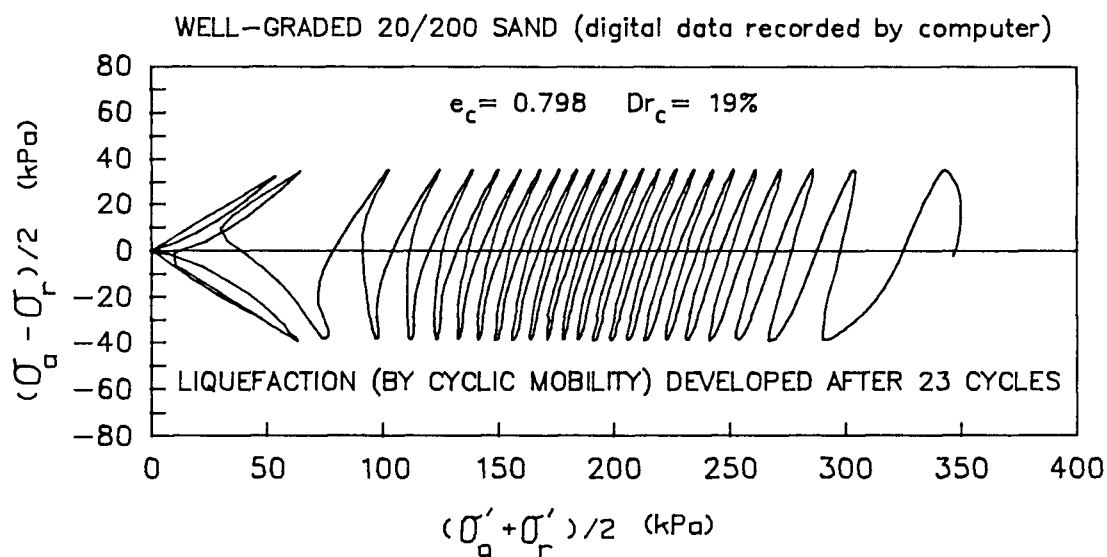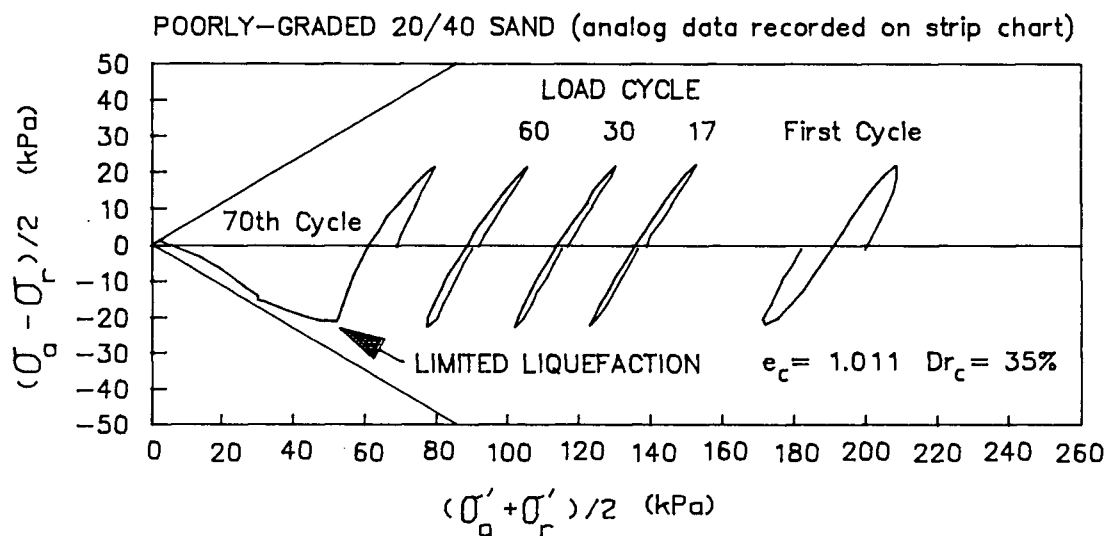
purposes it is prudent to observe the effects of cyclic loading with stress and strain reversal.

For the reasons described above, it is believed that isotropically consolidated triaxial specimens which are symmetrically loaded in extension and compression phases provide the most useful cyclic triaxial test data for general correlation purposes.

For the purposes of this research, liquefaction in undrained triaxial loading is defined as the development of 2.5% single amplitude axial strain (5% peak to peak axial strain between extension and compression loading phases). If steady-state liquefaction or limited liquefaction are not induced by cyclic loading, as is the case for the majority of cyclic tests performed on 20/200 sand, the development of 2.5% strain generally corresponds to the initial occurrence of a transient 100% pore pressure ratio. The number of load cycles required to induce liquefaction is defined as N_ℓ. A representative example of data obtained from a single cyclic triaxial test on silty 20/200 sand is shown in Figure 6.1.

The following sections present data obtained from 80 cyclic triaxial tests performed on silty 20/200 Brenda sand over a large range of densities, cyclic stress ratios, and number of cycles to liquefaction. The effects of silt content upon effective stress path, stress-strain response, pore pressure generation characteristics, shear strain generation, and resistance to liquefaction are discussed.

6.1 **GENERAL RESPONSE**

Two different types of response are observed under cyclic loading: (1) cyclic loading which leads to the initiation of steady-state liquefaction or limited liquefaction, with a very rapid generation of both pore pressure and shear strain below 100% pore pressure ratio, and (2) cyclic loading which produces a systematic increase in pore pressure and strain with each load cycle, with the development of large cyclic mobility strains only after a transient pore pressure ratio of 100% has been achieved. Steady-state liquefaction or limited liquefaction may only be initiated during cyclic loading if it is possible under monotonic loading conditions.   In addition, the sum of static and cyclic stress must exceed phase transformation strength (in either extension or compression phases).   The development of large cyclic mobility strain in relatively few loading cycles may follow the occurrence of limited liquefaction.

The cyclic loading response of silty 20/200 Brenda sand shown in Figure 6.1 is generally characteristic of the well-graded clean and silty sands tested.   The general character of the effective stress path of well-graded sand under cyclic loading does not show a great deal of variation with relative density, provided that limited liquefaction does not occur.   Limited liquefaction in the well-graded sand was only observed to occur in the extension phase of cyclic

loading (as observed in monotonic test results) and only in very loose well-graded sand samples which required less than 10 cycles to achieve 2.5% strain. For the majority of samples which failed by the development of cyclic mobility strain, the difference in loading response between loose and dense sands is mainly the magnitude of deviator stress required to induce 2.5% strain in a given number of cycles, and the ease with which cyclic mobility strains are developed once a transient state of zero effective stress has occurred. Axial strains much less than 1% were generally observed during pore pressure generation up to 60% pore pressure ratio. Axial strains larger than 1% occurred with the development of limited liquefaction and/or with the development of cyclic mobility. Loose to medium dense sands generally developed large cyclic mobility strains in excess of 15% very quickly within a few load cycles after development of initial zero effective stress, even when a large number of load cycles were required to achieve initial zero effective stress (see Figure 6.2). Denser sands required a greater number of load cycles to achieve large cyclic mobility strains after the occurrence of initial zero effective stress state, with very dense sands reaching a limited cyclic mobility strain level before the development of conjugate shear planes in the extension phase of loading. Strain development was observed to be uniform as a rule, except after a large number of cyclic mobility loading cycles in denser sands, or the development of conjugate

Figure 6.2 Development of shear strain in well—graded 20/200 sand during cyclic loading
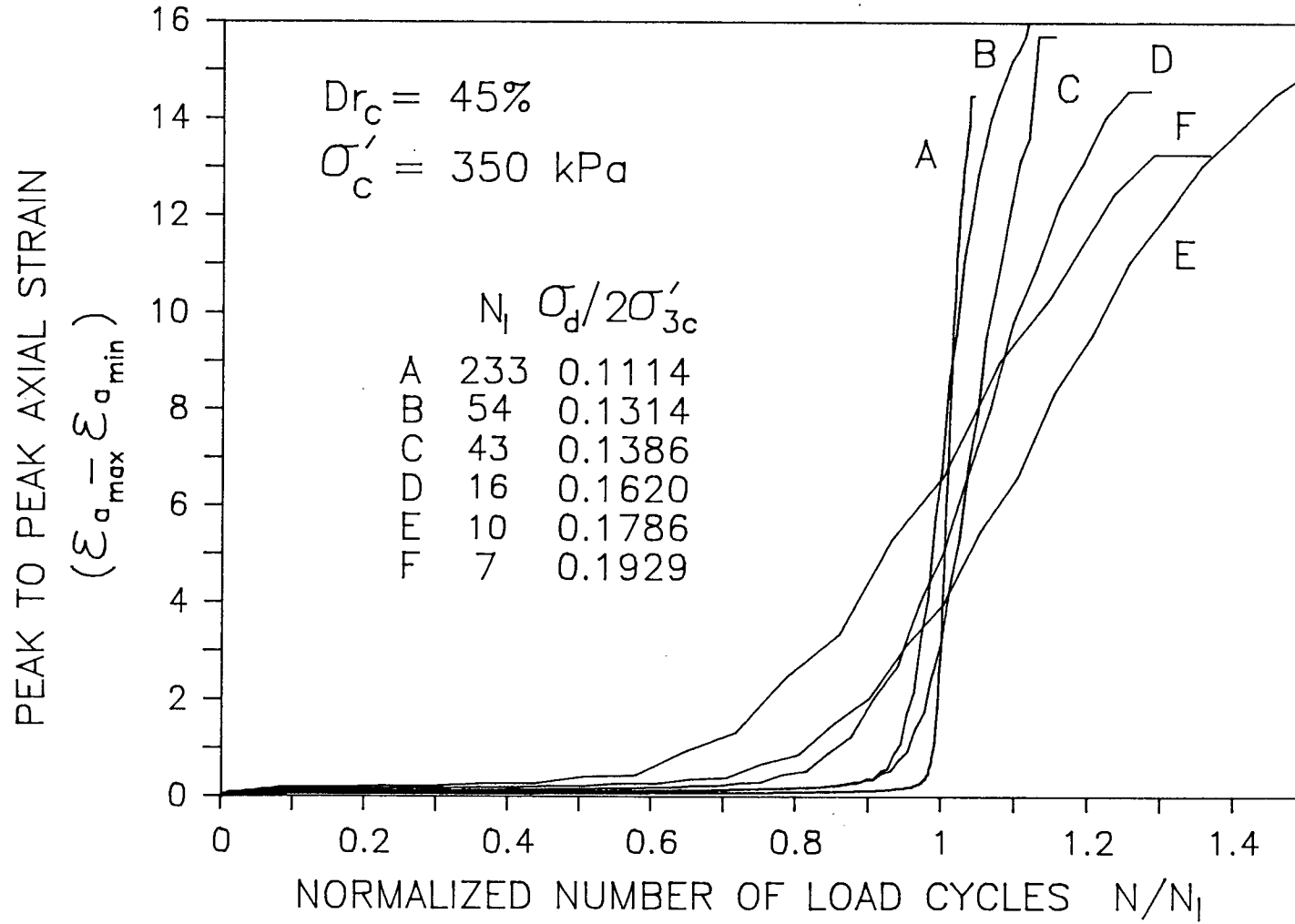
shear planes in extension loading after the development of large extension strains. The development of extension phase shear planes in a soil may be easily identified in test data, as effective stress path on a modified Mohr diagram deviates from the boundary envelope during cyclic mobility loading.

The major difference in cyclic loading response between well-graded and poorly-graded sands is the effect which gradation has upon steady-state liquefaction or limited liquefaction response. As observed in monotonic test results, poorly-graded sands are more susceptible to limited liquefaction than well-graded sand. Thus well-graded sand is more likely to fail by the development of cyclic mobility strain than poorly-graded sand. The range of cyclic strengths of well-graded and poorly-graded sands is similar, and within the range of cyclic strengths previously reported for other sands. This indicates that although more well-graded sands are less susceptible to limited liquefaction, both well-graded and poorly-graded sands are susceptible to pore pressure and cyclic mobility strain development under cyclic loading.

Well-graded and poorly-graded sands show a marked difference in the effective stress path produced by the intermediate stages of cyclic loading. During intermediate loading cycles, with development of pore pressure in the range from 20% to 60% of initial effective stress, the effective stress path of well-graded sand appears to be more

symmetric between compression and extension loading phases on the modified Mohr diagram (see Figure 6.1b). The effective stress path is closer to vertical on the modified Mohr diagram. This increased symmetry in effective stress path response is similar to that observed between monotonic compression and extension loading.

The effective stress path during intermediate cycles of loading could be considered to represent essentially elastic soil response. The recoverable changes in pore pressure during loading are due essentially to elastic soil response and changes in mean normal stress. The observation that pore pressure response during this stage of loading varies with gradation implies that pore pressure response is not only a function of change in mean normal stress, but also a function of the elastic volume changes induced during loading. The elastic stress-strain behaviour of a sand is thus shown to be a function of gradation. More well-graded sand is shown to have generally more contractive elastic strains in compression loading and more dilative elastic strains in extension loading than poorly-graded sand. This variation in elastic loading response with gradation is similar to that observed in plastic loading response (in monotonic test results), where more well-graded sand shows less anisotropy in dilatancy behaviour between compression and extension loading.

The boundary surface failure envelopes in extension and compression loading phases were found to have essentially

the same friction angles, although with some variation (plus or minus 1 degree) as observed in monotonic test results (Section 5.3.1). These friction angles were observed to change slightly with axial strain level, generally first increasing with increasing cyclic mobility strain, and then decreasing with larger strain, both in extension and compression loading phases as shown in Figure 6.3. Failure envelope friction angles were also observed to vary with trends in cyclic mobility strain development. The development of a trend towards residual extension phase cyclic mobility strain was observed to coincide with larger extension and smaller compression phase boundary friction angles. Similarly, the development of residual compression phase cyclic mobility strain was observed to coincide with larger compression and smaller extension phase boundary envelope friction angles. The majority of test samples generally developed larger extension strains than compression strains, thus extension phase boundary friction angles shown in Figure 6.4 are generally larger than compression phase friction angles. The development of larger strains in the extension phase is partially due to soil anisotropy and softer extension loading response, and partially due to the fact that soil samples were tested in a load controlled rather than a stress controlled manner, and thus changes in sample area produced larger extension and smaller compression maximum stresses at large strains. The observed variation in failure envelope friction angles with

Figure 6.3 Variation of boundary envelope friction angle during cyclic mobility loading

Upper plot: DEVELOPED FRICTION ANGLE (DEGREES) vs AXIAL STRAIN (%)

EXTENSION   COMPRESSION

SILTY 20/200 BRENDA
SAND WITH 4.35%
SILT BY WEIGHT

$Dr_c (\%)$ e_c

TOTAL   59.7   0.627
SAND
SKELETON   47.1   0.701

$\sigma_d / 2\sigma'_{3c} = 0.251$

$\sigma'_c = 350$ kPa

$N_I = 5$ CYCLES

Lower plot: DEVELOPED FRICTION ANGLE (DEGREES) vs NUMBER OF LOAD CYCLES N

COMPRESSION   EXTENSION
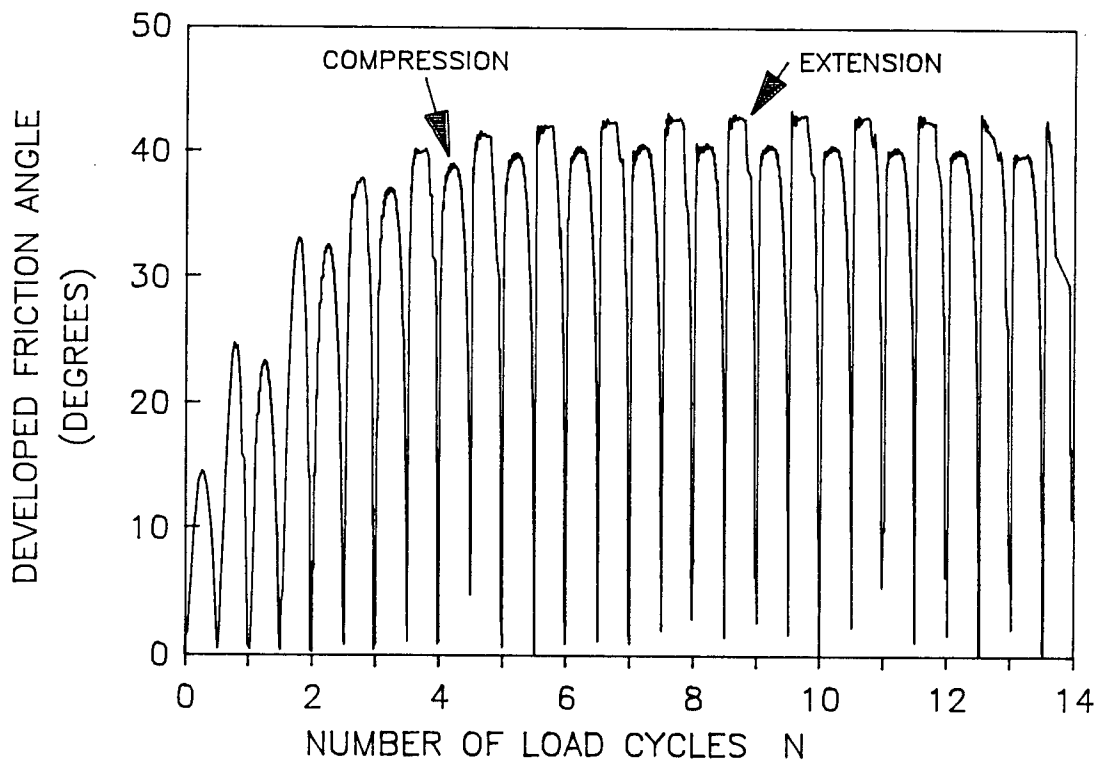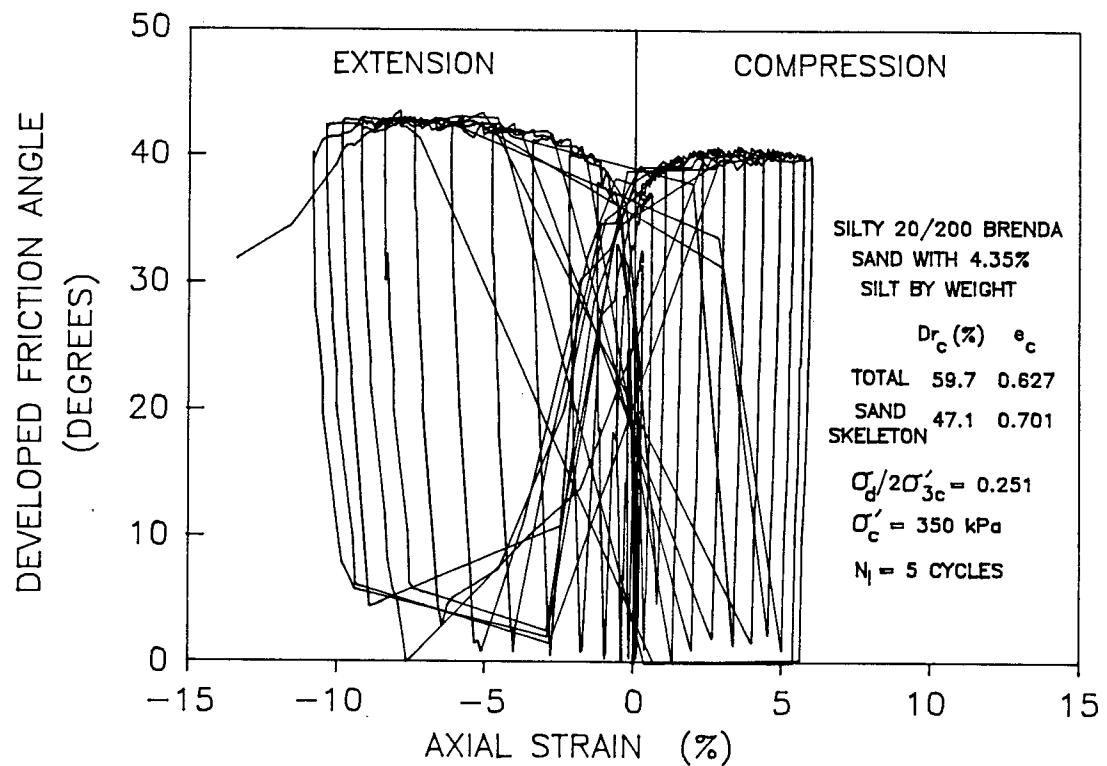
Figure 6.4 Variation of maximum boundary envelope friction angle of silty 20/200 Brenda sand with silt content and sand skeleton relative density
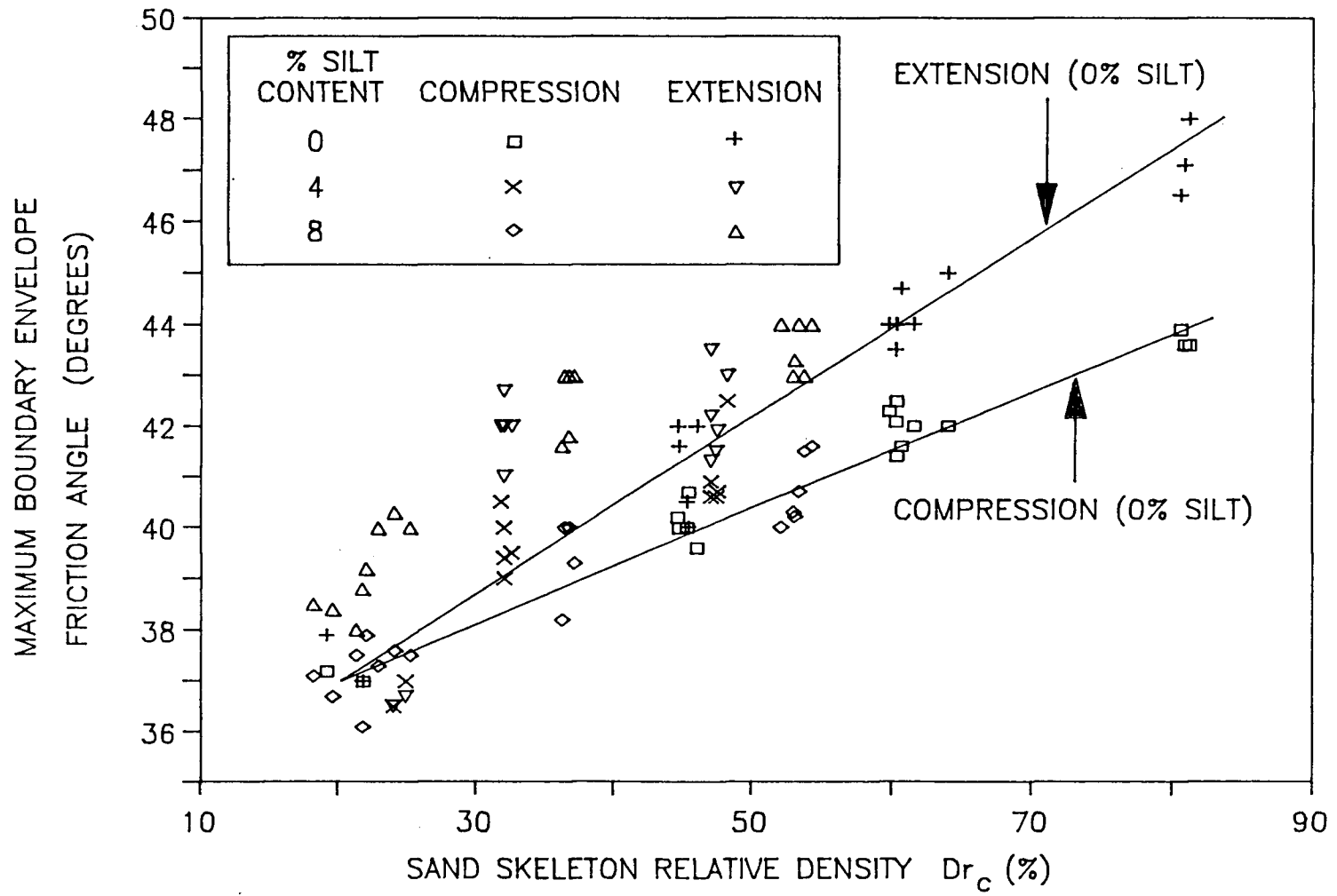
cyclic mobility strain development may be an indication of change in sand fabric with a change in cyclic mobility strain amplitude. The observed variations in boundary envelope friction angles with direction of loading and strain level may be qualitatively explained by considering the structures which control soil fabric, as described in Section 2.2.

Maximum obliquity friction angles were observed to increase with increasing sand skeleton relative density, as shown in Figure 6.4. The friction angles shown in Figure 6.4 generally have a scatter of plus or minus 1 degree. The scatter in maximum obliquity friction angles is probably due to the variation of friction angle with cyclic mobility strain development. Figure 6.4 also shows the variation of maximum obliquity friction angles with increasing silt content. The friction angles of loose sand (with a sand skeleton relative density less than 50 percent) was observed to increase somewhat with increasing silt content, as also observed in monotonic test results (Section 5.4). In contrast, maximum obliquity friction angles of moderately dense to dense sands (with a sand skeleton relative density greater than 50 percent) were observed to change little with increasing silt content.

6.2 STRESS-STRAIN RESPONSE WITHIN LOADING CYCLES

Figure 6.5, Figure 6.6, and Figure 6.7 show typical stress versus strain loops obtained during cyclic loading of clean and silty well-graded 20/200 sands. Several researchers have reported similar results for other sand types (for example Seed and Lee, 1966, Ishihara 1978). There are in general three characteristic types of undrained cyclic loading stress-strain response: (1) pre-liquefaction response at low induced strain and pore pressure level such as shown in Figure 6.5, (2) contractive response of the steady-state liquefaction or limited liquefaction types as shown in Figure 6.6, and (3) cyclic mobility response as shown in Figure 6.7, which develops with stress reversal following realization of transient states of zero effective stress. A single soil sample may undergo all three types of strain development, or just types (1) and (3).

In type (1) there is a general flattening of the hysteresis loops with increasing load cycles. Type (2) will occur only in cyclic loading if sand is contractive in monotonic loading, and only if cyclic stress exceeds phase transformation strength. In the well-graded sands tested, this is generally observed only in moderately loose to very loose sand, or at higher effective confining stress level. Type (1) and (2) stress-strain responses are in general governed by (a) the initial soil fabric, and (b) the mode of loading.

Figure 6.5 Typical cyclic loading stress—strain response at low strain level

WELL—GRADED 20/200 BRENDA SAND

$Dr_c = 45\%$

$\sigma'_c = 350$ kPa

$N_l = 10$ CYCLES

$\sigma_d/2\sigma'_{3c} = 0.1786$

FIFTH LOAD CYCLE

THIRD LOAD CYCLE

DEVIATOR STRESS σ_d (kPa)

AXIAL STRAIN (PERCENT)
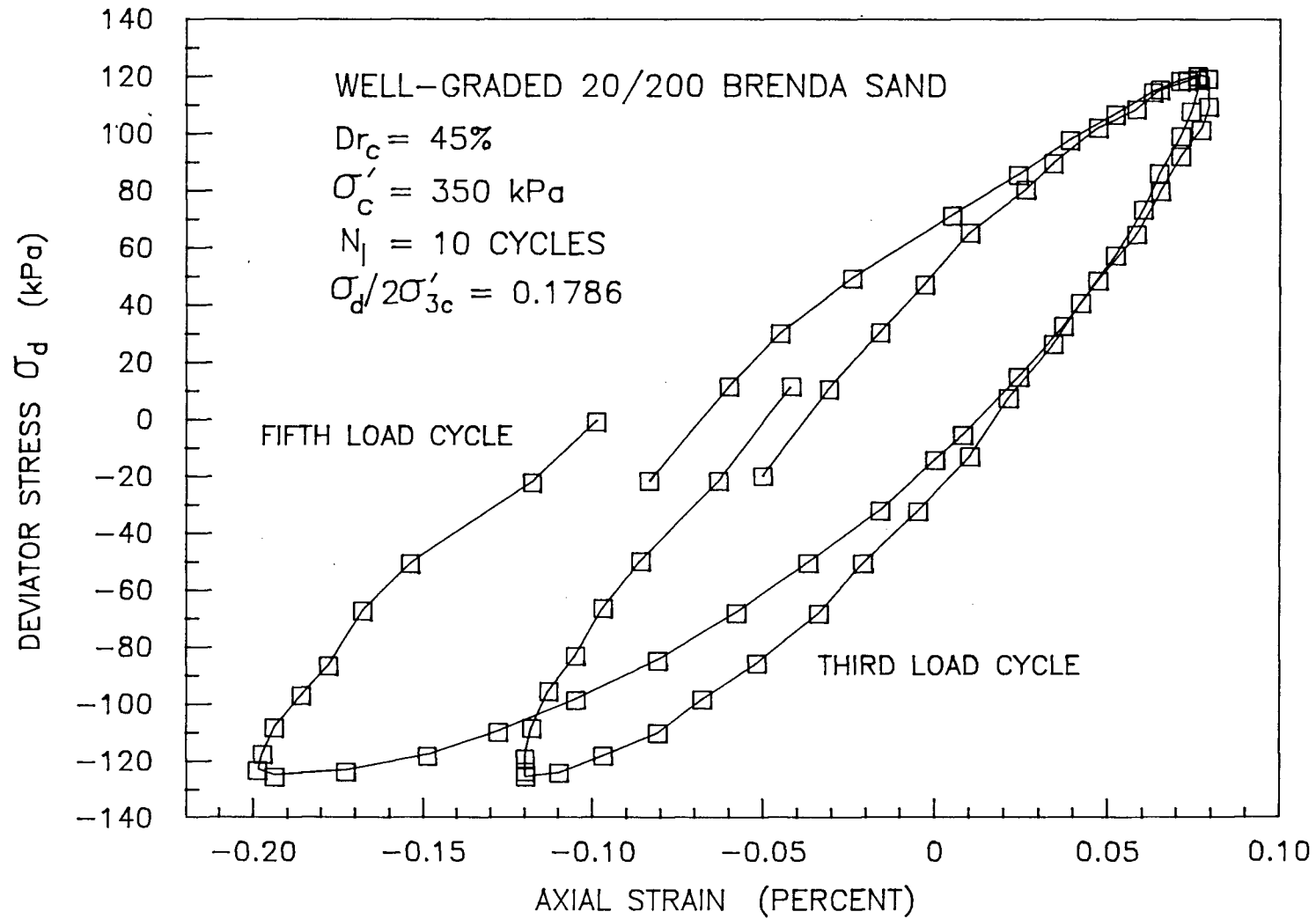
Figure 6.6 Cyclic loading stress—strain response of well—graded sand subject to limited liquefaction in extension loading

WELL GRADED 20/200
BRENDA SAND

$Dr_c = 22\%$

$\sigma'_c = 350$ kPa

$N_l = 6$ CYCLES

$\sigma_d/2\sigma'_{3c} = 0.147$

STRAIN HARDENING

LIMITED LIQUEFACTION
IN FIFTH LOAD CYCLE

DEVIATOR STRESS σ_d (kPa)

AXIAL STRAIN (PERCENT)
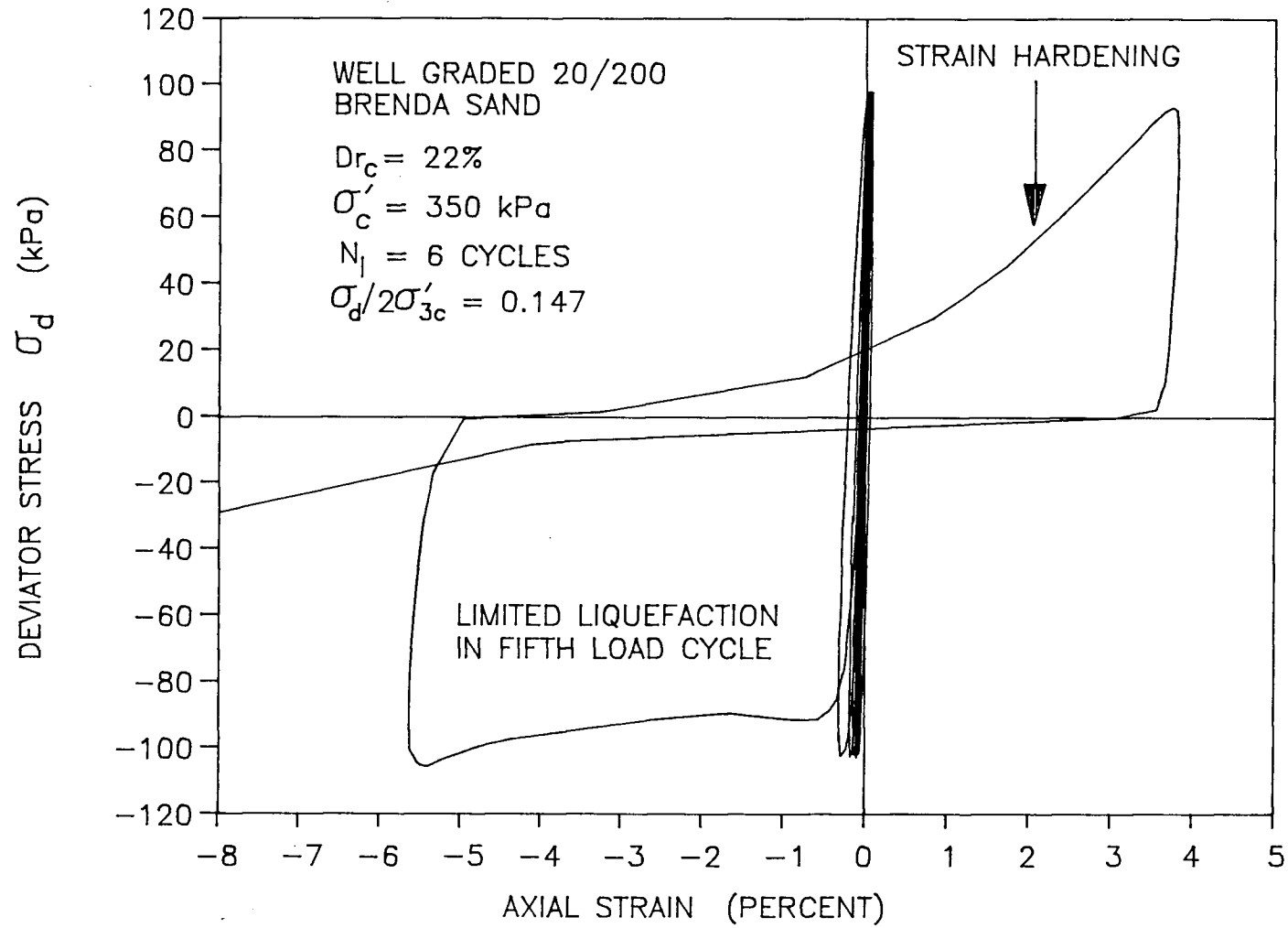
Figure 6.7 Development of cyclic mobility strain in loose silty well—graded
20/200 Brenda sand

SILTY WELL GRADED 20/200
BRENDA SAND (4.6% SILT)

$\sigma_c' = 350$ kPa

$N_l = 21$ CYCLES

$\sigma_d / 2\sigma_{3c}' = 0.147$

STRAIN HARDENING

	SAND	SKELETON
TOTAL		
e_c	0.6731	0.7536
$Dr_c(\%)$	46	32

Cycle 21

DEVIATOR STRESS σ_d (kPa)

AXIAL STRAIN (PERCENT)
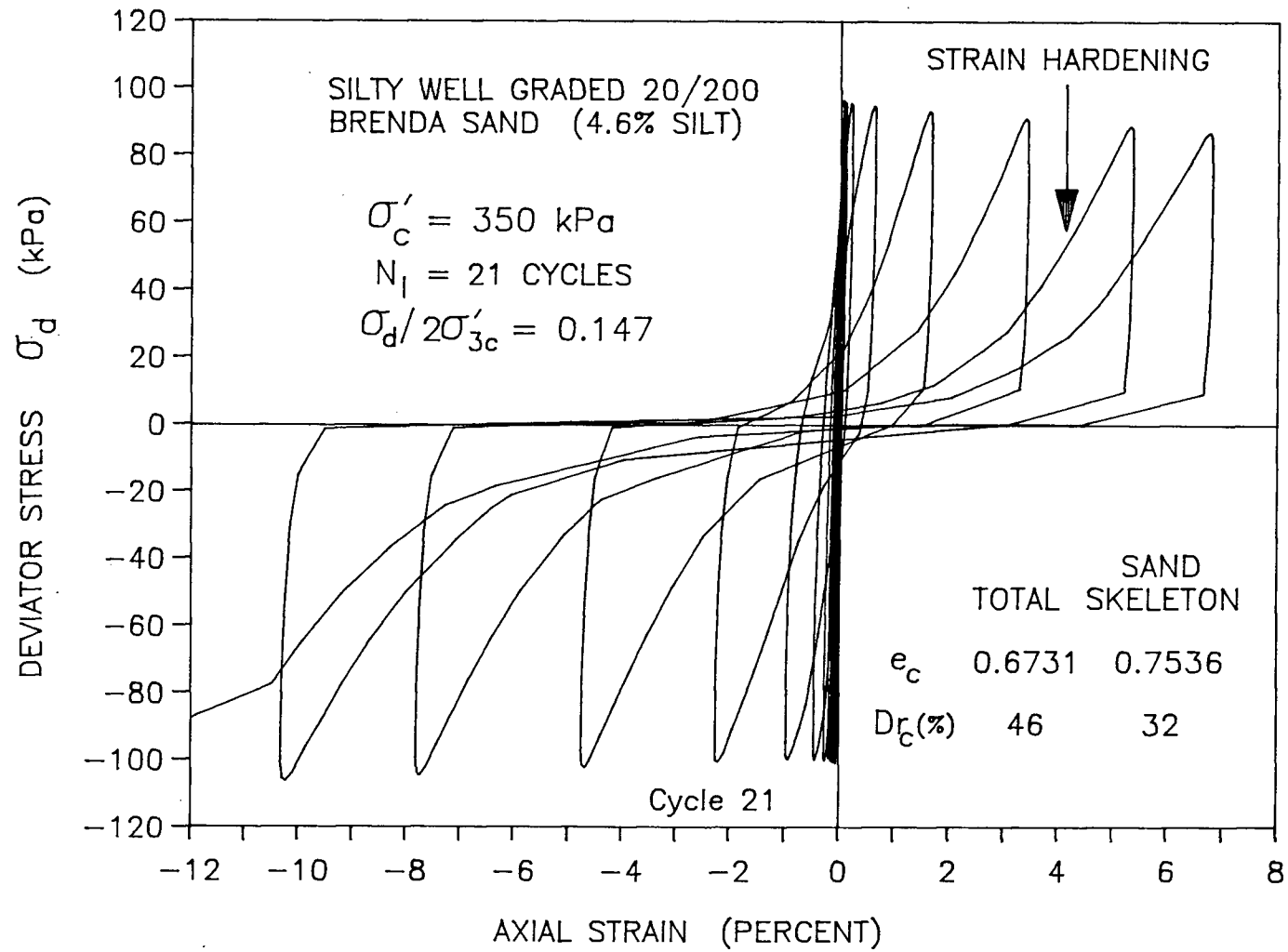
Type (3) response is governed mainly by stress and strain reversal rather than stress level. When applied stress is increased toward compression or extension during a single phase of loading, the stress-strain response is characterized by strain hardening. If stress reversal does not occur, cyclic mobility strains are generally small and may quickly reach a limiting value. If cyclic stress reversal does occur, very large strains may occur in relatively few load cycles, even though a large number of cycles of the same relatively low deviator stress amplitude were required to achieve an initial transient state of zero effective stress.

The development of strain hardening which is observed in each consecutive phase of mono-directional loading is indicative of a changing fabric within the sample during the development of cyclic mobility strain. Sample fabric becomes more dilative under increasing stress, which causes the material to stiffen in the direction of applied load. The stiffening of response in the direction of applied load is contrasted by a softening of the response when principal stresses are reversed. This indicates that the dilative and stable fabric established during loading in one direction is also highly contractive and unstable with the onset of principal stress reversal. The development of cyclic mobility strain occurs as a consequence of the fluctuation between soil fabrics which are stable under each phase of compression and extension loading. The character of stress-

strain curves in both phases of loading are similar, which indicates that a similar type of fabric is established in each direction of loading. The stable axis of the soil fabric developed in each phase of loading is parallel to the direction of maximum principal stress. The effective (boundary envelope) friction angle mobilized during each phase of loading is essentially the same, which also indicates a similarity in developed soil fabric between each mode of loading.

Incremental stress-strain loops in progressive load cycles are similar, although the magnitude of strains generated is significantly larger with each cycle. This fact suggests that the major difference between successive load cycles is the amount of induced strain required to initiate dilatant and hence strain hardening response.

Type (3) stress-strain loops show only small recoverable strain during unloading of deviator stress. This means a great deal of hysteretic work is absorbed by the soil in each cycle of loading. Perhaps the hysteretic work absorbed by the soil during loading could be used to quantify the directional soil fabric produced by the loading.

6.3 PORE PRESSURE GENERATION DURING CYCLIC LOADING

As in monotonic loading results (Section 5.1) pore pressure generation during undrained cyclic loading is a

function of total stress path. Figure 6.1 shows that there are generally large fluctuations in pore pressure with changing mean normal stress. The magnitude of these fluctuations is dependent upon total stress path. The cyclic effective stress path is, however, independent of total stress path if the principal stress directions remain constant. This dependence of induced pore pressure upon total stress path complicates the interpretation of pore pressure induced by cyclic loading. For laboratory testing purposes, previous workers have defined the residual pore pressure induced by cyclic loading as the pore pressure level which remains after each loading cycle has been completed. The total stress level at this point is equivalent to the initial total stress conditions. This definition of residual stress may not model cyclic loading conditions in the field, because the residual total stress after cyclic loading in the field has ceased may not correspond to the initial total stress conditions. The standard definition of residual pore pressure in laboratory test samples is adopted for the presentation of results in this thesis. Residual pore pressure is defined as the pore pressure at transient states of isotropic total stress, as all samples were initially consolidated under isotropic stress.

6.3.1 **Effect of Cyclic Stress Ratio**

Figure 6.8 shows how the residual pore pressure response of clean 20/200 sand (without silt) varies with change in cyclic stress ratio. The samples were isotropically consolidated to 350 kPa effective stress, with a relative density of 45% after vibratory densification and consolidation.

The number of cycles required to induce liquefaction increases with decreasing cyclic stress ratio, as expected. Residual pore pressure generation curves in Figure 6.8 have been normalized with respect to the number of cycles required to achieve liquefaction, in order to determine if the character of normalized pore pressure generation curves is similar, as suggested by De Alba (1976). Normalized curves are often used to estimate pore pressure generation in situ. This requires that the normalized curves have the same general shape.

Figure 6.8 shows that the normalized pore pressure generation curves do not have the same shape. There is a clear trend in the variation of pore pressure generation with changing cyclic stress ratio. At low cyclic stress ratio, or a large number of cycles to initial liquefaction, normalized pore pressure apparently builds relatively more quickly during initial loading up to 30% pore pressure ratio, and relatively more quickly after 70% pore pressure ratio. At higher cyclic stress ratio or few cycles to liquefaction, normalized curves are almost linear over the

Figure 6.8a Variation of pore pressure generation in loose clean 20/200 sand with change in cyclic stress ratio

$Dr_c = 45\%$

$\sigma_c' = 350 \text{ kPa}$

(RESIDUAL PORE PRESSURE CURVES)

	N_l	$\sigma_d/2\sigma_{3c}'$
A	233	0.1114
B	54	0.1314
C	43	0.1386
D	16	0.1620
E	10	0.1786
F	7	0.1929
G	4	0.2214

PORE PRESSURE RATIO $\Delta U/\sigma_{3c}'$

NORMALIZED NUMBER OF LOAD CYCLES N/N_l
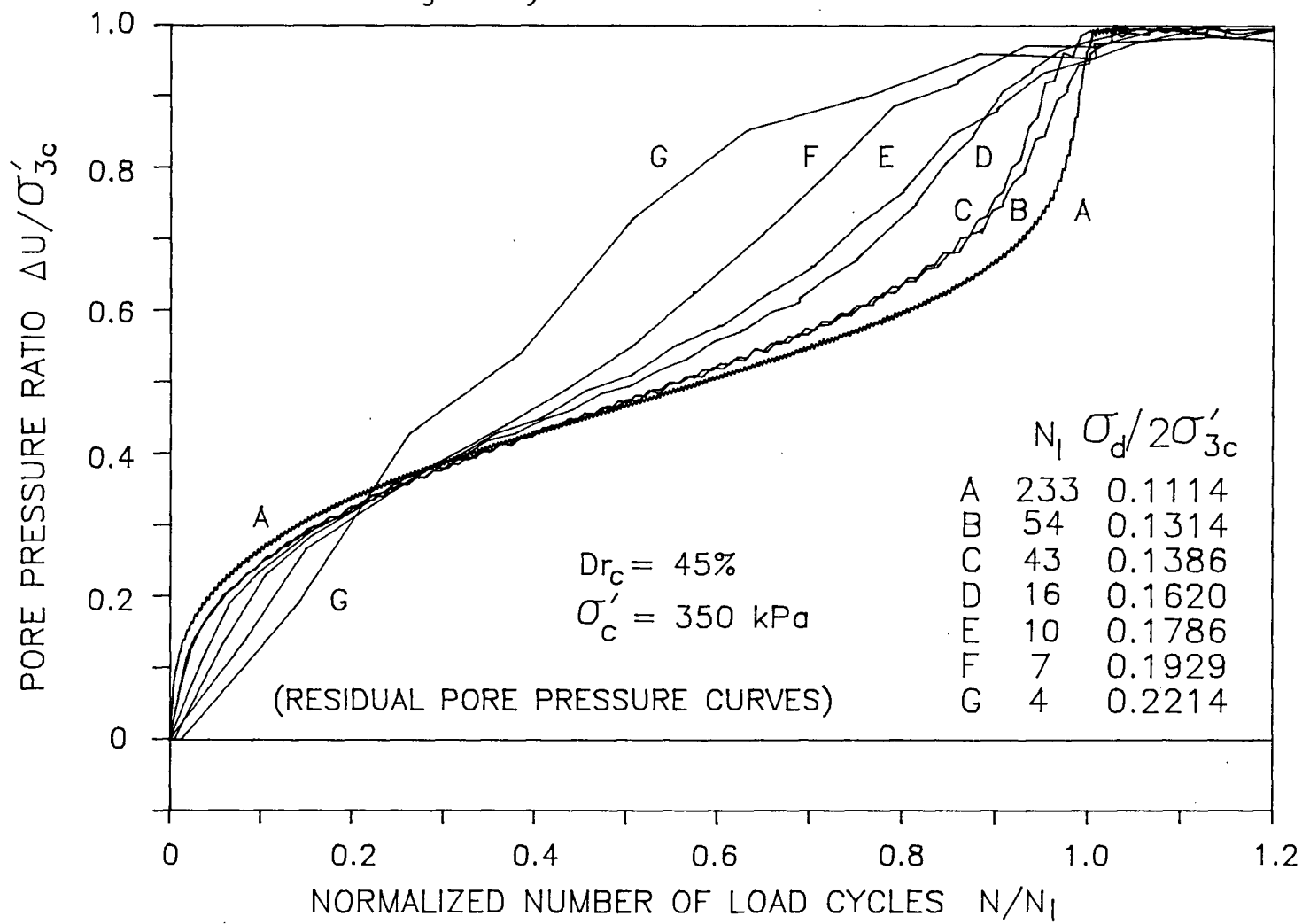
Figure 6.8b Variation of pore pressure generation in loose clean 20/200 sand with change in cyclic stress ratio

$Dr_c = 45\%$

$\sigma_c' = 350$ kPa

WELL—GRADED
20/200
BRENDA SAND

TEST	N_L	$\sigma_d/2\sigma_{3c}'$
A	233	0.1114
B	54	0.1314
C	43	0.1386
D	16	0.1620
E	10	0.1786
F	7	0.1929
G	4	0.2214

PORE PRESSURE RATIO $\Delta U/\sigma_c'$

NUMBER OF LOAD CYCLES N
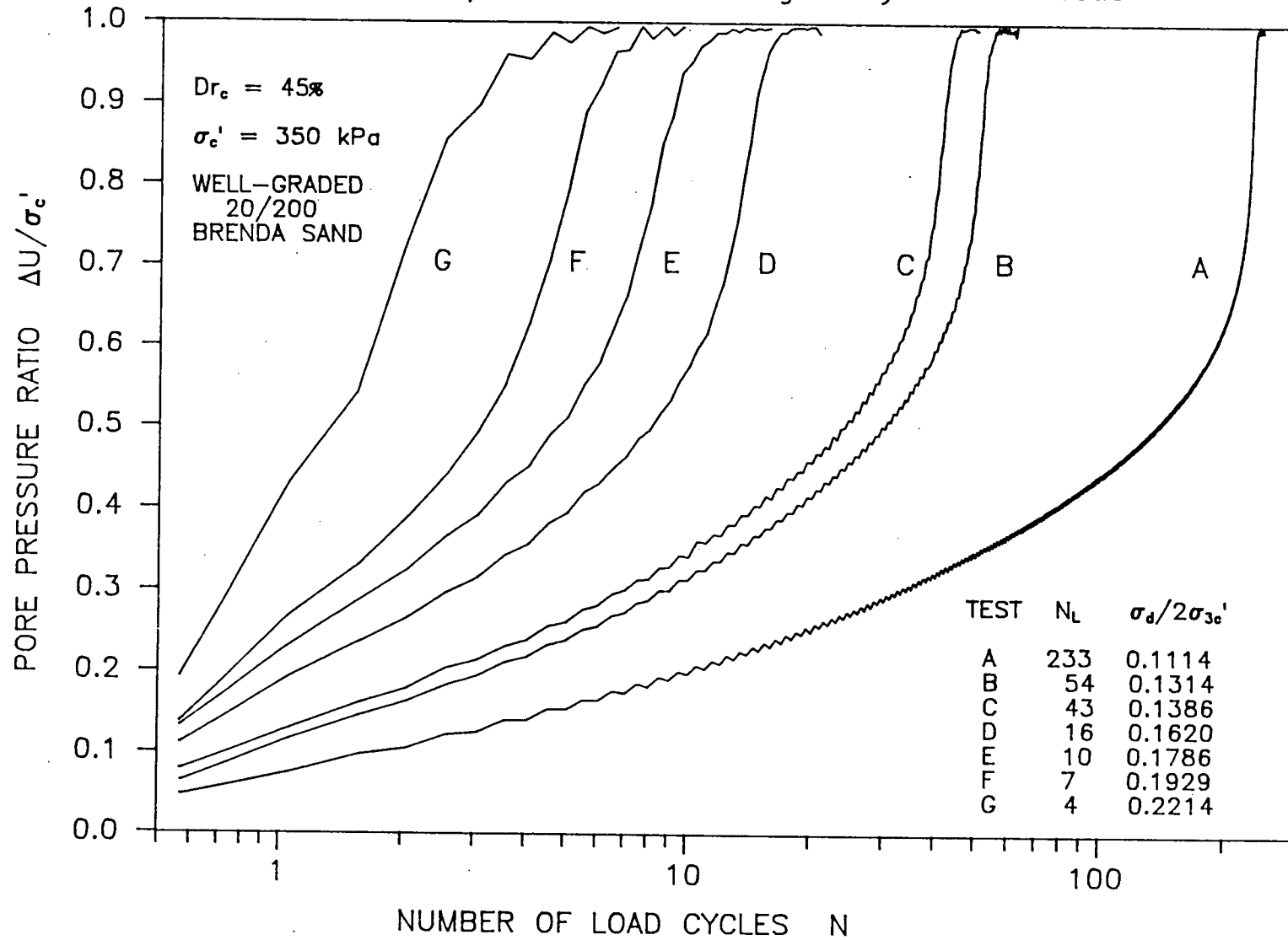
range of loading cycles. Steady-state or limited liquefaction was not observed in 45% relative density samples, regardless of the cyclic stress level.

6.3.2 Effect of Silt Content

Figure 6.9 and Figure 6.10 show how the residual pore water pressure generated by cyclic loading in silty 20/200 sand varies with change in silt content. The samples were prepared at near loosest state of slurry deposition and isotropically consolidated to 350 kPa, and thus have similar sand skeleton void ratios. The samples were subjected to a relatively large cyclic stress ratio and thus required a small number of cycles to achieve liquefaction.

Residual pore pressure response may be noted to be essentially the same for sand with 0 to 15% silt content. These samples all developed limited liquefaction during the sixth load cycle. In contrast, the sand with 20% silt content required 9 cycles to develop liquefaction without the occurrence of limited liquefaction, although the sand skeleton void ratio was bulked by the 20% silt content. Apparently a large silt content retards the development of limited liquefaction during cyclic loading. This was also observed in monotonic test results (Section 5.4)

Figure 6.11 and Figure 6.12 also show how the residual pore pressure generated by cyclic loading in silty 20/200 sand varies with change in silt content. As before, the samples were prepared at near loosest state of slurry

Figure 6.9 Variation of pore pressure generation with silt content in 20/200 sand subject to limited liquefaction
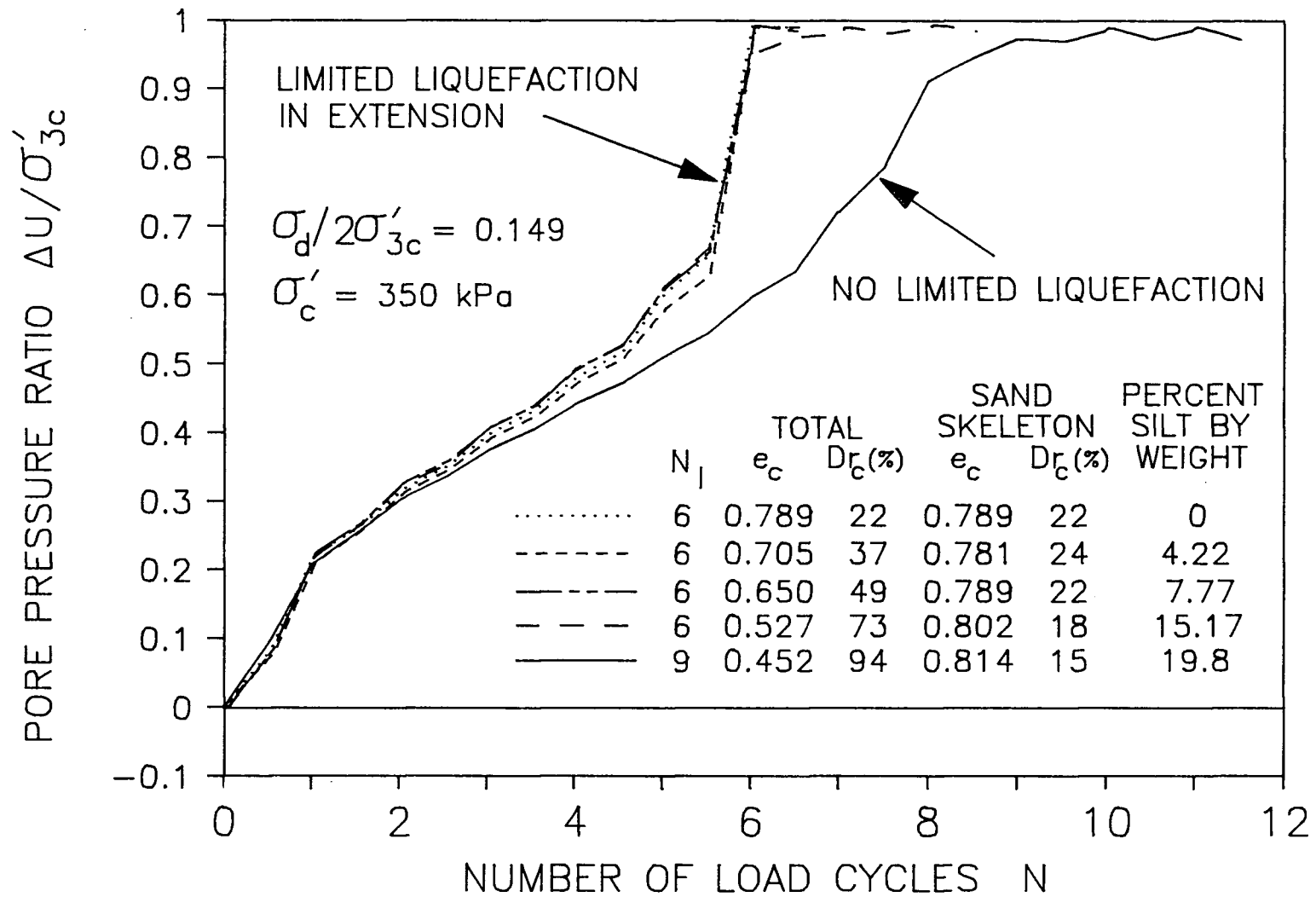
Figure 6.10 Variation of pore pressure generation with silt content in 20/200 sand subject to limited liquefaction

$$\sigma_c' = 350 \text{ kPa}$$

$$\sigma_d / 2\sigma_{3c}' = 0.149$$

			TOTAL	SAND SKELETON		PERCENT SILT BY
	N_l	e_c	$Dr_c(\%)$	e_c	$Dr_c(\%)$	WEIGHT
....	6	0.789	22	0.789	22	0
- - - - -	6	0.705	37	0.781	24	4.22
— - — -	6	0.650	49	0.789	22	7.77
— — —	6	0.527	73	0.802	18	15.17
———	9	0.452	94	0.814	15	19.8

PORE PRESSURE RATIO $\Delta U / \sigma_{3c}'$

NORMALIZED NUMBER OF LOAD CYCLES N/N_l
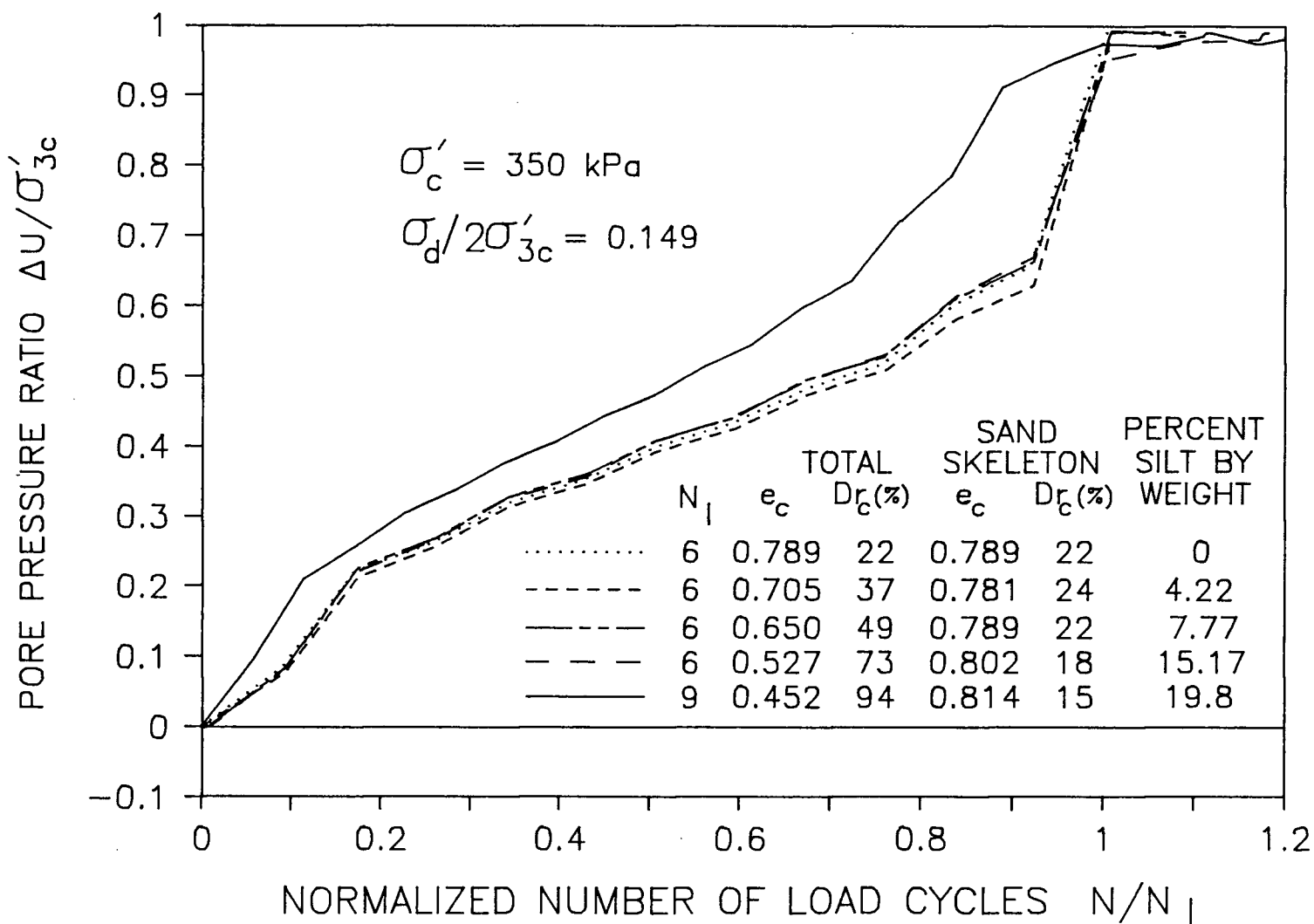
Figure 6.11 Variation of pore pressure generation with silt content in 20/200 sand not subject to limited liquefaction

$\sigma'_c = 350$ kPa

$\sigma_d / 2\sigma'_{3c} = 0.113$

	N_1	e_c	TOTAL $Dr_c(\%)$	SAND SKELETON e_c	$Dr_c(\%)$	PERCENT SILT BY WEIGHT
....	23	0.798	19	0.798	19	0
-------	35	0.708	37	0.778	25	3.91
—·—·—	46	0.660	46	0.803	18	7.88
— — —	43	0.533	72	0.790	22	14.3
———	32	0.440	98	0.826	11	21.0
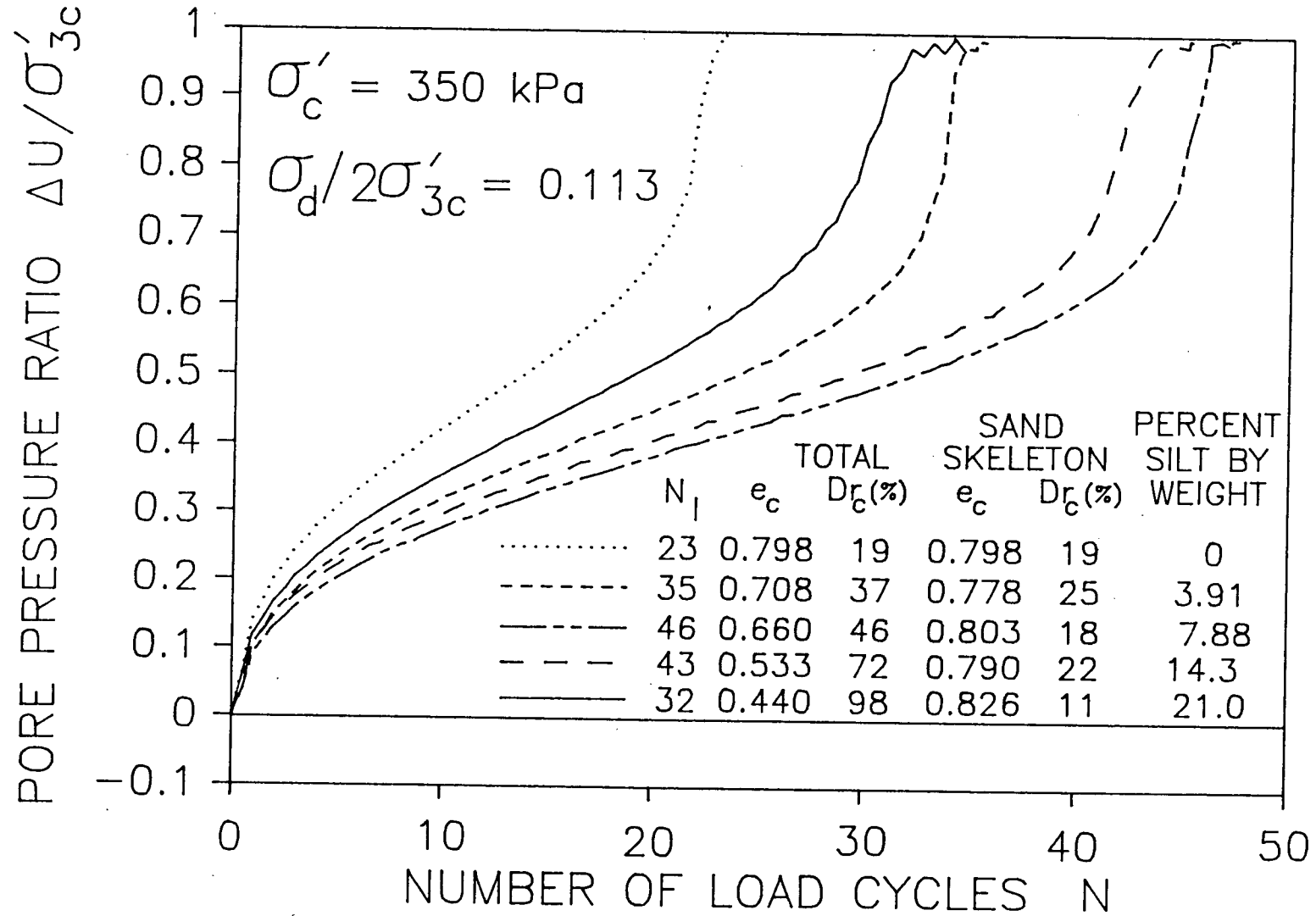
Figure 6.12 Variation of pore pressure generation with silt content in 20/200 sand not subject to limited liquefaction
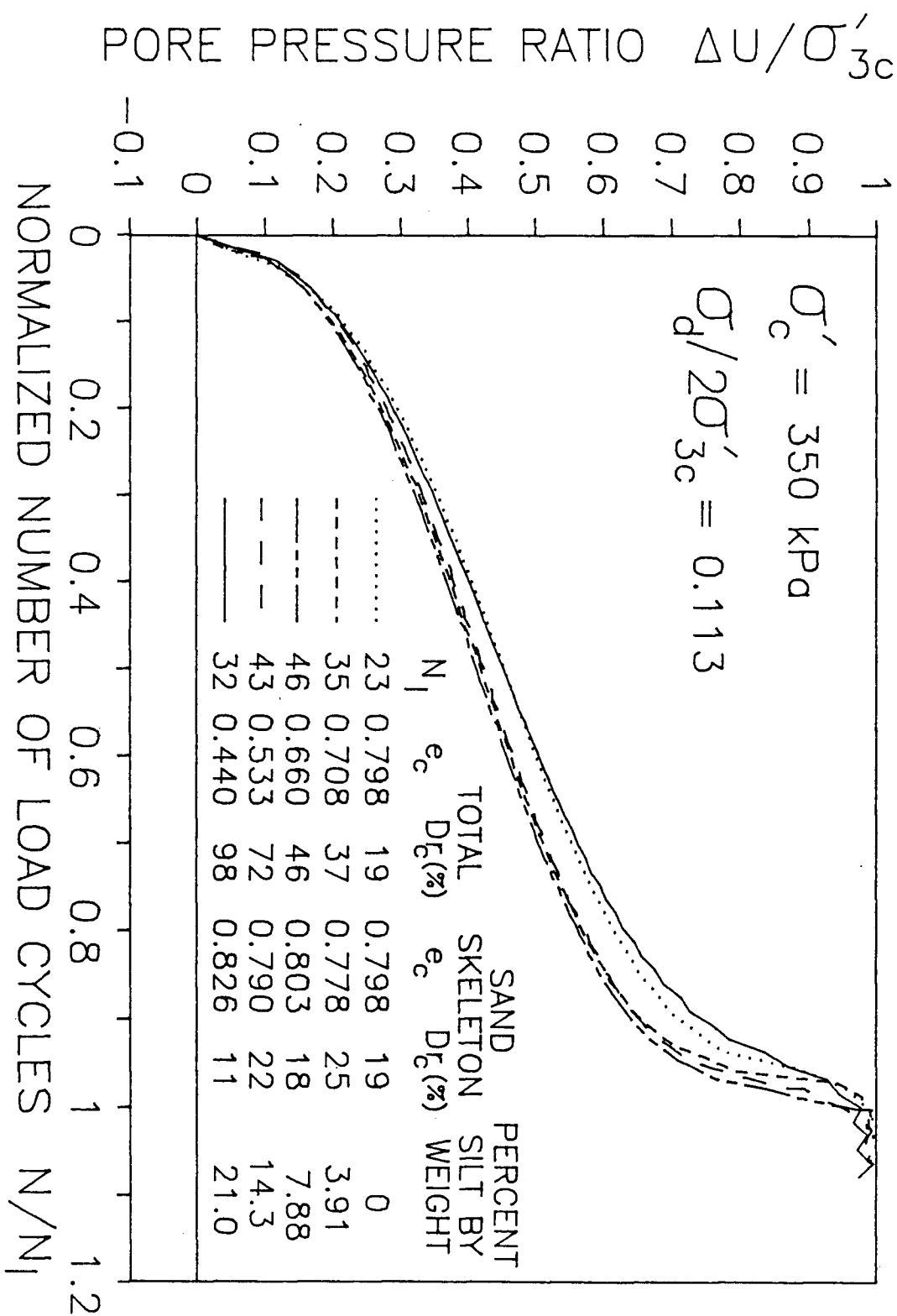
deposition and isotropically consolidated to 350 kPa, and thus have similar sand skeleton void ratios. The samples were subjected to a relatively low cyclic stress ratio, and thus required a larger number of cycles to achieve liquefaction.

Figure 6.11 indicates that susceptibility to liquefaction and generation of residual pore pressure is reduced by any addition of silt to the sand. The figure also indicates that the degree of increase in cyclic strength with addition of silt is not a direct function of percentage silt content. The variation of cyclic strength with increasing silt content appears to be fairly complex.

In contrast to the normalized residual pore pressure generation curves of clean sand shown in Figure 6.8, the normalized curves of silty sand shown in Figure 6.12 show little variation with increasing silt content. The silty sand normalized curves are representative of one cyclic stress ratio (0.113) while the clean sand normalized curves represent variable cyclic stress ratios. The shape of normalized curves appears to be more dependent upon magnitude of cyclic stress ratio and less dependent upon silt content.

6.3.3 Effect of Relative Density

Figures 6.13 and 6.14 show how the residual pore pressure generated in clean 20/200 sand during cyclic loading varies with relative density. There appears to be

Figure 6.13 Variation of pore pressure development in clean well—graded 20/200 sand with change in relative density

$\sigma'_c = 350$ kPa

SAMPLE	N_l	e_c	$Dr_c(\%)$	$\sigma_d/2\sigma'_{3c}$
A	6	0.789	22	0.147
B	43	0.705	46	0.147
C	154	0.656	60	0.146
D	27	0.584	81	0.249

PORE PRESSURE RATIO $\Delta U/\sigma'_{3c}$

NUMBER OF LOAD CYCLES N
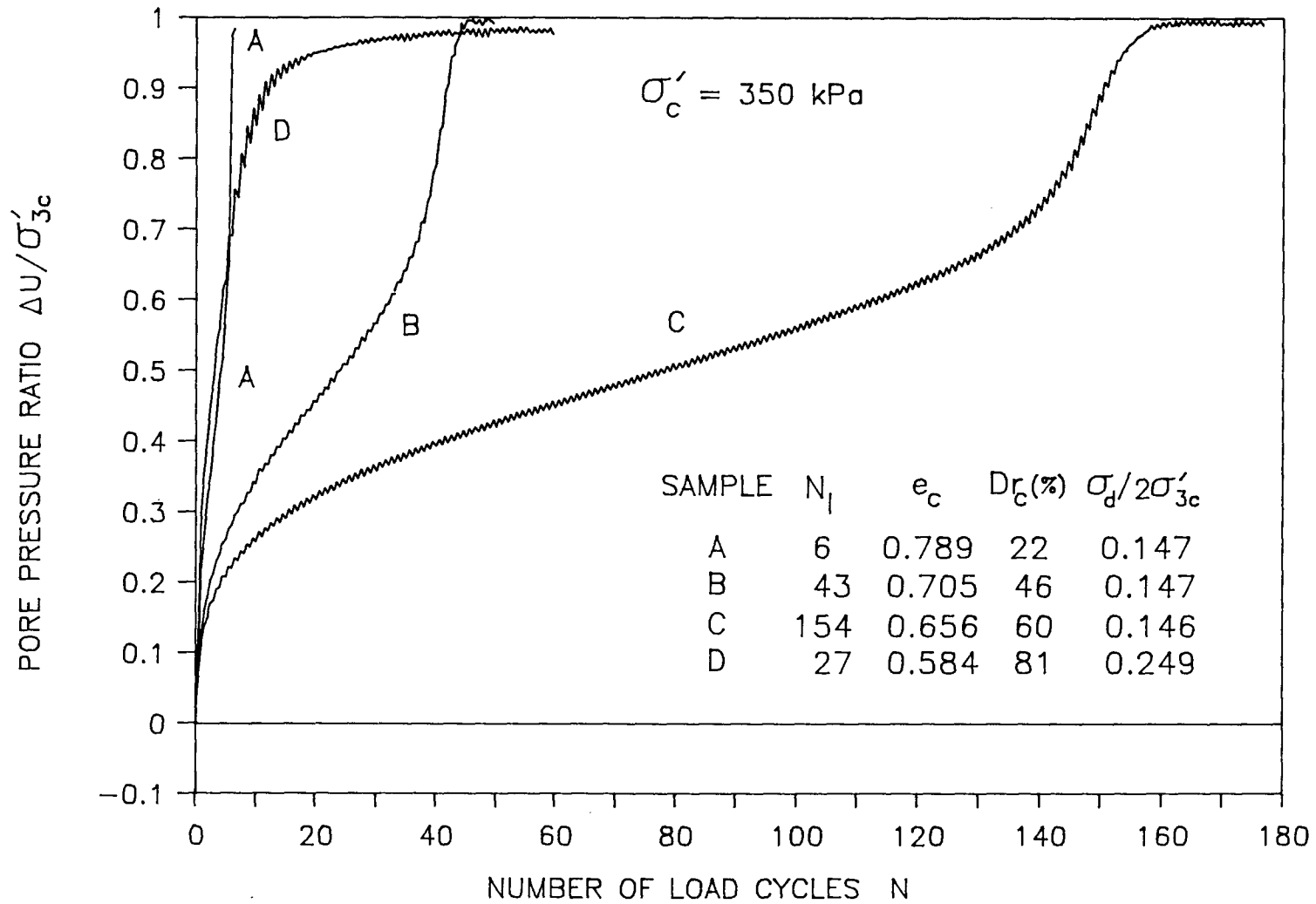
Figure 6.14 Variation of pore pressure generation in clean well—graded 20/200 sand with change in relative density

(RESIDUAL PORE PRESSURE CURVES)

	N_I	e_c	$Dr_c(\%)$	$\sigma_d/2\sigma'_{3c}$
A	6	0.789	22	0.147
B	43	0.705	46	0.147
C	154	0.656	60	0.146
D	27	0.584	81	0.249
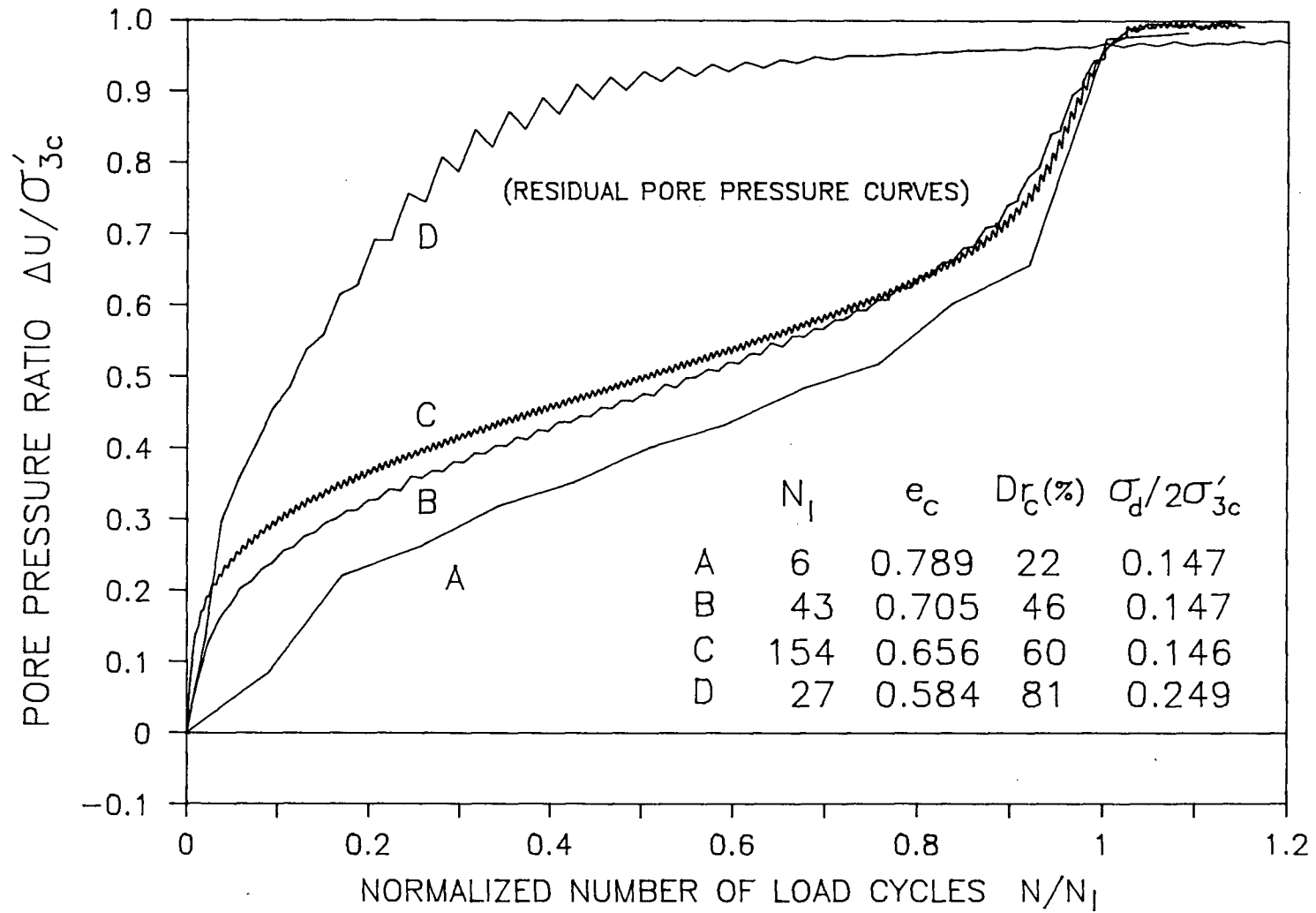
little variation in normalized curves for sands with a relative density between 45% and 60%. The loosest sample at 22% relative density suffered limited liquefaction in extension loading during the sixth load cycle, thus the initial part of the normalized curve suggests relatively lower pore pressure generation before the onset of liquefaction. The dense sample at 81% relative density shows a response which is considerably different than that of looser samples, because the dense material is generally dilative. A great deal of cyclic mobility strain must be developed before an initial state of zero effective stress is achieved.

6.3.4 Relationship Between Induced Strain and Residual Pore Pressure

Figure 6.15 shows how the residual pore pressure generated in clean 20/200 sand during cyclic loading varies with the development of shear strain. The only parameter which is varied in the figure is cyclic stress ratio and hence the number of cycles required to achieve liquefaction. Strain level is defined as the difference between peak extension and peak compression strain during a given load cycle. The figure shows that there is no direct relationship between residual pore pressure and shear strain level induced by cyclic loading. In fact, estimates of pore pressure based upon strain level may be off by 60% depending upon the magnitude of cyclic stress ratio.

Figure 6.15 Variation of pore pressure generation in clean 20/200 sand with shear strain level during cyclic loading

$Dr_c = 45\%$

$\sigma_c' = 350$ kPa

TEST	N_L	$\sigma_d/2\sigma_{3c}'$
A	233	0.1114
B	54	0.1314
C	43	0.1386
D	16	0.1620
E	10	0.1786
F	7	0.1929
G	4	0.2214

PORE PRESSURE RATIO $\Delta U/\sigma_{3c}'$

$\varepsilon_{a_{max}} - \varepsilon_{a_{min}}$
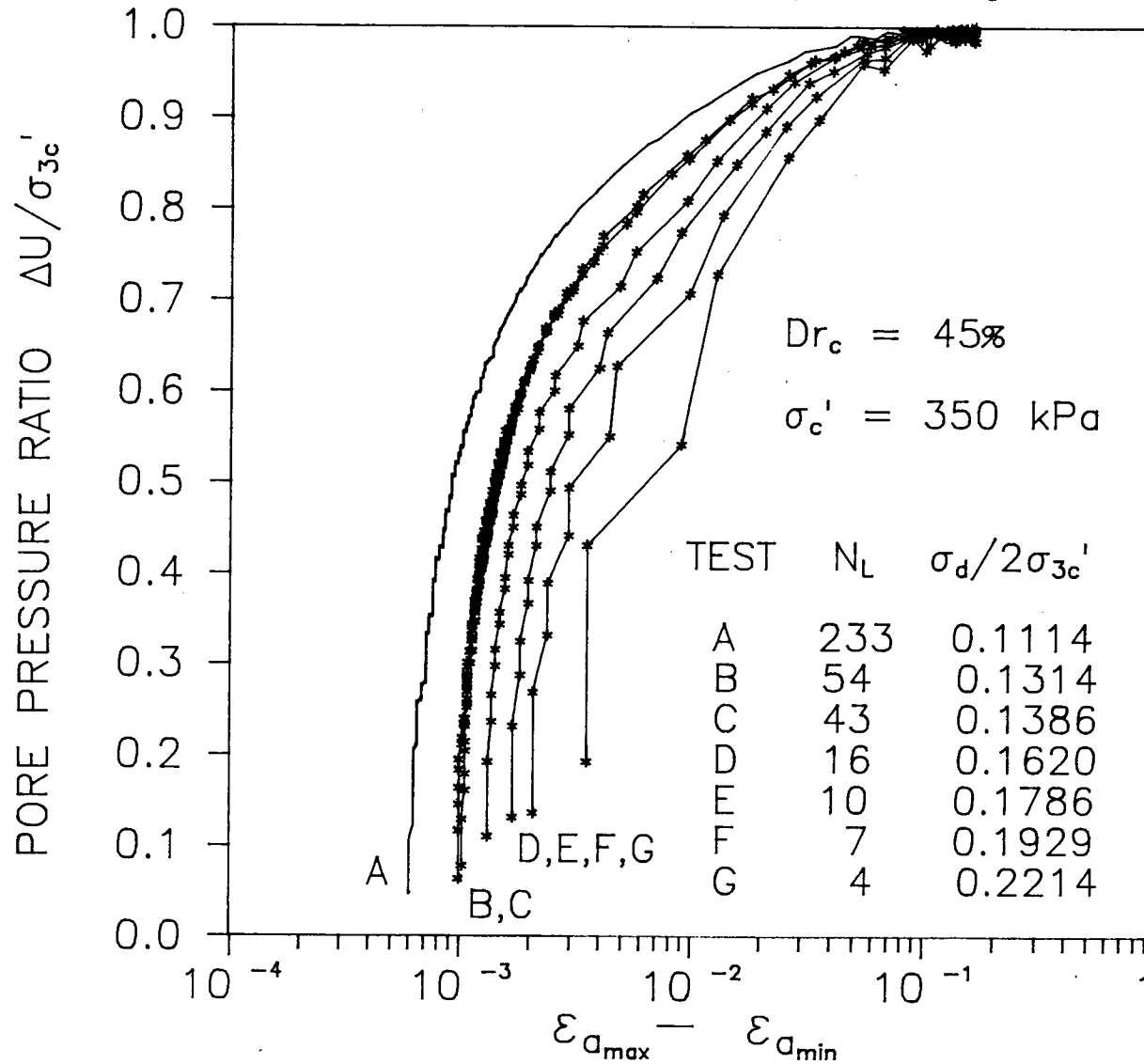
6.3.5 Relationship Between Residual Pore Pressure and Hysteretic Work

Some researchers have attempted to relate residual pore pressure to damage induced in a soil sample during cyclic loading (Finn and Bhatia, 1981). The damage induced within a soil specimen may be quantified by the irrecoverable work absorbed by the specimen during cyclic loading. This work may be easily calculated from the stress-strain loops observed during cyclic loading (Figure 6.16). Irrecoverable work absorbed per unit volume of soil is equal to the cumulative area within hysteretic stress-strain loops. The hysteretic work absorbed by a sand specimen during cyclic loading has been shown by Towhata and Ishihara (1985) to correlate well with induced residual pore pressure. Their hollow cylinder test results for Toyoura sand show that the correlation between hysteretic work and residual pore pressure is valid regardless of stress path and mode of loading.

The development of residual pore pressure in clean 20/200 sand during cyclic loading is plotted versus irrecoverable work absorbed by the soil (see Figure 6.17). A good correlation is observed between the two parameters for samples which undergo liquefaction in less than 60 cycles. The correlation is not as good for samples which require a large number of cycles to achieve liquefaction, possibly due to accumulation of error in the calculation of area within stress-strain loops, which increases proportionally to the number of loading cycles.

Figure 6.16 Calculation of irrecoverable work absorbed by a soil specimen from stress—strain response observed during cyclic loading

APPROXIMATION OF HYSTERETIC
WORK WITHIN STRESS—STRAIN LOOP

$Dr_c = 45\%$

$\sigma_c' = 350$ kPa

$N_l = 10$ CYCLES

$\sigma_d/2\sigma_{3c}' = 0.1786$

THIRD LOAD CYCLE
STRESS—STRAIN LOOP

WELL GRADED 20/200
BRENDA SAND

DEVIATOR STRESS σ_d (kPa)

AXIAL STRAIN (PERCENT)
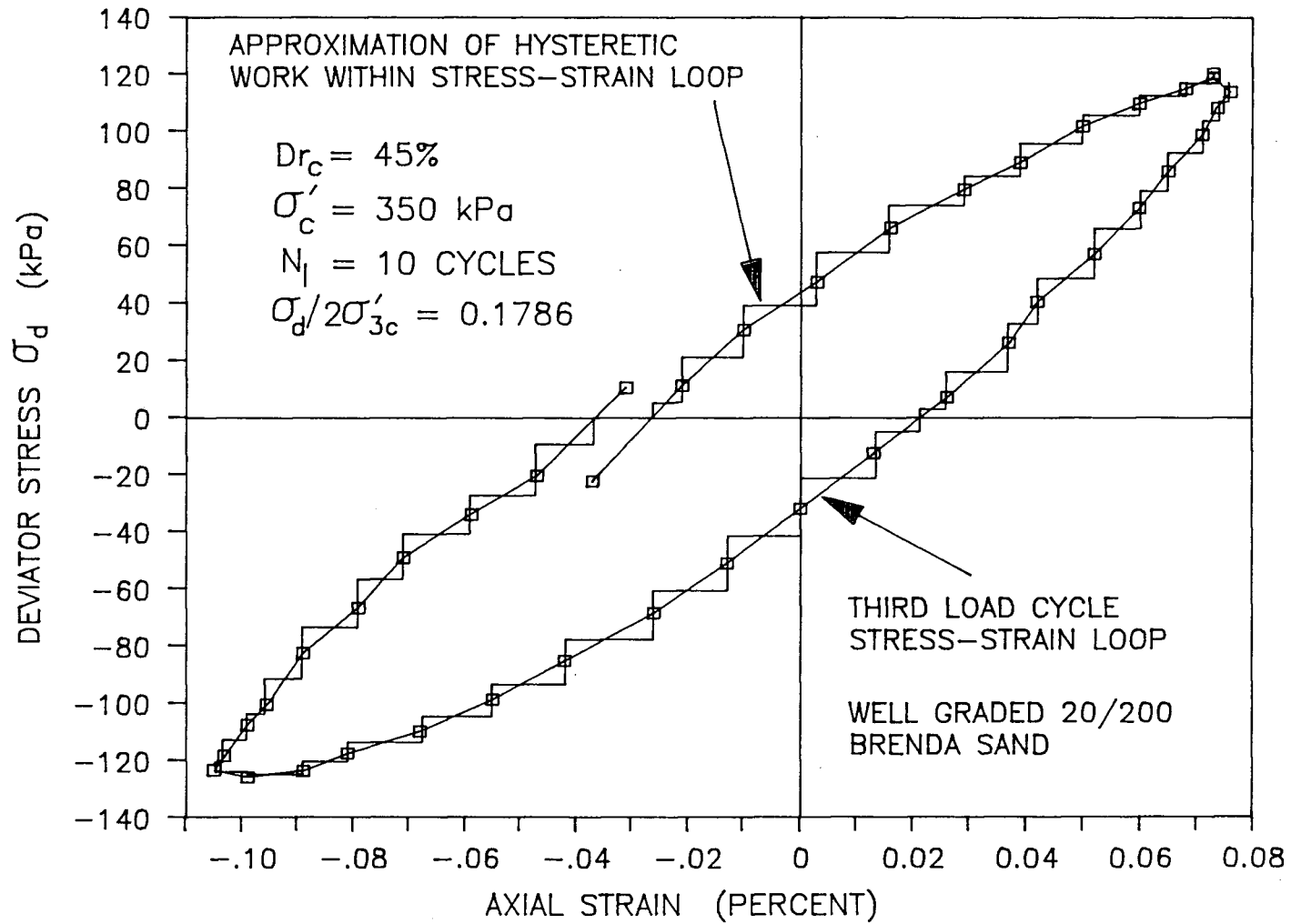
Figure 6.17 Variation of pore pressure generation in loose clean 20/200 sand with hysteretic work absorbed during cyclic loading

$Dr_c = 45\%$

$\sigma_c' = 350 \ kPa$

D,E,F,G   B,C A

TEST	N_L	$\sigma_d/2\sigma_{3c}'$
A	233	0.1114
B	54	0.1314
C	43	0.1386
D	16	0.1620
E	10	0.1786
F	7	0.1929
G	4	0.2214

PORE PRESSURE RATIO $\Delta U/\sigma_{3c}'$

IRRECOVERABLE SHEAR WORK ABSORBED PER UNIT VOLUME OF SOIL (kN/m^2)
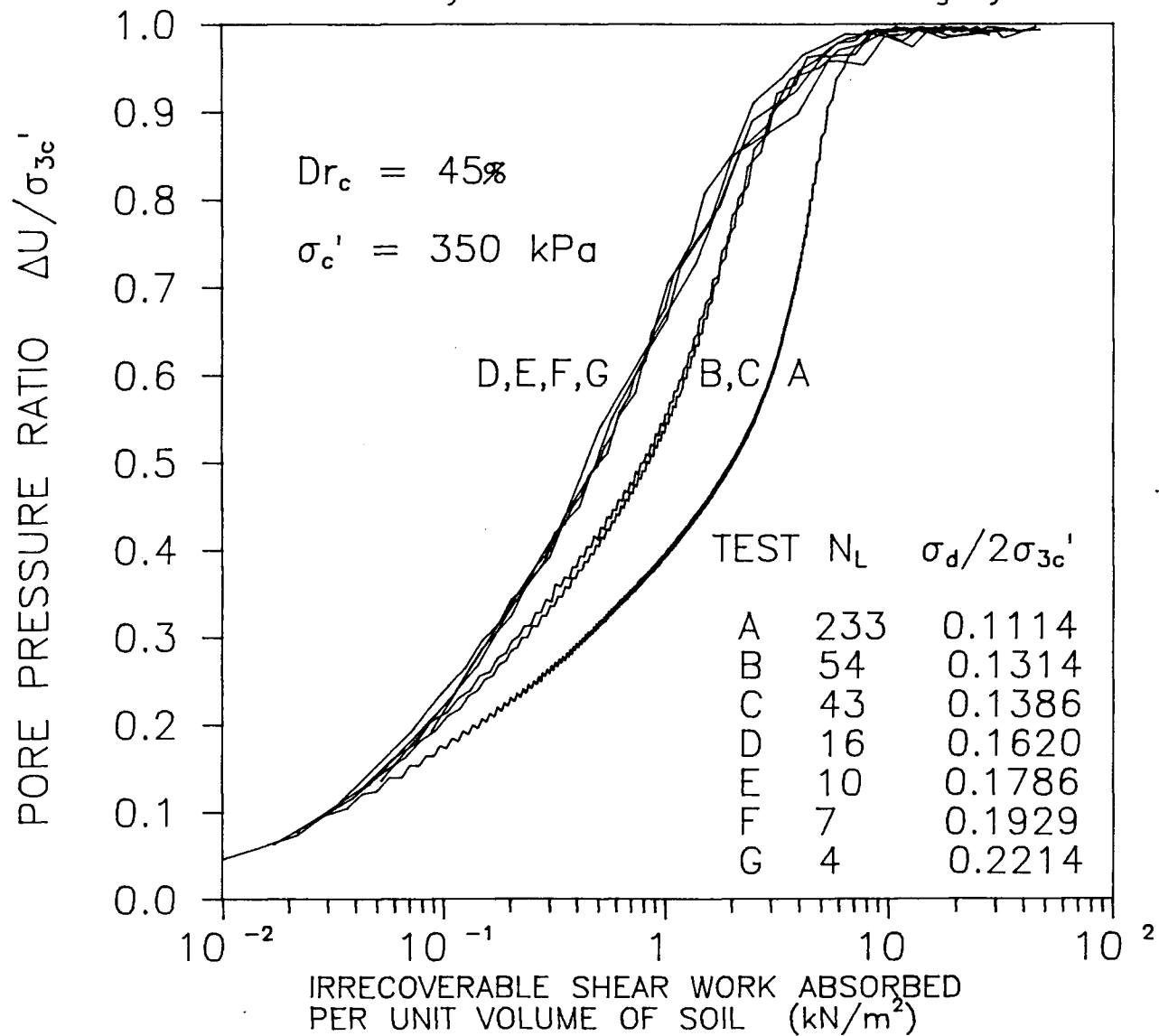
Figure 6.18 shows the relationship between the development of residual pore pressure and irrecoverable hysteretic work in clean sand at various relative densities. Again there is a good correlation between the two parameters, even though relative density, which controls the mode of failure of the various samples under cyclic loading, is varied from 20 to 80%.

Hysteretic work could provide an efficient method for the prediction of residual pore pressure, if stress-strain behaviour can be modelled sufficiently well to predict hysteretic damping.

6.4 CYCLIC RESISTANCE DATA

Cyclic triaxial tests were conducted on clean and silty well-graded Brenda 20/200 sand samples to determine the effect of silt content upon cyclic strength. To show trends in cyclic resistance, raw test data from a series of samples with constant silt content and density is processed by interpolation of curves into different forms to allow different methods of comparison.

6.4.1 Cyclic Resistance Curves at Constant Silt Content

Triaxial samples were prepared by controlling silt content and density. Thus the variation of cyclic strength with number of cycles to liquefaction on constant density contours can be directly observed from test data, as plotted in Section 6.4.1.1. To further reduce cyclic resistance

Figure 6.18   Variation of pore pressure generation in loose to dense clean
20/200 sand with hysteretic work absorbed during cyclic loading
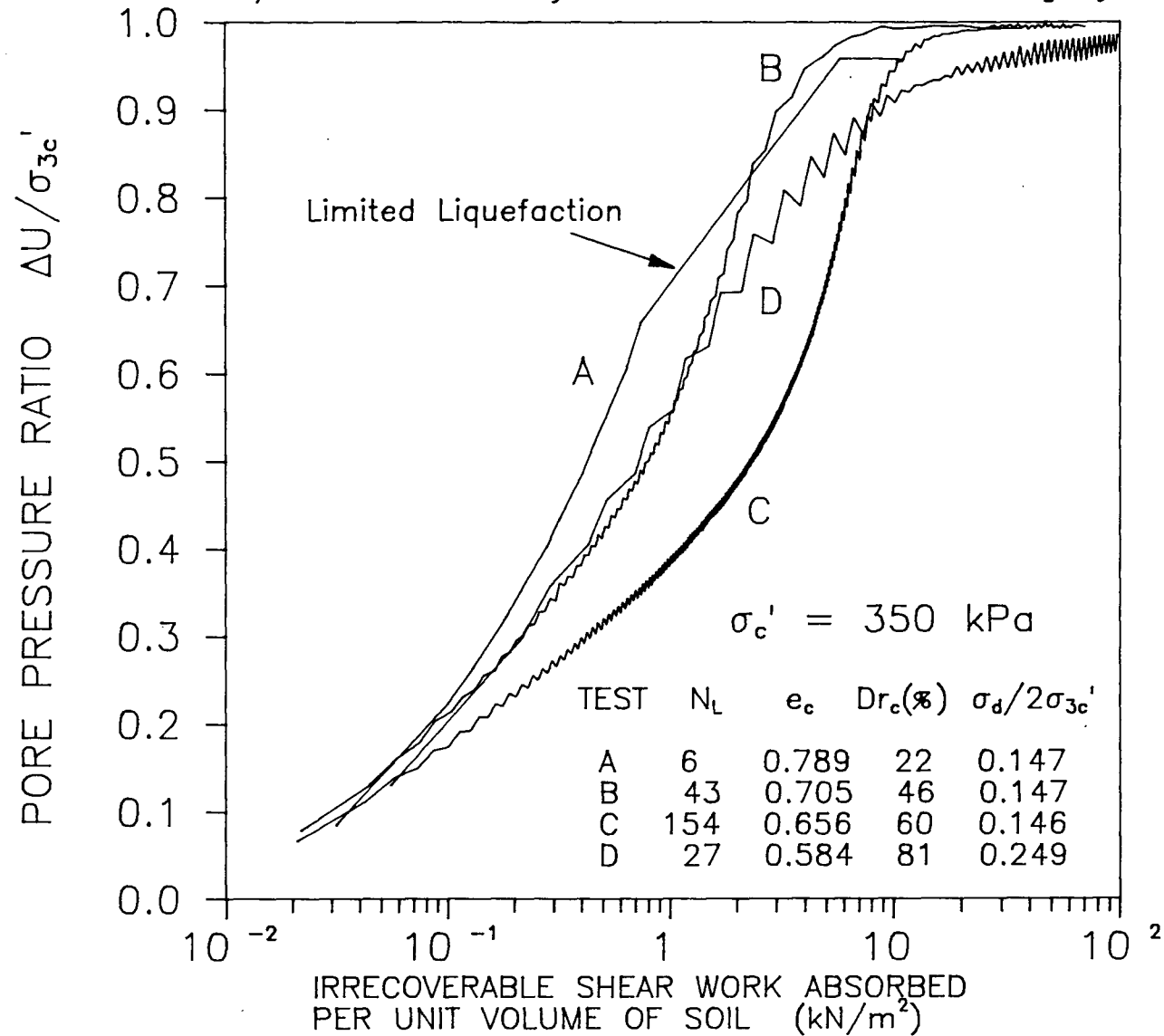
data such that the effects of relative density and silt content may be better understood, raw test data from Section 6.4.1.1 is interpolated to determine contours of constant number of cycles to liquefaction on cyclic stress ratio versus relative density plots presented in Section 6.4.1.2.

6.4.1.1   Raw Test Data Summary - Constant Density Contours

Figures 6.19 through 6.23 show cyclic stress ratio versus number of cycles to liquefaction for clean and silty 20/200 Brenda sand, with each sand at various relative densities.   The range of cyclic strengths shown (cyclic stress ratio from 0.08 to 0.30) is typical of loose to moderately dense sands and silty sands reported by other workers (for example Seed and Lee, 1966, Ishihara, 1980).

In general, cyclic resistance curves are concave upward or straight if the mechanism of strain development is by cyclic mobility (as is the case for most of the curves presented), and concave downward if the mechanism of strain development is by limited liquefaction or steady-state liquefaction.   Only very loose sand samples which were subjected to a relatively large cyclic stress ratio developed limited liquefaction in extension loading, as described in Section 6.1.

The variation of cyclic strength with silt content of samples prepared near loosest state of slurry deposition and isotropic consolidation to 350 kPa is shown in Figure 6.23. At near loosest state, any increase in silt content may be

Figure 6.19 Cyclic loading liquefaction resistance curves of clean 20/200 Brenda sand

CLEAN 20/200 BRENDA SAND

$$\sigma_c' = 350 \text{ kPa}$$

$e_c = 0.584 \pm .001$
$Dr_c = 80.8 \pm 0.3\%$

$e_c = 0.653 \pm .008$
$Dr_c = 61.0 \pm 1.0\%$

$e_c = 0.708 \pm .002$
$Dr_c = 45.2 \pm 0.8\%$

$e_c = 0.798 \pm .013$
$Dr_c = 20.0 \quad (18.5-25.5)\%$

$\oplus$ LIMITED LIQUEFACTION

CYCLIC STRESS RATIO $\sigma_d/(2 \cdot \sigma_{3c}')$

NUMBER OF CYCLES TO LIQUEFACTION (2.5% SINGLE AMPLITUDE STRAIN) N_l
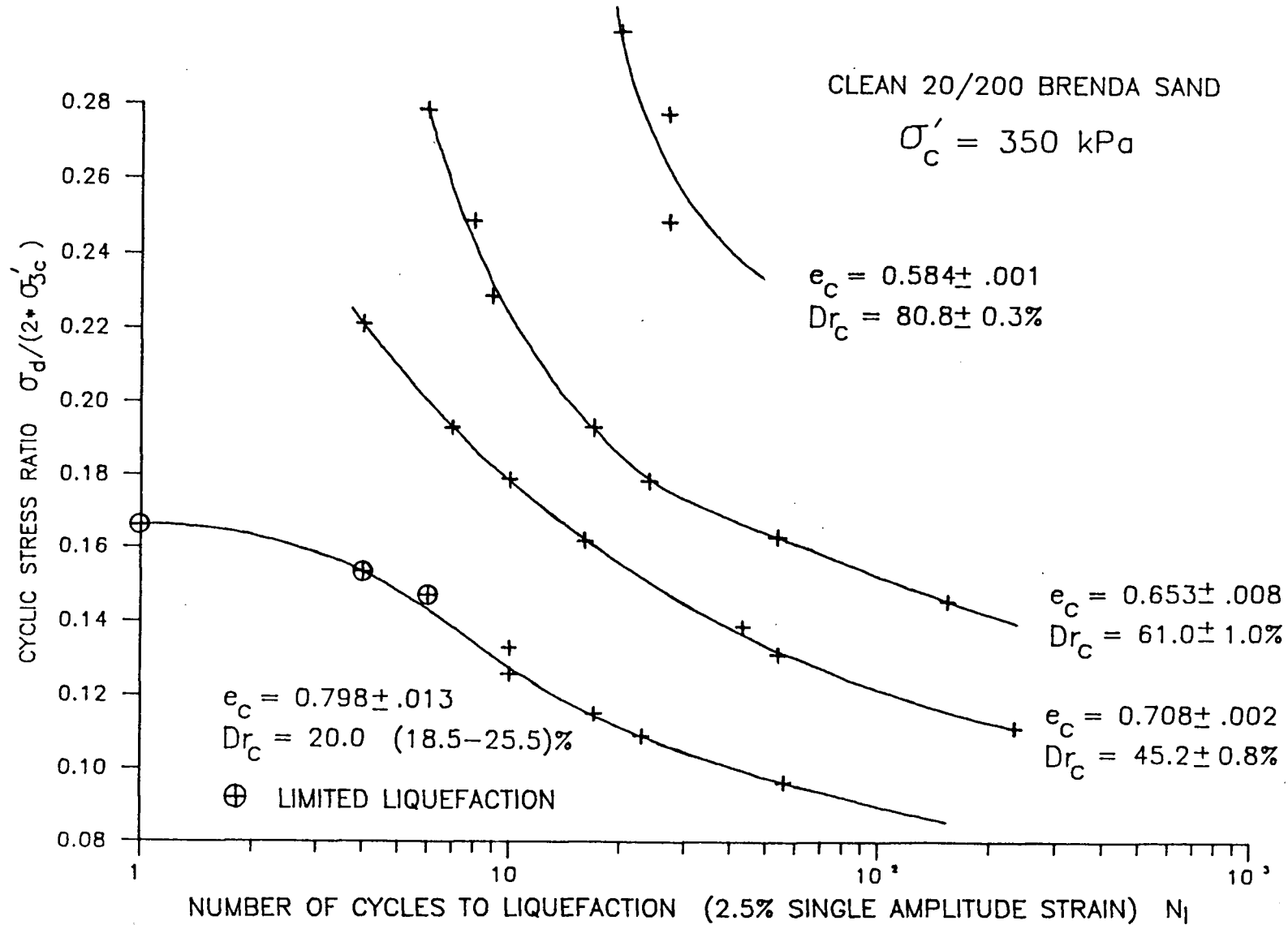
Figure 6.20 Cyclic loading liquefaction resistance curves of silty (4.3% silt) 20/200 Brenda sand

SILTY 20/200 BRENDA SAND

$$\sigma'_c = 350 \text{ kPa}$$

$4.34 \pm .15\%$ SILT

$\oplus$ LIMITED LIQUEFACTION

$e_c = 0.625 \pm .002$

$Dr_c = 60.0 \pm 0.5\%$

$Dr_c \text{ (skeleton)} = 47.5 \pm 0.5\%$

$e_c = 0.674 \pm .003$

$Dr_c = 46.0 \pm 0.5\%$

$Dr_c \text{ (skeleton)} = 32.3 \pm 0.5\%$

$e_c = 0.710 \pm .008$

$Dr_c = 35.0 \pm 2.1\%$

$Dr_c \text{ (skeleton)} = 22.6 \pm 2.2\%$

$4.0 \pm .20\%$ SILT

$4.5 \pm .21\%$ SILT

CYCLIC STRESS RATIO $\sigma_d/(2 * \sigma'_{3c})$

NUMBER OF CYCLES TO LIQUEFACTION (2.5% SINGLE AMPLITUDE STRAIN) N_l
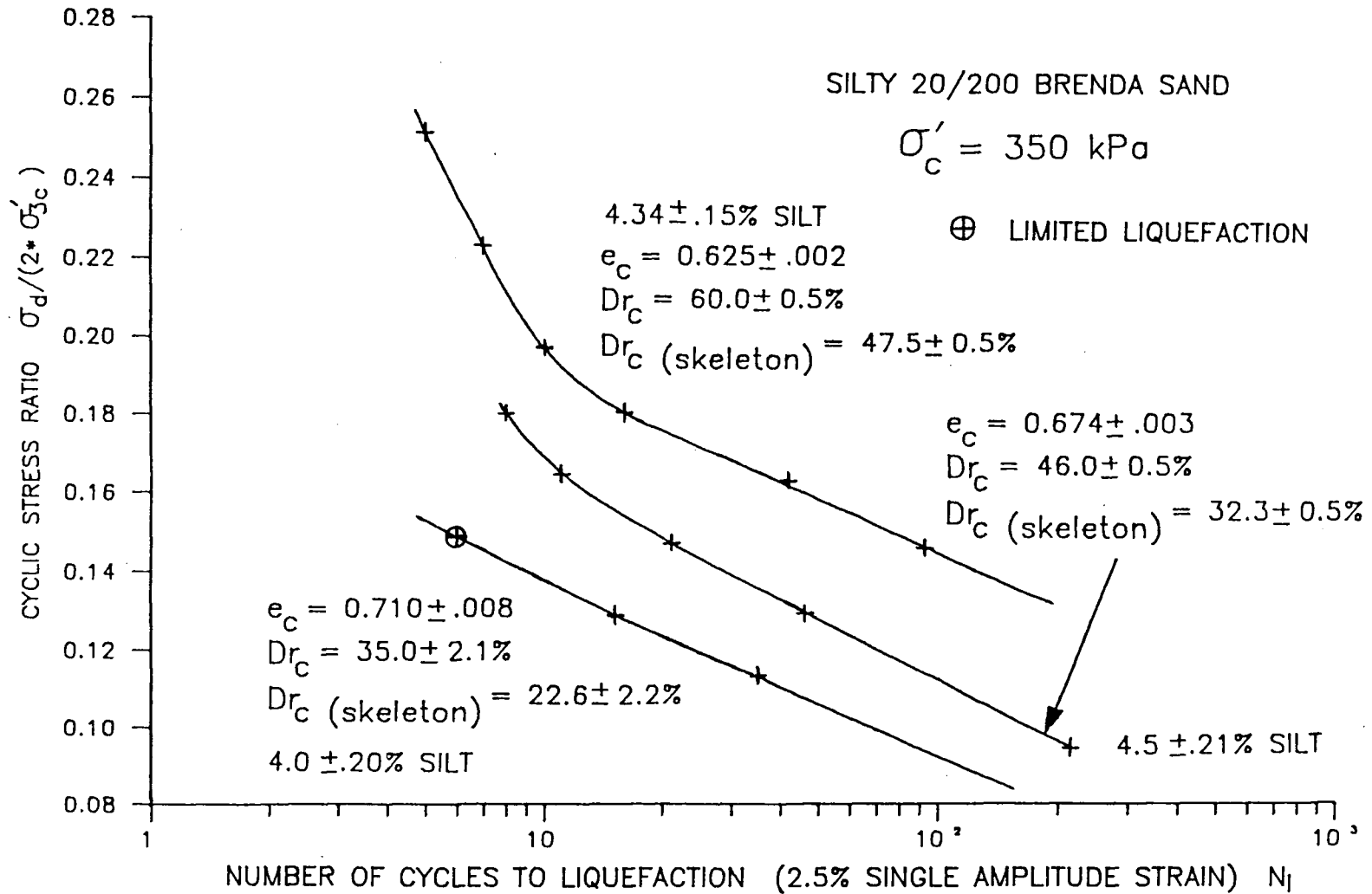
Figure 6.21   Cyclic loading liquefaction resistance curves of silty (7.5% silt) 20/200 Brenda sand

SILTY 20/200 BRENDA SAND

$$\sigma'_c = 350 \text{ kPa}$$

7.6 ±.30% SILT
$e_c = 0.605 \pm .005$
$Dr_c = 61.0 \pm 1.0\%$
$Dr_c \text{ (skel)} = 36.6 \pm 0.5\%$

7.3 ±.15% SILT
$e_c = 0.557 \pm .003$
$Dr_c = 74.5 \pm 0.7\%$
$Dr_c \text{ (skeleton)} = 53.2 \pm 1.0\%$

⊕   LIMITED LIQUEFACTION

7.76 ±.30% SILT
$e_c = 0.655 \pm .006$
$Dr_c = 47.2 \pm 1.5\%$
$Dr_c \text{ (skeleton)} = 20.0 \pm 1.5\%$

7.71 ±.10% SILT
$e_c = 0.643 \pm .006$
$Dr_c = 50.1 \pm 1.0\%$
$Dr_c \text{ (skel)} = 23.5 \pm 1.5\%$

CYCLIC STRESS RATIO $\sigma_d/(2 \cdot \sigma'_{3c})$

NUMBER OF CYCLES TO LIQUEFACTION   (2.5% SINGLE AMPLITUDE STRAIN) N_l
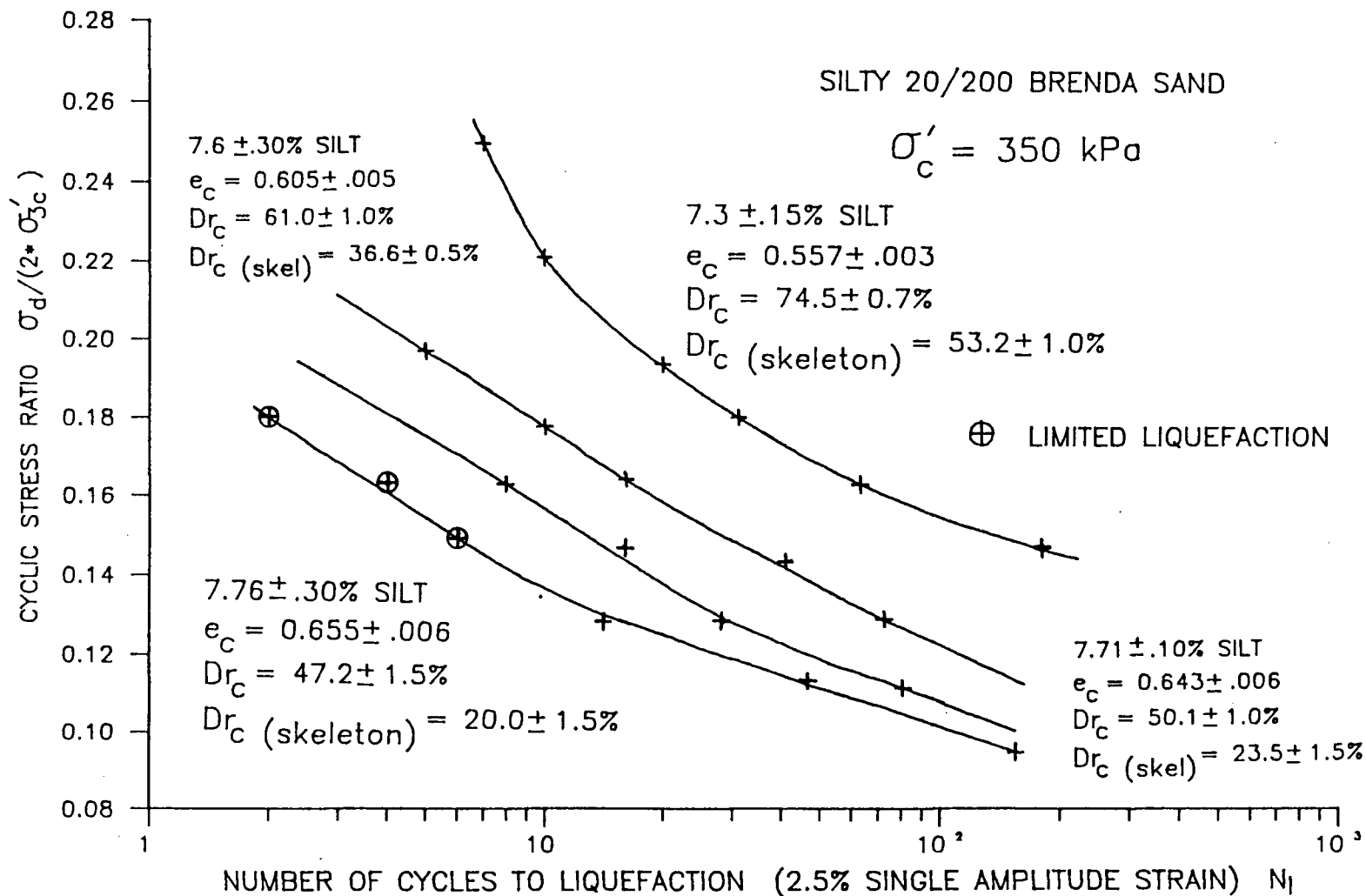
Figure 6.22   Cyclic loading liquefaction resistance curves of silty (13.5% silt) 20/200 Brenda sand

SILTY 20/200 BRENDA SAND

$$\sigma'_c = 350 \text{ kPa}$$

$\oplus$ LIMITED LIQUEFACTION

$13.33 \pm .15\%$ SILT
$e_c = 0.442 \pm .002$
$Dr_c = 94.9 \pm 0.6\%$
$Dr_c \text{ (skeleton)} = 57.5 \pm 0.1\%$

$13.94 \pm .13\%$ SILT
$e_c = 0.534 \pm .007$
$Dr_c = 71.0 \pm 2\%$
$Dr_c \text{ (skeleton)} = 20.0 \pm 2\%$

$13.67 \pm .14\%$ SILT
$e_c = 0.488 \pm .001$
$Dr_c = 83.1 \pm 0.3\%$
$Dr_c \text{ (skeleton)} = 40.0 \pm 0.5\%$

CYCLIC STRESS RATIO $\sigma_d/(2*\sigma'_{3c})$

NUMBER OF CYCLES TO LIQUEFACTION   (2.5% SINGLE AMPLITUDE STRAIN) N_l
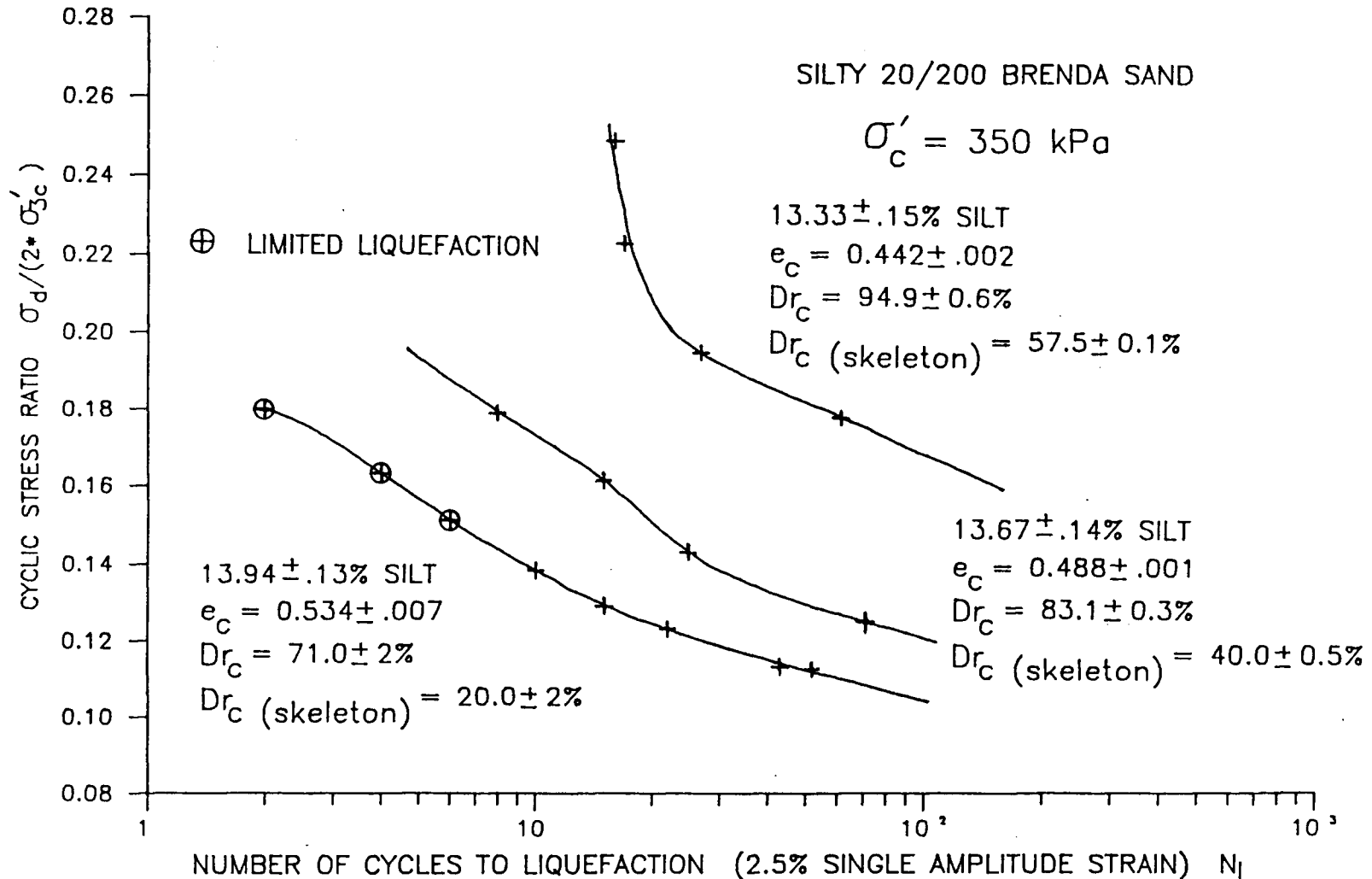
Figure 6.23 Cyclic loading liquefaction resistance curves of silty 20/200 sand at near loosest state of slurry deposition

PERCENTAGE SILT
CONTENT BY WEIGHT

0 ———————
4.3 —— —— ——
7.5 — — — — — ·
13.5 ············
21 —— —+—·—

SILTY 20/200 BRENDA SAND

$\sigma_c' = 350 \text{ kPa}$

$21 \pm 1.6\%$ SILT

$e_c = 0.446 \pm .006$

$Dr_c = 96 \pm 2.5\%$

$Dr_{c \text{ (skel)}} = 8 \ (-1.5 \text{ to } 14.6)\%$

CYCLIC STRESS RATIO $\sigma_d/(2 \cdot \sigma_{3c}')$

NUMBER OF CYCLES TO LIQUEFACTION (2.5% SINGLE AMPLITUDE STRAIN) N_l
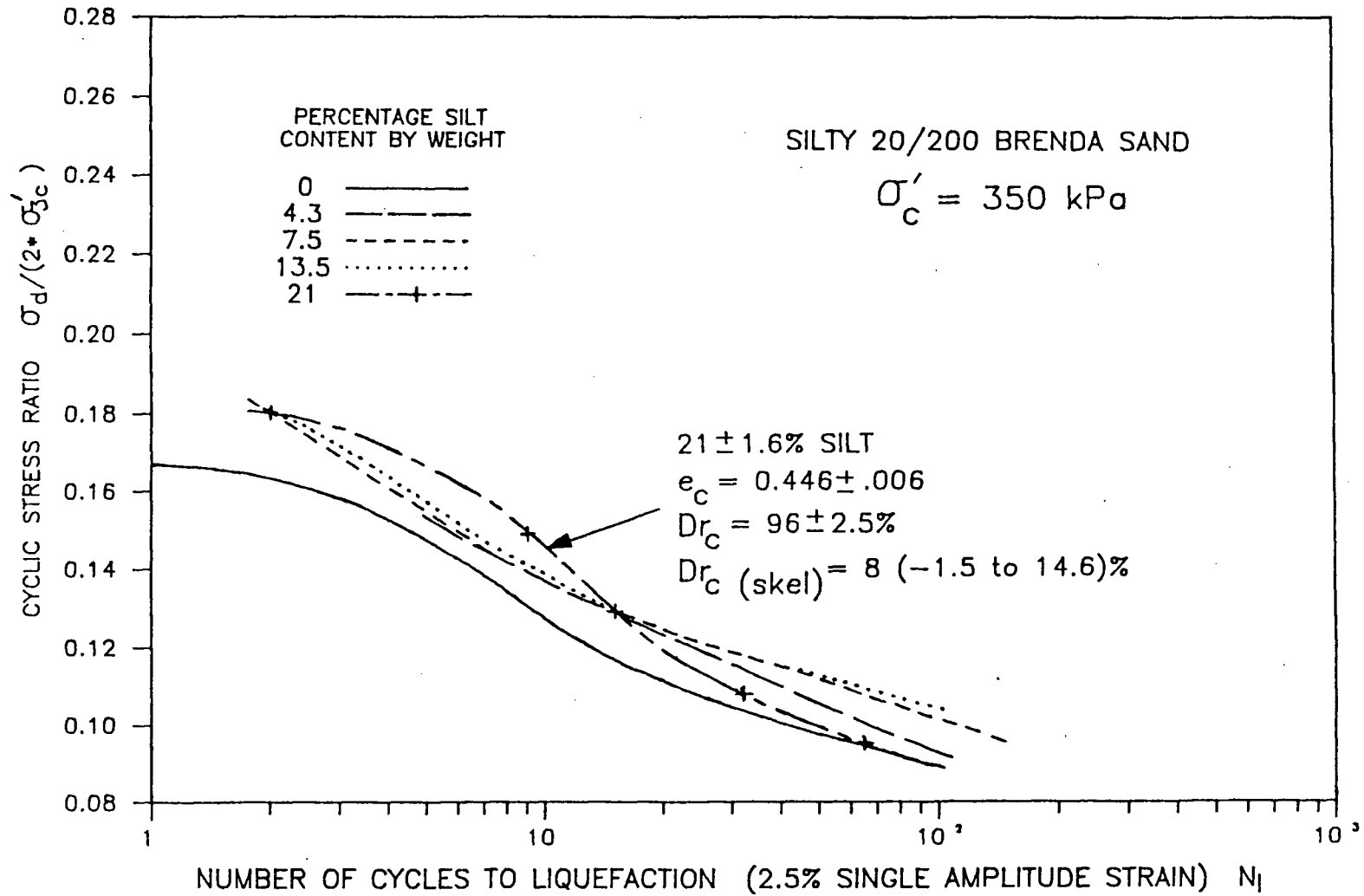
seen to increase the cyclic resistance of the sand. In some cases, a small increase in silt content may apparently increase cyclic strength more than a larger increase in silt content.

6.4.1.2 Comparison of Cyclic Strength in Fixed Number of Cycles to Liquefaction

Figures 6.24 through 6.27 show cyclic stress ratio versus standard relative density curves for several fixed number of cycles to liquefaction. The curves were interpolated from raw data presented in Section 6.4.1.1.

Although the range of cyclic strength does not change with silt content, standard relative density is shown to increase substantially with increase in silt content. When compared in terms of standard relative density (for the small range in which some curves overlap), silt content is shown to drastically reduce cyclic strength. This observation leads one to the conclusion made in Section 3.2.2.4, Section 5.4 and by other researchers (Ishihara, 1980, and ASTM D-2049-69) that the standard ASTM relative density provides a relatively poor basis for the comparison of mechanical properties of silty sand.

In Figure 6.25 and Figure 6.26 one can see that cyclic resistance drops off rapidly near loosest state of slurry deposition. Bulked silty sand samples with lower standard ASTM relative densities could be prepared by moist tamping or dry pluviation, as described in Section 3.3.1. Such samples would tend to be metastable under monotonic or

Figure 6.24   Cyclic loading liquefaction resistance curves of clean 20/200 Brenda sand

CLEAN 20/200 BRENDA SAND

$\sigma'_c = 350$ kPa

N_l = NUMBER OF CYCLES TO LIQUEFACTION
(2.5% SINGLE AMPLITUDE STRAIN)

$N_l = 10$

$N_l = 20$

$N_l = 50$

$N_l = 100$

CYCLIC STRESS RATIO $\sigma_d/(2*\sigma'_{3c})$

ASTM STANDARD RELATIVE DENSITY Dr_c (%)
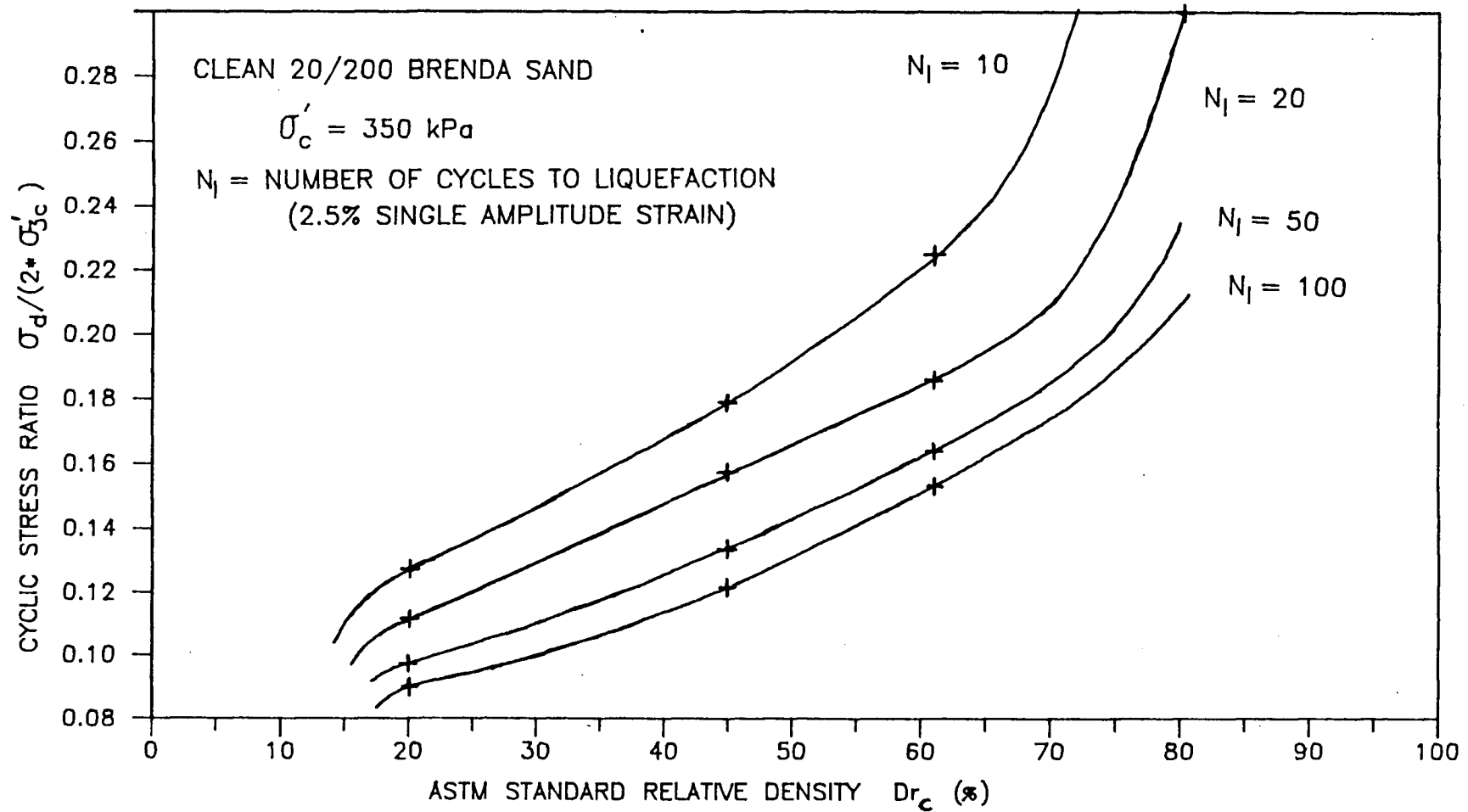
Figure 6.25 Cyclic loading liquefaction resistance curves of silty (4.3% silt) 20/200 Brenda sand
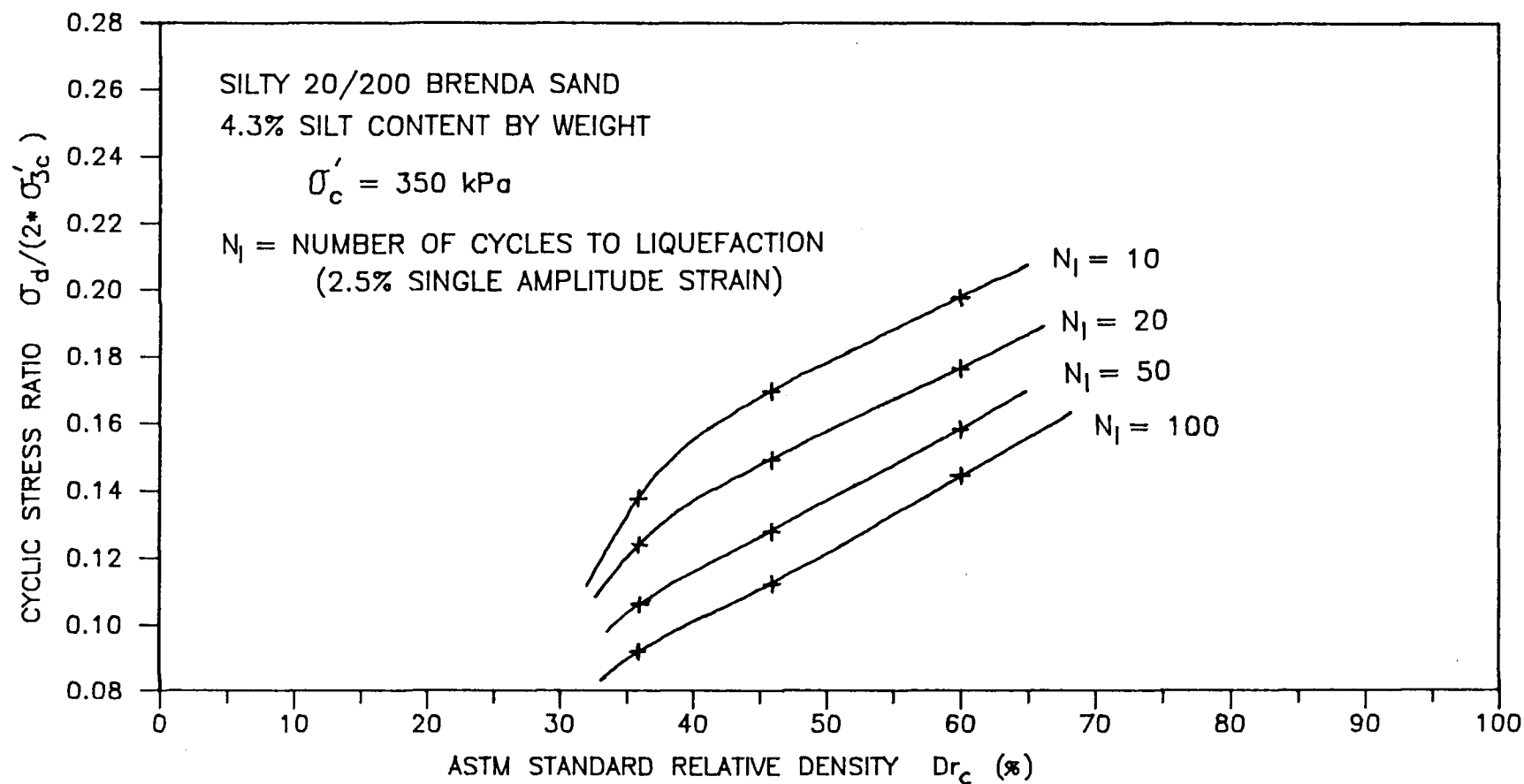
Figure 6.26 Cyclic loading liquefaction resistance curves of silty (7.5% silt) 20/200 Brenda sand
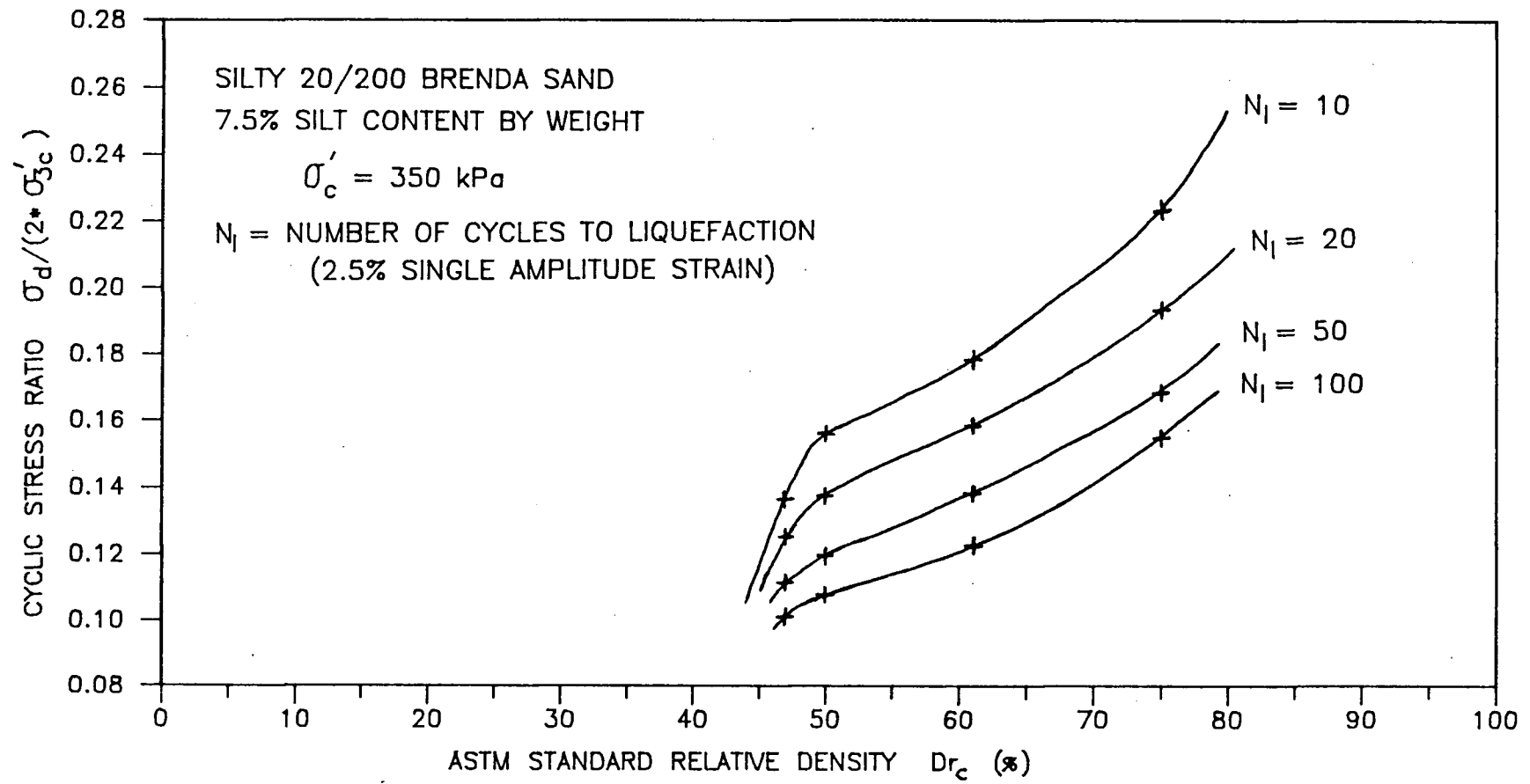
Figure 6.27 Cyclic loading liquefaction resistance curves of silty (13.5% silt) 20/200 Brenda sand

SILTY 20/200 BRENDA SAND
13.5% SILT CONTENT BY WEIGHT

$\sigma_c' = 350 \text{ kPa}$

N_l = NUMBER OF CYCLES TO LIQUEFACTION
(2.5% SINGLE AMPLITUDE STRAIN)

$N_l = 10$
$N_l = 20$
$N_l = 50$
$N_l = 100$

CYCLIC STRESS RATIO $\sigma_d/(2 * \sigma_{3c}')$

ASTM STANDARD RELATIVE DENSITY Dr_c (%)
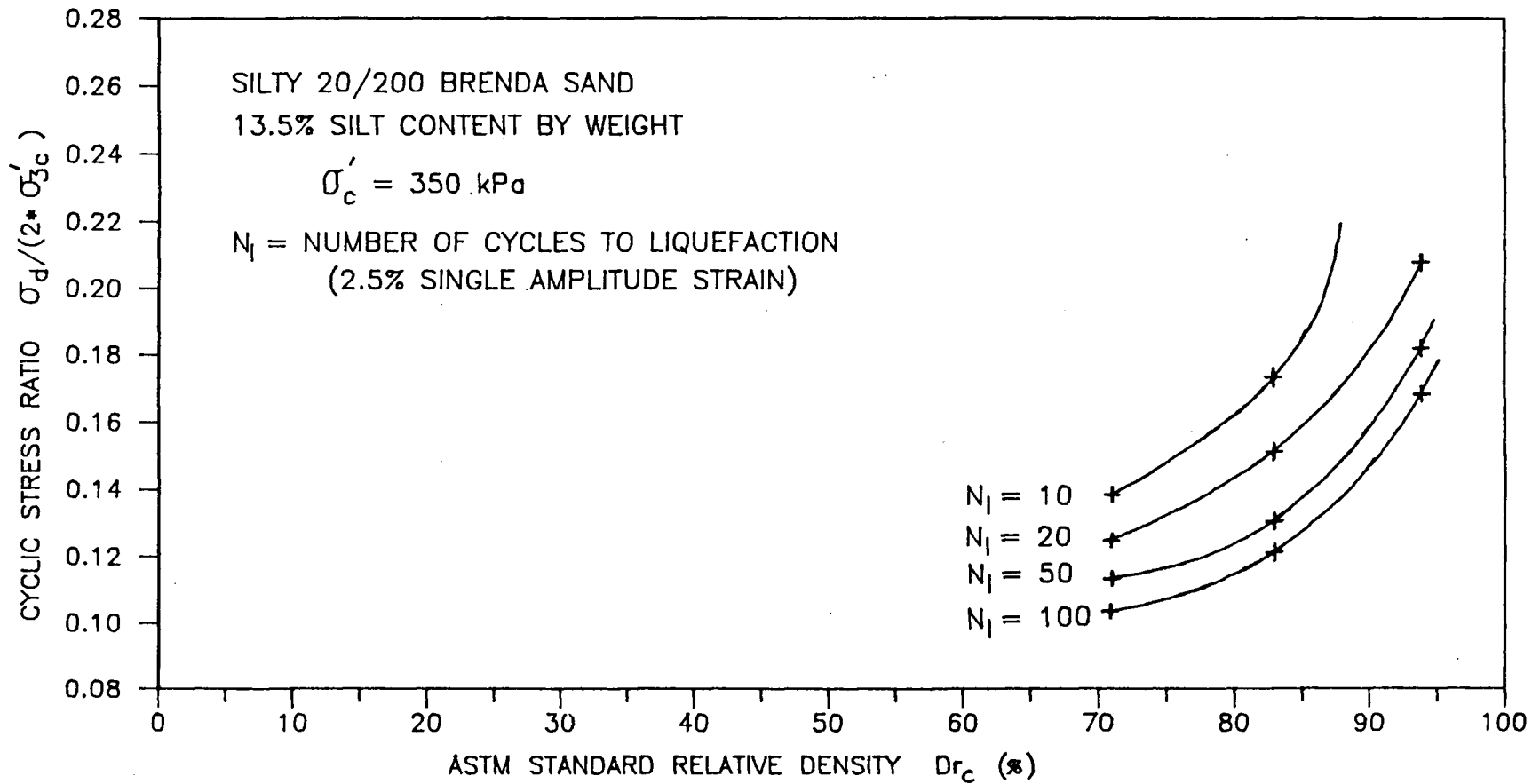
cyclic loading and would be subject to very low steady-state liquefaction strength as described by Castro (1969). Unsegregated water pluviated clean and silty 20/200 sand samples are possible only in the range of relative densities shown.

The data shown in Figures 6.24 through 6.27 is replotted in terms of sand skeleton relative density, as shown in Figures 6.28 through 6.30. In terms of sand skeleton relative density it is observed that the cyclic resistance curves for different silt contents are very similar. This indicates that cyclic strength is governed mainly by the sand portion of silty sand for up to about 20% homogeneous silt content. Silt content tends to increase cyclic strength somewhat when sand skeleton relative density is chosen as the basis for comparison.

6.4.2 Effect of Silt Content on Cyclic Resistance

Data presented in Section 6.4.1 may be interpolated to form a set of curves which show the effect of silt content on the cyclic strength of silty 20/200 Brenda sand. Such curves are presented in the following sections.

6.4.2.1 Variation of Cyclic Strength With Void Ratio

Ishihara et al. (1980) have suggested that in the case of silty sands, void ratio might be a better basis for the comparison of cyclic strength. Figure 6.31 through Figure 6.34 show such variation of cyclic strength for a given number of load cycles to liquefaction (10, 20, 50, and 100

Figure 6.28 Cyclic loading liquefaction resistance curves of silty (4.3% silt) 20/200 Brenda sand
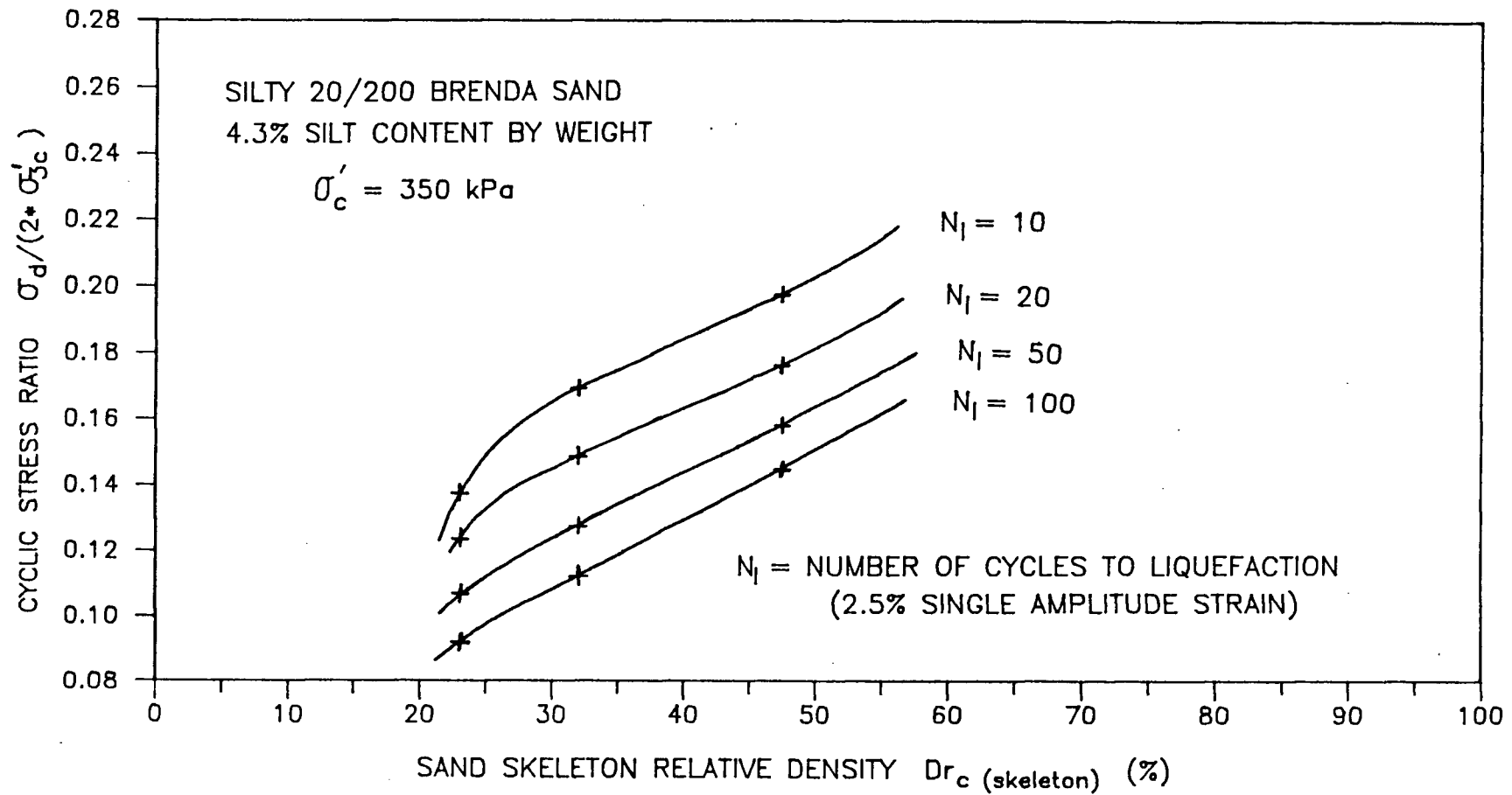
Figure 6.29 Cyclic loading liquefaction resistance curves of silty (7.5% silt) 20/200 Brenda sand

SILTY 20/200 BRENDA SAND
7.5% SILT CONTENT BY WEIGHT

$\sigma'_c = 350$ kPa

$N_l = 10$
$N_l = 20$
$N_l = 50$
$N_l = 100$

N_l = NUMBER OF CYCLES TO LIQUEFACTION
(2.5% SINGLE AMPLITUDE STRAIN)

CYCLIC STRESS RATIO $\sigma_d/(2 \cdot \sigma'_{3c})$

SAND SKELETON RELATIVE DENSITY Dr_c (skeleton) (%)
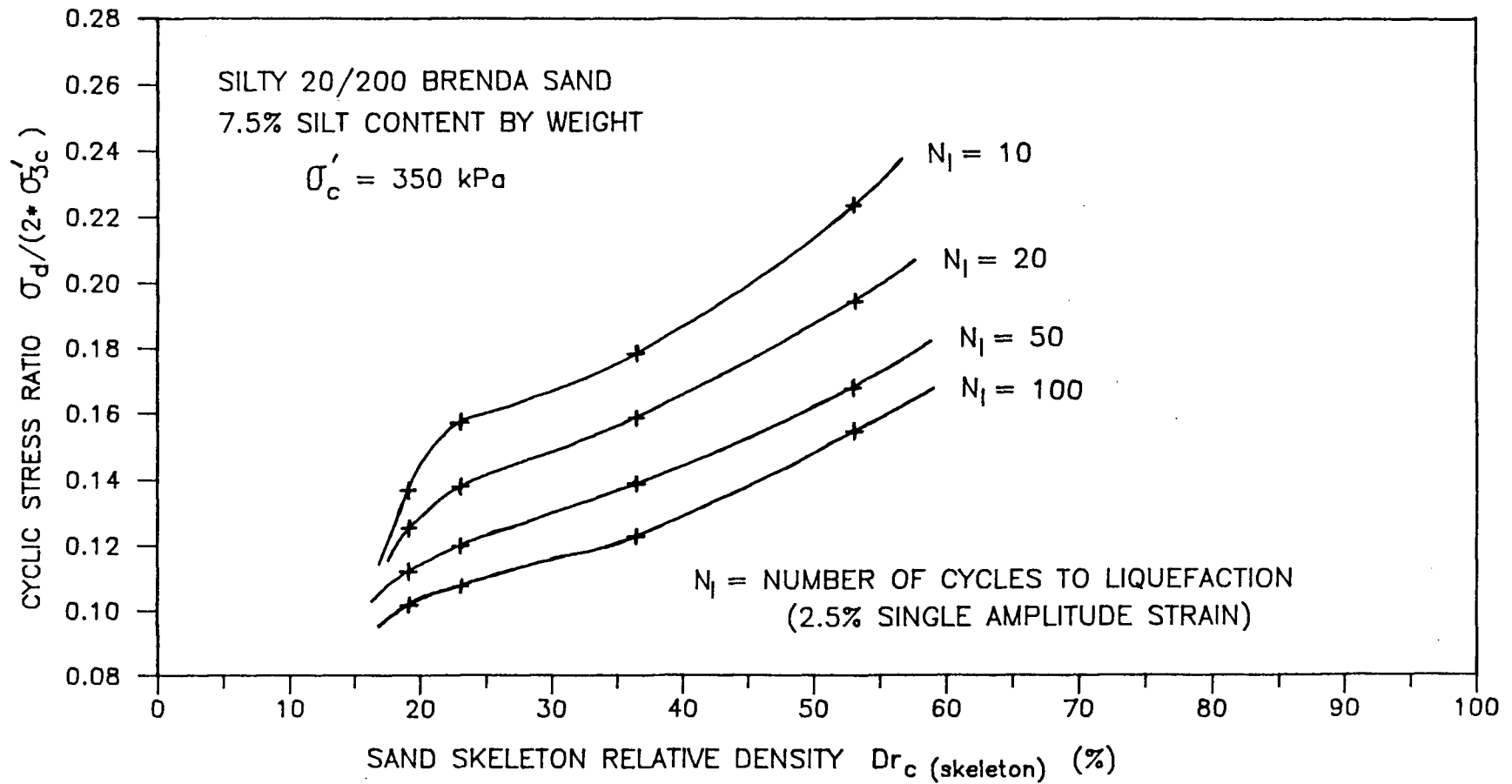
Figure 6.30 Cyclic loading liquefaction resistance curves of silty (13.5% silt) 20/200 Brenda sand
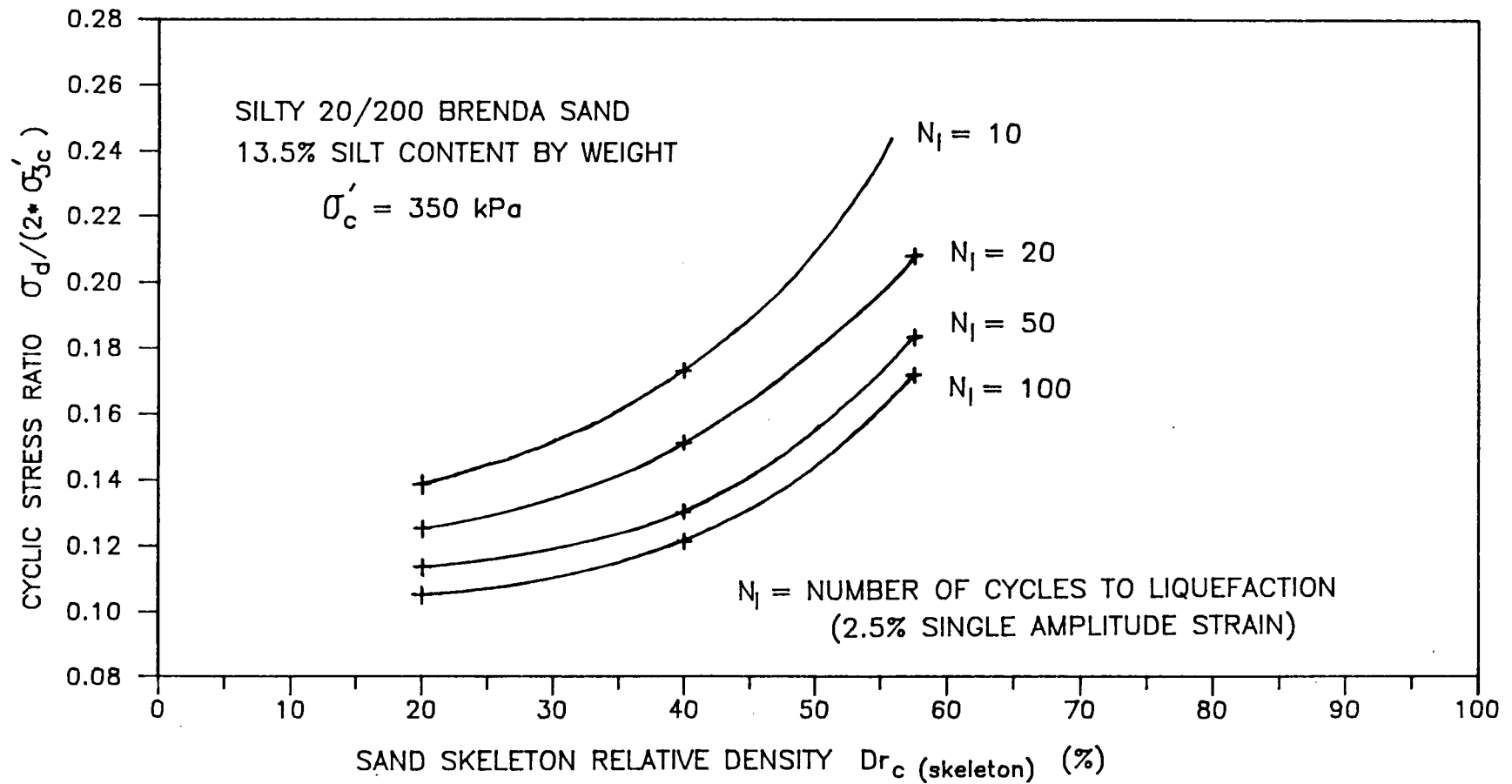
Figure 6.31 Variation of silty 20/200 sand resistance to liquefaction in 10 load cycles with consolidation void ratio
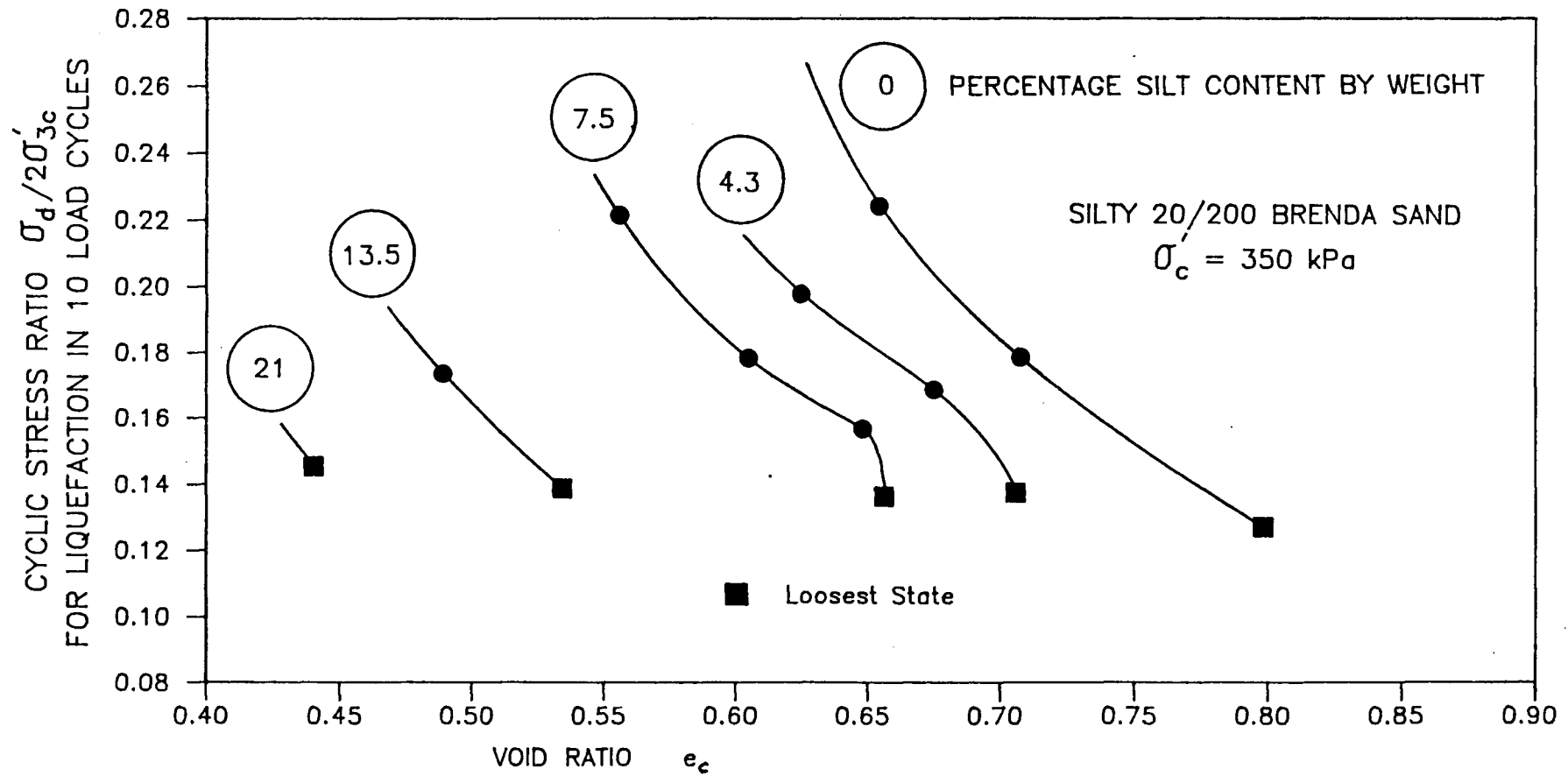
Figure 6.32 Variation of silty 20/200 sand resistance to liquefaction in 20
load cycles with consolidation void ratio
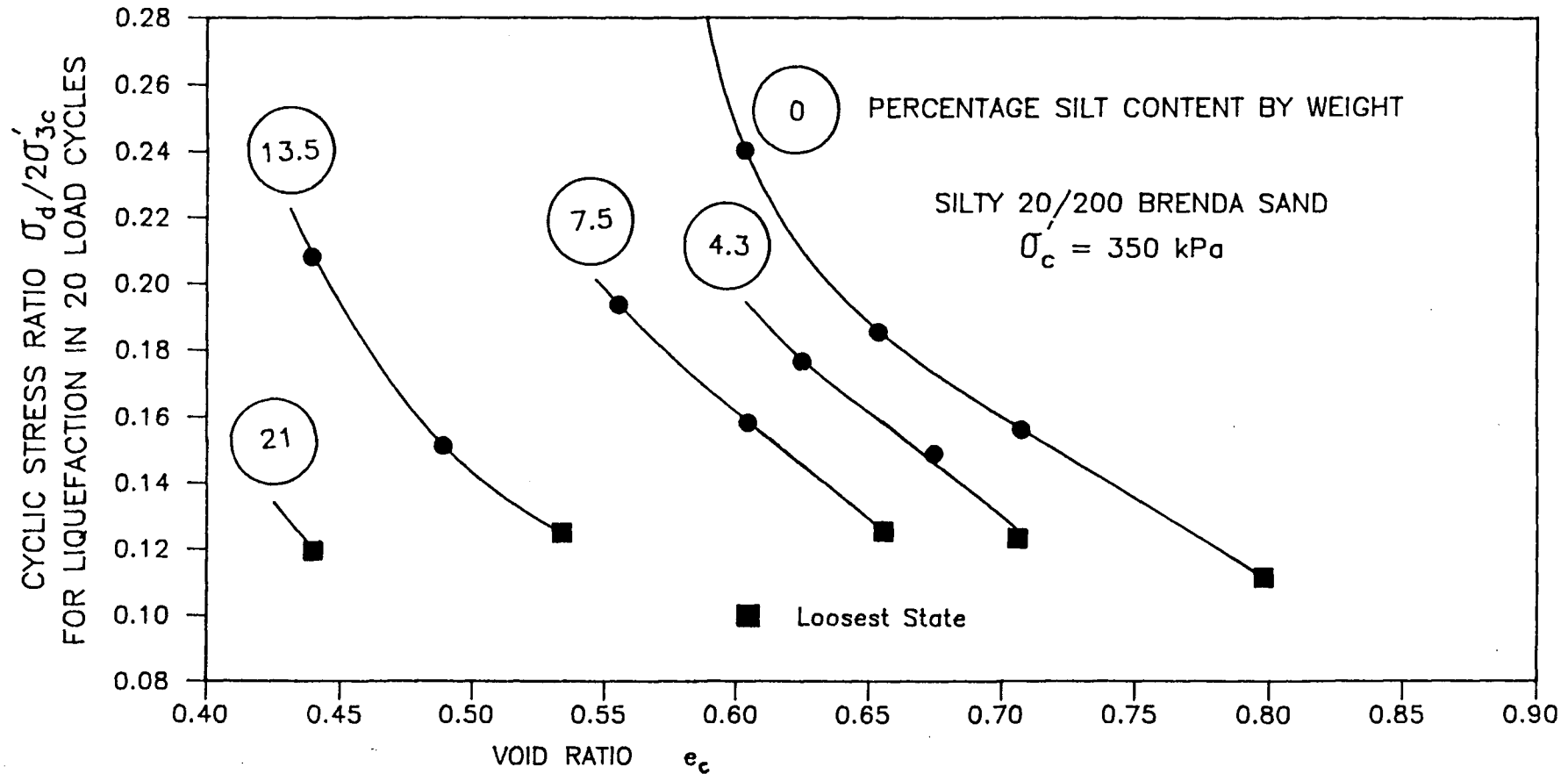
Figure 6.33 Variation of silty 20/200 sand resistance to liquefaction in 50 load cycles with consolidation void ratio
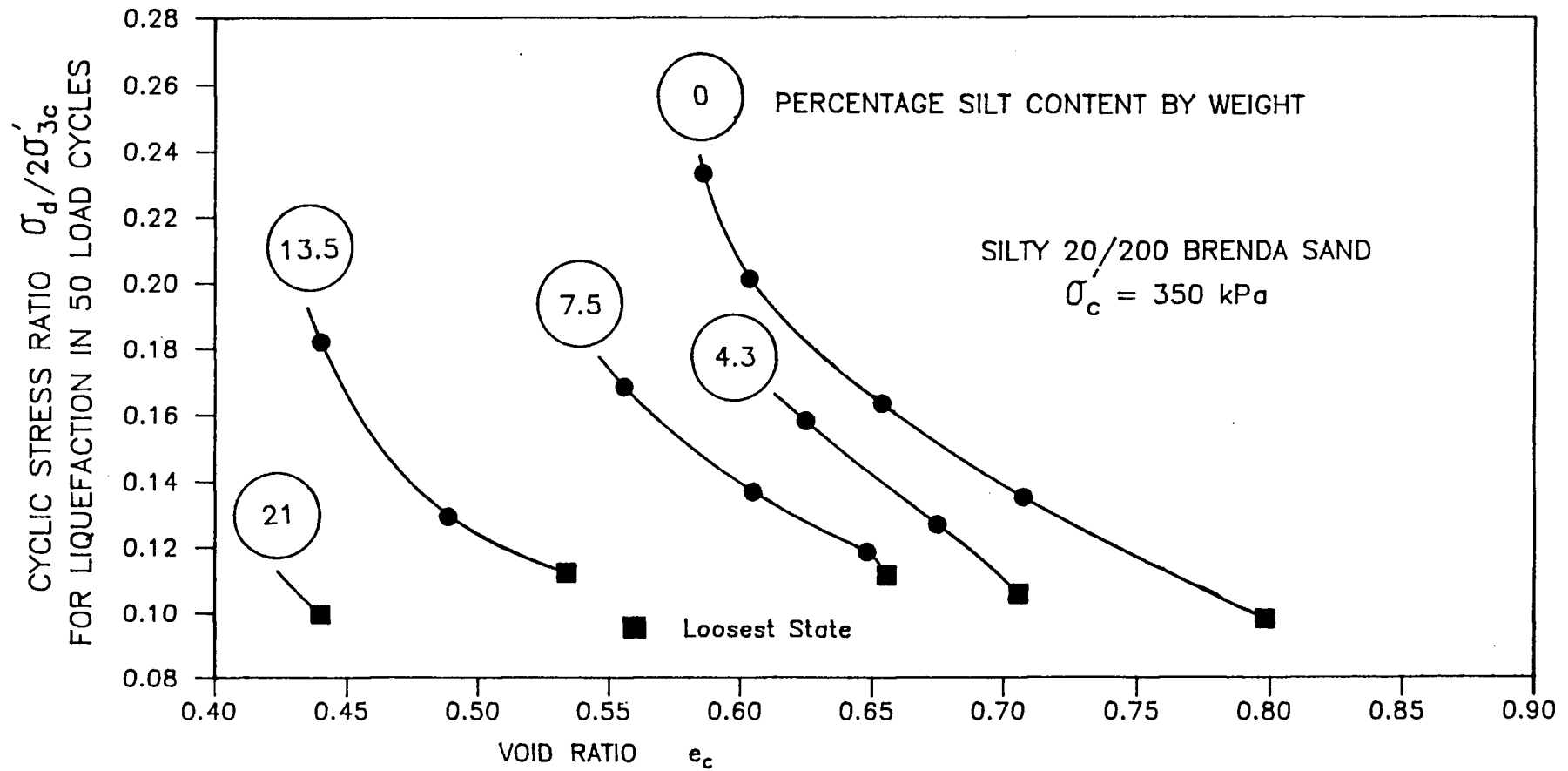
Figure 6.34 Variation of silty 20/200 sand resistance to liquefaction in 100 load cycles with consolidation void ratio
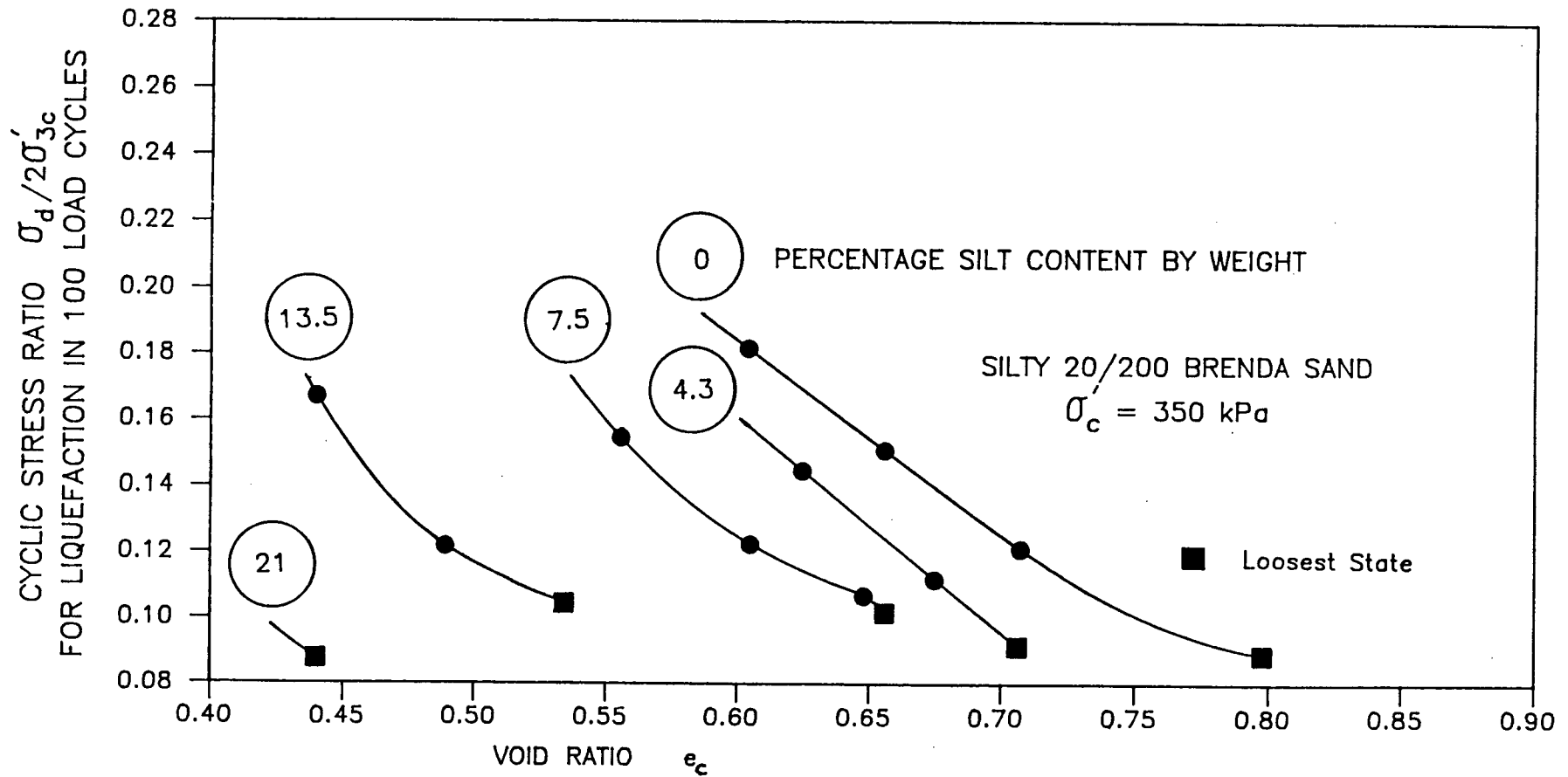
load cycles) for silty 20/200 sand. The figures show that near loosest state of deposition (the lowest data point on each curve), silty 20/200 sands have similar cyclic strength regardless of silt content, although there is a large difference in void ratios. The resistance curves are seen to shift horizontally toward lower void ratios as silt content increases. At each silt content there appears to be an approximately similar increase in cyclic resistance for a given decrease in void ratio. If compared at constant void ratio, silt content is shown to decrease severely the cyclic strength of a sand material, as observed in the variation of cyclic strength with standard ASTM relative density discussed in Section 6.4.1.2. As discussed previously, higher void ratios may be attained if silty sands are prepared by moist tamping or air pluviation. Such samples would tend to have very low cyclic and monotonic strength, which is uncharacteristic of water pluviated silty sand.

6.4.2.2 Variation of Cyclic Strength With Relative Density

Figure 6.35 through Figure 6.38 show how silt content affects the cyclic strength of silty 20/200 sand when sand skeleton relative density as opposed to ASTM standard relative density is used as the basis for comparison. As described in Section 6.4.1.2, if cyclic strength of silty sand is considered in terms of ASTM standard relative density, silt content is shown to substantially reduce cyclic strength. In contrast, if compared in terms of sand

Figure 6.35 Variation of silty 20/200 sand resistance to liquefaction in 10 load cycles with relative density
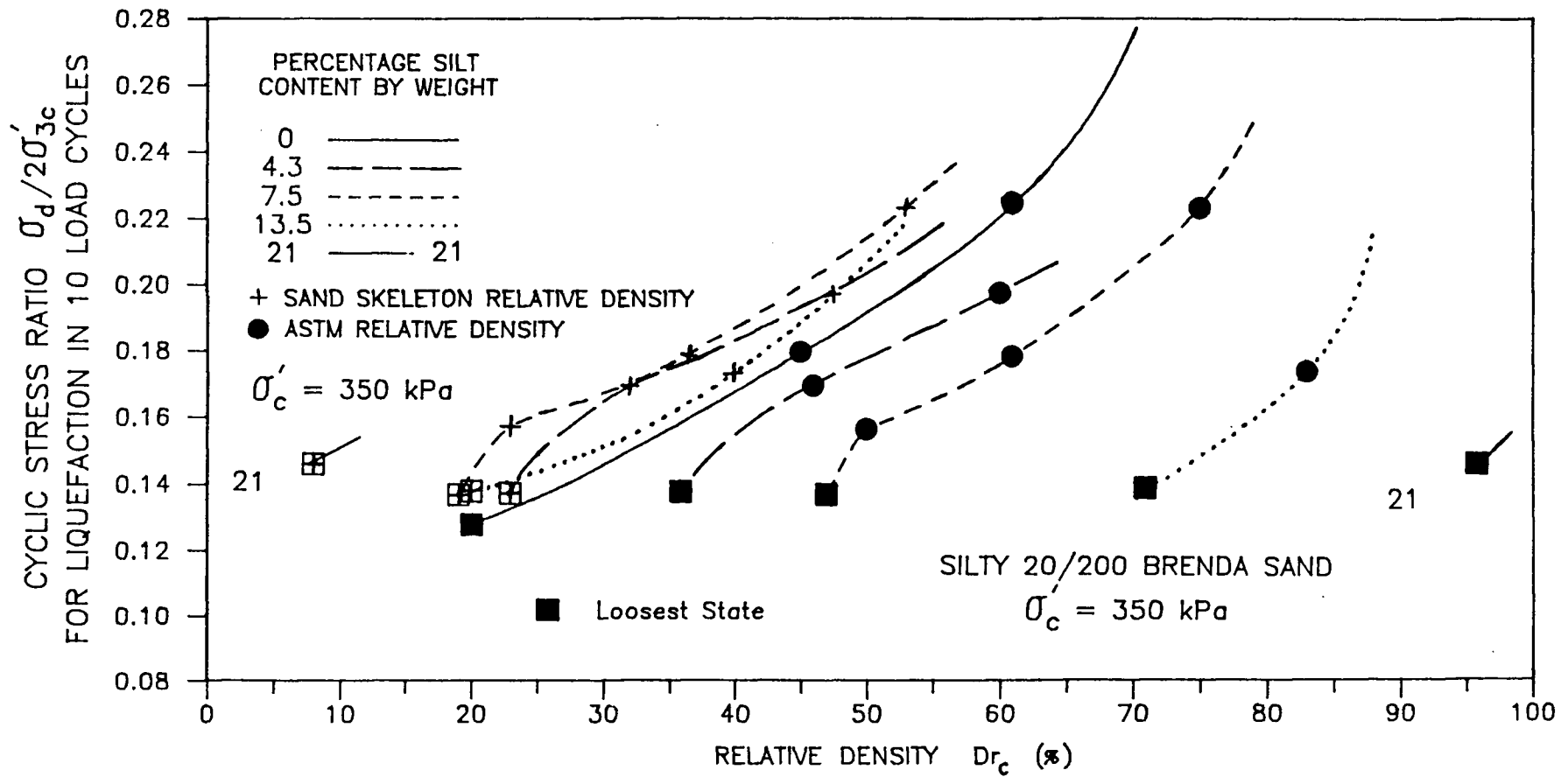
Figure 6.36 Variation of silty 20/200 sand resistance to liquefaction in 20 load cycles with relative density
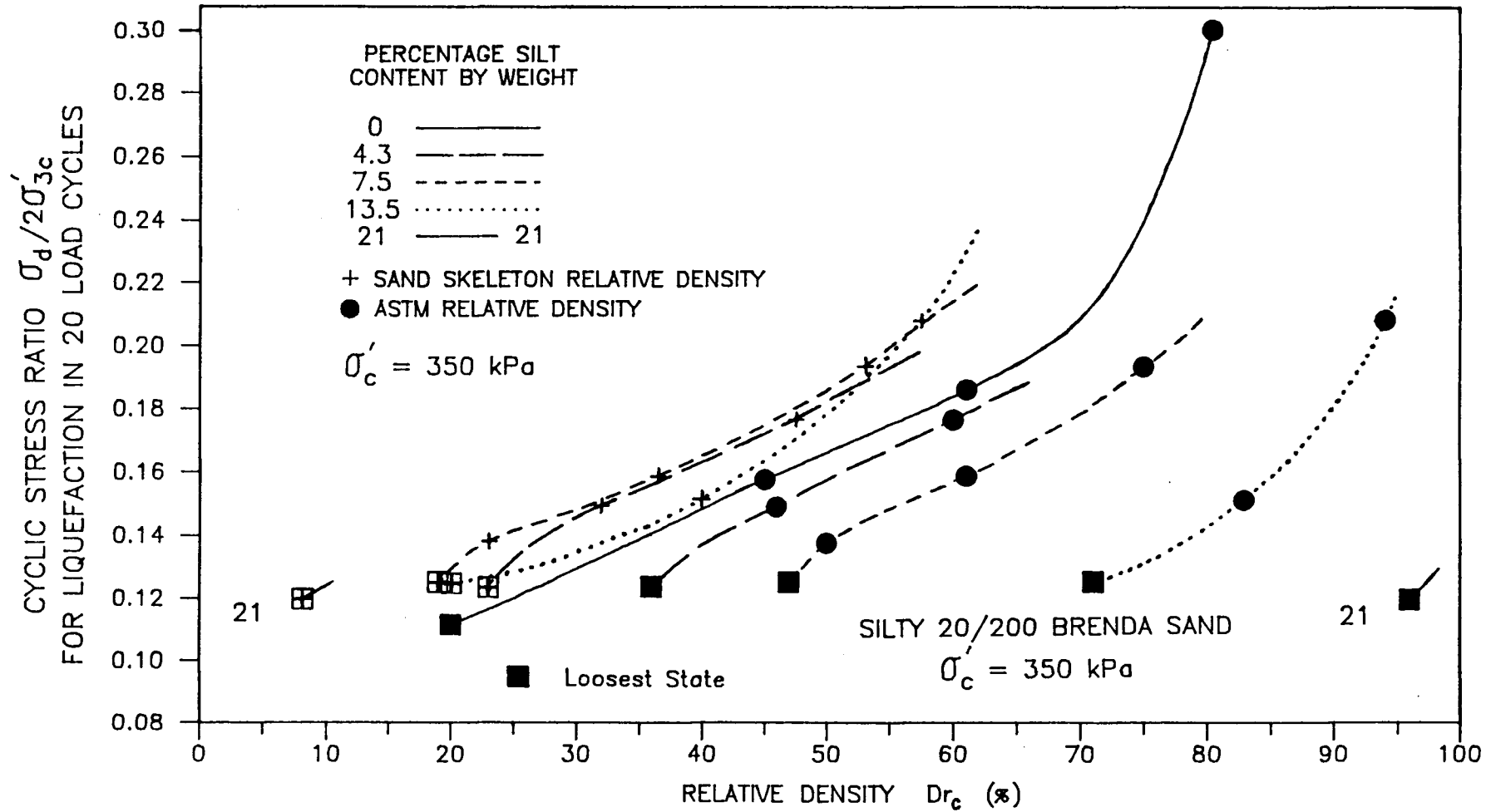
Figure 6.37 Variation of silty 20/200 sand resistance to liquefaction in 50 load cycles with relative density
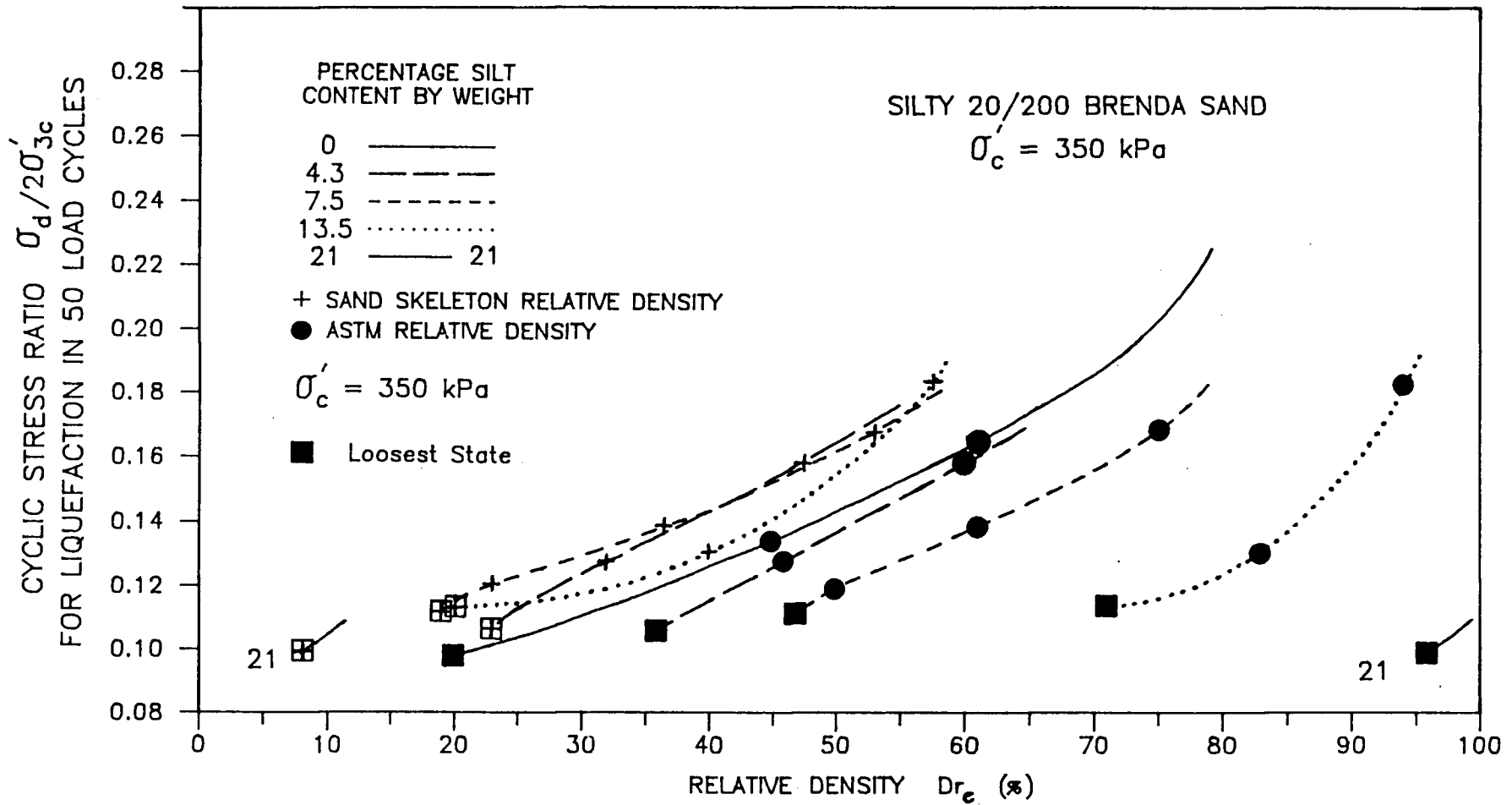
Figure 6.38 Variation of silty 20/200 sand resistance to liquefaction in 100 load cycles with relative density
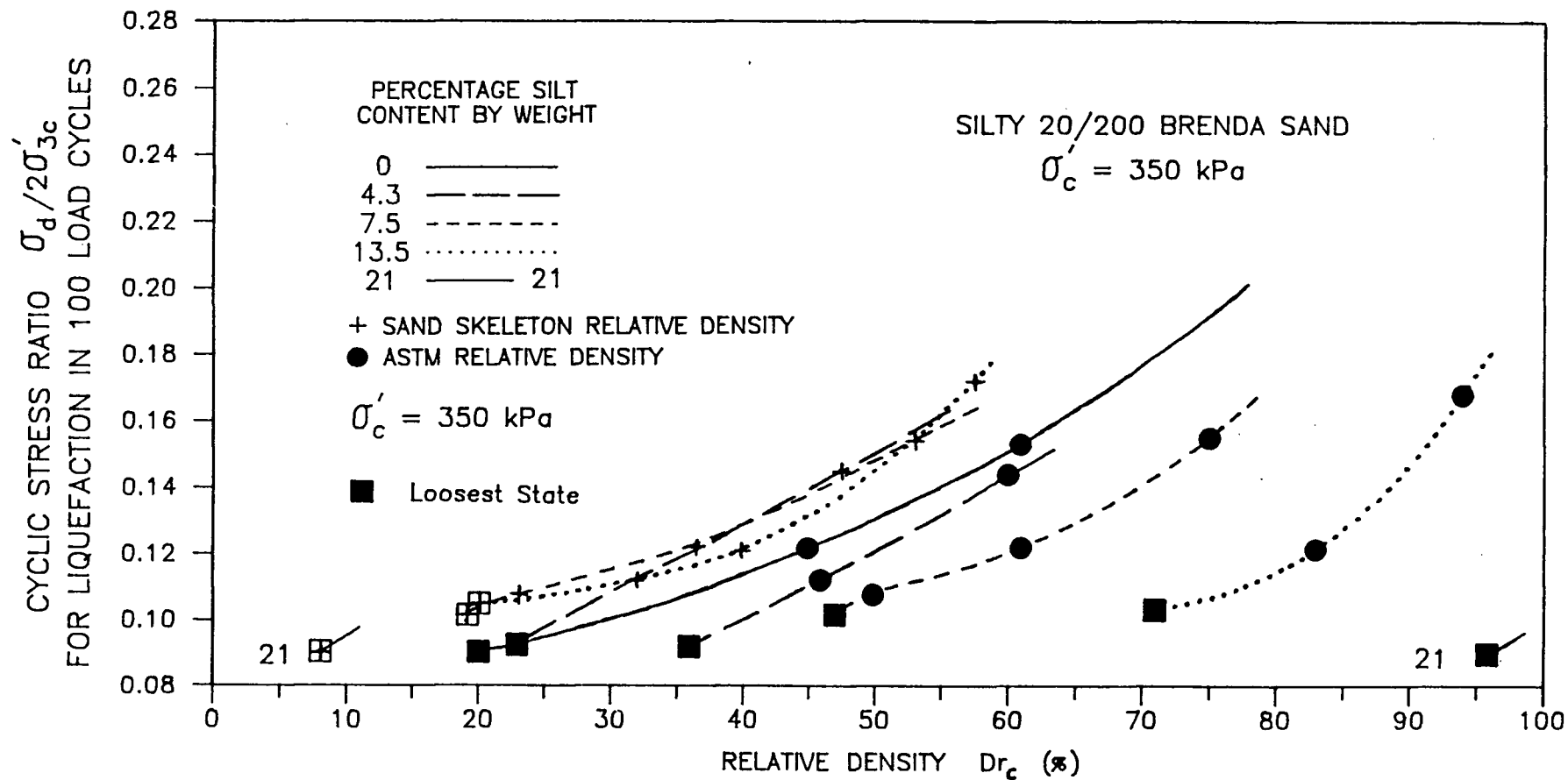
skeleton relative density, silt content is shown to have little effect upon cyclic strength, or infact slightly increase cyclic strength. The silt essentially fills void space within the sand without causing a large change in cyclic strength properties.

6.4.2.3   Variation of Cyclic Strength With Silt Content at Constant Sand Skeleton Relative Density

Interpolation of Section 6.4.2.2 cyclic resistance curves yields Figure 6.39, which shows that the cyclic strength of silty sand is increased up to 15% by any increase in silt content, when considered at constant sand skeleton relative density. A small addition of silt (4.3% by weight) may in fact increase cyclic strength more than a large addition of silt (13.5% by weight). This indicates that the increase in absolute density produced by an increase in silt content is not the only reason for an increase in cyclic strength with increasing silt content at constant sand skeleton relative density.

Test results in Fig. 6.39 indicate that the cyclic strength of hydraulic fill or fluvial silty sand which has been deposited through water sufficiently quickly to avoid deposition of segregated silt layers may be estimated conservatively by tests on clean sand of similar gradation and sand skeleton void ratio. The major difference in field loading behavior of clean and silty sands would be the extent of drainage possible during and after cyclic loading, a factor which is not considered in elemental undrained

Figure 6.39 Summary of the variation of silty 20/200 sand cyclic strength with variation of silt content at constant sand skeleton relative density
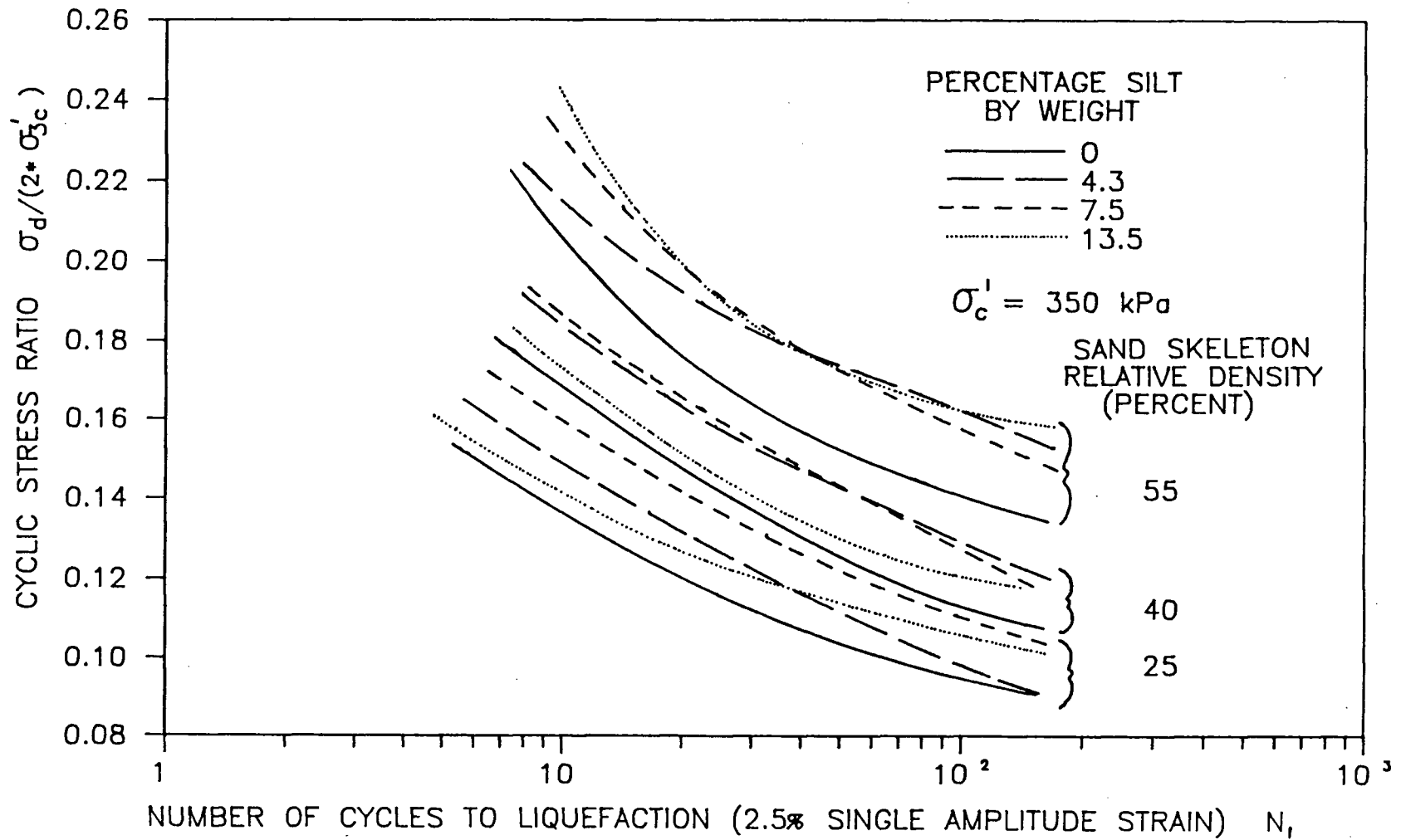
laboratory testing, because samples are maintained in an undrained state throughout testing.

6.4.2.4   Consistency of Interpolations

Figure 6.40 has been drawn from interpolated data derived from all previous cyclic resistance plots presented in Section 6.4, to show the variation of liquefaction resistance at constant applied cyclic stress ratio, and to check the validity of the interpolated data. The validity of interpolated plots is checked by plotting interpolated data from all other plots on Figure 6.40 to determine if the data form a set of smooth curves, as is observed to be the case. The same trends in cyclic resistance data as have been previously described are seen in Figure 6.40.

Figure 6.40 Variation of silty 20/200 sand cyclic strength with silt content at constant cyclic stress ratio
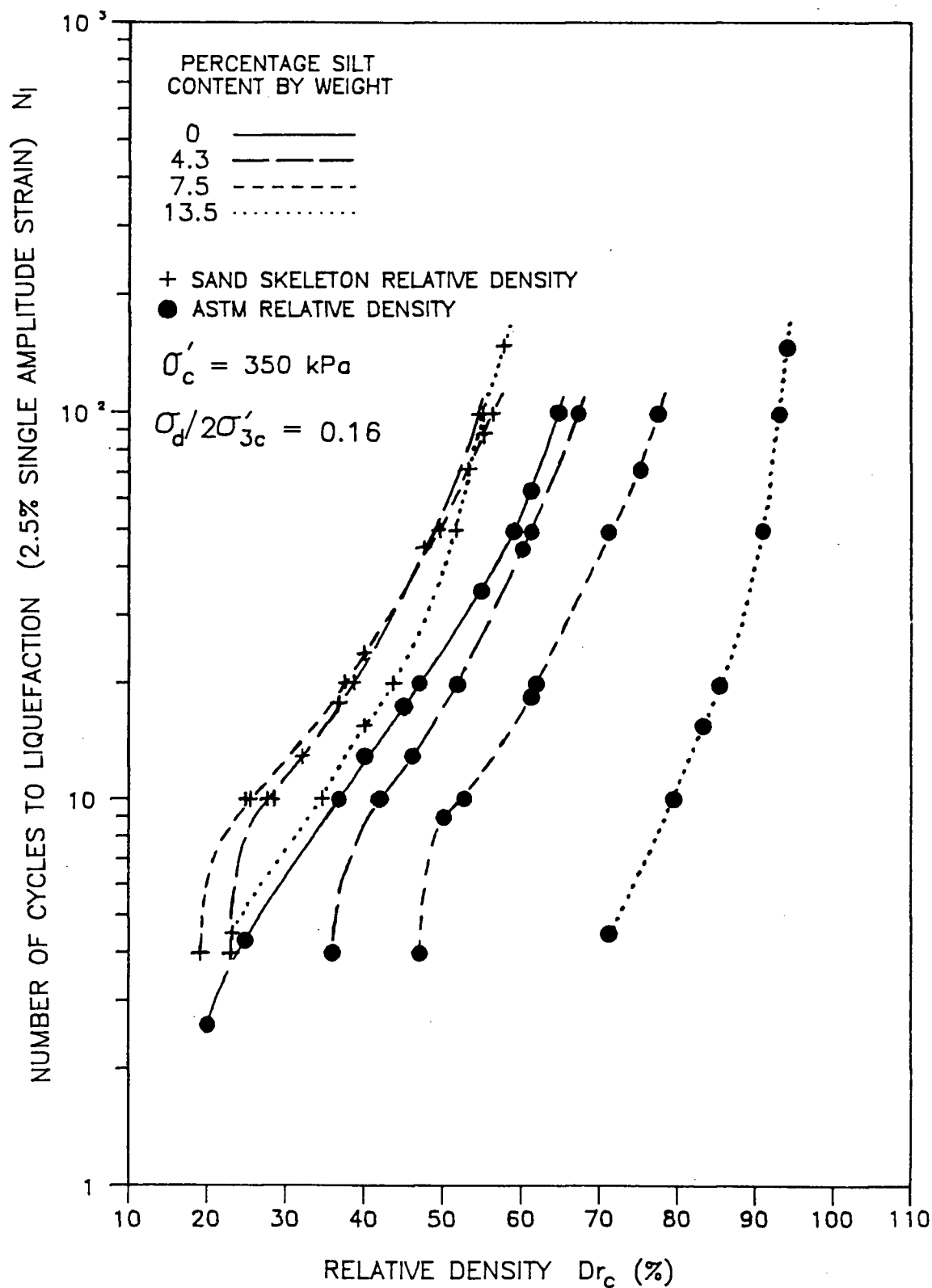
CHAPTER 7

DISCUSSION AND INTERPRETATION OF TEST RESULTS

The following features of the observed monotonic and cyclic loading behaviour of clean and silty sands deposited through water merit further discussion:

1) The monotonic compression loading behaviour of Brenda sand after consolidation from loosest state is observed to be generally dilative (i.e. steady-state or limited liquefaction is not observed during shear). This is true for both clean and silty sands regardless of their average grain size, gradation and silt content.

2) For samples prepared at loosest state, monotonic compression behaviour is dilative, yet extension behaviour is contractive (i.e. steady-state or limited liquefaction is observed during shear). All sands regardless of their gradation, average grain size and silt content behave in this manner over a range of confining stress. The same sand at a given void ratio is shown to be either contractive or dilative, depending upon direction of loading.

3) All sands tested display an initial decrease in effective confining stress under undrained loading, until a unique phase transformation or steady-state effective friction angle is mobilized. Once sheared past phase transformation state, the materials dilate with consequent increasing effective confining stress.

An essentially constant effective angle of friction is maintained within the material during dilation. This behaviour is observed regardless of direction of loading and the magnitude of maximum positive pore pressure developed.

Some of these aspects of material behaviour present radical departures from the generally accepted ideas regarding undrained behaviour of sands. Causes of these departures may lie in the sand type and the characteristic fabric of the water deposited materials used in this study. For example, water deposited Ottawa C109 sand at loosest deposition state shows steady-state or limited liquefaction response in both extension and compression loading (see Figure 3.12 and Chung, 1985), while Brenda sand shows steady-state or limited liquefaction response only in extension loading from an isotropic consolidation stress below 500 kPa. Although Ottawa sand shows limited liquefaction response in compression loading, extension response is still considerably more contractive than compression response. This anisotropy in loading response appears to be characteristic of water deposited sands, regardless of sand type.

Chung (1985) has shown that the anisotropy of water deposited sand may be radically altered by stress and strain history (see Figure 2.3). Thus the process of soil deposition must impart a specific fabric to the soil which

may only be altered by induced strain. The anisotropy of soil is shown to be only slightly changed by increasing consolidation stress level (which generally only induces small strain). Soil fabric is observed to be dependent upon stress ratio history (which may induce larger strain) and is observed to be essentially independent of magnitude of confining stress.

Most research on the undrained behaviour of sands, especially well-graded and silty sands, has been conducted using moist tamped samples. These samples may possess an entirely different fabric than that of water pluviated samples. Radical differences in the undrained behaviour of the two different types of reconstituted samples may be expected due to differences in fabric. In addition, most research has been concentrated on the study of soil strength behaviour under a single mode of loading, commonly triaxial compression loading and less commonly under triaxial extension or simple shear loading. Thus the opportunity to identify anisotropy in undrained response has most often been missed. The undrained behaviour of sands has been tacitly assumed to be isotropic. Some researchers have identified non-uniform strains in extension loading of moist tamped sands as the reason for not conducting triaxial extension tests (Castro, 1975). As in most laboratory testing techniques, the development of larger strain in triaxial samples invariably produces non-uniform stress and strain conditions (either in compression or extension

loading directions). This does not mean that the stress-strain behaviour observed before the development of non-uniform strains is invalid. The important factor to consider is at what point does stress-strain behaviour become invalid? Moist tamped specimens may be predisposed to the development of non-uniform strains in extension loading due to sample non-uniformity. Water pluviated samples maintain strain uniformity well past phase transformation state in extension loading (see Figure 3.13). Thus the soil strength behaviour obtained from extension test results is valid in the strain range which is of practical significance.

7.1 SAND FABRIC

Moist tamped sand samples have been shown to have steady-state or limited liquefaction response in compression loading over a range of void ratios (Castro et al., 1985) regardless of gradation, silt content, sand type or particle shape. Castro et al. (1982) present test results for Lornex tailings sand which has a similar mineralogy and angularity as Brenda tailings sand. Moist tamped Lornex sand is shown to be highly contractive in compression loading over a range of void ratios. Since all the water deposited angular sands tested in this study are generally dilative in compression loading, even in the loosest deposition state, the moist tamping technique must be imparting a fabric to the sand

which promotes contractive behaviour. Conversely, pluviation of sand through water must be imparting a fabric that promotes more dilative behaviour, at least under compression loading.

When moist sand is placed before tamping, it is generally in a bulked state with a relative density less than zero percent. Tamping is used to achieve any desired density. A moist sand is initially bulked and resistant to densification due to capillary tensions between grains. Casagrande (1976) has identified moist dumped sands to be particularly prone to liquefaction due to their "metastable honeycomb structure" which is induced by "capillary forces between moist grains". The magnitude of capillary tensions within a soil varies with grain size. Finer grained soils generate larger capillary tensions and thus may be subject to greater bulking and an increased resistance to densification by tamping.

At low stress level, capillary tensions control particle interaction within a moist soil. The effects of capillary forces upon soil fabric may be expected to persist in some form even after tamping to densities higher than the ASTM minimum. This is suggested by some laboratory studies, where loose moist tamped specimens of finer grained soils have been shown to experience large strains during the saturation process, even while being maintained under a consolidation vacuum (Marcuson, 1972; Chang et al., 1982; Sladen et al., 1985). This collapsing characteristic on

mere removal of capillary tensions suggests a fabric which is metastable. This fabric is likely to result in contractive behaviour during shear.

In contrast to moist tamped sands, water pluviated sands are deposited under gravitational forces and drag forces during settlement through water. Upon deposition, particle interaction is governed by interparticle friction, and not capillary tension forces.

Deposition of dry coarse sand through air could be expected to yield a similar fabric as deposition through water, because upon deposition, particle interaction is governed by interparticle friction. This is indicated by the similarity between ASTM and slurry deposition maximum void ratios shown in Table 3.2. In contrast to coarse grained sands, air versus water pluviated fine and silty sands may give rise to different fabrics, as indicated by the loosest state void ratios shown in Figure 3.5 and Figure 3.6. The large increase in maximum sand skeleton void ratio with increase in silt content in dry air pluviated silty sands is due to the pronounced electrostatic forces between fine silt grains in the dry state. In the dry state, electro-static forces between silt grains may be considered to bulk the sand in much the same manner as capillary tension forces in moist sand. Thus both air pluviated and moist tamped samples may neither duplicate the fabric nor the accessible range of void ratios possible in water deposited soils.

7.2 INTERPRETATION OF FACTORS WHICH PRODUCE AND CONTROL FABRIC OF WATER PLUVIATED SAND

Water pluviated sands show a characteristic trend in strength behaviour and anisotropy. Thus the fabric of water pluviated sand must have specific features which are derived from the process of pluviation through water. For the purposes of explaining and possibly predicting the behaviour of water pluviated sands, it is important to identify the factors which produce and control their fabric.

Much of the behaviour observed in the test results reported can be explained in terms of Rowe's two dimensional particulate model as described in Section 2.2. Rowe's model can be used to show that the dilatancy and stress-strain response of a particulate material is controlled by interparticle contact angle β and particle dimension factor α. Dilatancy is also shown to be a function of direction of loading and strain level (see Section 2.2). The physical parameters α and β of Rowe's model are applicable to the description of sand fabric in a general manner because sand is simply an assemblage of particles. The difference between Rowe's model and a natural assemblage of sand particles is that a sand has a statistical distribution or population of particle contact angles (β) and structure dimension factors (α). As long as the deformation in a sand is controlled mainly by the frictional resistance between

particles, Rowe's model may be expected to provide a reasonable simulation of deformation behaviour.

Strain behaviour in a sand is controlled by the combinations of α and β which are rendered unstable and produce slip between particle contacts as stress ratio is increased. Figure 7.1 shows the range of stable population of α and β for various levels of stress ratio. A comparison of Figure 7.1a and Figure 7.1b shows how the intrinsic angle of friction on particle surfaces affects the range of stable population of particle contacts. The actual population of α and β within a sand may vary within the stable zone, depending upon stress-strain history and method of sample preparation, as described in the following paragraphs.

7.2.1 Sample Preparation

During pluviation through water, sand particles are subjected to gravitational forces and viscous drag forces. Flatter shaped particles may tend to orient themselves with their longer axes in a horizontal direction, and shortest axis in the vertical direction, due to water drag forces. Upon sedimentation, the particles would tend to settle upon the deposition plane with this preferred orientation, in addition to having particle contact normals which are preferably oriented closer to vertical in order to support self-weight. Both of these factors would tend to induce a concentration of lower α values and higher β values in the particle contact population. Thus the particle contact

Figure 7.1a   Stability contours for Rowe's particulate model as a function of
particle dimension factor α and interparticle contact angle β

ZONE OF MODE B SLIP WHEN
$\sigma_v/\sigma_h \leq \tan(\beta - \phi_\mu) * \tan(\alpha)$

5.0

4.0

3.0

2.0

1.5

$\sigma_v/\sigma_h = 1.0$

$\sigma_v/\sigma_h = 1.0$ 1.5   2.0   3.0 4.0   5.0

ZONE OF MODE A SLIP WHEN
$\sigma_v/\sigma_h \geq \tan(\beta + \phi_\mu) * \tan(\alpha)$

SLIP MODE A = SLIP IN DIRECTION OF
              MAXIMUM PRINCIPAL STRESS

SLIP MODE B = SLIP AGAINST DIRECTION OF
              MAXIMUM PRINCIPAL STRESS

$\phi_\mu = 25°$

STRUCTURE DIMENSION FACTOR α (DEGREES)

INTERPARTICLE CONTACT ANGLE β (DEGREES)
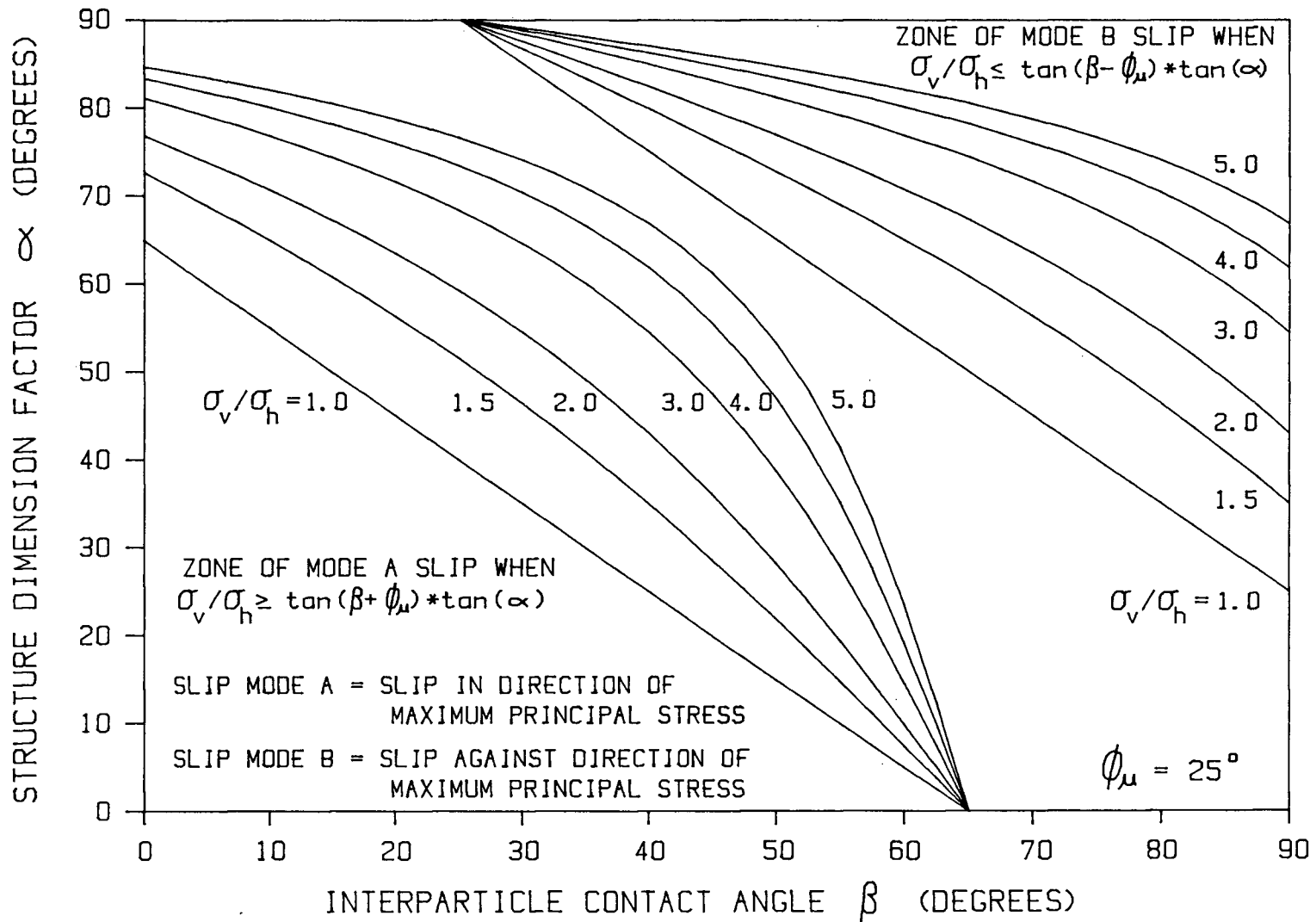
Figure 7.1b Stability contours for Rowe's particulate model as a function of particle dimension factor α and interparticle contact angle β
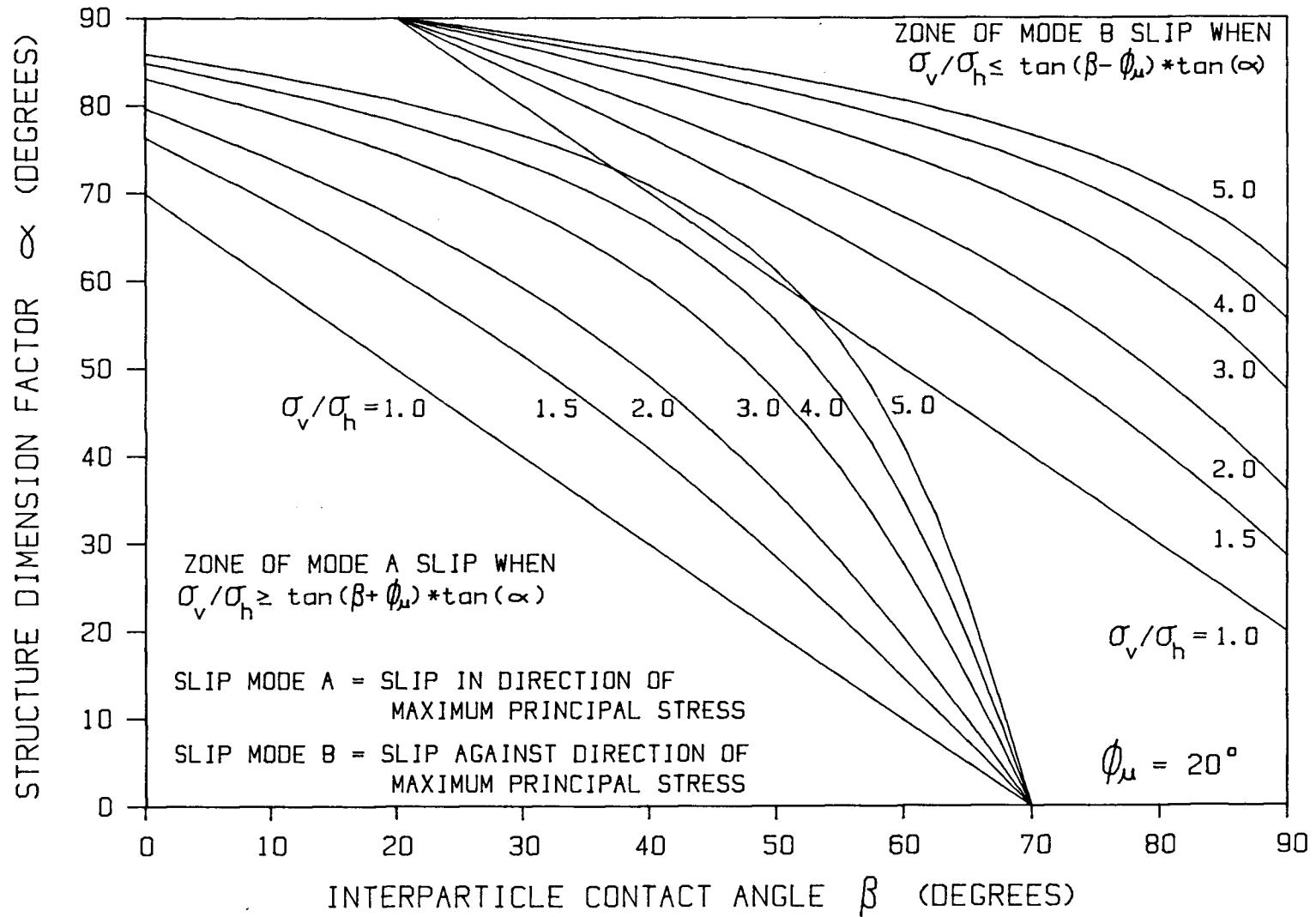
Fig. 7.2 Constant incremental strain ratio contours for Rowe's particulate model as a function of particle dimension factor α and interparticle contact angle β
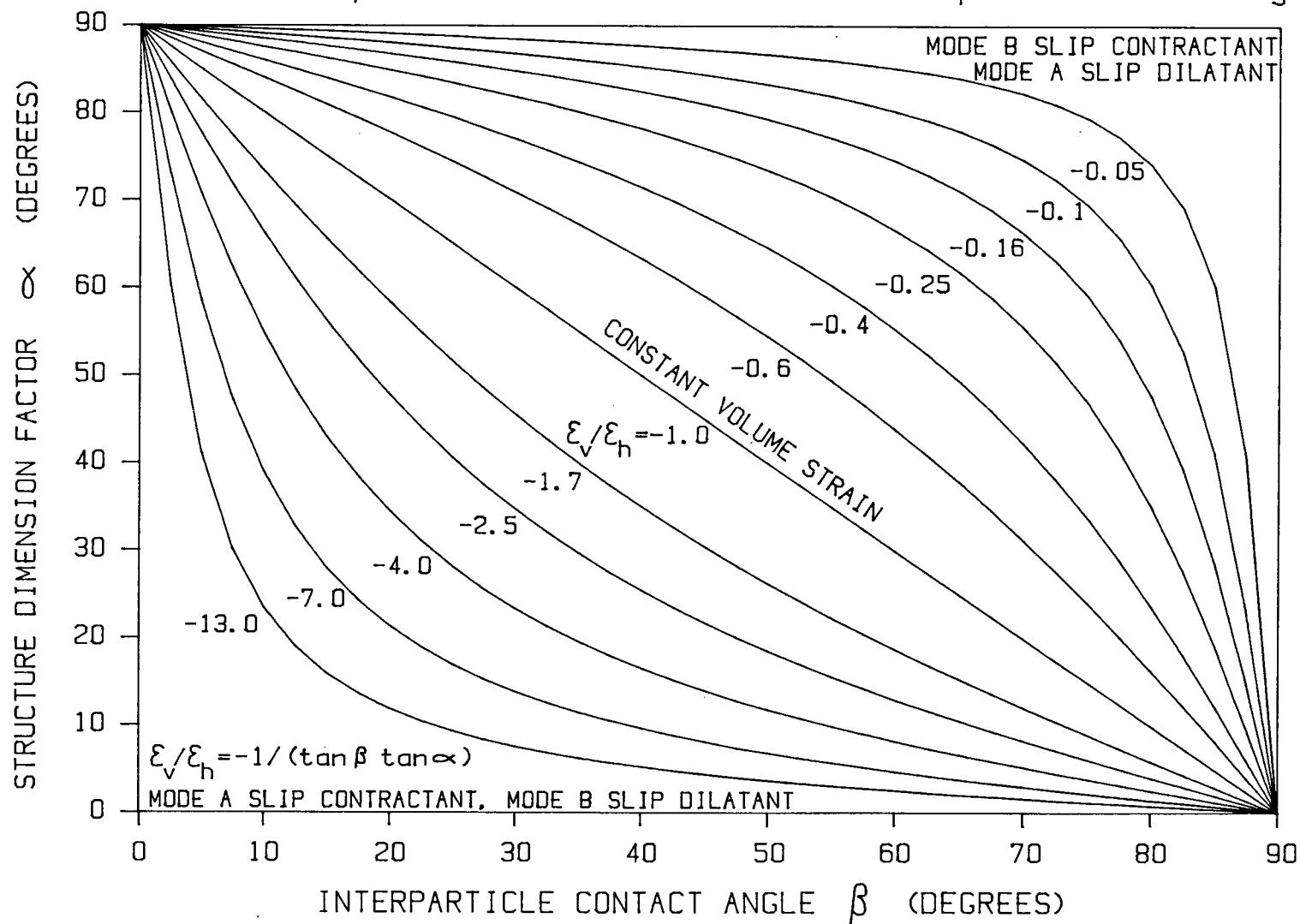
population would tend to be concentrated in the lower right hand corner of Figure 7.1 and Figure 7.3.

7.2.2 Sample Consolidation

Following the settlement of particles, a state of K_O consolidation is established under self-weight within the material. This produces and maintains a stress ratio of approximately 2.0 within the material, which implies a range of stable particle contacts as shown in Figure 7.3.

As laboratory samples are isotropically consolidated from as deposited K_O state, the range of stable particle contacts is transformed to the population shown in Figure 7.4. The particulate model implies that mode B contractive volumetric strains are induced during the transformation from K_O consolidation to isotropic consolidation, because a zone of previously stable contacts is exposed to the mode B strain unstable zone, as shown in Figure 7.5. Mode B strain implies slip against the direction of external maximum principal stress (see Section 2.2). In a K_O consolidated triaxial specimen, this would imply an increase in sample height when radial stress is increased to the magnitude of vertical stress in order to induce isotropic consolidation. This form of strain development was observed and verified at low confining stress during the preparation of tailings sand samples. Saturated samples were K_O consolidated after deposition by maintaining an 80 kPa vacuum between the former tube and the outside surface of the sample membrane,

Figure 7.3   Range of stable particle contacts after Ko consolidation

Chart axes and labels:

Y-axis: STRUCTURE DIMENSION FACTOR α (DEGREES)

X-axis: INTERPARTICLE CONTACT ANGLE β (DEGREES)

ZONE OF MODE B SLIP WHEN
$$\sigma_v / \sigma_h \leq \tan(\beta - \phi_\mu) * \tan(\alpha)$$

5.0
4.0
2.0
3.0

$\sigma_v / \sigma_h = 1.0$ 1.5   2.0

ZONE OF MODE A SLIP WHEN
$$\sigma_v / \sigma_h \geq \tan(\beta + \phi_\mu) * \tan(\alpha)$$

SLIP MODE A = SLIP IN DIRECTION OF
              MAXIMUM PRINCIPAL STRESS

SLIP MODE B = SLIP AGAINST DIRECTION OF
              MAXIMUM PRINCIPAL STRESS

STABLE PARTICLE
CONTACT POPULATION
AFTER PLUVIATION AND
Ko CONSOLIDATION

Figure 7.4 Range of stable particle contacts after isotropic consolidation
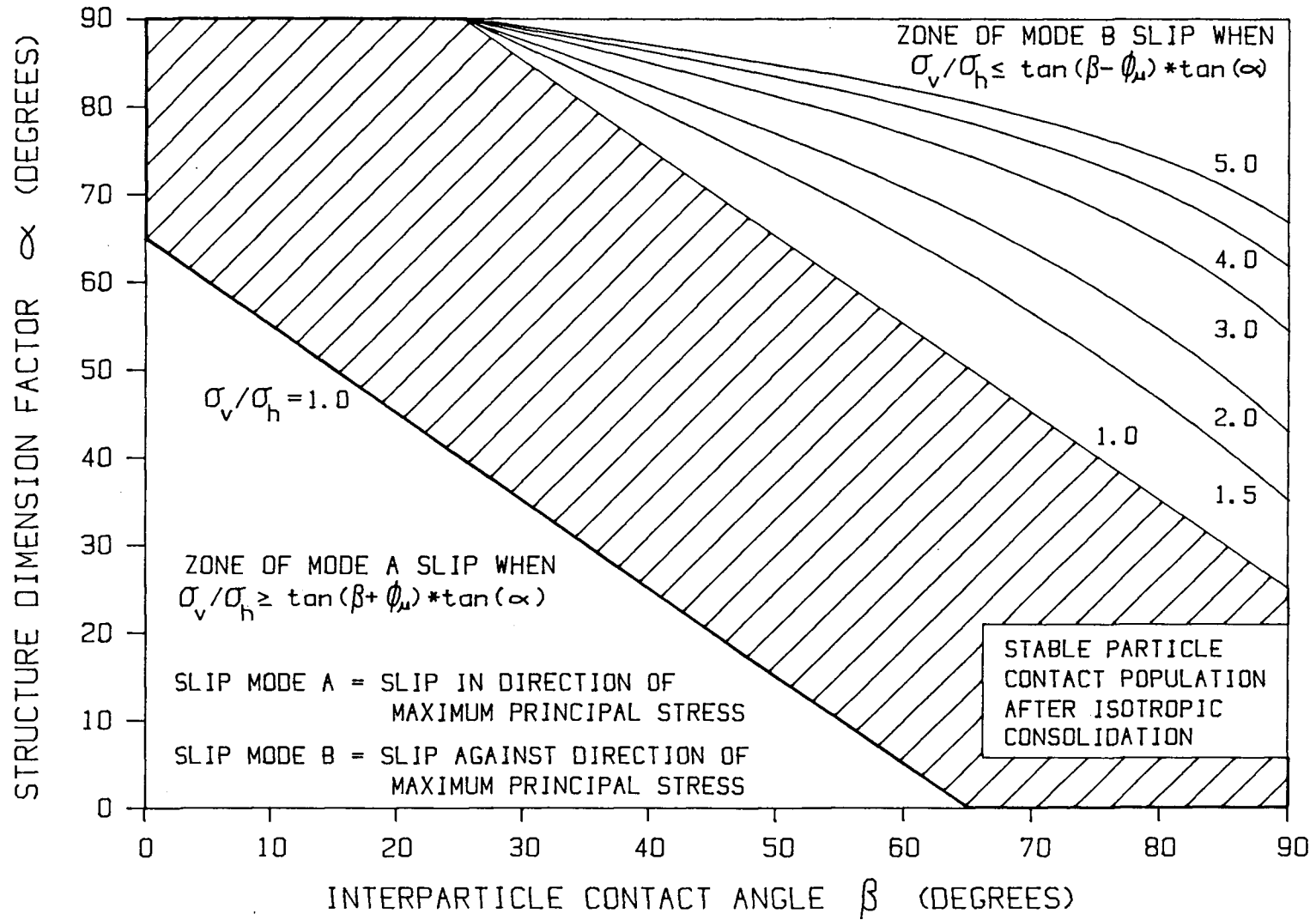
Figure 7.5 Range of particle contacts which undergo Mode B slip in the transformation from Ko to isotropic consolidation
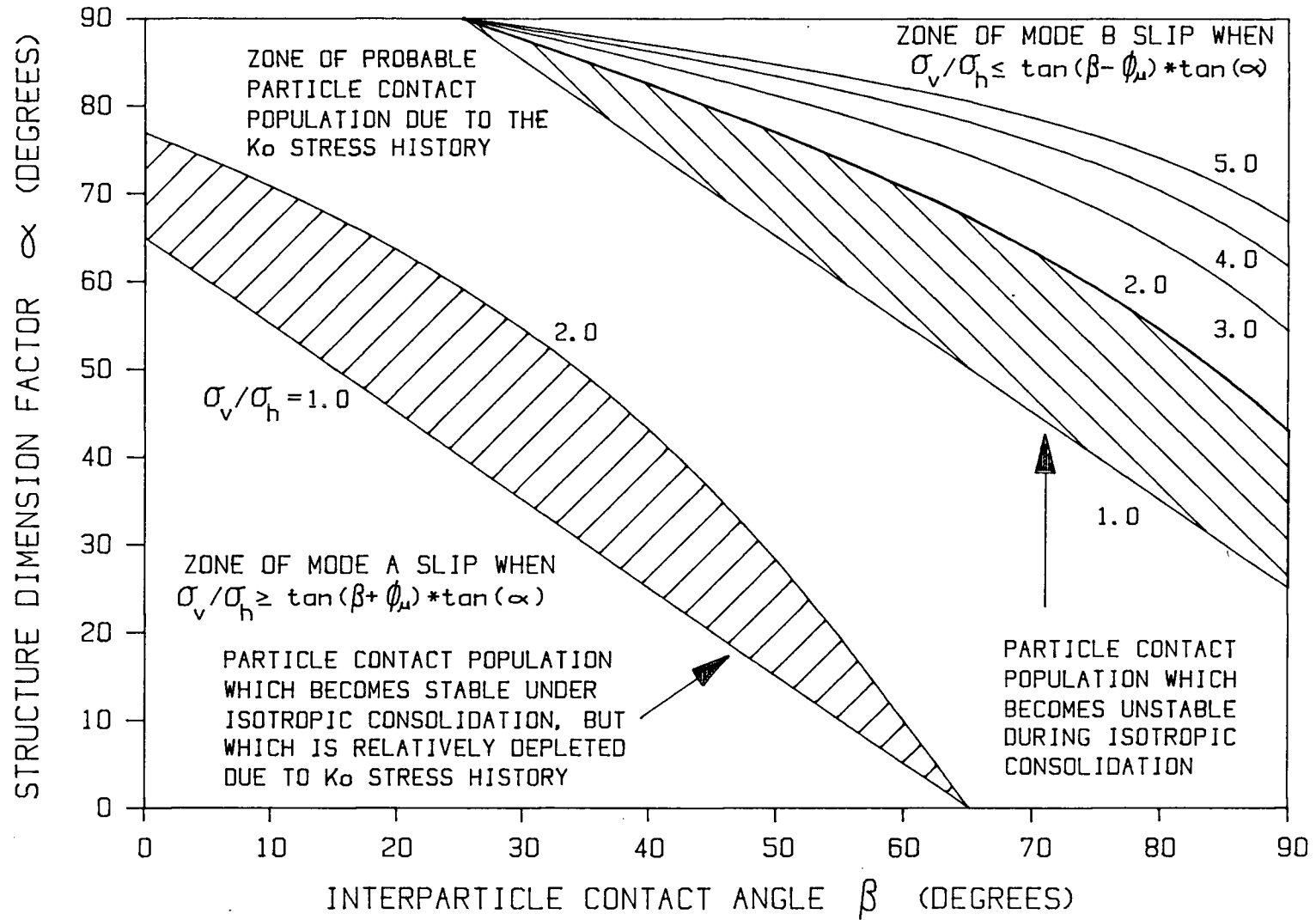
while a 20 kPa vacuum was applied in increments to the sample. Thus the vertical stress on the sample was 20 kPa, and radial stress a lower amount corresponding to K_O consolidation, because zero radial strain was imposed on the sample. Now, without disturbing the sample, the external 80 kPa vacuum on the outside surface of the sample was released, so that the sample would be transformed from K_O consolidation to isotropic consolidation without a change in vertical stress. Sample height was observed to increase, while large contractive volumetric strains indicated the occurrence of large compressive radial strains. The predicted range of incremental strain ratio induced by a change in population of stable particle contacts due to a change in stress ratio can be determined from Figure 7.2. During the transformation from K_O to isotropic consolidation, contractive mode B deformation is predicted to occur. Incremental vertical to horizontal strain ratio is estimated to be greater than -0.4, which indicates a considerably larger radial than axial strain, as has been observed in triaxial test results. Test results thus confirm that mode B strains are indeed possible within a sand, and that Rowe's particulate model can be effectively used to explain otherwise unexplainable observed behaviour.

Rowe's particulate model assumes that strain within a particulate material may only be induced by slip between particle contacts. Individual particles are assumed to be completely rigid. The result of these assumptions is that

strain is only predicted to be induced by a change in stress ratio, and not by a change in the magnitude of stress. The model suggests that when a particulate material is stable at one magnitude of consolidation stress, it will remain stable under increasing or decreasing consolidation stress (i.e. slip at particle contacts will not be induced) as long as stress ratio is held constant. This contention is reasonable for completely rigid particles whose intrinsic angle of surface friction is not a function of normal stress level. The relatively small amount of strain induced in sand during consolidation at constant stress ratio must then be due to factors other than slip between rigid particles.

The majority of strain induced in sand during isotropic consolidation is expected to be due to particle contact crushing and the elastic strain of non-rigid particles. These two mechanisms of strain development are not considered in Rowe's particulate model. The strain induced by these two mechanisms could also induce unstable changes in α and β particle contact populations, which could in turn, induce slip at particle contacts. The magnitude of particle contact slip during isotropic consolidation is expected to be coupled to the magnitude of strain developed by crushing at particle contacts and the magnitude of elastic strain.

The relatively small consolidation strains observed in crush resistant Ottawa C109 sand (see Figure 4.5) and the substantially larger strains observed in angular Brenda

sand, which is considerably less resistant to particle crushing, confirm that particle crushing is an important factor in the development of strain during isotropic consolidation.

The proportion of recoverable or elastic strain in loosest state Ottawa sand after virgin isotropic consolidation from 50 kPa to 550 kPa and unloading again to 50 kPa (see Figure A.3) is approximately 97% axial strain and 51% radial strain, while that of Brenda sand is much less at 36 to 32% axial strain and 21 to 23% radial strain (see Figure A.2). This correlation of greater particle crushing resistance in Ottawa sand with lower magnitude of consolidation strain and a high percentage of recoverable elastic strain tends to support the interpreted mechanism of coupled strain development under isotropic consolidation.

The strains observed under virgin isotropic consolidation are always compressive or positive in both axial and radial directions (see Figure 4.11). This indicates that the strains induced by particle contact crushing and elastic deformation predominate during isotropic consolidation, because the strains induced by mode A or mode B particle contact slip require that there be a combination of both compressive and extensional strain components which result in a negative strain ratio (see Figure 2.4). The elastic component of strains induced during virgin consolidation may be estimated from the strains induced during isotropic unloading. The strains

recovered during isotropic unloading are essentially isotropic and elastic (see Section 4.4, Appendix A, and Vaid and Negussey, 1984). When the elastic component of strain is subtracted from virgin strain, the remaining component of irrecoverable axial strain is still compressive but considerably less compressive than the remaining component of irrecoverable radial strain. The irrecoverable strain component must be due to particle contact crushing, and induced slip between particle contacts which have been made unstable by elastic and crushing strain. If particle crushing strain is assumed to be isotropic, then the remaining strain component due to particle contact slip is inferred to be of the mode B type, similar to that observed during sample preparation when switching from K_O consolidation to isotropic consolidation. Since induced particle crushing and elastic strains are relatively small during virgin isotropic consolidation, only small changes in the particle contact population α and β may be expected during virgin isotropic consolidation. Thus only the particle contact population which is close to slip failure (a stability boundary in Figure 7.4) could be expected to become unstable during isotropic consolidation. The inference that particle slip during virgin consolidation is of the Mode B type implies that the majority of particle contacts which become unstable during virgin isotropic consolidation are close the mode B stability boundary shown in Figure 7.4. This might be expected because of the

previous K_o consolidation stress history. This previous stress history has insured that stable particle contacts have never been failed close to the mode B strain boundary, while the mode A strain boundary has only recently been shifted into a previously unstable zone, and thus one would not expect a large population of stable particle contacts close to this boundary (between the stress ratio of 1.0 and 2.0 contours as shown in Figure 7.5). Thus the particulate model may also be used to explain the relatively larger irrecoverable horizontal strain component of water pluviated sand under virgin isotropic consolidation.

7.2.3 Compression Loading Response

After isotropic consolidation, a test sample is expected to have a population of particle contacts as shown in the middle zone of Figure 7.5. As vertical stress is increased in compression loading, the zone of stable particle contacts shifts to the right of Figure 7.5 or 7.1, thus exposing previously stable particle contacts to mode A strain. Because of the K_o consolidation stress history after sample preparation (see Section 7.2.2) there is a deficiency of stable particle contacts below the 2.0 stress ratio contour. Thus only minor mode A strain is generated below a stress ratio of 2.0. In addition, because of settlement through water, the majority of particle contacts is concentrated in the bottom right hand corner of Figure 7.5, with higher β value and lower α value. Under

compression loading, this zone remains stable up to very large stress ratio (see Figure 7.1) thus one could again predict fairly small mode A strains. A prediction of the incremental strain ratio and dilatancy induced by an increase in stress ratio may be made from Figure 7.2.

Under initial increases in stress ratio from 1.0, the model indicates that vertical strain is greater in magnitude than horizontal strain, thus induced strain is predicted to be contractive (e.g., to show a reduction in effective confining stress during undrained loading), as observed in all soil tests in the low stress ratio range. As stress ratio is increased, the particulate model predicts that contractant response will be transformed into dilatant response. The stress ratio at which this occurs cannot be directly determined from the particulate model, as one stress ratio contour (Figure 7.1) is crossed by several strain ratio contours (Figure 7.2). Strains induced by an increase in stress ratio are governed by the population of α and β particle contacts which exist within the soil.

Due to the previous K_O consolidation stress history in water pluviated sands, and the resulting deficiency in particle contacts which may slip below a stress ratio of 2.0, the triggering of steady-state or limited liquefaction response is not expected below a stress ratio of 2.0. In undrained loading of water pluviated sands, the triggering of steady-state or limited liquefaction is expected in the contractive range of loading response from a stress ratio of

2.0 to the phase transformation state. This is indeed observed in the undrained loading response of Ottawa sand, which has a constant CSR of approximately 2.0 (mobilized friction angle of 20 degrees). Thus CSR is shown to correlate well with the initiation of increased particle contact slip predicted in water pluviated sand by the particulate model.

The essentially constant ultimate friction angle maintained on the undrained failure envelope is interpreted to represent the state where a similar population of particle contacts is both created and destroyed under increasing strain. Such a mechanism could explain the observed increase in ultimate friction angle with increasing sand density (see Figure 6.4), because one could expect a greater resistance to particle rearrangement in a denser sand.

7.2.4 Extension Loading Response

If the particle contact population which is interpreted to exist within an isotropically consolidated water pluviated sand (the same sand as that described in the previous section) is subjected to extension loading, the values of α and β must be transformed to $\alpha' = 90-\alpha$ and $\beta' = 90-\beta$. This transformation accounts for the reversal of principal stress direction in loading (see Figure 2.4). The resulting initial population of particle contacts is shown in Figure 7.6.

Figure 7.6 Range of particle contacts which are subjected to slip in extension loading, after a Ko and isotropic consolidation stress history

ZONE OF MODE B SLIP WHEN
$\sigma_h/\sigma_v \le \tan(\beta' - \phi_\mu) * \tan(\alpha')$

ZONE OF PROBABLE PARTICLE CONTACT POPULATION DUE TO THE Ko STRESS HISTORY AND ISOTROPIC CONSOLIDATION

PARTICLE CONTACT POPULATION WHICH BECOMES STABLE UNDER ISOTROPIC CONSOLIDATION, BUT WHICH IS RELATIVELY DEPLETED DUE TO Ko STRESS HISTORY

1.0

1.0

REVERSED STRESS DIRECTION:

$\sigma_h > \sigma_v$ $\alpha' = 90 - \alpha$

$\beta' = 90 - \beta$

ZONE OF MODE A SLIP WHEN
$\sigma_h/\sigma_v \ge \tan(\beta' + \phi_\mu) * \tan(\alpha')$

STRUCTURE DIMENSION FACTOR α' (DEGREES)

INTERPARTICLE CONTACT ANGLE β' (DEGREES)

234

Due to the sample preparation and isotropic consolidation stress history, there is a large population of particle contacts which are exposed to mode A slip in extension loading as stress ratio is increased. This contrasts with the sparse population of particle contacts which are exposed to mode A slip in compression loading as stress ratio is increased from 1.0 to 2.0. The population of contacts in extension loading which are subject to slip in the same stress ratio range (1.0 to 2.0) have never been subjected to slip during sample preparation. Thus a large amount of plastic contractive strain is induced even at low stress ratio during extension loading. This difference in soil fabric between extension and compression loading offers a reasonable explanation for the observed differences in critical stress ratio (CSR) behaviour between extension and compression loading (see Sections 2.1 and 5.3). CSR is observed to be essentially constant in compression loading, which is believed to be due to the sparcity of particle contacts which may undergo slip below a K_0 consolidation stress ratio, due to the previous K_0 consolidation stress history. Particle contacts which are subject to slip by an increase of stress ratio above 2.0 have never been caused to slip by previous stress history, thus when stress ratio is increased close to 2.0, large contractive strains are induced. If these contractive strains are sufficient to produce a reduction in sand strength, a CSR of close to 2.0 is observed. In contrast to compression loading CSR,

extension loading CSR is observed to be a function of deposition void ratio (Chung, 1985). CSR is generally much lower than observed in compression loading (see Table 5.1), with loosest state samples having the lowest CSR, and denser samples showing a gradual increase in CSR. The behaviour of CSR in extension loading can be attributed to the reduced contractive behaviour of sand with increasing density. Although there is a tendency toward volume contraction of sand during shear up to phase transformation stress ratio regardless of density, the magnitude of contraction is diminished with increasing density. In undrained loading, the potential for a sufficient amount of pore pressure generation to trigger liquefaction or limited liquefaction is reduced with increasing sand density, thus CSR is increased with increasing density, unless it is fixed by previous stress ratio history as observed in compression test results.

Greater contraction is observed in extension loading because a larger number of particle contacts are subjected to contractive slip under extension loading. This population of contacts exists within the sand because they have not been rendered unstable by previous stress history. A second factor which yields greater contractive strain in extension loading is the initial concentration of particle contacts produced by deposition through water (see Section 7.2.1) which results in generally lower α and higher β values. When these values are transformed to their

equivalent in the extension loading direction, generally higher α' and lower β' values result. Thus the major concentration of particle contacts produced by deposition through water is in the upper left hand corner of Figure 7.6. This zone of particle contacts is subject to slip under extension loading, while the same population was not subject to slip under compression loading. Due to this concentration of particle contacts produced by pluviation of particles through water, more contractive strains are again predicted in extension loading.

7.2.5 Stress Reversal

As stress ratio is increased in one direction of loading, the stable zone of particle contact population is shifted, as shown in Figure 7.7 for compression loading. All newly established particle contacts which are induced by strain must exist within the new stable zone, in order for the particulate material to remain stable. A peak stress ratio is achieved when the mode A strain stable zone boundary can no longer be pushed to a higher stress ratio contour. In other words, the stable particle contact population produced by slip is the same as that before slip occurred.

If stress ratio is reduced following loading, the zone of stable particle contacts is shifted again. One could expect mode B strains as the previously stable zone is exposed to the mode B strain unstable zone. Because the

Figure 7.7 Zone of stable particle contacts at high stress ratio during compression loading
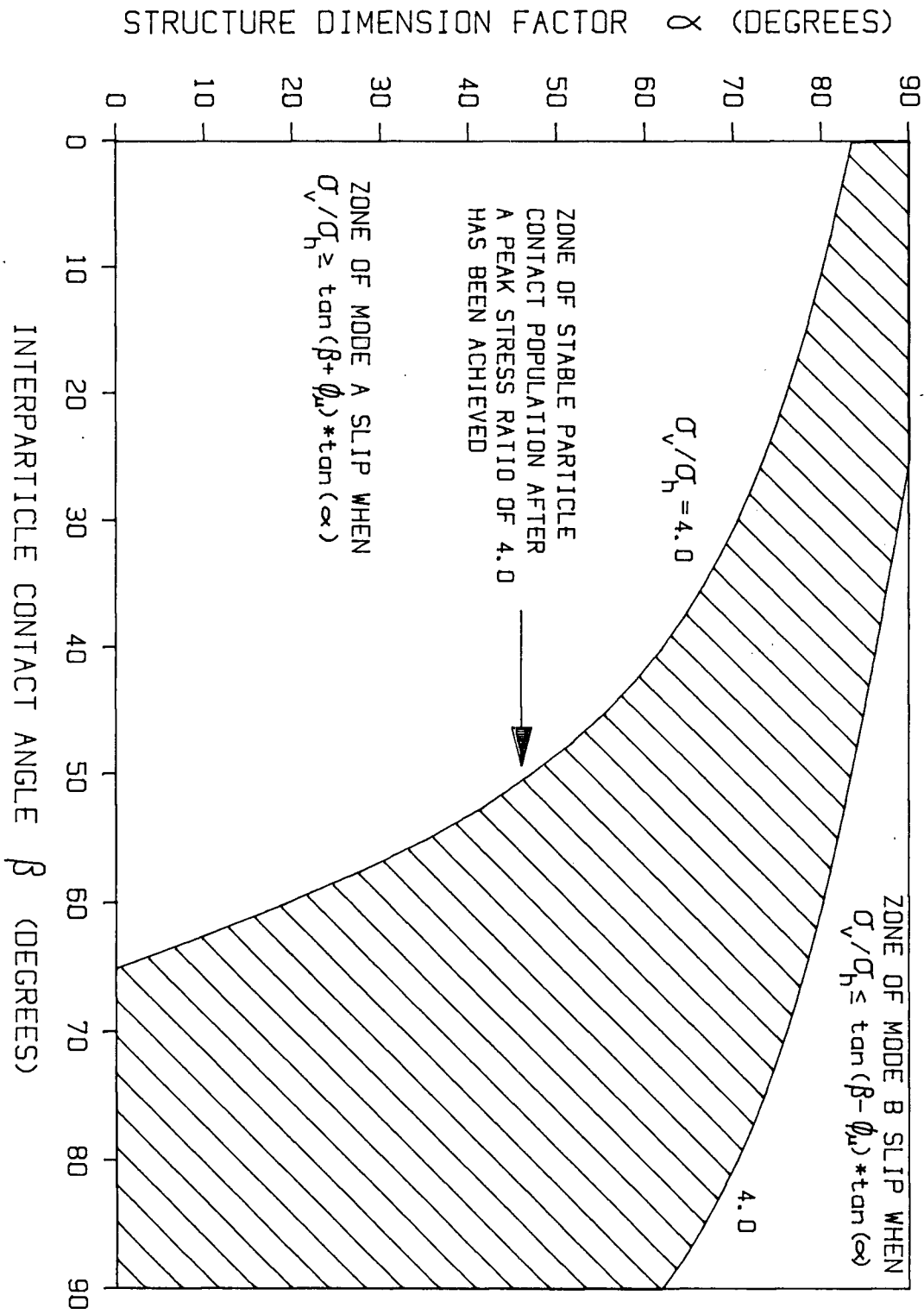
mode B strain stable zone boundary above the 1.0 stress ratio contour has only recently been made stable by increasing stress ratio, one could not expect a large concentration of particle contacts within this zone. Thus one could expect unloading strains to be small in comparison to loading strains. The mode B strains which do occur on unloading are predicted by the particulate model to be contractive, as observed in cyclic loading test results (see Section 6.0). In contrast, the reduction of mean normal stress which generally accompanies a reduction in stress ratio in undrained loading implies that elastic strains on unloading should be dilative. The contractive strains observed in the unloading of undrained test samples thus indicates that the mode B strains induced by a reduction of stress ratio are larger than the elastic strains induced by the reduction of mean normal stress.

Figure 7.8 displays what happens to the stable population shown in Figure 7.7 with the occurrence of stress reversal. Compression loading α and β values have been transformed to extension loading α' and β' values. The majority of the previously stable zone produced by compression loading is shown to fall into the mode A strain unstable zone under extension loading. Thus one would predict large contractive strains to occur upon stress reversal and extension loading. This behaviour is indeed observed in undrained tests, and leads to the development of large cyclic mobility strains in sands which are generally

Figure 7.8 Explanation of the large contractive strains associated with principal stress reversal following loading to a high stress ratio

ZONE OF MODE B SLIP WHEN

$\sigma_h/\sigma_v \leq \tan(\beta' - \phi_\mu) * \tan(\alpha')$

THE PARTICLE CONTACT POPULATION WHICH WAS PREVIOUSLY STABLE AT A STRESS RATIO OF 4.0 (SEE PREVIOUS FIGURE) SUBJECT TO UNLOADING AND REVERSAL OF PRINCIPAL STRESS DIRECTION. THE PARTICLE CONTACT DISTRIBUTION IS VERY UNSTABLE UNDER THE NEW DIRECTION OF LOADING, AND LARGE CONTRACTIVE STRAINS OCCUR UNTIL A MORE STABLE MATERIAL FABRIC IS REESTABLISHED.

ORIGINAL STRESS DIRECTION:

$\sigma_v > \sigma_h$ (σ_v/σ_h) max = 4.0

REVERSED STRESS DIRECTION:

$\sigma_h > \sigma_v$ $\alpha' = 90 - \alpha$

$\beta' = 90 - \beta$

ZONE OF MODE A SLIP WHEN

$\sigma_h/\sigma_v \geq \tan(\beta' + \phi_\mu) * \tan(\alpha')$

STRUCTURE DIMENSION FACTOR α' (DEGREES)

INTERPARTICLE CONTACT ANGLE β' (DEGREES)

dilative under monodirectional loading. The development of cyclic mobility strain is considered to be due to the fluctuation of sand fabric between extremes generated in different directions of loading. With each extreme fluctuation of sand fabric, the tendency for volume contraction is increased. Thus greater dilative strains must be produced in each load cycle in order to increase effective stress and soil strength to carry the applied load.

7.2.6 The Effect of Stress History Upon CSR

A K_o consolidation stress history which induces a stress ratio of 2.0 during sample preparation has been interpreted as the reason why water pluviated sand has a CSR of 2.0 in compression loading (see Sections 7.2.3 and 7.2.4). This interpretation implies that CSR may be changed to a given stress ratio by simply prestraining a contractive sand to this given stress ratio. Data presented by Chung (1985) on the effects of sample prestrain upon CSR and limited liquefaction response show that CSR may indeed be increased to a specific value by prestraining to an equivalent stress ratio value. As long as limited liquefaction behaviour is maintained after prestraining and reconsolidation, and the direction of preloading and reloading are the same, the CSR value obtained during reloading is very close to the maximum stress ratio achieved during preloading. This is true in both compression and

extension loading directions. The observed effect of prestrain upon measured CSR values is consistent with the particulate interpretation of factors which contribute to the fabric and behaviour of water pluviated sands.

7.3 INTERPRETATION OF FACTORS WHICH PRODUCE AND CONTROL MOIST TAMPED SAND FABRIC

At low confining stress, the internal structure within a moist sand sample is controlled by capillary tensions between grains. This is because capillary tension forces are considerably larger than self-weight forces. Thus one could expect particle contacts to be essentially random within the sample, because the water tension forces which control soil structure are independent of direction. The process of compaction by tamping may tend to induce a less random structure in higher density samples. In loose samples, the random structure may have α and β particle contact values which are unbounded by stress ratio contours, because water tension forces and not frictional resistance between particles maintain the sample in a stable state. One could thus expect relatively large and contractive strains in a moist sand as an external stress which exceeds interparticle capillary tensions is applied to the sample. One might also expect large strains during the saturation process, as capillary tension forces are removed from within the sample. Such large strains induced during saturation while the moist sand is maintained under a consolidation

vacuum have been reported by Marcuson et al. (1972), Chang et al. (1982) and Sladen et al. (1985).

The initial stress history applied to a moist sand sample could be expected to establish the initial fabric and anisotropic character of the sample. Under normal conditions, an isotropic stress is applied by creating a vacuum within the sample. This might be expected to create a population of α and β particle contacts which exists within the stress ratio = 1.0 contours of Figure 7.1. Within the stable zone, particle contacts could be expected to be essentially random, unlike that of water pluviated sand which has been subjected to isotropic consolidation stress after preparation at a K_0 consolidation state (see Section 7.2.).

Depending upon the strain allowed in the moist sample during initial application of a confining vacuum, the stresses induced within the sample may not be isotropic. Castro et al. (1969, 1982) describes the standard method employed by himself and many other researchers for the preparation of moist tamped soil specimens. This method requires that the loading platens on each end of the sample be vertically supported by the split former tube which radially encases the sample. As an initial vacuum is applied to the inside of the sample, the rubber membrane on the sides of the sample is drawn in, and the sample is free to contract in the radial direction. Thus the radial stress on the sample equals the vacuum pressure. But because the

loading platens at either end of the sample are separated by the rigid former tube, essentially zero strain may occur in the axial direction. The reaction due to the vacuum on the end platens is carried by the former tube, and only the K_o component of stress generated in the axial direction of the sample due to the higher radial stress. As this is equivalent to K_o consolidation in the ground but with reversed directions of principal stress, the axial stress on the sample could be expected to be only half the radial stress, until the split former tube is removed.

Upon removal of the former tube, a state of isotropic stress would be established within the sample. This stress history would result in a fabric which is preloaded in the radial direction, but not preloaded in the axial direction. Thus subsequent strains induced by extension loading would be predicted to be relatively small in comparison to subsequent strains induced by compression loading. This is opposite to the trend predicted and observed in water pluviated sands (see Section 7.2).

If the moist tamped sand were truely isotropically consolidated during initial sample preparation, one could expect shear induced pore pressures under subsequent undrained loading to be essentially independent of direction of loading. In comparison to water pluviated sands, one could again predict greater shear induced pore pressures in the compression loading response of moist tamped sand.

The predicted differences in sand fabric between water pluviated and moist tamped sands offers a reasonable explanation for differences in CSR behaviour of the two sand types. In water pluviated sands, CSR is observed to be constant in compression loading, but variable and generally lower in extension loading (see Section 2.1 and Section 5.3). CSR behaviour in water pluviated sand is interpreted to be a consequence of the soil fabric produced by settlement of particles through water (see Section 7.2.3 and 7.2.4). In compression loading, water pluviated sand is interpreted to have a CSR equal to the K_O stress ratio of approximately 2.0 because the K_O consolidation stress history following sand deposition has ensured that there is a deficit of particle contacts which may slip and cause contractive deformation below a stress ratio of 2.0. In extension loading, no such stress history has occurred, thus the particle slip and induced contraction which triggers liquefaction may occur at lower and variable CSR values.

CSR behaviour of moist tamped sand in compression loading has been described by Castro (1982), Sladen et al. (1985) and Mohamad and Dobry (1986). CSR has been shown to be variable, generally increasing with increasing density. Very low CSR values have also been reported in compression loading. Thus the CSR behaviour of moist tamped sand in compression loading is more like that observed in water pluviated sand under extension loading. This is explained by the difference in interpreted sand fabric between the two

sand types. Moist tamped sand is interpreted to have a compression stress history only due to the tamping history during sample preparation, thus the particle contact population which may fail under compression loading is controlled by the degree and method of tamping. In relatively loose sands, there is no deficit of particle contacts which may fail during compression loading, thus CSR may be low and tend to increase with increasing density.

In general, one could predict that moist tamped sands could be more contractive than water pluviated sands in compression loading, and possibly less contractive than water pluviated sands in extension loading. The difference in behaviour of the two sand types is due to differences in fabric produced by sample preparation.

CHAPTER 8

PRACTICAL IMPLICATIONS

The mechanism of placement of a sand and its stress-strain history invariably induces an inherent fabric which imparts anisotropic strength properties to the sand. The variation of strength properties with direction of maximum principal stress is in direct conflict with the basic premise of the steady-state theory, which states that steady-state soil strength is solely dependent upon void ratio. Test results presented in this thesis indicate that at a given consolidation state, a sand may be either contractive or dilative, depending upon the orientation of principal stresses during shear. Thus the use of steady-state theory may lead to either conservative or unconservative estimates of soil strength, depending upon the procedure employed to determine soil strength.

In order to determine the undrained strength characteristics of natural fluvial or hydraulic fill sands, we must either obtain representative undisturbed samples from an in situ deposit, or if this is not possible, the deposition process and stress history expected in the field must be simulated in reconstituted laboratory test specimens.

Water pluviated sand has a characteristic behaviour under loading; it has relatively low compressibility under vertical loading and relatively high compressiblity under

horizontal loading. This anisotropy in compressibility results in an undrained loading response which is dependent on the inclination α of the maximum principal stress with the deposition direction. An α value of 0 degrees results in relatively less contractive response (as in triaxial compression loading), while an α value of 90 degrees results in relatively more contractive response (as in triaxial extension loading). Hollow cylinder tests performed by Symes et al. (1985) and Shibuya and Hight (1987) show a systematic weakening (increasing contractiveness and reduction in phase transformation strength) in water pluviated sand with increase in α from 0 to 90 degrees, which suggests that compression and extension tests provide the extremes of behaviour possible in a given water pluviated sand. Although the trend in inherent anisotropy is similar for all water pluviated sands which have been tested, the degree of anisotropy is dependent upon sand type. For example, water pluviated Ottawa sand is shown to have limited liquefaction behaviour in both extension and compression loading when loaded at loosest state, while in the same stress range, angular tailings sand is shown to have limited liquefaction behaviour only in extension loading. Figure 8.1 shows that although Ottawa sand is subject to limited liquefaction in compression loading over a range of void ratios, the material is still subject to substantial dilation once it is strained past phase transformation state. The contrast in loading behaviour of

Fig. 8.1 Undrained loading response of water deposited
Ottawa Sand C109 at various densities

$\sigma'_{3c} = 2.0 \ \text{kgf/cm}^2$

$K_c = 1.0$

SAMPLE SET	$Dr_i(\%)$	$Dr_c(\%)$
□ 1	32.5	36
△ 2	36.0	40.5
○ 3	39.0	43.0
○ 4	43.5	46.5
+ 5	60	62.5

$(\sigma_V - \sigma_H)$ (kgf/cm^2)

AXIAL STRAIN ε_a (%)
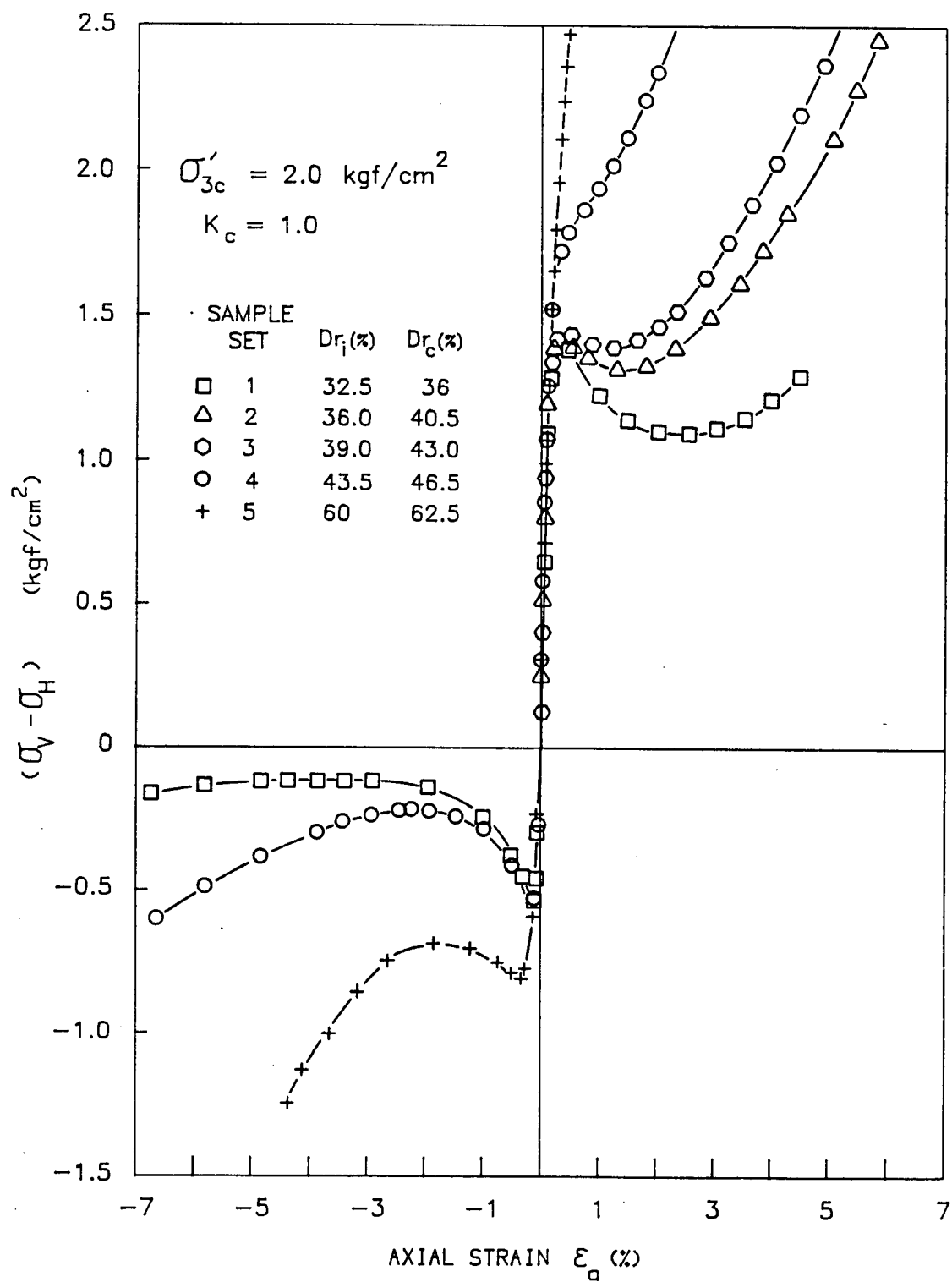
Ottawa sand and Brenda sand indicates that it is well worth while to conduct laboratory tests on representative samples of a given sand in order to characterize its properties.

The anisotropic properties of water pluviated sands may lead to modes of failure and mechanisms of triggering failure in a soil mass which are both unexpected and difficult to predict using presently available analytical methods. Soil masses which are subject to any form of lateral loading, such as in offshore islands and harbour facilities which are subject to ice, wave or boat loading, may be highly susceptable to liquefaction. In contrast, a soil mass which is subject to mainly vertical loading may be relatively resistant to liquefaction. Problems with current methods of evaluation arise in the majority of practical cases where a soil mass may be subjected to a combination of loading conditions. The following paragraphs attempt to identify and explain some of the practical implications of water pluviated sand fabric and properties upon the performance of a common structure, a soil embankment.

An embankment constructed of water pluviated sand should be relatively resistant to liquefaction under static loading conditions, due to the relatively low compressibility and high undrained strength of water pluviated sand under vertical loading. Terzaghi and Peck (1967) state that "A clean sand deposited under water is stable, although it may be loose, because the grains roll down into stable positions. In a sand capable of

spontaneous liquefaction, some agent must interfere with this process". The relatively small number of reported liquefaction failures of hydraulic fill embankments under static loading conditions tends to support the idea that most of these embankments are resistant to liquefaction under normal conditions.

The fact that some hydraulic fill embankments have been observed to fail under static loading suggests that some specific features of either the sand used or the method of construction has resulted in failure. Test results presented in this thesis indicate that different sands at loosest state after deposition may indeed have varying degrees of resistance to liquefaction under vertical loading. A comparison of the properties of Ottawa C109 sand and Brenda tailings sand suggests that rounded quartz sand which has a lower angle of intrinsic friction on particle surfaces is more susceptable to the development of flow failure under vertical loading than angular felsic sand which has on average a higher angle of intrinsic friction on particle surfaces.

The amount of air entrapped within a hydraulic fill sand may also interfere with the development of a stable sand fabric during deposition. A sand slurry which is deposited below water level may be expected to have a small percentage of entrapped air, which would have very little effect on water pluviated sand fabric due to small capillary tension forces. A sand which is deposited into water may

contain relatively more entrapped air, while a sand slurry which is deposited above water may contain a large amount of entrapped air, and thus develop a fabric which is more like that of moist tamped sand. A sand which has a large content of entrapped air is generally more unstable under vertical loading than sand which is deposited in a saturated state, due to the bulking effect and influence of capillary tension forces between grains. If a sand which is deposited above water is re-graded by a bulldozer without significant compaction, the sand may be bulked and its fabric altered further to produce a material which is considerably less stable under vertical loading.

The mechanism of hydraulic fill placement may have a significant affect upon its performance, thus it is very important to specify and control the mechanism of fill placement.

The mechanism of hydraulic fill placement in a fully saturated state may also affect the in situ fabric and material performance. Laboratory prepared slurry deposited test specimens of sand and silty sand are homogeneous and thus represent elemental material properties. Natural fluvial and hydraulic fill sands, in practice, will undergo some degree of particle segregation. The effect of particle segregation may be assessed from the results of tests performed on Ottawa sand C109 (see Figure 3.12). One set of compression and extension tests was performed on homogeneous slurry deposited sand specimens (with no segregation) and

another set of tests was conducted on water pluviated sand specimens (some visible segregation - Ottawa sand has C_u = 1.5). All tests were conducted on essentially loosest state specimens at similar density. Segregation is shown to increase both the peak strength as well as the phase transformation strength in compression. The same effect, though to a smaller extent, is observed in extension loading. The effect of particle size segregation upon undrained compression response is similar to the effect of gradation upon compression response in Brenda sands (see Figure 5.5). When compared at loosest state after deposition, the compression loading response of homogeneous poorly-graded sand (Figure 5.5) and segregated sand (Figure 3.12) is shown to be initially stiffer at small strain level and somewhat softer at large strain level than the compression response of homogeneous well-graded sand (Figure 5.5) or unsegregated sand (Figure 3.12). In addition, both segregated sands and poorly-graded sands are shown to have lower density at loosest state than unsegregated or well-graded sand (see Figure 3.8, Figure 3.9 and Table 3.2). One may conclude from these observations that particle segregation tends to make an otherwise well-graded sand behave as if it were more poorly-graded. This would be true if loading response is compared at either loosest state after slurry deposition, or at constant density. Since poorly-graded sands are more susceptible to liquefaction or limited liquefaction in extension loading than well-graded

sands, when consolidated from loosest state after deposition, some segregated sands could also be expected to be more contractive than unsegregated sands under extension loading at loosest state.

In situ sands which invariably have some degree of particle size segregation could be expected to be slightly more susceptible to liquefaction under horizontal loading and slightly less susceptible to liquefaction under vertical loading than unsegregated samples of equivalent gradation which are also consolidated from loosest state.

In laboratory studies, the deposition of sand through water occurs in the vertical direction, with settlement of particles upon a horizontal deposition plane. This results in the vertical loading direction having the least and horizontal loading the most contractive response. The axis of least contractive response in a hydraulic fill sand deposited on a slope may shift from vertical towards a direction normal to the slope. This could have the damaging effect of decreasing the resistance to liquefaction along a potential failure surface if the slope was constructed outwards from the central core. An opposite effect, or an increase in resistance to liquefaction could occur if the embankment was constructed by filling on a slope that dips from the outer shell towards the central core. Such a technique of construction could also limit the damaging effect of finer grained or silty beds and lenses within the embankment slope, because these less permeable beds would be

dipping downwards towards the central core, opposite the dip of the embankment slope and a potential failure surface. This orientation of finer grained beds would cause faster dissipation of pore pressures from within the embankment, and would also limit the effect which any particular weaker or impermeable bedding layer might have upon the orientation of a failure surface.

The results presented in this study show that water deposited silty sands could be slightly less susceptable to liquefaction than clean sand. The permeability of silty sands, however, decreases with increase in silt content. Thus, under field conditions, a condition of strictly undrained loading could occur more readily in silty sands than in clean sands, which could make silty sands more vulnerable to liquefaction.

The stress conditions on a potential failure surface through an embankment vary from the condition of a vertical maximum principal stress at and below the crest of the embankment, towards horizontal maximum principal stress at the toe of the embankment. The direction of maximum principal stress undergoes continuous rotation from the crest towards the toe of the embankment. In order to calculate a Factor of Safety for a given slope, it is important to determine this variability of soil strength with direction of loading. This is especially important in analyzing the stability of hydraulic fill embankments, because hydraulic fill properties are highly anisotropic. A

consequence of the relatively lower strength of hydraulic fill sand with the rotation of maximum principal stress toward the horizontal direction is that one could expect a relatively deep seated failure surface within an embankment. A major portion of the failure surface would be predicted to be fairly flat, as observed in the failure zone of the lower San Fernando hydraulic fill dam (Castro et al., 1985; Seed et al., 1975). On the relatively flat failure zone of the lower San Fernando Dam, the undrained strength would correspond to loading with $\alpha = 45 + \phi_S/2$, where ϕ_S is the friction angle at steady-state. With $\phi_S = 37^O$, $\alpha = 63^O$, which is closer to a horizontal direction than a vertical direction of maximum principal stress. If suitable α dependent values of steady-state strength were used in the analysis of the stability of the dam, it would probably not be necessary to apply a reduction factor of 20 to the measured triaxial compression test steady-state strength in order to obtain back-analysed strength at failure (as reported by Castro et al., 1985). Densification of sand samples taken from the dam could be blamed for an overestimate of in situ steady-state strength, but its effects are probably overstated due to a neglect of α dependence of steady-state strength. An estimate of the magnitude of anisotropy between compression and extension loading modes may be obtained from the results reported in this thesis. Loose Ottawa sand C109 has extension phase transformation strength that is at most 10% of that in

compression (Figure 3.12, Figure 8.1), while angular tailings sands do not even show contractive behaviour in compression (Figure 5.2 through Figure 5.4).

The low strength of water pluviated sands under horizontal loading may play a role in the initiation of contractive flow in a hydraulic fill embankment. Once lateral stresses at the toe of an embankment are large enough to initiate strain softening, the toe region may develop very low strength. The development of low strength at the toe of the embankment is essentially equivalent to unloading the toe of the embankment. As would be observed in unloading the toe of any embankment, this reduction of soil strength at the toe would cause a redistribution of the driving stresses deeper within the embankment, which may be sufficient to initiate progressive or entire failure of the embankment. Any factors which contribute to increased lateral loading of the toe of the embankment may cause initiation of toe failure and subsequent progressive failure of the entire slope. Increased lateral load may be induced by external cyclic loading due to seismic loading, or an increase in porewater pressure under the conditions of either static of cyclic loading. The mechanism whereby increased pore pressure may induce an increase in lateral stress is described in the following paragraphs.

Increased pore pressure within an embankment may be induced by rapid rates of construction, by seepage through an embankment which retains water, by the initiation of

strain softening contractive response, or by cyclic loading. Beneath the crest of an embankment, vertical total stress distribution is a function of soil unit weight and depth within the embankment. The distribution of vertical total stress below the embankment crest is essentially constant, and may only be altered by a change in embankment height. Vertical effective stress is in addition a function of porewater pressure. In contrast, both horizontal total and effective stresses are a function of porewater pressure and the mobilized angle of friction within each soil element. Assuming that vertical total stress distribution is constant (i.e. that the embankment height is not changed) one may derive Equation 8.3 which relates the variation of horizontal total stress on a soil element beneath the crest of an embankment with the mobilized friction (effective mobilized stress ratio R) and pore pressure within the soil element.

Equation 8.3 shows that an increase in pore pressure within a soil element beneath the crest of an embankment would probably also induce an increase in horizontal total stress. Horizontal total stress within these soil elements could be expected to vary from a minimum corresponding to K_O consolidation state, up to a maximum when vertical and horizontal total stress are equal at a state of zero effective stress. The horizontal total stress generated within these soil elements beneath the crest of an embankment must be transfered and carried by adjacent soil

elements within the embankment slope. This spreading of lateral stress would tend to rotate the direction of maximum principal stress away from vertical and towards horizontal within soil elements in the embankment slope. Within these elements, horizontal total stress would not be limited by the magnitude of initial vertical stress, as beneath the crest of the embankment. Horizontal total stress may in fact exceed initial vertical total stress, giving rise to a triaxial extension type of loading towards the toe of the embankment slope.

If pore pressure is increased within an embankment, this may also lead to a spreading of lateral total stress in the embankment, which could trigger strain softening at the toe of the embankment. If strength at the toe is reduced, this would simulate unloading of the toe, which may produce progressive or complete failure of the embankment. This mechanism of triggering flow deformation is particularly relevant to hydraulic fill embankments, due to the characteristic strength anisotropy of water pluviated sand.

For a soil element beneath the embankment crest:

$$R = (\sigma_v - U)/(\sigma_h - U) \qquad (8.1)$$

where

R   =   effective mobilized principal stress ratio

σ_v =   vertical total stress

σ_h = horizontal total stress

U = porewater pressure

Then

$$\sigma_h = U + (\sigma_v - U)/R \qquad\qquad (8.2)$$

Differentiating Equation (8.2):

$$d\sigma_h = dU + d(\sigma_v/R) - d(U/R)$$

$$d\sigma_h = dU + d\sigma_v/R - \sigma_v dR/R^2 - dU/R + U dR/R^2$$

$$\Delta\sigma_h = (1-1/R_1)(U_2-U_1)+(\sigma_{v2}-\sigma_{v1})/R_1+(U_2-\sigma_{v2})(1/R_1-1/R_2)$$

when σ_v = constant:

$$\Delta\sigma_h = (1-1/R_1)(U_2-U_1)+(U_2-\sigma_v)(1/R_1-1/R_2) \qquad (8.3)$$

where:

R_1 = initial mobilized stress ratio

R_2 = final mobilized stress ratio

$\Delta\sigma_h$ = change in horizontal total stress

U_1 = initial pore pressure

U_2 = final pore pressure

(see Figure 8.2)

Fig. 8.2 Change in lateral total stress with change in effective stress state for a soil element beneath the crest of an embankment

$$\Delta \sigma_h = (1 - 1/R_1)(U_2 - U_1) + 1/R_1 (\sigma_{v2} - \sigma_{v1}) + (U_2 - \sigma_{v2})(1/R_1 - 1/R_2)$$
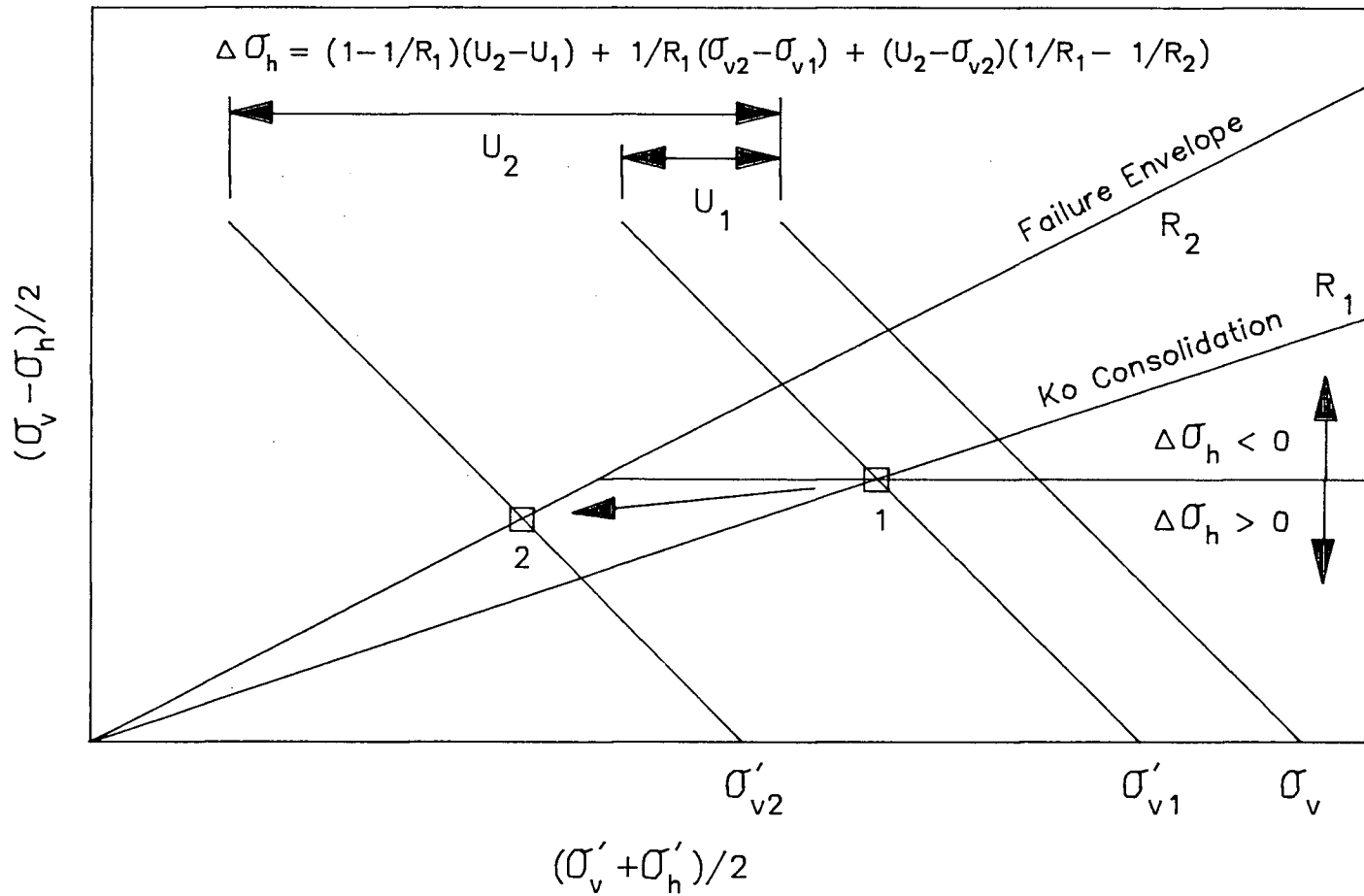
CHAPTER 9

SUMMARY AND CONCLUSIONS

In the past, our knowledge of the fundamentals of sand liquefaction behaviour has been derived from laboratory tests and observations. To ensure that fundamental material strength properties determined in the laboratory are applicable to practical field problems, two basic questions must be considered: (1) is the soil sample tested in the laboratory representative of the in situ soil being modelled, and (2) does the laboratory testing technique employed simulate the loading conditions that occur in situ. Previous studies have shown that sand liquefaction behaviour in the laboratory is controlled by both method of sample preparation and mode of soil testing.

A majority of loose sandy soils which are prone to liquefaction and of practical concern in geotechnical designs are deposited by natural fluvial deposition or artificial hydraulic fill placement. These deposits are often well-graded with some fines content. A majority of laboratory testing in the past has been conducted on poorly-graded sands in order to ensure sample uniformity, which is required in most laboratory tests in order to measure elemental soil properties. The study of well-graded sands and sands with some fines content has been relatively limited. Since these sands are relatively common in the field, the study of the effect of gradation and fines

content upon sand behaviour has been identified as a major research objective by the U.S. N.R.C. (1985) report on earthquake engineering. Most sands which have been tested in the past have been reconstituted in the laboratory using the moist tamping or dry pluviation techniques of sample preparation. These techniques may not simulate either the density range or strength behaviour possible in a sand which is pluviated through water, as in a fluvial or hydraulic fill sand deposit.

In order to model the behaviour of fluvial and hydraulic fill sands in the laboratory, the slurry deposition method of sample preparation has been developed. This method simulates the mechanism of hydraulic fill or fluvial sand deposition through water very well, yet yields homogeneous well-mixed samples which are essentially unsegregated, regardless of gradation and fines content. A comparison of the soil strength properties of poorly-graded water pluviated and slurry deposited sand samples indicates that both sample preparation techniques yield similar test results.

In order to observe the effect which gradation and fines content have upon the properties of sands which have been pluviated through water, a series of undrained triaxial tests have been conducted on samples of poorly-graded, well-graded and silty angular tailings sands derived from the Brenda Mine, British Columbia. This tailings sand is representative of generally more well-graded and silty sands

found in seismically active mountainous areas, and tailings sands which are derived from granitic rock. The use of tailings sand derived from crushed rock ensures that sand mineralogy is essentially independent of grain size. Both triaxial compression and extension tests were employed, in order to show the effect of direction of loading upon strength behaviour.

The fabric of water pluviated sand is shown to produce a characteristic anisotropy in undrained loading response. Water pluviated sand is substantially more contractive when loaded under a horizontal maximum principal stress, and substantially less contractive when loaded under a vertical maximum principal stress. The substantial directional dependence of sand strength at constant void ratio conflicts with the main premise of steady-state concepts, which states that the ultimate undrained strength of sand is only a function of soil void ratio, and independent of factors such as soil fabric, direction of loading and consolidation state. The use of steady-state concepts and triaxial compression test results to characterize the behaviour of water pluviated sand would result in high estimates of sand strength. The use of such estimates in design could result in designs which are highly unconservative.

In water pluviated sands consolidated from loosest state of deposition, as might be expected in a hydraulic fill deposit, triaxial compression stress-strain response is essentially the same for various gradations of sand. In

contrast, triaxial extension response is highly dependent upon soil gradation. Well-graded sand is shown to be substantially less contractive than poorly-graded sand in extension loading. Well-graded sand thus shows less anisotropy, or less of a difference between extension and compression test response than poorly-graded sand. One may conclude that well-graded sand is in general more resistant to liquefaction than poorly-graded sand.

In poorly-graded sand, smaller grain size tends to produce slightly more dilative response in compression loading, yet more contractive response in extension loading. Strength anisotropy of isotropically consolidated sand is shown to be greatest at low consolidation stress and least at high consolidation stress. The process of isotropic consolidation is thus observed to slightly alter strength anisotropy, or soil fabric.

Gradation generally has a greater effect upon material properties of sand than non-cohesive fines content, especially if the sand portion is coarser grained. An increase in silt content up to 20% in loosest state slurry deposited 20/200 sand makes monotonic compression loading behaviour somewhat more dilative and extension loading behaviour somewhat less contractive. The rather small change in loading behaviour with increasing silt content can be explained by the fact that sand skeleton void ratio remains virtually unaltered with increasing silt content. Silt essentially fills sand skeleton void space and does not

greatly affect soil behaviour. On the other hand, silty sands need not have a large void ratio to be susceptible to liquefaction, as long as sand skeleton void ratio and silt portion void ratio are high.

Silty 20/200 sands at loosest state show only a slight increase in cyclic strength with increasing silt content, despite a large reduction in void ratio. When compared at constant sand skeleton void ratio, cyclic strength is shown to increase slightly with increasing silt content.

If the silt fraction of a soil is segregated into silty lenses, as often is the case in hydraulic fill or fluvial soil deposits, cyclic strength of the material may be expected to be lower than if the material is well mixed (when considered at loosest state of consolidation), simply because elements of the segregated soil are more poorly-graded. If a segregated sand and a well mixed sand with the same grain size gradation and void ratio are compared, the segregated soil would tend to be more resistant to liquefaction, because it is effectively more poorly-graded and thus at an effectively denser state.

For practical purposes it is conservative to ignore silt content in a hydraulic fill silty sand, when considering undrained soil strength, as long as the water pluviated reconstituted silt free material tested in the laboratory has a similar sand gradation and sand skeleton void ratio as the silty sand being modelled.

The conclusion that silt content generally makes a laboratory soil sample more resistant to liquefaction (when compared at both loosest state or constant sand skeleton void ratio) does not take into account drainage and migration of porewater as may occur in a field embankment. In general, a silty sand embankment of similar sand skeleton density and gradation as a clean sand embankment may be more susceptible to strain development due to: (1) greater retension of pore pressure during loading, and (2) migration and build-up of pore pressure at silty layer barriers.

The characteristic loading response and anisotropy of water pluviated sand may be explained by considering the mechanics of frictional resistance to particle contact slip during loading. For an assembly of rigid particles, dilatancy during loading is shown to be a function of particle structure or fabric (the spacial distribution and orientation of particle contacts), direction of loading, stress ratio level and strain level. The fabric of a sand is interpreted to be a function of sample preparation and stress ratio history. The soil fabric and properties derived from a specific method of deposition may be explained by considering the physical processes which are active during deposition.

The method selected for soil placement in the field may influence the stability of a soil mass considerably. The method of soil deposition has been shown to have a large effect upon: (1) the range of void ratios possible within a

soil deposit, (2) the range of undrained loading response possible, (3) the range of soil anisotropy possible, and (4) the magnitude of soil strength at a given void ratio. Moist or dry soil may be prepared at much larger void ratios than possible in similar water pluviated soil. Thus much lower strengths may be obtained by moist or dry preparation of a sand, simply because much higher void ratios are possible. At the same void ratio, water pluviated sand may be weaker or stronger than air pluviated or moist tamped sand, depending upon soil fabric and direction or mode of loading.

Laboratory observations concerning the effect of soil deposition method upon soil properties may be used in evaluating and perhaps designing better field construction techniques. The hydraulic fill form of construction is shown to be fairly good in that lower depositional void ratios can generally be attained with no compactive effort, as long as the hydraulic fill technique ensures saturation of the fill material. In addition, hydraulic fill is relatively less compressible under vertical loading, which is often beneficial under field loading conditions.

The characteristic properties of water pluviated sand would result in characteristic modes of failure and triggering failure within a soil mass which may be difficult to predict. The variation of material properties with direction of loading should be considered during design. The method of stability analysis employed in design should be able to account for the variation of undrained strength

with the inclination of maximum principal stress to the fill deposition direction. The relatively low strength of water pluviated sand under lateral loading conditions would tend to induce a deep seated failure surface in an embankment. In addition, undrained failure of an embankment is likely to be triggered by initial liquefaction failure at the toe, which is induced by increased lateral stress in the embankment. Liquefaction at the toe under a maximum principal stress which is close to horizontal would simulate unloading of the embankment toe, which could lead to progressive or complete failure of the embankment. Liquefaction at the toe may be triggered by any mechanism which induces an increase in lateral stress in the embankment slope, including dynamic loading or an increase in pore pressure within the embankment.

REFERENCES

ASTM D2049-69 "Standard Test Method for Relative Density of Cohesionless Soils," Annual Book of ASTM Stadards, 1983, Section 4, Soil and Rock; Building Stones.

Atkinson, J.H. and Bransby, P.L. (1978). "The Mechanics of Solids, An Introduction to Critical State Soil Mechanics," McGraw Hill Book Company (UK) Ltd.

Berre, T. (1982). "Triaxial Testing at the Norwegian Geotechnical Institute," Geotechnical Testing Journal, Vol. 5, No. 1/2, pp. 3-17.

Bishop, A.W. (1971). "Shear Strength Parameters for Undisturbed and Remolded Soil Specimens," Roscoe Mem. Symp., Cambridge University, pp. 3-58.

Bishop, A.W. and Henkel, D.J. (1957). "The Measurement of Soil Properties in the Triaxial Test," Edward Arnold Publishers Ltd., London, England.

Bishop, A.W. and Wesley, L.D. (1975). "A Hydraulic triaxial Apparatus for Controlled Stress Path Testing", Geotechnique, Vol. 25.

Bjerrum, L. (1972). "Embankment on Soft Ground," ASCE Spec. Conf., Earth and Earth Supported Structures, Vol. 1, Purdue University.

Casagrande, A. (1936). "Characteristics of Cohesionless Soils Affecting The Stability of Slopes and Earthfills," Journal of the Boston Society of Civil Engineers, reprinted in Contributions to Soil Mechanics, 1925 to 1940, Boston Society of Civil Engineers, Oct. 1940, pp. 257-276.

Casagrande, A. (1975). "Liquefaction and Cyclic Deformation of Sands - A Critical Review," Proc. 5th American Conf. on Soil Mechanics and Foundation Engineering, Buenos Aires, Vol. 5, pp. 79-133.

Casagrande, A. (1976). "Liquefaction and Cyclic Deformation of Sands - A Critical Review," Harvard Soil Mechanics Series No. 88, Harvard University, Cambridge, Mass.

Castro, G. (1969). "Liquefaction of Sands," Ph.D. Thesis, Harvard University, Cambridge, Mass.

Castro, G. (1975). "Liquefaction and Cyclic Mobility of Saturated Sands," J. of the Geot. Engng. Div., ASCE, Vol. 101, No. GT6, Proc., 551-569.

Castro, G. and Poulos, S.J. (1977). "Factors Affecting Liquefaction and Cyclic Mobility," J. of the Geot. Engng. Div., ASCE, Vol. 103, No. GT6, 501-506.

Castro, G., Poulos, S.J., France, J.W. and Enos, J.L. (1982). "Liquefaction Induced by Cyclic Loading, Report to National Science Foundation, March, 1982.

Castro, G., Poulos, S.J. and Leathers, F.D. (1985). "Re-Examination of Slide of Lower San Fernando Dam," J. Geotech. Eng., ASCE, Vol. 111, No. 9, pp. 1093-1107.

Chaney, R. and Mulilis, P.J. (1978). ASTM Geotechnical Testing Journal, Vol. 1, No. 2, 1978, pp. 107-108.

Chang, N.Y., Yey, S.T. and Kaufman L.P. (1982). "Liquefaction Potential of Clean and Silty Sands," Proc. Third Microzonation Conf., Seattle, pp. 1018-1032.

Chern, J.C. (1985). "Undrained Response of Saturated Sands with Emphasis on Liquefaction and Cyclic Mobility," Ph.D. Thesis, The University of British Columbia, Vancouver, Canada.

Chung, E.K.F. (1985). "Effects of Stress Path and Prestrain History on the Undrained Monotonic and Cyclic Loading Behaviour of Saturated Sand," M.A.Sc. Thesis, The University of British Columbia, Vancouver, Canada.

De Alba, P., Chan, C.K., and Seed, H.B. (1976). "Sand Liquefaction in Large-Scale Simple Shear Tests," J. Geotech. Engrg. Div., ASCE, 102(9), pp. 909-927.

DeGroff, W., Donaghe, R., Lade, P. and La Rochelle, P. (1988). "Correction of Strength for Membrane Effects in the Triaxial Test," Geotechnical Testing Journal, Vol 11 (1).

Dobry, R. (1985). Unpublished data, presented in N.R.C. (1985) report.

Duncan, J.M. and Seed, H.B. (1967). "Corrections for Strength Test Data," Jour. Soil Mech. Div., Proc. ASCE, Vol. 93, No. SM5, pp. 121-137.

El-Sohby, M.A. (1969). "Deformation of Sands Under Constant Stress Ratios," Proc., Seventh International Conference on Soil Mechanics and Foundation Engineering, Mexico, Vol. 1, pp. 111-119.

El-Sohby, M.A. and Andrawes, K.Z. (1972). "Deformation Characteristics of Granular Materials Under Hydrostatic Compression," Canadian Geotech. Journal, 9, pp. 338-350.

Emery, J.J., Finn, W.D.L. and Lee, K.W. (1973). "Uniformity of Saturated Sand Samples," ASTM STP 523, 1973, pp. 182-194.

Finn, W.D.L., and Bhatia, S.K. (1981). "Prediction of Seismic Pore-Water Pressures," pp.201-206 in Proceedings in the Tenth International Conference on Soil Mechanics and Foundation Engineering, Volume 3, A.A. Balkema Publishers, Rotterdam, Netherlands.

Finn, W.D.L., Pickering, D.J., and Bransby, P.L. (1971). "Sand Liquefaction in Triaxial and Simple Shear Tests," Journal of the Soil Mechanics and Foundations Division, ASCE, Vol. 97, No. SM4, Proc. Paper 8039, pp. 639-659.

Finn, W.D.L., Bransby, P.L. and Pickering, D.J. (1970). "Effect of Strain History on Liquefaction of Sands," Journal of the Soil Mechanics and Foundations Division, ASCE, Vol. 96, No. SM6, pp. 1917-1934.

Fukushima, S. and Tatsuoka, F. (1984). "Strength and Deformation Characteristics of Saturated Sand at Extremely Low Pressures," Soils and Foundations, Vol. 24, No. 4, pp. 30-48.

Hanzawa, H. (1980). "Undrained Strength and Stability of Quick Sand," Soils and Foundations, Vol. 20 (2), pp. 17-29.

Hedberg, J. (1977). Ph.D. Thesis, M.I.T., Cambridge, Massachusetts.

Henkel, D.J. (1960). "Shear Strength of Saturated Remolded Clays," ASCE, Research Conf. on Shear Strength of Cohesive Soils, Boulder, Colorado, pp. 533-554.

Henkel, D.J. and Gilbert, G.D. (1952). "The Effect of the Rubber Membrane on the Measured Triaxial Compression Strength of Clay Samples," Geotechnique, Vol. 3, No. 1, March 1952, pp. 20-29.

Horne, M.R. (1965). "The Behaviour of an Assembly of Rotund, Rigid, Cohesionless Particles," Proc. Roy. Soc. A, 286, pp. 63-97.

Ishihara, K., Tatsuoka, F. and Yasuda, S. (1975). "Undrained Deformation and Liquefaction of Sand Under Cyclic Stresses," Soils and Foundations, Vol. 15, No. 1, pp. 29-44.

Ishihara, K. and Okada, S. (1978). "Effects of Stress History on Cyclic Behaviour of Sand," Soils and Foundations, Vol. 18, No. 4, pp. 31-45.

Ishihara, K., Troncoso, J., Kawase, Y. and Takahashi, Y. (1980). "Cyclic Strength Characteristics of Tailings Materials," Soils and Foundations, Vol. 20, No. 4, pp. 127-142.

Ishihara, K. and Okada, S. (1982). "Effects of Large Preshearing on Cyclic Behaviour of Sand," Soils and Foundations, Vol. 22, No. 4, pp. 109-125.

Ladd, R.S. (1977). "Specimen Preparation and Cyclic Stability of Sands," Journal of the Geotechnical Engineering Division, ASCE 103(GT6):535-547.

Ladd, R.S. (1974). "Specimen Preparation and Liquefaction of Sands," Journal of the Geotechnical Engineering Division, ASCE 100(GT10):1180-1184.

Lambe, T. W. (1951). "Soil Testing for Engineers," The Massachusetts Institute of Technology, John Wiley & Sons, Inc., New York.

Lee, K.L., et. al. (1975). "Properties of Soil in the San Fernando Hydraulic Fill Dams," J. Geotech. Engrg., ASCE, 101(8), 801-821.

Lee, K.L. and Fitton, J.A. (1969). "Factors Affecting the Cyclic Loading Strength of Soil," Vibration Effects of Earthquakes on Soils and Foundations, ASTM STP 450, pp. 71-95.

Lee, F.H. and Schofield, A.N. (1988). "Centrifuge Modelling of Sand Embankments and Islands in Earthquakes," Geotechnique 38, No. 1, pp. 45-58.

Lee, K.L., and Seed, H.B. (1967). "Cyclic Stress Conditions Causing Liquefaction of Sand," Journal of the Soil Mechanics and Foundations Division, ASCE, Vol. 93, No. SM1, pp. 47-70.

Marcuson, W.F., III and Gilbert, P.A. (1972). "Earthquake Liquefaction Potential at Patoka Dam, Indiana," Army Engineer Waterways Experimental Station Miscellaneous Paper S-72-42, 62p.

Marcuson, W.F., III and Townsend, F.C. (1974). "The Effects of Reconstitution on Cyclic Triaxial Results," Preliminary Report U.S. Army Corps. of Engineers, Waterways Experimental Station, Vicksburg, Miss.

Matsuoka, H. and Takeda, K. (1980). "A Stress-Strain Relationship for Granular Materials Derived from Microscopic Shear Mechanism," Soils and Foundations, Vol. 20, No. 3, pp. 45-58.

Mehrabadi, M.M., Nemat-Nasser, S. and Oda, M. (1982). "On Statistical Description of Stress and Fabric in Granular Materials," Int. J. Num. An. Methods Geomechanics, Vol. 6, pp. 95-108.

Mejia, C.A., Vaid, Y.P. and Negussey, D. (1988). "Time Dependent Behaviour of Sand," International Conf. on Rheology and Soil Mech., Coventry, England, Elsevier Publications.

Miura, S. and Toki S. (1982). "A Sample Preparation Method and its Effect on Static and Cyclic Deformation - Strength Properties of Sand," Soils and Foundations, Vol. 22, No. 1, pp. 61-77.

Miura, S., Toki, S. and Tanizawa, F. (1984). "Cone Penetration Characteristics and its Correlation to Static and Cyclic Deformation-Strength Behaviors of Anisotropic Sand," Soils and Foundations, Vol. 24, No. 2, pp 58-74.

Mohamad, R., and Dobry, R. (1986). "Undrained Monotonic and Cyclic Triaxial Strength of Sand," Journal of the Geotechnical Engineering Division, ASCE 112(GT10):941-958.

Molenkamp, F. and Luger, H.J. (1981). "Modelling and Minimization of Membrane Penetration Effects in Tests on Granular Soils," Geotechnique, Vol. 31, No. 4, pp. 471-486.

Mulilis, J.P., Chan, C.K. and Seed, H.B. (1975). "The Effects of Method of Sample Preparation on the Cyclic Stress-Strain Behavior of Sands," EERC-75-19, University of California, Berkeley.

Mulilis, J.P., Seed, H.B., Chan, C.K., Mitchell, J.K., and Arulanandan, K. (1977). "Effects of Sample Preparation on Sand Liquefaction," Journal of the Geotechnical Engineering Division, ASCE 103(GT2): pp 91-108.

National Research Council (1985). "Liquefaction of Soils During Earthquakes," Report No. CETS-EE-001, Committee on Earthquake Engineering, National Academy Press, Washington, D.C.

Negussey, D., Wijewickreme, W.K.D., and Vaid, Y.P. (1986). "Constant Volume Friction Angle of Granular Materials," Soil Mechanics Series No. 94, Department of Civil Engineering, The University of British Columbia, Vancouver, Canada.

Negussey, D. (1984). "An Experimental Study of the Small Strain Response of Sand," Ph.D. Thesis, The University of British Columbia, Vancouver, Canada.

Negussey, D. (1989). Personal Communication, Unpublished Data.

Nemat-Nasser (1980). "On Behaviour of Granular Materials in Simple Shear," Soils and Foundations, Vol. 20, No. 3, pp. 59-73.

Oda, M. (1972a). "Initial Fabrics and Their Relationships to Mechanical Properties of Granular Material," Soils and Foundations, Vol. 12, No. 1, pp. 17-36.

Oda, M. (1972b). "The Mechanism of Fabric Change During Compressional Deformation of Sand," Soils and Foundations, Vol. 12, No. 2, pp. 1-18.

Oda, M., Koishikawa, I. and Higuchi, T. (1978). "Experimental Study of Anisotropic Shear Strength of Sand by Plane Strain Test," Soils and Foundations, Vol. 18, No. 1, pp. 25-38.

Oda, M. and Konishi, J. (1974). "Microscopic Deformation Mechanism of Granular Material in Simple Shear," Soils and Foundations, Vol. 14, No. 4, pp. 25-38.

Oda, M., Nemat-Nasser, S., Konishi, J. (1985). "Stress Induced Anisotropy in Granular Masses," Soils and Foundations, Vol. 25, No. 3, pp. 85-97.

Ponce, V.M. and Bell, J.M. (1971). "Shear Strength of Sand at Extremely Low Pressures," Journal of the Soil Mech. and Foundations Div., ASCE, Vol. 97, No. SM4, pp. 625-638.

Rowe, P.W. (1962). "The Stress-Dilatancy Relation for Static Equilibrium of an Assembly of Particles in Contact," Proc. Roy. Soc. A, 269, 500.

Rowe, P.W. (1971). "Theoritical Meaning and Observed Values of Deformation Parameters for Soil," Discussion Session 2, Proceedings of the Roscoe Memorial Symposium, Cambridge University, pp. 143-194.

Seed, H.B. (1987). "Design problems in Soil Liquefaction," Journal of the Geotechnical Engineering Div., ASCE, Vol. 113, No. 8, pp. 827-845.

Seed, H.B. (1983). "Earthquake Resistant Design of Earth Dams," Proc. Symp. on Seismic Design of Embankments and Caverns, ASCE, pp. 41-64.

Seed, H.B. (1979). "Soil Liquefaction and Cyclic Mobility Evaluation for Level Ground During Earthquakes," Journal of the Geotechnical Engineering Division, ASCE 105(GT2): pp. 201-255.

Seed, H.B., Mori, K. and Chan, C.K. (1975). "Influence of Seismic History on the Liquefaction Characteristics of Sands," Report No. EERC 75-25, Earthquake Engineering Research Center, University of California, Berkeley, California.

Seed, H.B., and Lee, K.L. (1966). "Liquefaction of Saturated Sands During Cyclic Loading," Journal of the Soil Mechanics and Foundations Division, ASCE 92(SM6):105-134.

Seed, H.B., Lee, K.L., Idriss, I.M., and Makdisi, F.I. (1975). "The Slides in the San Fernando Dams During the Earthquake of February 9, 1971," Journal of the Geot. Eng. Div., Proc. of the ASCE, Vol. 101, No. GT7.

Shibuya, S., and Hight, D.W. (1987). "A Bounding Surface for Granular Materials," Soils and Foundations, Vol. 27, No. 4, pp. 123-136.

Symes, M.J., Shibuya, S., Hight, D.W., and Gens, A. (1985). "Liquefaction with Cyclic Principal Stress Rotation," Eleventh International Conference on Soil Mechanics and Foundation Engineering, Vol. 4, San Francisco.

Sladen, J.A., D'Hollander, R.D. and Krahn, J. (1985). "The Liquefaction of Sands, a Collapse Surface Approach," Canadian Geotech. Journal. Vol. 22, pp 564-578.

Soregaroli, A.E. (1974). "Geology of the Brenda Copper-Molybdenum Deposit in British Columbia, Canadian Mining and Metallurgical (CIM) Bulletin, Vol. 67, No. 750.

Tatsuoka, F., Ochi, K., Fujii, S. and Okamoto M. (1986). "Cyclic Undrained Triaxial and Torsional Shear Strength of Sands for Different Sample Preparation Methods," Soils and Foundations, Vol. 26, No. 3, pp. 23-41.

Tatsuoka, F., Toki, S., Miura, S., Kato, H., Okamoto, M., Yamada, S., Yasuda, S., and Tanizawa, F. (1986). "Some Factors Affecting Cyclic Undrained Triaxial Strength of Sand," Soils and Foundations, Vol. 26, No. 3, pp. 99-116.

Terzaghi, K. and Peck, R.B. (1967). "Soil mechanics in Engineering Practice," John Wiley & Sons, New York.

Towhata, I. and Ishihara, K. (1985). "Shear Work and Pore Water Pressure in Undrained Shear," Soils and Foundations, Vol. 25, No. 3, pp. 73-84.

Troncoso, J.H., and Verdugo, R. (1985). "Silt Content and Dynamic Behaviour of Tailings Sands," Proc. of the Eleventh International Conference on Soil Mechanics and Foundation Engineering, Vol. 3, San Francisco.

Vaid, Y.P. and Chern, J.C. (1983). "Effect of Static Shear on Resistance to Liquefaction," Soils and Foundations 23(1):47-60.

Vaid, Y.P. and Chern, J.C. (1985). "Cyclic and Monotonic Undrained Response of Saturated Sands," Advances in the Art of Testing Soils Under Cyclic Conditions, ASCE Convention, Detroit, pp. 120-147.

Vaid, Y.P. and Negussey, D. (1984). "Relative Density of Pluviated Sand Samples," U.B.C. Soil Mechanics Series No. 82, The University of British Columbia.

Vaid, Y.P. and Negussey, D. (1984). "A Critical Assessment of Membrane Penetration in the Triaxial Test," Geotechnical Testing Journal, Vol. 7, No. 2, pp. 70-76.

Vaid, Y.P. and Negussey, D. (1986). "Preparation of Reconstituted Sand Specimens," U.B.C. Soil Mechanics Series No. 98, The University of British Columbia, 26p.

Vaid, Y.P., Negussey, D. and Zergoun, M. (1988). "A Stress- and Strain-Controlled Monotonic and Cyclic Loading System," ASTM STP 977.

Appendix A:. Membrane Penetration Correction

Volumetric and radial strains during consolidation have been corrected
for membrane penetration errors using Method 2 described by Vaid and Negussey
(1984). Method 2 membrane penetration corrections are determined by conducting
an isotropic consolidation load and unload test on a single soil sample. In
isotropic consolidation loading, soil specimen strains need not be isotropic
due to soil anisotropy, but in isotropic consolidation unloading, soil specimen
strains have been found to be isotropic. The deviation of triaxial test soil
specimen unloading strain from isotropy with respect to axial strain is shown
to be due to membrane penetration effects in the radial direction of loading.
The correction to radial strain required to maintain isotropic unloading strain
is the correction required to account for membrane penetration effects. The
unit membrane penetration correction ε_m is calculated as shown in Equation A.1:

$$\varepsilon_{V_{tu}} = \varepsilon_m \, A_s / V_o + 3\varepsilon_{au} \qquad \text{Eqn. A.1}$$

Where: ε_m = unit membrane penetration correction or membrane penetration
volume per unit surface area of membrane

$\varepsilon_{V_{tu}}$ = total volumetric strain measured in an unloading step

ε_{au} = axial strain measured in an unloading step

$3\varepsilon_{au}$ = true volumetric strain in the unloading step if there is no membrane
penetration (top and bottom platens must be rigid)

A_s = surface area of soil sample covered with rubber membrane

V_o = initial volume of soil sample within membrane

Equation A.1 may be rewritten in terms of soil sample diameter, Equation A.2:

$$\varepsilon_m = (\varepsilon_{V_{tu}} - 3\varepsilon_{au}) D_o / 4 \qquad \text{Eqn. A.2}$$

Where: D_o = soil sample diameter

Unit membrane penetration ε_m varies approximately linearly with logarithm
of effective consolidation stress (see Figure A.1, after Vaid and Negussey,
1984). The slope (m, Equation A.3) of unit membrane penetration with logarithm
of effective stress is essentially constant, and may be used in Equation A.4
to calculate true volumetric strain within a soil specimen whose m value is
known.

$$m = \varepsilon_m / \log(\sigma_c' / \sigma_{ci}') \qquad \text{Eqn. A.3}$$

$$\varepsilon_v = \varepsilon_{v_T} - 4m\log(\sigma_c' / \sigma_{ci}')/D_o \qquad \text{Eqn. A.4}$$

Where: m = membrane penetration function slope (see Figure A.1)

σ_c' = consolidation effective stress on membrane

σ_{ci}' = initial consolidation effective stress on membrane

ε_v = true volumetric strain corrected for membrane penetration

FIGURE A.1 Unit membrane penetration of various Brenda sand gradations determined by the single specimen method

After Vaid and Negussey (1984)

$$m = \varepsilon_m / \log(\sigma_c' / \sigma_{ci}')$$

Consolidation from loosest state of slurry deposition

20/40 Sand
m = 0.00566 cm

20/200 Sand
m = 0.00078 cm

60/100 Sand
m = 0

100/140 Sand
m = 0

UNIT MEMBRANE PENETRATION ε_m (cm)

EFFECTIVE ISOTROPIC CONSOLIDATION STRESS σ_c' (kPa)
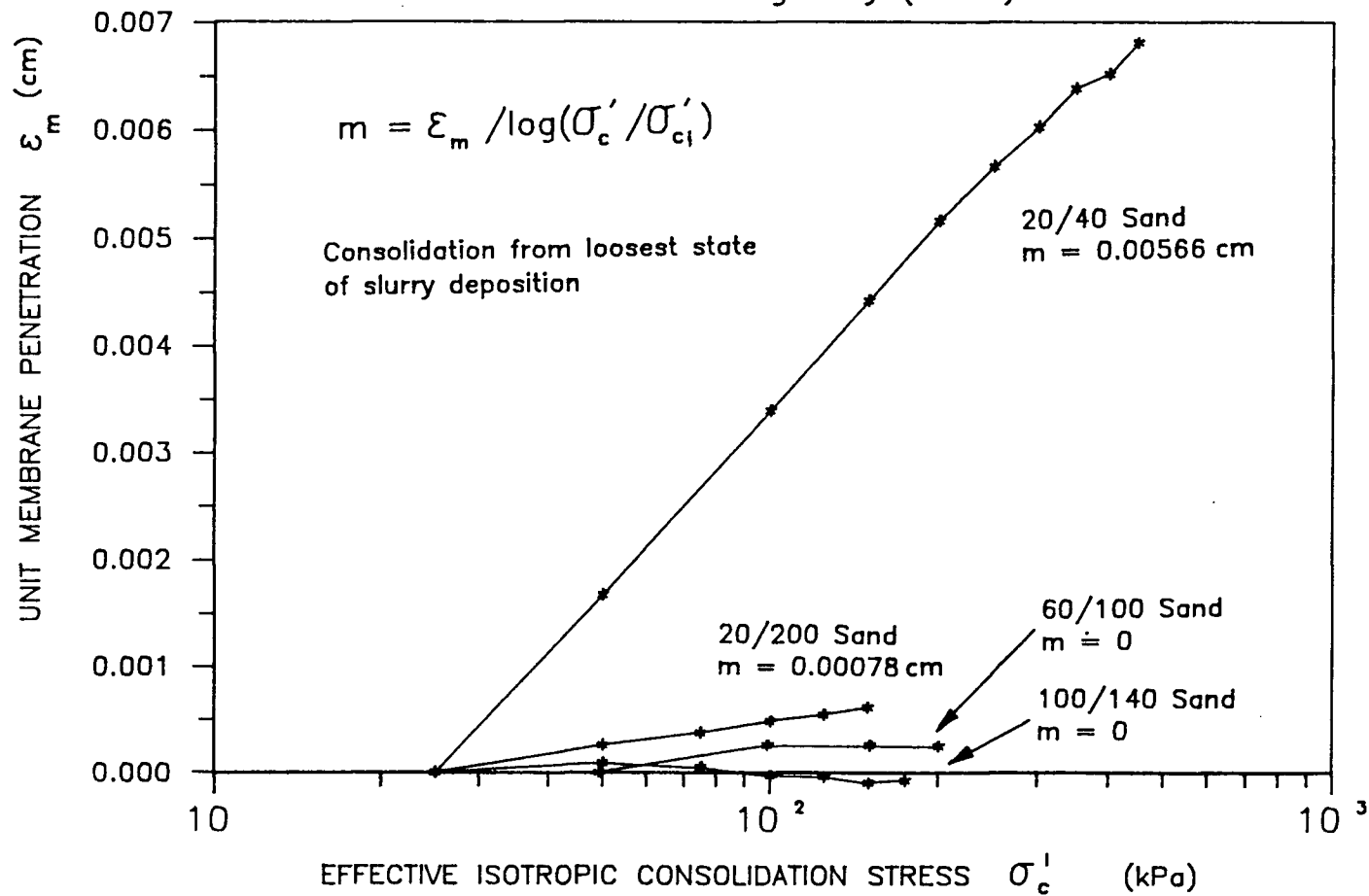
Figure A.2 Strain in Various Gradations of Brenda Sand
Under Virgin Isotropic Consolidation and Unloading

All samples consolidated
from near loosest state.

100/140

60/100

20/40

20/200

$\varepsilon_a = \varepsilon_r$

RADIAL STRAIN ε_r (%)

AXIAL STRAIN ε_a (%)

Sand Type	Dr_i (%)	e_i	$\sigma'_{c\,max}$ (kPa)
20/40	7	1.110	525
60/100	28	1.076	450
100/140	34	1.054	200
20/200	19	0.799	400

Figure A.3   Strain in Ottawa sand C109 during isotropic virgin consolidation and unloading
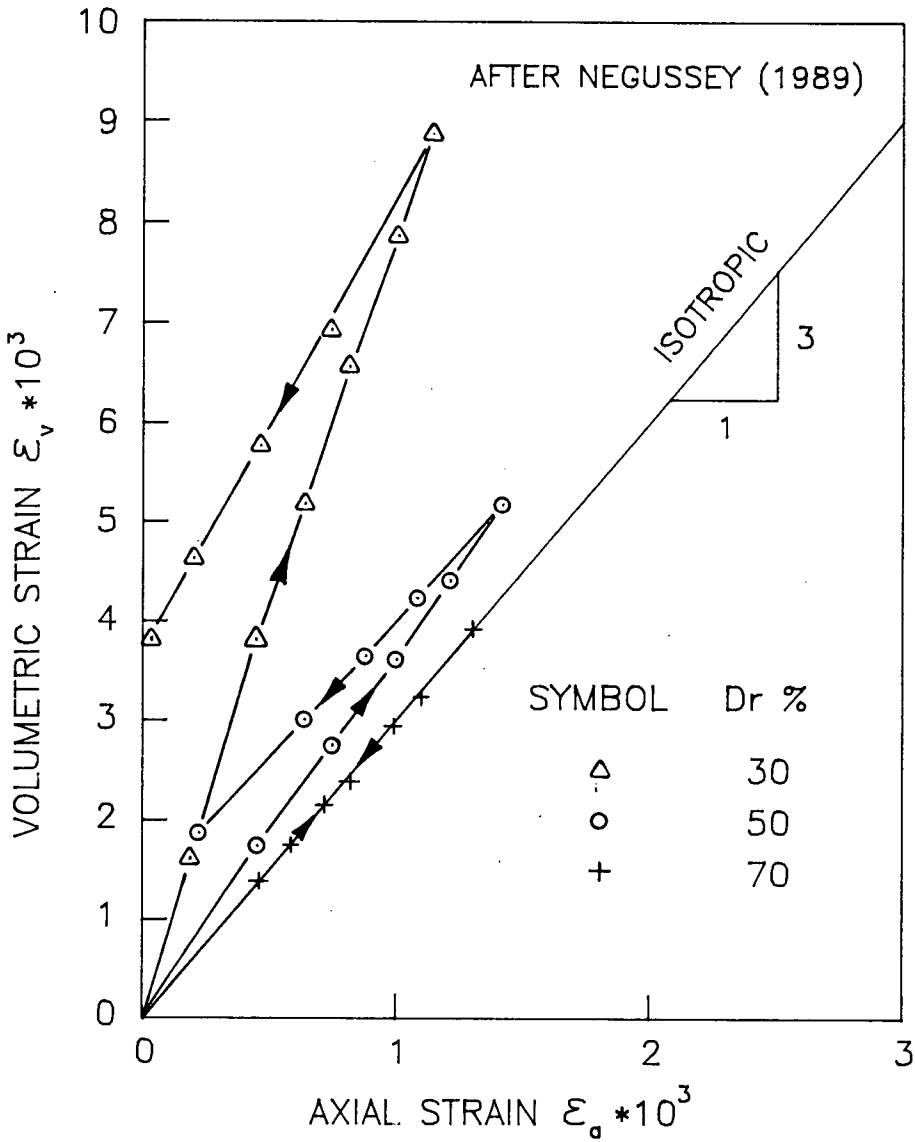
Appendix B: Calculation of Membrane Stress Correction

Various methods for calculating the stresses applied to a soil sample by its confining rubber membrane have been described in soil mechanics literature. These corrections are based on a number of assumptions which may or may not be true, depending upon test conditions.   There are three general types of membrane correction assumptions as follows (from Fukushima and Tatsuoka, 1984): Method 1) the membrane is assumed to maintain the shape of a thin wall cylindrical shell, such that elastic thin shell compression theory can be used; Method 2) it is assumed that axial deformation occurs independently of radial and circumferential deformations; and Method 3) it is assumed that the resistance of a membrane against axial deformation is neg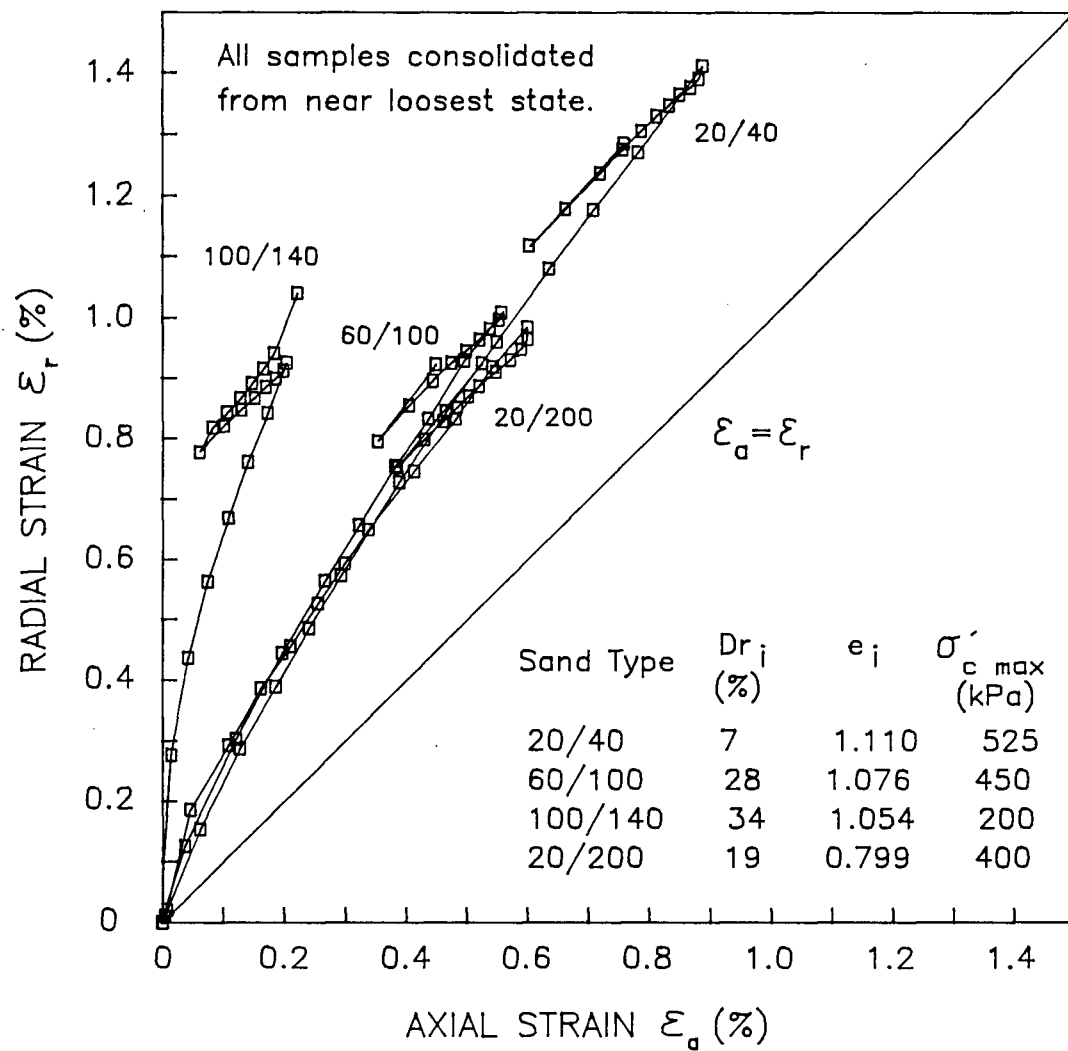ligible due to membrane buckling, and only membrane "hoop stresses" are applied to the soil sample.   Method 2 is thought to be unreliable because it neglects elastic theory.   Method 3 is useful for compression test corrections at larger strain level if buckling can be visually observed, especially in the testing of soft clay samples which are prone to large consolidation strains and are generally tested with very thin membranes.   Method 1 is generally preferable to the other methods of correction at smaller strain levels as long as membrane buckling is not observed and if soil samples are tested in both compression and extension loading.   Method 1 is particularly useful for testing sandy materials for susceptability to liquefaction, as low stress levels are encountered, larger membrane thicknesses which are less susceptable to buckling are used to overcome membrane penetration and damage problems, consolidation strains which may increase susceptability to buckling are small, and samples may be loaded in both extension and compression directions.   Method 1 type corrections have been derived and used by numerous workers, for example Henkel and Gilbert (1952), Duncan and Seed (1967), Berre (1982), Ponce and Bell (1971), Molenkamp and Luger (1981) and DeGroff et. al. (1988).   Although the same general method of evaluation has been used, different researchers have used different formulations which may or may not take into account the following factors which should be considered: 1) stress and strain induced in the membrane during sample preparation, 2) change in soil membrane thickness during strain, 3)

change in membrane modulus with strain level, 4) change in membrane stress and strain during sample saturation and consolidation, and 5) change in membrane stress with axial and radial strain during loading; it is important to note that according to elasticity theory, axial and radial membrane strains have an effect upon both axial and radial stresses, depending upon Poisson's ratio. In addition to theoretical formulation of membrane stress corrections, experimental verification of corrections should be undertaken to validate their reliability.

A formal derivation of Method 1 corrections which takes into account all of the factors described above and which simplifies the calculation of membrane stress correction is presented in the following pages. Experimental verification of the derived membrane stress correction factors is provided by a strain controlled undrained extension and compression test upon a triaxial test sample membrane filled with water.

Calculation of membrane stress correction by Method 1 (elastic shell theory):

The elastic strains in an elastic membrane cylindrical shell are as follows:

$$\varepsilon_{Ma} = (\sigma_{Ma} - \nu\sigma_{Mc} - \nu\sigma_{Mt})/E_M \qquad \text{Eqn. 1}$$

$$\varepsilon_{Mc} = (-\nu\sigma_{Ma} + \sigma_{Mc} - \nu\sigma_{Mt})/E_M \qquad \text{Eqn. 2}$$

$$\varepsilon_{Mt} = (-\nu\sigma_{Ma} - \nu\sigma_{Mc} + \sigma_{Mt})/E_M \qquad \text{Eqn. 3}$$

Where: ε_{Ma} = axial strain in cylindrical membrane

ε_{Mc} = circumferential strain in cylindrical membrane

ε_{Mt} = radial strain, or strain in thickness of the cylindrical membrane

E_M = Young's modulus of membrane rubber

ν = Poisson's ratio of membrane rubber

σ_{Ma} = axial stress in membrane

σ_{Mc} = circumferential stress in membrane

$\sigma_{Mt} \doteq \sigma_r$ = radial stress in cylindrical membrane

From the cylindrical dimensions of the membrane and radial stress upon the inside of the membrane, a relationship between σ_{Mc} and σ_{Mt} may be determined:

Figure B.1 Rubber membrane shell

$$D*H*\sigma_r = \sigma_{Mc}*2*t*H$$

$$\sigma_r = \sigma_{Mc}*2*t/D$$
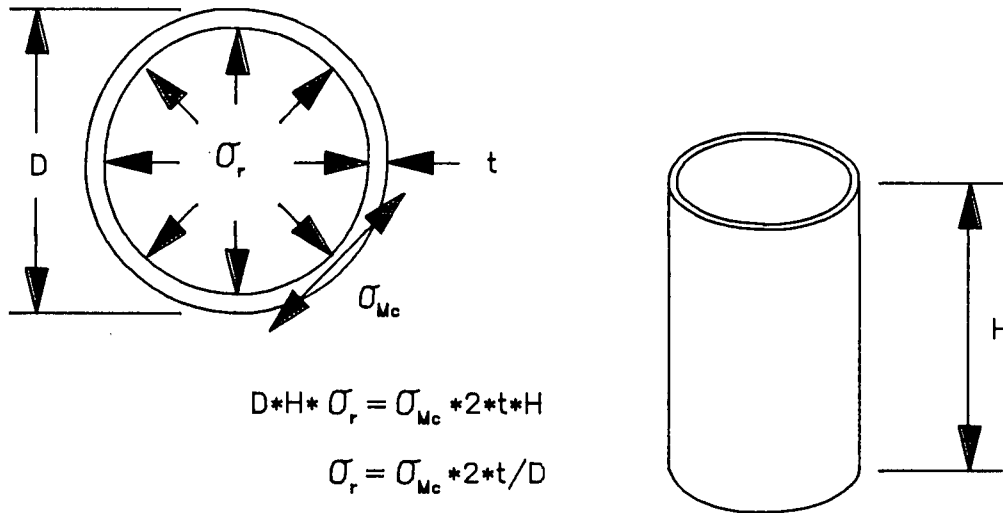
If t << D (for a thin cylindrical elastic shell) $\sigma_r << \sigma_{Mc}$, thus one can assume that $\sigma_r \doteq \sigma_{Mt} \doteq 0$, and may be ignored; from Equations 1 and 2:

$$\varepsilon_{Ma} = (\sigma_{Ma} - \nu\sigma_{Mc})/E_M \qquad \text{Eqn. 4}$$

$$\varepsilon_{Mc} = (-\nu\sigma_{Ma} + \sigma_{Mc})/E_M \qquad \text{Eqn. 5}$$

Hence:

$$\sigma_{Ma} = (\varepsilon_{Ma} + \nu\varepsilon_{Mc})*E_M/(1-\nu^2) \qquad \text{Eqn. 6}$$

$$\sigma_{Mc} = (\nu\varepsilon_{Ma} + \varepsilon_{Mc})*E_M/(1-\nu^2) \qquad \text{Eqn. 7}$$

Corrected stresses on a cylindrical soil sample within a confining membrane are

$$\sigma'_{am} = \sigma'_a - 4*(t/D)*\sigma_{Ma} \qquad \text{Eqn. 8}$$

$$\sigma'_{rm} = \sigma'_r - 2*(t/D)*\sigma_{Mc} \qquad \text{Eqn. 9}$$

Where: σ'_{am} = corrected axial stress on soil sample

σ'_{rm} = corrected radial stress on soil sample

σ'_{a} = axial stress on soil sample

σ'_{r} = radial stress on soil sample

t = present membrane thickness

D = present sample diameter

Thus membrane corrected sample stresses are:

$(6)+(8)$ $\sigma'_{am} = \sigma'_{a} - 4*(t/D)*E_M*(\varepsilon_{Ma} + \nu\varepsilon_{Mc})/(1-\nu^2)$ Eqn. 10

$(7)+(9)$ $\sigma'_{rm} = \sigma'_{r} - 2*(t/D)*E_M*(\nu\varepsilon_{Ma} + \varepsilon_{Mc})/(1-\nu^2)$ Eqn. 11

(Compression stress and strain is positive)

With a membrane rubber Poisson's ratio of $\nu = 0.5$ as is commonly measured (which implies that the membrane rubber undergoes zero volume change when strained):

from (10) $\sigma'_{am} = \sigma'_{a} - 8*(t/D)*E_M*(2\varepsilon_{Ma} + \varepsilon_{Mc})/3$ Eqn. 12

from (11) $\sigma'_{rm} = \sigma'_{r} - 4*(t/D)*E_M*(\varepsilon_{Ma} + 2\varepsilon_{Mc})/3$ Eqn. 13

With no volume change in rubber during strain ($\nu = 0.5$):

$$\varepsilon_{Mv} = \varepsilon_{Ma} + \varepsilon_{Mc} + \varepsilon_{Mt} = 0$$ Eqn. 14

Where: ε_{Mv} = volumetric strain in rubber

Considering circumferential strain in membrane:

$$S = \pi D$$

$$S_o = \pi D_o$$

$$\Delta S = \pi \Delta D$$ Eqn. 15

Where: S = circumference of cylindrical membrane

S_o = nominal unstretched membrane circumference

D = diameter of cylindrical membrane

D_o = nominal unstretched membrane diameter

$$\varepsilon_{Mc} = \Delta S/S_o = \pi \Delta D/\pi D_o = \Delta D/D_o = \varepsilon_r \qquad \text{Eqn. 16}$$

$$\varepsilon_r = (D_o - D)/D_o$$

$$D = (1 - \varepsilon_r) * D_o \qquad \text{Eqn. 17}$$

Where: ε_r = radial strain of cylindrical membrane dimensions referenced to initial unstretched membrane diameter

Considering radial strain in membrane (or change in membrane thickness):

$$\varepsilon_{Mt} = (t_o - t)/t_o = -(\varepsilon_r + \varepsilon_{Ma}) \qquad \text{Eqn. 18}$$

$$t = t_o (1 + \varepsilon_{Ma} + \varepsilon_r) \qquad \text{Eqn. 19}$$

Where: t_o = nominal undisturbed membrane thickness

Considering volume contained within membrane:

$$\varepsilon_v = (V_o - V)/V_o = (\varepsilon_{Ma} + 2\varepsilon_r) \qquad \text{Eqn. 20}$$

$$\varepsilon_r = (\varepsilon_v - \varepsilon_{Ma})/2 \qquad \text{Eqn. 21}$$

from (21)+(17) $$D = D_o (2 + \varepsilon_{Ma} - \varepsilon_v)/2 \qquad \text{Eqn. 22}$$

$$V_o = \pi D_o^2 H_o/4$$

Where: V_o = nominal volume within unstretched cylindrical membrane

H_o = nominal height of unstretched membrane which contains sample

ε_v = volumetric strain of volume within the stretched membrane referenced to unstretched membrane volume

Considering axial stress on soil sample:

$$\sigma'_{am} = \sigma'_a - 8*(t/D)*E_M*(2\,\varepsilon_{Ma} + \varepsilon_{Mc})/3 \qquad \text{Eqn. 12}$$

$(12)+(19) \quad \sigma'_{am} = \sigma'_a - 8*(t_o/D)*E_M*(1+\varepsilon_r+\varepsilon_{Ma})(2\varepsilon_{Ma}+\varepsilon_r)/3$

$+(21) \quad \sigma'_{am} = \sigma'_a - 2*(t_o/D)*E_M*(2+\varepsilon_v+\varepsilon_{Ma})(3\varepsilon_{Ma}+\varepsilon_v)/3$

$$+(22) \quad \sigma'_{am} = \sigma'_a - \frac{4*t_o*E_M(2+\varepsilon_v+\varepsilon_{Ma})(3\varepsilon_{Ma}+\varepsilon_v)}{3*D_o(2-\varepsilon_v+\varepsilon_{Ma})} \qquad \text{Eqn. 23}$$

Considering radial stress on soil sample:

$$\sigma'_{rm} = \sigma'_r - 4*(t/D)*E_M*(\varepsilon_{Ma}+2\varepsilon_{Mc})/3 \qquad \text{Eqn. 13}$$

from $(13)+(19)+(22)+(21)$

$$\sigma'_{rm} = \sigma'_r - \frac{8*E_M*t_o(1+\varepsilon_{Ma}+\varepsilon_r)\varepsilon_v}{3*D_o(2-\varepsilon_v+\varepsilon_{Ma})}$$

$$\sigma'_{rm} = \sigma'_r - \frac{4*E_M*t_o(2+\varepsilon_v+\varepsilon_{Ma})\varepsilon_v}{3*D_o(2-\varepsilon_v+\varepsilon_{Ma})} \qquad \text{Eqn. 24}$$

Thus soil stresses corrected for axial and radial membrane loading are:

$$\sigma'_{am} = \sigma'_a - \frac{4*t_o*E_M(2+\varepsilon_v+\varepsilon_{Ma})(3\varepsilon_{Ma}+\varepsilon_v)}{3*D_o(2-\varepsilon_v+\varepsilon_{Ma})} \qquad \text{Eqn. 23}$$

$$\sigma'_{rm} = \sigma'_r - \frac{4*E_M*t_o(2+\varepsilon_v+\varepsilon_{Ma})\varepsilon_v}{3*D_o(2-\varepsilon_v+\varepsilon_{Ma})} \qquad \text{Eqn. 24}$$

Note: All strains are measured with respect to nominal unstretched membrane dimensions.

Determination of membrane Young's modulus E_M :

In the previous derivation of membrane stress corrections, present membrane thickness and dimensions are used in the calculation of membrane stresses. The experimental technique for the determination of membrane Young's modulus described by Bishop and Henkel (1962), which requires that a strip of rubber membrane be hung between two glass rods and loaded with known mass to measure induced deformation in the membrane, is adequate for the determination of membrane Young's modulus as long as stretched membrane area is used in the calculation of induced membrane stress and thus Young's modulus. The original method of Young's modulus calculation described by Bishop and Henkel does not account for changes in stretched membrane dimensions.

If stretched membrane area is used in the calculation of membrane stress, Young's modulus is found to be constant from 0 to 25% extension loading strain (see Table B.1). If initial membrane area is used to calculate induced stress and thus Young's modulus, Young's modulus is shown to decrease up to 25% with 25% extension strain. Thus the calculation of Young's modulus using present induced membrane stress is also preferable because calculated modulus is found to be constant with changing stress and strain level. Poisson's ratio can also be verified to be 0.5 when Bishop and Henkel's experimental method is used to determine Young's modulus, by simply measuring the width and thus lateral strain in the test membrane as load is applied.

Calculation of membrane stress corrections:

To use Equations 23 and 24 to calculate membrane stresses on a soil sample, the following procedure is employed during sample preparation:

1) Initial membrane unstretched thickness t_0 and nominal diameter D_0 are determined.

2) Horizontal lines 10 cm apart are drawn with a marker pen on the unstretched membrane, so that initial axial sample preparation strain in the membrane may be determined by measuring the distance between

Determination of membrane Young's modulus E_M for a Geotest membrane (2.36" diameter by 0.012" thick by 8" high):

Figure B.2   Measurement of membrane modulus after Bishop and Henkel (1962):

wire hanger

glass rod

2"

W
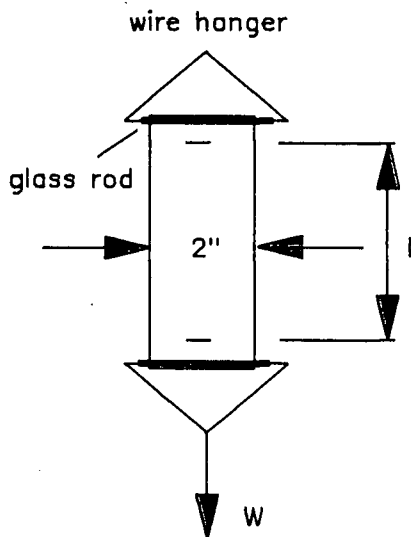
l = length between marks on membrane

W = load on membrane

E_M^* = Young's Modulus by Bishop and Henkel method of calculation, using initial dimensions of sample membrane.

E_M = Young's Modulus using loaded thickness and width of membrane to calculate stress on membrane.

Table B.1   Calculation of a Geotest membrane modulus

Load W (kg)	Length l (cm)	Width (cm)	ε_l	ε_w	E_M^* (kg/cm^2)	E_M (kg/cm^2)
0	7.85	5.05	0	0		
0.25	8.26		0.0522		15.46	16.31
0.5	8.70		0.1083		14.91	16.66
0.75	9.26		0.1796		13.48	16.28
1.0	9.92	4.38	0.2637	0.1327	12.25	16.25

$\mathcal{V}$ = 0.1327/0.2637 = 0.503   (used to calculate membrane area and stress)

Use E_M = 16.3 kg/cm^2 = 1600 kPa

Note: One should use present membrane dimensions to calculate stress in membrane and thus membrane modulus.

pen marks after sample preparation has been completed.

3) The length of membrane which covers the sample after sample preparation has been completed is adjusted for axial strain induced in the membrane during sample preparation to determine the unstretched height H_o which covers the soil sample.

4) The unstretched volume of membrane which contains the sample is determined from H_o and D_o .

5) The axial and volumetric strains used in Equation 23 and 24 are calculated from unstretched membrane dimensions, and updated every time the soil sample within the membrane undergoes axial or volumetric strain.

It should be noted that the probability of membrane buckling can be reduced or completely avoided by prestretching the membrane during sample preparation. If a membrane is axially prestretched 5 to 10% during sample preparation, which is not uncommon if the membrane is initially of smaller diameter than the soil sample and stretched to the sides of a sample former tube by an external vacuum, then the membrane will be under axial tension up to 5 to 10% soil sample compression strain and maintain an unbuckled shape at higher compression strain level. The initial load on the soil sample due to the sample membrane is not a problem as it may be accurately calculated using Equations 23 and 24.

Equations 23 and 24 have been validated by assembling a rubber membrane within a triaxial test cell with only de—aired water filling it to its initial cylindrical sample shape. The water filled membrane was loaded undrained in a strain controlled testing apparatus, to determine the load—strain response of the membrane experimentally as shown in Figure B.3. The predicted load—strain response calculated using Equation 23, as also shown in Figure B.3, provides a good estimate of membrane load—strain response. The membrane does not buckle until compression strain is greater than 5%; buckling resistance is better in a soil test because membrane shape is maintained by the soil sample within the membrane.

Figure B.3 Cylindrical rubber membrane stress correction verification by triaxial test constant rate of strain loading of a Geotest membrane filled with water

Predicted load from elastic shell theory:

$$L = \pi t_o D_o E_M (2 + \varepsilon_v + \varepsilon_{Ma})(3\varepsilon_{Ma} + \varepsilon_v)(2 - \varepsilon_v + \varepsilon_{Ma})/12 + \text{uplift on rod} - \text{buoyant weight of top cap}$$

Geotest membrane specifications:
2.36" Dia. x 0.012" x 8"
E_M = 1600 kPa = 16.3 kg/cm^2

Membrane state before loading:
H_I = 13.00 cm V_I = 413.8 cm^3
ε_{Ma_I} = 0.008 ε_{V_I} = −0.119

Unstretched membrane dimensions:
H_o = 13.104 cm V_o = 369.77 cm^3
t_o = 0.0305 cm

Rod area = 0.3167 cm^2
Cap buoyant weight = 0.2412 kg
Cell pressure = 142 kPa

Compression

Friction on rod = 0.22 kg

Extension

Predicted load versus strain using elastic shell theory

Measured undrained load versus strain response of a rubber membrane filled with water (corrected for LVDT spring)

Axial load L (kg)

Sample axial strain $\varepsilon_A = \dfrac{H_I - H}{H_I}$ (percent)